UCTEA Turkish Chamber of Civil Engineers

Teknik Dergi

Technical Journal

Volume 32 Issue 2 March 2021

TEKNİK DERGİ PUBLICATION PRINCIPLES

Teknik Dergi is a scientific and technical journal indexed by the Science Citation Index Expanded. Annually six issues are published, three in Turkish in the months of January, May and September, three in English in March, July and November. Its main principles of publication are summarized below:

1. Articles reporting original scientific research and those reflecting interesting engineering applications are accepted for publication. To be classified as original, the work should either produce new scientific knowledge or add a genuinely new dimension to the existing knowledge or develop a totally new method or substantially improve an existing method.
2. Articles reporting preliminary results of scientific studies and those which do not qualify as full articles but provide useful information for the reader can be considered for publication as technical notes.
3. Discussions received from the readers of the published articles within three months from publication are reviewed by the Editorial Board and then published together with the closing remarks of the author.
4. Manuscripts submitted for publication are evaluated by two or three reviewers unknown to the authors. In the light of their reports, final decision to accept or decline is taken by the Editorial Board. General policy of the Board is to get the insufficient manuscripts improved in line with the reviewers' proposals. Articles that fail to reach the desired level are declined. Reasons behind decisions are not declared.
5. A signed statement is taken from the authors, declaring that the article has not been published as a "journal article or book chapter". In case the Editorial Board is in the opinion that the article has already been published elsewhere with minor changes or suspects plagiarism or a similar violation of ethics, then not only that article, but none of the articles of the same authors are published.
6. Papers reporting works presented as conference papers and developed further may be considered for publication. The conference it was presented to is given as a footnote in the first page.
7. Additionally, a document signed by all authors, transferring the copyright to UCTEA Chamber of Civil Engineers is submitted together with the manuscript.

UCTEA Turkish Chamber of Civil Engineers

Teknik Dergi

Technical Journal

Volume 32 Issue 2 March 2021

UCTEA *(TMMOB)*
Turkish Chamber of Civil Engineers *(İnşaat Mühendisleri Odası)*
Necatibey St. No: 57, Kızılay 06440 Ankara, Turkey
Tel: +90.312.294 30 00 - Faks: +90.312.294 30 88
E-mail: imo@imo.org.tr - www.imo.org.tr

Publisher *(Sahibi)*:
Taner YÜZGEÇ
On behalf of UCTEA Turkish Chamber of Civil Engineers

Administrative Officer *(Yazı İşleri Müdürü)*:
Özer AKKUŞ

Volume 32 - Issue 2 - March 2021 *(Cilt 32 - Sayı 2 - Mart 2021)*

Published bi-monthly. Local periodical. *(İki ayda bir yayınlanır, yerel süreli yayın)*

Date of Print: 1 March 2021 *(Baskı Tarihi: 1 Mart 2021)*

Number of copies: 1.000 *(1.000 adet basılmıştır)*

ISSN: 1300-3453

Printed by *(Baskı)*:
Boyut Tanıtım Matbaa Basım Yayın San. Tic. Ltd. Şti.
İvedik Organize Sanayi 1354. Cad. Fora İşmerkezi No: 138/18 - Yenimahalle /Ankara
Tel: 0.312.385 72 12 - Faks: 0.312.385 72 13

UCTEA Turkish Chamber of Civil Engineers

Teknik Dergi

Teknik Dergi is indexed by
- Science Citation Index Expanded
- Scopus
- Journal Citation Reports / Science Edition
- Engineering Index
- Concrete Abstracts (American Concrete Institute)
- National Technical Information Service (US NTIS)
- CITIS
- Ulrich's International Periodical's Directory
- TÜBİTAK / ULAKBİM

Teknik Dergi is a peer reviewed open access periodical publishing papers of original research and interesting practice cases. It addresses both the research community and the practicing engineers.

Reviewers:

This list is renewed each year and includes reviewers who served in the last two years of publication.

Süleyman ADANUR
Ali Mardani AGHABAGLOU
Ayda Şafak AĞAR ÖZBEK
Perviz AHMEDZADE
Ragıp AKBAŞ
Sami Oğuzhan AKBAŞ
Şeref Doğuşcan AKBAŞ
Rıfat AKBIYIKLI
Özge AKBOĞA KALE
Hüseyin AKBULUT
Burcu AKÇAY ALDANMAZ
Cihan Taylan AKDAĞ
Adem AKPINAR
Muhammet Vefa AKPINAR
Atakan AKSOY
Hafzullah AKSOY
Hakan AKSU
Tülay AKSU ÖZKUL
Büşra AKTÜRK
Güzin AKYILDIZ ALÇURA
Zuhal AKYÜREK
Uğurhan AKYÜZ
Sadık ALASHAN
Cenk ALHAN
Sinan ALTIN
Selim ALTUN
Adlen ALTUNBAŞ
Ahmet Can ALTUNIŞIK
Yalçın ALVER
Egemen ARAS
Ergin ARIOĞLU
Yalçın ARISOY
Musa Hakan ARSLAN
Deniz ARTAN İLTER
Şenay ATABAY
Ali Osman ATAHAN
Hakan Nuri ATAHAN
Abdullah AVEY
Ersin AYDIN
İsmail AYDIN
Mustafa Tamer AYVAZ
Ela BABALIK
Can Elmar BALAS
Selim BARADAN
Türkay BARAN
Bekir Oğuz BARTIN
Eyüp Ensar BAŞAKIN
Cemal BAŞARAN
Özgür BAŞKAN
İdris BEDİRHANOĞLU
Niyazi Özgür BEZGİN
Senem BİLİR MAHÇİÇEK
Ahmet BİRİNCİ
İlknur BOZBEY
Zafer BOZKUŞ
Atıl BULU
Burcu BURAK BAKIR
Halil İbrahim BURGAN
Yusuf CALAYIR
Erdem CANBAY
Zekai CELEP
Cihan CENGİZ
Halim CEYLAN
Hüseyin CEYLAN
Ömer CİVALEK
Özgür ÇAKIR
Melih ÇALAMAK
Gülben ÇALIŞ
Erkan ÇELEBİ
Kutay ÇELEBİOĞLU
Tevfik Kutay ÇELEBİOĞLU
Ahmet Ozan ÇELİK
Oğuz Cem ÇELİK
Osman Nuri ÇELİK
Semet ÇELİK
Hilmi Berk ÇELİKOĞLU
Mecit ÇETİN
Gökhan ÇEVİKBİLEN
Mesut ÇİMEN
Safiye Feyza ÇİNİCİOĞLU
Erdal ÇOKÇA
Şevket ÇOKGÖR
İsa ÇÖMEZ
Atilla DAMCI
Yakup DARAMA
Osama M.F. DAWOUD
Özgür DEĞERTEKİN
Abdullah DEMİR
Cem DEMİR
Uğur DEMİR
Ender DEMİREL
Mehmet Cüneyd DEMİREL
Fatih DİKBAŞ
Seyyit Ümit DİKMEN
İrem DİKMEN TOKER
Ali Ersin DİNÇER
Selim DÜNDAR
Nurhan ECEMİŞ ZEREN
Alper ELÇİ
Şebnem ELÇİ
Muhammet Emin EMİROĞLU
Hakan ERDEM
Sinan Turhan ERDOĞAN
Esin ERGEN PEHLEVAN
Ayşen ERGİN
Gökmen ERGÜN
Ebru ERİŞ
Bülent ERKMEN
Barış ERKUŞ
Esra Ece ESELLER BAYAT
Tuğba ESKİŞAR TEFÇİ
Burak FELEKOĞLU
Okan FISTIKOĞLU
Abdullah GEDİKLİ
Ergun GEDİZLİOĞLU
Mohammad Ali GHORBANİ
Ömer GİRAN
Konuralp GİRGİN
Zehra Canan GİRGİN
Ilgın GÖKAŞAR
Çağlar GÖKSU
Serdar GÖKTEPE
Fazlı Erol GÜLER
Hakan GÜLER
Ilgın GÜLER
Gürkan GÜNAY
Taylan GÜNAY
Abdurrahman GÜNER
Samet GÜNER
Ülker GÜNER BACANLI
Oğuz GÜNEŞ
Mehmet Şükrü GÜNEY
Tuba GÜRBÜZ
BÜYÜKKAYIKÇI
Melike GÜREL
İbrahim GÜRER
Aslı Pelin GÜRGÜN
Gürşans GÜVEN IŞIN
Iman HAJİRASOULİHA
Soner HALDENBİLEN
Murat HAMDERİ
Ufuk HANCILAR
Ingo A. HANSEN
Mustafa HATİPOĞLU
Nejan HUVAJ SARIHAN
Metin HÜSEM
Zeynep IŞIK
Hande IŞIK ÖZTÜRK
Sabriye Banu İKİZLER
Ragıp İNCE
Eren İNCİ
Pınar İNCİ KOÇAK
Sedat KABDAŞLI
Volkan KAHYA
Mehmet Rifat KAHYAOĞLU
Volkan KALPAKÇI
Alper KANYILMAZ
Murat KARACASU
Tanay KARADEMİR
Halil KARAHAN
Ali KARAİPEKLİ
Cenk KARAKURT
Mustafa KARAŞAHİN
Zülküf KAYA
Mustafa Kubilay KELEŞOĞLU
Mustafa Erol KESKİN
Havvanur KILIÇ
İsmail Emrah KILIÇ
Sami And KILIÇ
Fahriye KILINÇKALE
Ufuk KIRBAŞ
Veysel Şadan Özgür KIRCA
Güven KIYMAZ
Young Hoon KİM
Gökhan KİRKİL
Salih KOÇAK
Niyazi Uğur KOÇKAL
Önder KOÇYİĞİT
Mehmet Melih KOŞUCU
Baha Vural KÖK
Mete KÖKEN
Fuat KÖKSAL
Şerife Yurdagül KUMCU
Murat KURUOĞLU
Akif KUTLU
Semih KÜÇÜKARSLAN
Abdullah KÜRKÇÜ
Hilmi LUŞ
Kasım MERMERTAŞ
Mehmet Murat MONKUL
Hamid MORTEZAİE
Yetiş Şazi MURAT
Sepanta NAİMİ
Öcal NECMİOĞLU
Sinan Melih NİĞDELİ
Elif OĞUZ
Didem OKTAY
Derviş Volkan OKUR
Volkan OKUR
Mehmet Hakkı OMURTAG
Engin ORAKDÖĞEN
Şeref ORUÇ
Akın ÖNALP
Halil ÖNDER
Jülide ÖNER
Bihrat ÖNÖZ
Mustafa ÖZAKÇA
Bergüzar ÖZBAHÇECİ
Ceyhun ÖZÇELİK
Gökhan ÖZDEMİR
İlker ÖZDEMİR
Osman Nuri ÖZDEMİR
Halit ÖZEN
Murat ÖZEN
Pelin ÖZENER
Cem ÖZER
Hasan ÖZER
Serkan ÖZGEN
Eren Arman ÖZGÜVEN
Hakkı Oral ÖZHAN
Yener ÖZKAN
M. Hulusi ÖZKUL
Gülen ÖZKULA
Turan ÖZTURAN
Hasan Tahsin ÖZTÜRK
Mustafa ÖZUYSAL
Polat ÖZYİĞİT
Gülizar ÖZYURT
TARAKÇIOĞLU
Onur PEKCAN
Elişan Filiz PİROĞLU
Cengiz POLAT
Selim PUL
Selçuk SAATÇİ
Selman SAĞLAM
Mehmet SALTAN
İlyas SARIBAŞ
Afşin SARITAŞ
Altuğ SAYGILI
Serdar SELAMET
Senem SEYİS
Alper SEZER
Faiz Uddin Ahmed SHAİKH
Osman SİVRİKAYA
Behzad SOLTANBEİGİ
Celal SOYARSLAN
Serdar SOYÖZ
Tayfun Altuğ SÖYLEV
Aleksandar STEVANOVİC
Erol ŞADOĞLU
Güvenç ŞAHİN
Remzi ŞAHİN
Yuşa ŞAHİN
Mustafa ŞAHMARAN
Nermin ŞARLAK
Ömer Lütfi ŞEN
Burak ŞENGÖZ
Aynur ŞENSOY ŞORMAN
Okan ŞİRİN
Ali Arda ŞORMAN
Ali Ünal ŞORMAN
Özcan TAN
Gülüm TANIRCAN
Kürşat TANRIÖVEN
Serhan TANYEL
Yüksel TAŞDEMİR
Kerem TAŞTAN
Gökmen TAYFUR
İlker TEKİN
Beytullah TEMEL
Egemen TEOMETE
Serdal TERZİ
Berrak TEYMUR
H. Onur TEZCAN
Hüseyin Onur TEZCAN
Mesut TIĞDEMİR
Şahnaz TİĞREK
Salih TİLEYLİOĞLU
Vedat TOĞAN
Onur Behzat TOKDEMİR
Cengiz TOKLU
Nuray TOKYAY
Ali TOPAL
İlker Bekir TOPÇU
Cem TOPKAYA
Selçuk TOPRAK
Kamile TOSUN FELEKOĞLU
Gökçe TÖNÜK
Nursu TUNALIOĞLU
Kağan TUNCAY
Gürsoy TURAN
Ö. Tuğrul TURAN
Cüneyt TÜZÜN
Latif Onur UĞUR
Mehmet Fevzi UĞURYOL
Berna UNUTMAZ
Volkan Emre UZ
Nihal UZCAN ERATLI
İbrahim Mert UZUN
Deniz ÜLGEN
Mehmet ÜLKER
Cüneyt VATANSEVER
Syed Tanvir WASTI
Nazmiye YAHNİOĞLU
Cem YALÇIN
Mehmet Cem YALÇIN
Aslı YALÇIN DAYIOOĞLU
Ahmet Cevdet YALÇINER
İsmail Özgür YAMAN
Arcan YANIK
Mert Yücel YARDIMCI
Ufuk YAZGAN
Anıl YAZICI
Halit YAZICI
Kasım YENİGÜN
Seda YEŞİLMEN
İrem Zeynep YILDIRIM
Mehmet YILDIRIMOĞLU
Osman YILDIZ
Çetin YILMAZ
Fatih YILMAZ
Koray Kamil YILMAZ
Mehmet YILMAZ
Murat YILMAZ
Mustafa Tuğrul YILMAZ
Veysel YILMAZ
Yüksel YILMAZ
Fatih YONAR
Recep YURTAL
İsmail YÜCEL
Ömer YÜKSEK
Ercan YÜKSEL
Yeliz YÜKSELEN AKSOY
Ahmet Şahin ZAİMOĞLU
Abdullah Can ZÜLFİKAR

UCTEA Turkish Chamber of Civil Engineers

Teknik Dergi

Volume: 32 Issue: 2 March 2021

CONTENTS

Foreword

ON THE FUTURE OF BILINGUAL PUBLICATION POLICY

Since adoption of the bilingual publication policy, Teknik Dergi annually publishes three issues in Turkish and three in English as of January 2018. Initially, the Editorial Board had been concerned about a sustainable inflow of English manuscripts. However, this concern faded away soon as the manuscripts in English outnumbered the Turkish ones. Observations over the last two years give the impression that this tendency will probably continue, it may even get stronger. This imbalance could so far be compensated by including a larger number of papers in the issues in English. Evidently, this approach is not sufficient by itself any more, since a sizeable accumulation of English manuscripts is building up.

In view of the statistical analyses and a comprehensive evaluation of the publication principles, it was concluded that publication of four issues in English and two issues in Turkish would be feasible. The current publication regime will be continued throughout 2021, since the issues to be published that year have already been organised. As of the beginning of the following year, January, March, July and September issues will be published in English and May and November issues in Turkish. The Editorial Board has decided to have the forthcoming issues organised accordingly.

In the case if the number of English Manuscripts increases further, regular publication of the Turkish issues may become hard, even unfeasible, and a different publication regime may become unavoidable. Various alternatives are being considered in this respect, the final decision will be taken in the light of the developments observed in due course.

Turkish engineers have lately improved their foreign language (English in particular) reading and writing capabilities. This is probably the result of the improvements in English teaching in universities, besides the ever-increasing use of the Internet. The academia, on the other hand, are improving their communication and collaboration activities globally. Consequently, the authors of Teknik Dergi are becoming more enthusiastic to draft their papers in English. Although the drafting language of the recently received papers appear to be improving, some manuscripts still reflect an unacceptably poor English. The authors are encouraged to have their manuscripts reviewed by someone having a good command of English, a native speaker if possible.

With our best wishes…

Tuğrul Tankut
On behalf of the Editorial Board

Teknik Dergi, 2021 10577-10610, Paper 604

Damage Identification Analyses of a Historic Masonry Structure in T-F Domain

Kemal BEYEN[1]

ABSTRACT

Fatih mosque, a landmark structure in Istanbul, has suffered structural damage during 1999 Kocaeli earthquake. Using spectral, time-domain (OKID/ERA for SISO and MIMO models) and T-F domain (WT, HHT) techniques on ambient vibrations, damage identification has been performed. Results of parametric and spectral analyses indicate close global peaks. Northwest arch (O_3) that was expected to move in harmony with other arches cannot display such a consistent behavior and produces additional local frequency at 24Hz due to damage. Southeast arch (O_1) also has comparable damage producing another locality at 38Hz. Extending linear approaches into nonlinear-nonstationary methods, decompositions in WT and HHT improved the results in the temporal-frequency energy distribution. Estimated individual and global structural behavior are consistent with visually inspected damage states for O_3 and O_1. On a global scale, damage additionally generates significant nonstationarity on the neighbors in touch. Northeast arch (O_2) is affected strongly by the anomalies appeared at stations O_3 and O_1. Especially neighbor stations O_6 and O_7 located at the springing points of the arch (O_3) and others O_5 and O_6 located at the springing points of the arch (O_2) are strongly affected due to tension rod failure causing the dome base to open outwards. T-F analysis detects and localizes any anomalous system behavior and can adequately capture the system dynamics of any instrumented part of the structure at any particular time epoch. For historical masonry structures with vulnerable components like large central dome and arches that have low redundancy, there is a need to develop automatic signal/image processing through, machine vision, and pattern recognition for early diagnosis and warning of gradual deteriorations.

Keywords: Damage identification, nonstationary, nonlinear, wavelet analysis, HHT, T-F analysis, stone masonry structure.

Note:
- This paper has been received on May 24, 2018 and accepted for publication by the Editorial Board on October 22, 2019.
- Discussions on this paper will be accepted by May 31, 2021.
- https://dx.doi.org/10.18400/tekderg.426728

1 Kocaeli University, Department of Civil Engineering, Kocaeli, Turkey - kbeyen@kocaeli.edu.tr
https://orcid.org/0000-0001-8878-0985

1. INTRODUCTION

Turkey has a long history of destructive earthquakes. The 17 August 1999 M_w 7.4 Kocaeli earthquake was one of the largest earthquakes of the North Anatolian fault zone over the last five centuries. It caused widespread damage in the densely populated epicentral region. Structural damages were observed as far away as the western suburbs of Istanbul, about 110 km from the epicenter. Stone- masonry cultural structures were subjected to strong shaking during the Kocaeli earthquake and they are in areas of high seismic hazard from future events.

Arches and domes are vulnerable important components of stone masonry cultural structures. Damage characteristics and unique failure mechanisms of such structural systems are key issues to be identified before effective seismic risk mitigation schemes can be developed. P*ost-earthquake* failures in aging stone masonry structures that may develop over time are also possible. Such damage patterns will become apparent as excessive cracks and inevitably, element-level spallings are initiated by seismic activities. Fatih mosque, which was originally built more than 500 years ago, suffered various kinds of damage due to large-scale earthquakes during its lifetime. During the great earthquake of 1766, many domes and arches of monumental buildings in the city, including Fatih mosque, collapsed (it was subsequently reconstructed). In the 1999 Kocaeli earthquake, the structure suffered various kinds of damage and parts of its facades fell off in many locations. Progressive damage and partial failure may destabilize the adjacent members and eventually develop a post-earthquake structural collapse. Collapse of the east arch of Hagia Sophia three years after a major earthquake in 1344 [1] is a remarkable example of a post-earthquake structural failure. To prevent such possible failures initiating collapse, real-time damage detection in a scheduled task is essential. This task can be realized within the frames of nondestructive vibration-based damage identification in a health-monitoring program.

Despite the structural simplicity and morphological clarity of the stone made dome-arch type structures, understanding and describing mechanical behavior especially under seismic loading condition is still challenging problem due to complex and nonlinear behavior of masonry structures [2]. As it is summarized by Lourenço [3], experimental and numerical issues in modelling of the mechanical behavior of masonry construction are still developing with the computational technologies. Lourenço also proposes possible guidelines with illustrations from different numerical analysis tools for historical constructions [3]. Kennedy proposed experimental modal analysis that is the first and perhaps the most significant one in 1947 [4]. Vibration based damage assessment for bridge structures was seen in the early 1980's [5]. Field tests of civil engineering structures that were studied comprehensively dates back to the early nineties [6, 7]. Today, influence of existing cracks on the dynamic behavior of buildings, constitutive models for masonry [8, 9] and level of changes in dynamic properties realistically describing the masonry building damages are some topics under consideration [10]. Moreover today, long-term structural monitoring and FEM-based damage assessment through linear [11, 12, 13] and nonlinear analysis [14] represent complementary techniques to identify the complex behavior of ancient buildings. Importance of the structural monitoring has been well understood in recent decades by the community as an identification tool for model upgrading [15, 16, 17, 18, 19], a diagnosis tool for tracing progressive damage and condition assessment [11, 12, 13, 14] and control tool after the restoration or strengthening [20, 21, 22].

In general, ambient vibration data provides knowledge about the characteristic behavior of a structure that has two broad applications; (1) Updating member properties in an analytical model of the structure provides a rational basis for validation [16, 23]. (2) Identification of deterioration and probable failure mechanism. However, ambient vibration data recorded from historical structures contains low amplitude structural vibration signal and large amplitude wide-band noise. Therefore, in case of damage identification currently used classical methods are usually not suitable. Furthermore, analysis of deterioration requires multi-epoch ambient vibration measurements in a properly designed and continuously operated structural health-monitoring network. For the Fatih mosque, measurement program was performed in 2005, after the Kocaeli earthquake to assess the existing condition of the historical large-scale building in the class of the Imperial Ottoman mosques. The vibrations of the dome + arch type structural system are valuable post-earthquake records for the stone made structures. Recorded data sets were used first in the identification of the structural characteristics for the report, which was prepared for the restoration work undertaken by Istanbul Metropolitan Municipality [24, 25]. Later, although all were linear approaches and consistency was limited for damage identification, advanced algorithms were implemented and responses to the August 17, 1999 Kocaeli earthquake were simulated based on code proposed spectrum [26]. In this study, the aim is to identify and correlate the damage with strong evidences using nonlinear and nonstationary techniques for accurate estimation. Since as a priority, structural characteristics and as well as damage information are not known before recording, it is inevitable that the various methods are always tested with the data sets to see the level of sensitivity. Consistency between the Time-Frequency results is also investigated to assess the accuracy for each applied technique. Early results [26] were also described in part of this study. Such linear-stationary outcomes is particularly important at this time, when concerns about the nonlinear and nonstationary features of the dynamic behavior exist.

In modern construction, for instance for moment resisting-shear frame systems, damage is mostly a local phenomenon that is captured by utilizing high frequency modes, whereas the low frequency modes are related to the global response of the structure. In case of vibration-based damage detection, studies have shown that the resonant frequencies have less random measurement errors (i.e., less effect of sampling variation) than other modal parameters, which may have many sources of error [27]. Therefore, the resonant frequency can be a robust damage indicator for historical structures with small structural redundancy. As shown in Fig. 1, the building is approximately square in plan with vertical load carrying members at the corners. Failure of any one of these members may initiate the collapse mechanism, due to poor redundancy. Damage, or lack thereof, can be evaluated comparing vibration characteristics between damaged and undamaged states of identical components. Due to reflective symmetry in both directions, considering for a moment a damaged member to be investigated and an undamaged identical member on the symmetry site referred to as a control member, frequency information of both identical structural members may correlate with each other, if no damage occurs; otherwise, comparison will reveal the detectable differences in peak frequencies [26]. Large changes will certainly give a strong anomaly, which needs to be examined in detail. A similar methodology might be applied in structural condition assessment for the cultural structures. Progressive damage might be better detected by an operational monitoring network. Simple seeking of natural/dominant frequency shift and peak drop in allowable limits over the time may be basic algorithm for detection.

The objectives of the past studies [24, 26] are to infer the structural characteristics and identify the damage potential based on linearized approaches. Some of the core subjects in this research include (1) declaring the shortage of the linear techniques, (2) identifying nonstationary and nonlinear behavior in the structural response, (3) identifying the possible damage at the earliest possible stage from recorded input-output data and (4) implementing all of these procedures for the historical stone masonry structure. For a striking application, earthquake-induced damage in large components of the Ottoman royal mosque Fatih was considered as the working structure.

History of the working structure dates back to 15th century. It was built in İstanbul between 1463 and 1470 along with a well-integrated group of appurtenant buildings. Much of it was destroyed during the 1766 earthquake. After altering the old structural system to the present one, it was reopened in 1772. However, little trace of this complex survives today. As a load-bearing system, central dome structure rests on four pointed-arches, which rise from springings of four heavy corner piers [1, 28, 29, 30]. Four semi domes and four cupolas also support the central dome system. Cupolas are carried on four spherical triangular pendentives, which enable the force transition from the circular base of the dome to the rectangular base below and ultimately to the foundation by the piers. Buttresses on the sides provide important contribution to lateral resistance against the lateral forces of the earthquakes.

In the current study, the following provides a brief description of the content of the text that follows. Section 2 explains the behavior of the masonry structure with typical photographs of the damages developed in the Fatih mosque. Section 3 describes failure modes of the stone masonry arch-dome system in detail with typical photographs of the system failures from Fatih mosque. Section 4 briefly explains the time-frequeny domain advanced algorithms such as wavelet and Hilbert transforms, which have workable solutions to this challenging problem in vibration identification. In sub sections, background of the algorithms and efficiencies/drawbacks will be shortly discussed. Section 5 describes the instrumentation of the structure and data processing. Section 6 extensively discusses the results of the above-mentioned techniques, improvements of the resolutions based on intrinsic mode functions, proposed improvement over the classic harmonic decompositions (i.e., FT) and efficiency of damage identification based on ambient vibration data sets. The Conclusion is given in section 7. This study would be beneficial example in order to apply for other monuments prone to earthquake damage. Techniques applied in this study would also bring a different perspective to civil engineers point of view other than classic approaches for conservation of historical structures.

2. BEHAVIOR OF THE MASONRY STRUCTURE

A conceptual framework, which is customary in testing documented performances with the observations, was used in this section to verify the expected cause and effect correlation in the structural behavior. While the behavior of the masonry structure is given in detail, typical photographs will be shared as damage examples of the Fatih mosque.

Mostly the accumulated effects of material degradation, ageing, overloading and foundation settlements damage historical unreinforced stone masonry structures. Due to additional loading because of change in functioning or boundary conditions due to supplementary losses

or failures on neighbor members or due to seismic forces for which the structure had not been designed originally, structural members may undergo damage. Among the structural members, the most important members that are primarily vulnerable to earthquake damage are the vertical load carrying members, which are principally designed to resist gravity and wind loads with little or no consideration of the forces generated by the seismic effects. Nevertheless, under seismic forces they tend to interact with the surrounding frame and may result in different desirable failure modes. In general, behavior of the masonry structure is usually brittle with little or no ductility and both structural and non-structural parts suffer various types of damages varying from invisible cracking to crushing and eventually disintegration. William et al. [31] describes limitations in simulating the seismic behavior of masonry structures as follows: **'**Steel and reinforced concrete are ductile materials that have linear elastic properties and good post-elastic strength characteristics. After yielding, these materials maintain most of their strength while undergoing substantial plastic deformations and they can be analyzed with reasonable accuracy using analytic or computational methods. In contrast, after cracks are initiated, the behavior of brittle, unreinforced materials, such as stone, brick, or adobe, is extremely difficult to predict even with today's advanced computational capabilities. In a brittle material, once yielding occurs, cracks develop and there is a complete loss of tensile strength.**'** Such a strength failure at any point in the structural member reduces the monolithic behavior of the structure and breaks down the load path. William et al., [31] also suggested that **'**after cracks have developed, the seismic behavior of adobe building is dominated by the interactions among large cracked sections of the walls that rock out-of-plane and collide or rub against each other in-plane**'.** The primary cause of the most often observed damage is the low tensile strength of brick-mortar connections, as observed in Figure 2b. Both shear and flexural stresses develop because of the low tensile strength of the structure. Principally in-plane forces may cause tensile strength failure and diagonal cracking. Out-of-plane forces cause flexural stresses and cracking [32]. Further development of the in-plane cracks can result in a classic pier or arch failure as seen in Figures 2, 3 and 4 [34, 35]. The failure of the corner member results from a combination of flexural and tensile stresses. Once the corner vertical member has failed, the adjacent arches meeting at the damaged pier are more likely to fail as the cases observed in Fatih mosque (see Figures 2 and 4 [34]) demonstrate. In contrast to this mechanism, other strength reductions take place specifically in the joint region of the dome base and main arches. Domes are very susceptible to local base problems and foundation problems due to insufficient tensile strength in the component materials. Damage at the base level of the main dome is the most probable source of loosened joint. Loosening affects the integrity at the joint between the stone blocks within a short time if the bond failure is not strengthened. Otherwise, an outward opening is triggered and large tension cracks on the body produce irreversible changes in the behavior of arch system. Such gradual deterioration may be externally detected after peeling the top lead coverage because inaccessible areas may not be detected by visual examination (see Figures 5, 6 and 7 [33, 34, 35]). As a result, the collapse of the dome will not be surprising. Such dome failures were reported in the literature for major historical earthquakes [1, 30]. Signs and symptoms of weaknesses that are not practically detectable may require regular monitoring through image processing, machine vision, and pattern recognition. Further signs that may be seen on physical examination mostly affect the stability of the structure, since stone made masonry construction has a brittle behavior. Structural collapse might occur without warning due to (1) very low tensile

strength, (2) fragile behavior of the blocks and joints, and (3) very massive body, which generates large inertia forces during earthquake shaking.

3. FAILURE MODES OF THE STONE MASONRY ARCH-DOME SYSTEM

Some failure modes for masonry structures that might not be expected may be well captured by fundamental mode vibration properties (mainly involving local but critical damage to arches), whereas others involving distributed deformations and damage should be reflected in the fundamental mode response. Stone masonry arches can collapse as a result of three possible failure mechanisms, namely a shear mechanism, a hinge mechanism and a combined shear-hinge mechanism. Plastic shear deformations in the bare arch system produce cracks that can kinematically define potential sliding blocks. Progressive cracks and sliding masonry units of arch skeleton will form the collapse mechanism. Transverse cracks appear at locations where the tensile strength capacity is exceeded. The hinge mechanism forms when the compressive strength capacity is reached, causing plastic deformations that produce the hinge. In combined shear-hinge mechanism, failure is developed by sliding between components under large compressive forces exceed strength capacity. On the other hand, two hinges are sufficient for collapse for a single span two-hinged arch system, which has first order indeterminacy. Critical damage location causing the collapse mechanism in a single span arch is not at the center of the span but at a quarter of the span. Main arches that work as single span vertical members in the arch plane should supply the continuity of the force flow down to the foundation. If load transfer to the springing points of the main arches, to the main piers, and to the foundations, respectively, is not realized on a regular basis, functional continuity is broken down. Broken load transmission consequently causes severely nonsymmetrical load distributions, which have the potential for causing the arch system to collapse. On the other hand, broken load flow in the arches leading to damage also causes the tension rod connection failure (bond beam failure), as seen in Fig. 7 [34], which breaks down the balance of forces and causes the dome base to open outwards. Tension rod failure on top of the arches affects the global modes at first since tension bars at the dome base act together as a diaphragm providing horizontal bracing system to resist lateral loads and transfer the loads to the vertical members. Main vertical structural members that support the adjacent arches from spring points at the corners offer little resistance to horizontal movement. This low-level redundancy known as component level redundancy affects the low frequency modes; consequently, the fundamental frequency of the structural system is shifted downward as is the case discussed in the first publication [26]. Measurements of fundamental mode frequencies and their shift between members (or over time) may have a limited ability to detect damage of the types described above that can lead to arch collapse. It is well known that frequency shifts have considerable limitations depending on structure types. For the structure under the study, substantial damage would be required to create significant frequency shift [26].

Any loose or cracked bond between stone masonry blocks that becomes visible at the face would be expected to weaken the bearing capacity of the member and decreases the compression force capacity (see Fig. 2 [25]). Such reductions will also decrease the shear strength capacity of the arch. In the absence of such damage, domes are relatively stable structures with high resistance to lateral deformations due to inherent advantages of their geometry.

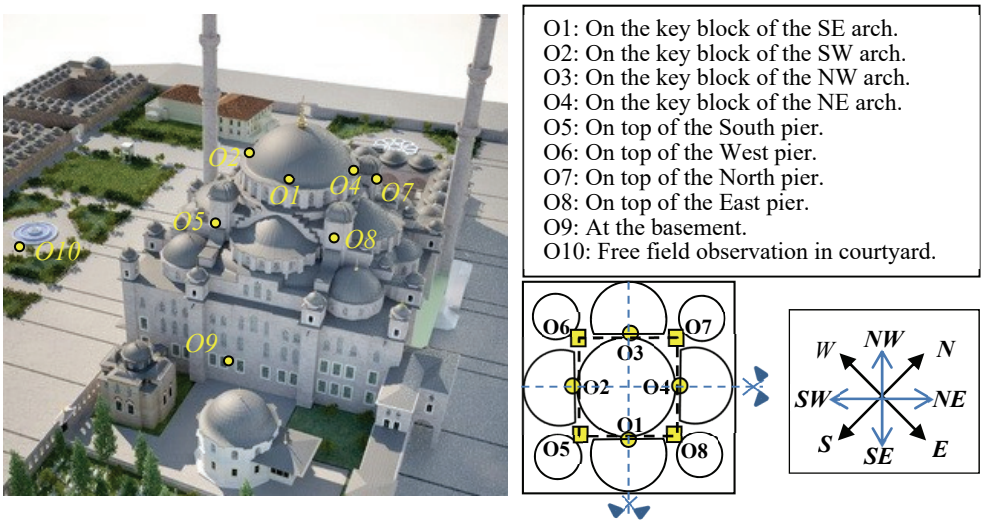

Fig. 1 - Seismometer locations from SE courtyard towards NW. Reflective symmetry in both directions in plan view is seen in the right.

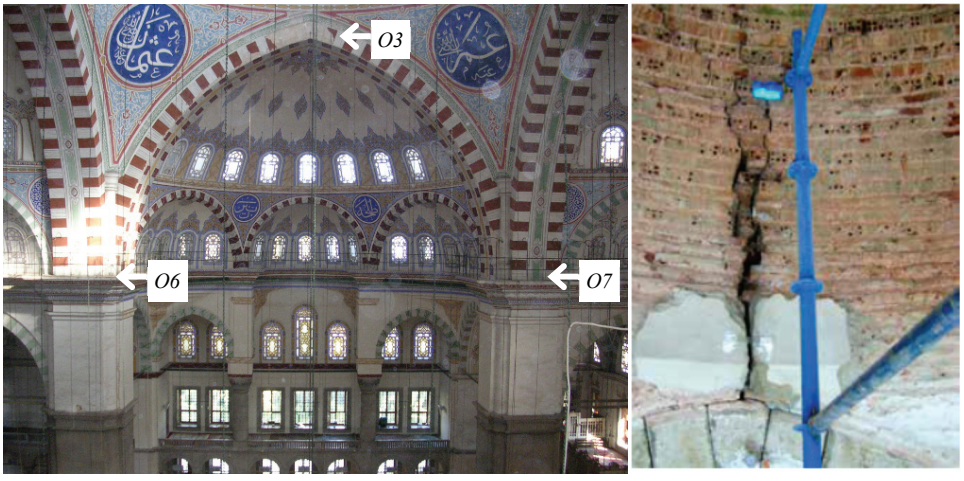

Fig. 2 - (a) From inside close look towards Northwest for station 3 at the crown of the main arch that received damage during Kocaeli earthquake of 1999; (b) Typical cracks in mortar and masonry units after scraping the top coat [25].

In case of the main arches with the interaction of dome, vaults and pillars, high lateral load resistance is possible in arch plane under static gravity and seismic loads (i.e., dynamic gravity). However, combinations of earthquake induced adverse vertical inertia forces and gravity may change the stress state from compression to tension. Such alteration may lead to stress drop, which causes damage and associated reductions in compressive capacity to

members that typically experience only compression. Resultant tension cracks around the station 8 with lack of tension capacity and typical local openings in the window border can be seen respectively in Figures 2 and 8 [35]. In addition to this deterioration, out of plane arch deformations will further degrade the strength capacity. Such strength reductions in the arch system and at the base of the central dome cause distributed deformations and damage.

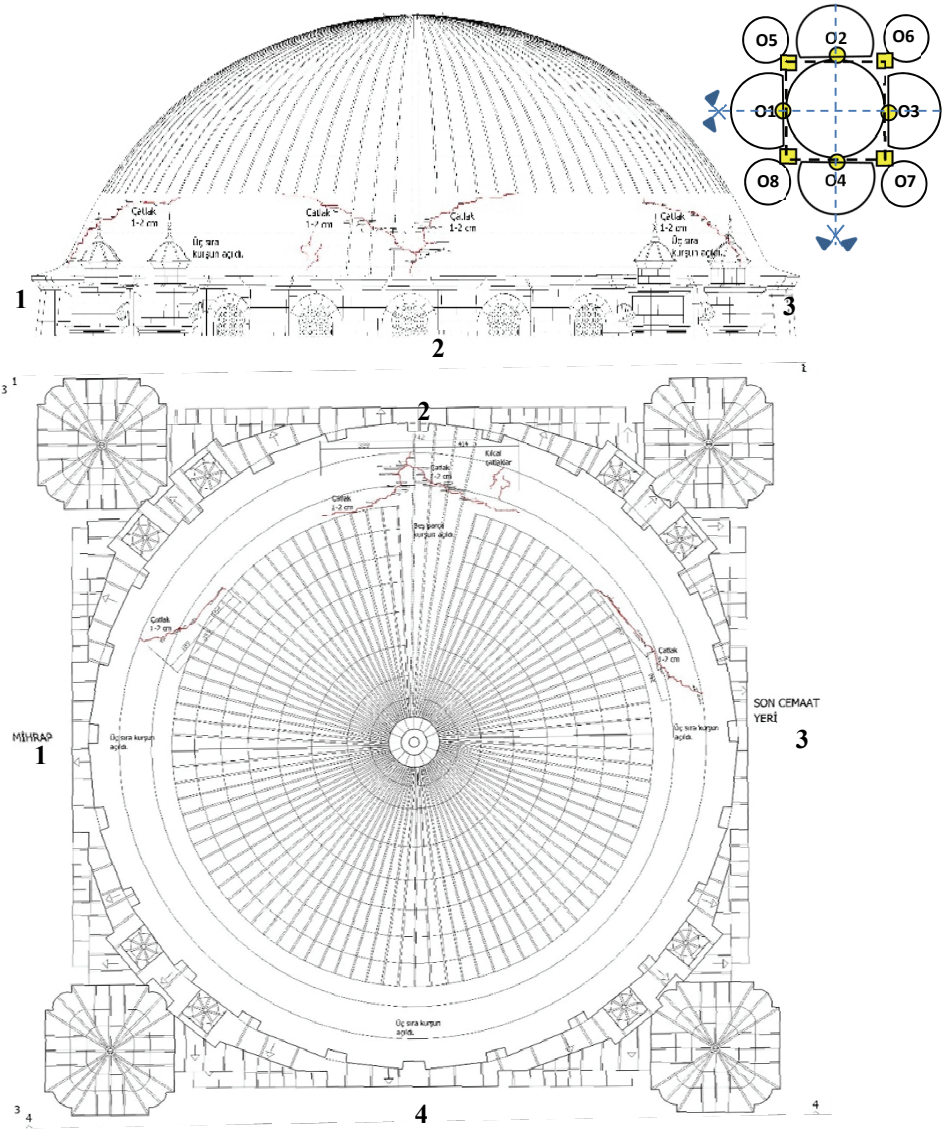

Fig. 3 - Damage patterns on the main dome in plan view (low). Damage around the stations 1, 2 and 3 from West view (top). The upper right corner (reoriented) sketch shows the instrument layout in plan view [33].

After removing the lead cover, tension cracks in the main dome was observed as seen in Fig. 3 [33] and large deformations on windows under the main dome base can be distinguished from Figure 4 [34, 35]. Corner dome failure next to the main pier station 7 [33, 34] also reflects the weakening of the horizontal strength between the members due to tension rod failure. The effects of such large-scale damage are observed at low frequencies [26]. In the case of the Hagia Sophia, a post-earthquake ambient vibration survey showed a drop from the pre-earthquake condition of the first two modal frequencies of approximately 4% – 5% [36].

Fig - 4a Damage around station 2 [34].

Fig. 4b - Side dome view around the station 4 from outside [34]

Fig. 5 - Cap view from the top of the main piers 6 and 7 [34, 35]

Fig. 6 - Top view from the damaged corner dome next to the main pier station 7 [33, 34]

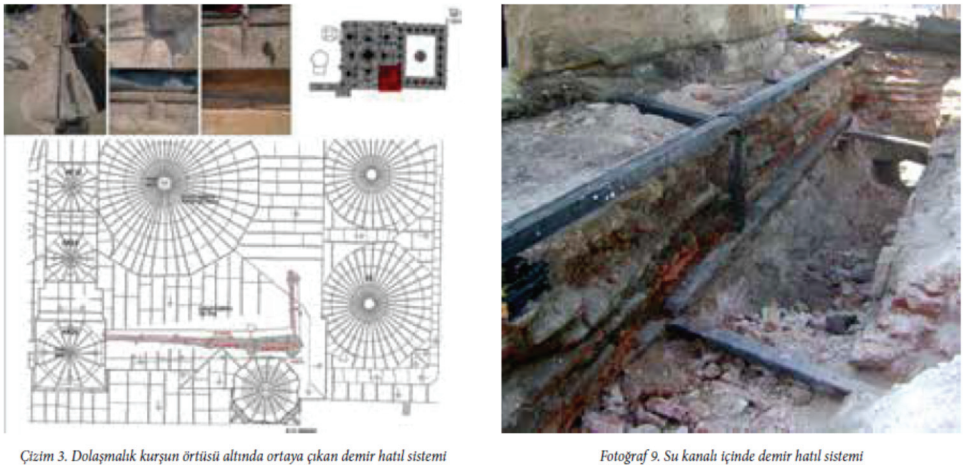

Fig. 7 - Top view from the damaged corner dome next to the main pier station 7 and corroded tension rods changed by new ties to prevent the progressive opening of the main dome [33].

Damage mechanisms of the Fatih Mosque from historical large scale events also verify the similar weak structural components as reported in the literature. It is worth mentioning that one compilation [30] describes damage from the 1509 earthquake that was localized at the supporting members of the dome (O_1, O_2, O_3, and O_4) and at the top of the four main piers (O_5, O_6, O_7, and O_8) as shown in Fig. 1. This same collection [30] also describes sequential collapse of the main dome and the main piers during the 1766 earthquake. Fatih Mosque that received damages on several parts by the 17 August 1999 Kocaeli earthquake was restored significantly between 2007 and 2012 [33].

Fig. 8 - Resultant tension cracks around the station 8. Windows were damaged due to tension rod failure causing the dome base to open outwards. Tension rod connection provides horizontal bracing as a diaphragm [34].

4. THEORETICAL FRAMEWORK

It is an observable fact that the dynamic system produces responses by modifying the input excitation and the response is not a linear function of the input excitation for most of the structural systems in civil engineering. Therefore, nonlinear behavior is a usual situation rather than the exceptional linear system behavior. Such dynamic systems cannot be identified appropriately by applying physical principles, since complete knowledge of the physical parameters of the structure may not be known; therefore, it is not possible to analytically determine the underlying differential equations. The complexity of the structure on the other hand may preclude an accurate analysis. Remarkably complex dynamic relationships also cannot be described fully in distributed nature in numerical simulations; consequently, simple representative systems like lumped mass are preferred for simulations.

This article will focus on single-input single-output (SISO) system, since it is the most prevalent and it is tested by several engineering disciplines. The SISO models can be combined also to create multi-input, multi-output (MIMO) and single input multi-output (SIMO) mathematical models for consistency check if necessary. Transfer function estimated from the candidate SISO predictive model may also identify the structural behavior of the test building based on representative lumped-mass model of uncoupled rigid diaphragm floor with single horizontal degree of freedom. The key feature of such simplification corresponds to the full diagonal stiffness matrix with zero off-diagonal terms. Interaction between the stories may also be considered for lumped mass rigid diaphragm floor structure based on SIMO predictive model. Transfer function in this case can be efficient and powerful estimation tool to understand better the performance of a well-balanced stable hyper-static structural behavior. Such story interaction corresponds to the full stiffness matrix with non-zero off-diagonal terms representing contributions/interactions among the stories. All these prediction models can be applicable only for linear and stationary dynamics in accordance with input-output conditions. In case of nonlinearity as well as non-stationarity, Time-frequency (T-F) algorithms are preferred.

In the study, cross validation is followed using results obtained from both spectral and parametric methods. Characteristic structural transfer functions in parametric approach are estimated from pairs of input-output observations based on two mathematical relationship models, as explained above namely, SISO and MIMO models. The models are linear dynamic systems handling parametric estimations for representative transfer functions that identify all detectable modes from the experimental data streams. The philosophy behind these models is that the global modal properties do not vary noticeably from one FRF to another FRF. Results of this first part that will be discussed in following sections manifest the limits of the linear approaches. On the other hand, advanced analysis techniques such as T-F methods receive considerable attention in case of progressive anomalies or in case of the insufficient physical examination for some parts, which cannot be accessible. Wavelet Transform (WT) and Hilbert Transform with Huang (HHT) (i.e., intrinsic mode functions (IMF)) among available T-F techniques were chosen based on their better performances for complex nonlinearity in nonstationary signals and they may perform more reliable estimations for nonlinear structural properties.

Structural damage detection methods are, in principle, based on the assumption that damage will change the structural properties, which further lead to changes in modal properties. Changes in the modal properties that have important effects on dynamic behavior are used to trace back the causes of large variations in dynamic parameters [37]. Based on practical experiences, another method entails the derivation of the structural stiffness matrix from the experimental modal data [38]. Other techniques for determination of the extent of damage may include Eigen structure assignment [39], probabilistic methodologies [40], matrix perturbation methods [41], and sub matrix approaches in model updating [42]. Recently, estimated Frequency Response Function (FRF) can also be used for feature extraction of a structure and for damage detection in careful systematic studies [43]. FRF estimations based on in-situ measurements are certainly free from extensive numerical errors (in fitting response function, for instance). Within the time domain methods, Complex Exponential (CE), Least-Squares Complex Exponential (LSCE) and the Eigen system Realization Algorithm (ERA) techniques comprise just a few of the most widely used approaches. Among these, ERA with Observer Kalman Identification method (OKID/ERA) [44, 45, 46]

based on the concepts of the control theory is a more general approach for handling the effect of noise and numerical errors in advanced modal parameter identification techniques.

4.1. Spectral Method in Damage Identification

In general, ambient vibration data recorded from historical masonry structures hold low amplitude structural vibration signal and large amplitude wide-band noise. Therefore, in case of damage identification Fourier based spectral methods are usually not suitable for noisy measurements. Time domain system identification technique using test data can be focused on as an alternative. Based on another study [26], it was shown that parametric model estimation fits quite well with the spectral estimation although different data sets recorded in different periods were used. From the discussion, it was evident that the frequency response of the structure and parametric model response provide valuable insight and represent well enough underlying dynamics of the structure if sampling and recording time are suitable [26]. In practice, signals may show nonstationary characteristic and therefore, their frequency content change over time. The advantages of using time-frequency techniques over frequency-domain or time-domain of a signal will be discussed in the following sections.

FRF (*H(w)*) describes the relationship between output response of a structural point (*Y(t)*) and input force history (*F(t)*) at the free field. Eq (1a) indicates that an FRF is defined as the ratio of the FT of an output response (*Y(w)*) divided by the FT of the input force history (*F(w)*) that caused the output. Applying FT to the cross (R_{FY}) and auto (R_{FF} and R_{YY}) correlations, spectral density functions (S_{FY}, S_{FF}, S_{YY}) can be obtain for alternative expressions for the FRF. To minimize the effects of noise on the output, alternatively $H_1(w)$ may be defined as seen in Eq(1b) and to minimize the effects of noise at the input, alternatively $H_2(w)$ of Eq(1c) may be defined.

$$H(w) = \frac{Y(w)}{F(w)} \tag{1a}$$

$$H_1(w) = \frac{S_{FY}(w)}{S_{FF}(w)} \tag{1b}$$

$$H_2(w) = \frac{S_{YY}(w)}{S_{YF}(w)} \tag{1c}$$

It is clearly seen that in the absence of measurement errors, they verify the identity as follow; $H(w)=H_1(w)=H_2(w)$. To verify the reliability and quality of the measurement, coherence function $\gamma^2(w)$ can be tested by the following expression [26];

$$\gamma^2(w) = \frac{|S_{FY}(w)|^2}{S_{FF}(w).S_{YY}(w)} \tag{2}$$

This indicates how the response is consistent with the excitation. If $\gamma^2(w) < 0.75 - 0.80$, quality of the experimental data might be qualified as unreliable in the sense that the signal/noise (*S/N*) ratio is low. Low values of coherence might be caused from both the presence of high noise or nonlinear behavior of the structure [26].

4.2. Time Domain (OKID/ERA) Method

OKID/ERA algorithm based on state-space model, coded in Matlab [47] is composed of the following three major computational steps: (1) The observer Markov parameters are calculated with OKID. (2) From the observer Markov parameters, OKID, this time, retrieves the system Markov parameters. (3) ERA is utilized with the system Markov parameters to realize the discrete time state-space (*SS*) system matrices, *A*, *B, C* and *D*. Markov parameters forming the basis for identifying mathematical models are the unit sample response or pulse response histories of the system. In the classical approach, Markov parameters might be extracted from inverse Fourier Transform (IFT) of the frequency response function (FRF), which is defined as the ratio of the Fourier Transforms (FT) of the measured output and input data. Due to aliasing and numerical ill-conditioned problems, calculating accurate Markov parameters in this way is impractical. FT algorithm requiring appropriately long time histories has another disadvantage in calculations. In contrast to the classical technique, OKID finds the Markov parameters more quickly and accurately than FFT-IFFT. Moreover, since OKID has an asymptotically stable observer, influence of the noise and other problems appearing in the estimation of the system Markov parameters from direct input-output data are bypassed. Further details of the theory with derivations are described in Juang [44, 45].

4.3. Time-Frequency Analysis

, Dynamic systems may have frequency properties that can change over time or have unusual interruptions or anomalies because of inelastic deformations at different times in their service life. Using the sinusoid type hyperbolic function as the basis, decomposing non-stationary behavior in finite length signal into sinusoids in usual Fourier Transformation (FT) may not capture and properly represent all components of the entire signal and frequency change in time. Fourier transform, *F(w)* of a time series *f(t)* and the inverse Fourier transform as seen in Eq. (3) can be obtained by combining the whole signal and this causes to get lost the local features changing with time and frequency. When *F(w)* is transformed back to time domain, the transformed signal that will repeat itself every time interval *t* shows no localization in time.

$$F(w) = \int_{-\infty}^{\infty} f(t) e^{-i\omega t}\, dt \qquad f(t) = \int_{-\infty}^{\infty} F(w) e^{i\omega t}\, dw \tag{3}$$

The difficulty with localizing frequencies in the spatial domain is one of major weaknesses of the FT in analyzing signals. FT decomposes the signal down to the sinusoids that theoretically extend from minus to plus infinity unlike the wavelet. In contrast, frequency of an irregular and almost non-symmetrical wavelet varies over the length of the waveform and it is better at describing non-stationary problems. By stretching (dilating) and shifting (translating) the waveforms, wavelets that come in various shapes and sizes are used to detect the hidden event and approximate its frequency and location in time. A particular mother wavelet shape that may match or correlates the event unusually well when stretched and shifted suitably may exactly regenerate the whole signal. Even if a wavelet is transformed from time domain into frequency domain, still the relative phase relations of different contributing frequencies determine the position in time.

Focusing on the localization in time and frequency is at least not the only property that is characteristic about the wavelet transform. Much earlier, short-time Fourier transform (STFT) that is also localized in time and frequency is introduced to overcome the limitations of the FT by Gabor [44] and it provides information about where in time a certain frequency occurs, since it is essentially collection of the FTs applied consecutively onto the windowed (i.e., small) portions of the signal. The signal in the sliding window is assumed approximately stationary. Using the inner product notation, the STFT can be expressed as

$$STFT(\tau, f) = \int x(t) g(t-\tau) e^{-i\omega t} dt \tag{4}$$

STFT employs a sliding window function *g(t)* centered at time τ of the window. FT is performed on the signal *x(t)* within the window. Through such consecutive operations, FT of the entire signal decomposes into a two dimensional T-F representation. Recorded field data is generally not known a priori, selection of a suitable window size for effective signal decomposition or for processing nonstationary events in the STFT is difficult. For instance, in contrast to the STFT technique where the window size is fixed and is not suitable for nonstationary data, the wavelet transform enables flexible window sizes in analyzing different frequency components within a signal. By comparing the level of similarities between the signal and a set of patterns obtained from dilating and contracting the original period (i.e., scaling represented by *s*) and translating along the time axis (i.e., shifting, τ) of a base wavelet $\psi(t)$, T-F characteristic may be mapped remarkably. Using inner product, the wavelet transform (WT) of a signal *x(t)* can be expressed as;

$$wt(s, \tau) = \frac{1}{\sqrt{s}} \int_{-\infty}^{\infty} x(t) \psi^* \left(\frac{t-\tau}{s} \right) dt \tag{5}$$

where the scaling parameter, *s* greater than zero, which determines the time and frequency resolutions of the scaled base wavelet $\psi\langle(t-\tau)/s\rangle$. The specific values of *s* are inversely proportional to the frequency. The symbol $\psi^*(\cdot)$ denotes the complex conjugate. WT is capable of extracting the inherent components within time series over its entire spectrum, by using small scales (corresponding to higher frequencies) and large scales (corresponding to lower frequencies) for decomposing frequencies.

The Hilbert-Huang transform (HHT), developed by Huang et al. [48] as an empirical approach, may also solve the nonstationary structure. The HHT consists of self-adaptive empirical mode decomposition (EMD) and Hilbert spectral analysis (HSA). Steps are summarized below and details may found in Huang et al. [48]. The EMD was designed based on the assumption that the data set consists of simple different intrinsic mode functions (IMF) of oscillations with harmonic or nonsinusoidal coexisting characteristics derived recursively from the data. First mean m_1 is calculated and subtracted from the whole data, *X* and difference h_1 called IMF candidate as a first component since it satisfies all the conditions of an IMF as detailed in Huang et al. [48].

$$h_1(t) = X(t) - m_1(t) \tag{6}$$

However remaining data $h_1(t)$ that is treated as the recent data and previous process, called the sifting, is repeated;

$$h_{11}(t) = h_1(t) - m_{11}(t) \tag{7}$$

In this case, m_{11} becomes mean of the upper and lower envelopes of h_1. Consequently, other rounds of sifting process are carried out k times until the residue becomes constant (monotonic) or represents an negligible trend (baseline passing from zero at most two times).

$$h_{1k}(t) = h_{1(k-1)}(t) - m_{1k}(t) \tag{8}$$

$$c_1(t) = h_{1k}(t)$$

Then the recent $h_{1k}(t)$ is nominated as the first IMF component c_1, which contains highest frequency content of the signal $X(t)$. c_1 is removed from the data $X(t)$ to obtain the residue r_1, which contains lower frequency components. The r_1 is treated as the new data and subjected to the same sifting process. This procedure is repeated to obtain all the subsequent r_i functions;

$$r_1(t) = X(t) - c_1(t) \tag{9}$$

$$r_i(t) = r_{i-1}(t) - c_i(t), \qquad i = 2,3,4, \dots \dots, n$$

After completing the decomposition, the original signal can be collected by summing n IMF components plus the final residue.

$$X(t) = \sum_{i=1}^{n} c_i(t) + r_n(t) \tag{10}$$

In HSA, signal $c_i(t)$ and its *HT*, $H[c_i(t)]$ can be combined to form the analytical signal $Z_i(t)$ in a complex structure,

$$Z_i(t) = c_i(t) + j\, H[c_i(t)] = a_i(t)\, e^{j\theta_i(t)} \tag{11}$$

and HT is defined as

$$H[c_i(t)] = \frac{P}{\pi} \int \frac{c_i(u)}{t-u} du \tag{12}$$

where P denotes the Cauchy principle value. With this newly defined analytical signal, time-dependent $a(t)$ and phase $\theta(t)$ become observable over the time and the instantaneous frequency can be defined as,

$$a_i(t) = \sqrt{{c_i}^2(t) + H[c_i(t)]^2} \tag{13a}$$

$$\theta_i(t) = arctan \frac{H[c_i(t)]}{c_i(t)} \tag{13b}$$

$$w(t) = \frac{d\theta(t)}{dt} \tag{13c}$$

Applying the HT to the *n* IMF components of X(t) but excluding residue r_n, X(t) can be written in terms of amplitude and instantaneous frequency corresponding to each component *i* as functions of time.

$$X(t) = \Re \sum_{i=1}^{n} a_i(t) e^{j \int w_i(t) dt} \quad (14)$$

Eq. (14) differs from the time-independent amplitude and phase in the FT. It improves the flexibility of the expansion and tracks the nonstationary characteristic. The T-F distribution of the amplitude called as the Hilbert spectrum *H(w,t)* defined as

$$H(w,t) = \sum_{i=1}^{n} \widetilde{H}_i(w,t) = \sum_{i=1}^{n} a_i(t) \quad (15)$$

Where $\widetilde{H}_i(w,t)$ stands for *i*th component of the total Hilbert spectrum *H*. The square of *H* also gives the energy distribution (i.e., energy density). Another very important definition is the marginal spectrum *h(w)* provides a measure of total amplitude contribution from each frequency, in which *T* denotes the time length of the signal.

$$h(w) = \sum_{i=1}^{n} \tilde{h}_i(w) = \sum_{i=1}^{n} \int_0^T a_i(t) dt \quad (16)$$

5. DESCRIPTION OF THE INSTRUMENTATION AND DATA PROCESSING

Sensor locations was decided by first performing analytical modal analysis and then it was finalized based on modal participation factors of the candidate observation points in the mode shapes according to preliminary observations (i.e., test data). Structurally important eight observation points were instrumented by two-component seismometers for principal horizontal directions to track the global behavior of the superstructure and one was used at the basement to capture the true structural input characteristics, as seen in Fig. 1, and described in Table 1. Another one records the free field motion as micro-tremors at the far site in the courtyard. Deciding seismometer as a sensor type was motivated by the experiences from past experimental studies, it is certain that the velocity peaks of low frequency input motion (i.e., accelerating momentums in free vibration) have high impact on structures. Structural response is also directly related to the input energy, which is proportional to the velocity. Naturally, low frequency signals give dominant low frequency content but non-stationarity may be introduced. The equipment used for the measurement and the data acquisition are as follows; Analog to digital converter, DT-2827 A/D board with 16 bit A/D converter at the speed of 100 KHz accommodating both single-ended and differential analog inputs, manufactured by Data Translation Inc., Multiplexer card, DI-64x4-V2 manufactured by Quesing Electronics, accepting up to 64 channels at 1000Hz sampled data and signal conditioner, SC-1 manufactured by Kinemetrics. From Mark products, L22 type low frequency seismometers, with peak-to-peak 0.15-inch amplitude precision, were utilized for the tests. Allowable accuracy of the synchronic acquisition was examined in detail on the site and adjusted at a sampling rate of 122Hz through the A/D converter. Four sets of ambient vibration measurement were recorded for 5 minutes from structure and the courtyard for test and verification purposes. The calibration measurement was performed at the basement right after collecting structural data by collocating instruments next to each other

parallel to the structural axes. Control test data were utilized for qualifying linearity and distortion in recordings based on wavelet analysis. Finally, band pass filtering was decided between frequencies of 0.1Hz and 50Hz (as the Nyquist frequency band) to eliminate the effects of white noise, hardware problems and effects of the different cable lengths. Base-line correction (linear and nonlinear if necessary) and re-decimation for eliminating high frequency spikes in the record were also performed when they were needed. Ambient displacement time histories of the structural points are plotted on the same scale for the same time window for SE-NW direction, as a typical example shown in Fig. 9.

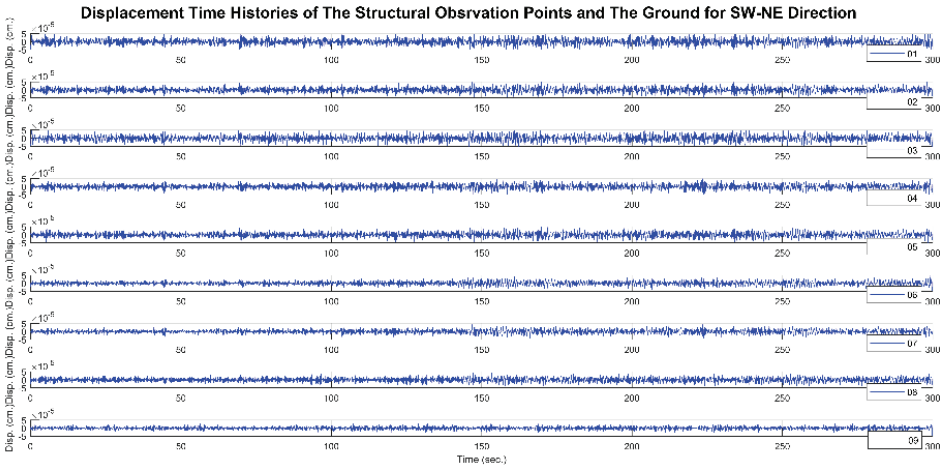

Fig. 9 - Displacement time histories for the structural observation points O1 through O8 and ground station O9 for SE-NW direction.

6. ANALYSIS OF THE RECORDINGS

In this section, first tradational approaches from frequency domain and time domain are performed to illustrate that linear-and-stationary data analysis provides incomplete or biased information for damage detection. Then, wavelet and HHT analysis from T-F techniques are adopted to demonstrate logic and direct information in damage identification. Matlab implementations of the all algorithms used in this study have been developed since 1990s using Matlab macro scripts [47].

6.1. Nonparametric (Spectral) Analysis

Instrumentally corrected records were Fourier transformed and to reduce the undesired noise components the power spectra for SE-NW direction is plotted in Fig. 10. Stations 1 and 3 (O_1, O_3) yield larger spectral amplitudes in both low and high frequency regions but in global region such extraordinary amplitudes are not observed. Some other sharp peaks are seen at 24Hz for O_3 and around 38Hz for O_1.

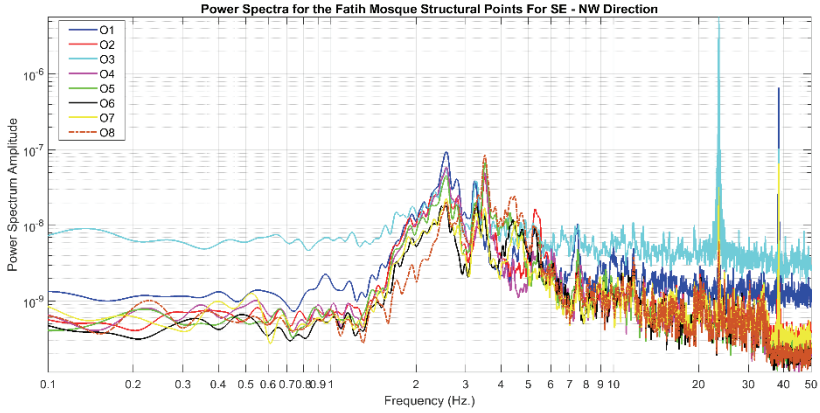

Fig. 10 - SE-NW component power spectra for the structural observation points.

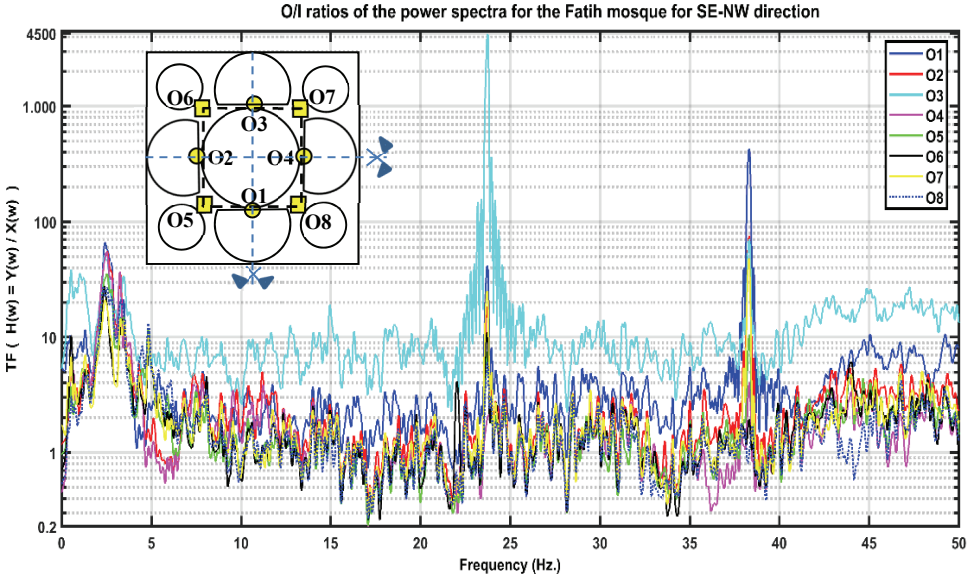

Fig. 11 - Spectral transfer functions for SE-NW direction between structural responses and base input motion (defined by the expression in Eq. (1)).

In Fig. 11, spectral transfer functions for SE-NW direction between structural responses and reference base input motion have been calculated as defined by the expression in Eq. (1). Spectral peaks at the cornice-level stations at the four springing points of the main arches (O_5, O_6, O_7, O_8) and those at the crowns of the main arches at the dome-base (O_1, O_2, O_3, O_4) are seen almost at the global frequencies. Stations O_3 and O_1 that envelope the others in the all frequency range have two broadband peaks with high amplitude values of 30 and 10 at around 1.2Hz and 1.8Hz, respectively, while other stations oscillate at around 1 in low

frequency region. In the high frequency region, around 24Hz O_3 and around 38Hz O_1 has sharp peak. Such peaks that may be sign of coherence with ground input motion can also indicate local failure. This is not the case for other stations. In Fig. 12, magnitude squared coherences ($\gamma^2(w)$) between the structural responses and the input motion are calculated for SE-NW direction. Average value little exceeds the critical value of 0.75 and rises to 0.8 that indicates that the *S/N* ratio is acceptable for linear analysis but it might be also noteworthy sign for the nonstationarity and nonlinearity. In another study [26], de-noising procedure was applied to test data sets to reconstruct the original signal based on the orthogonal wavelet packet decomposition procedure. Close estimation was observed and it is concluded that the reconstructed signal with retained energy of 82% appears reasonable and consistent for the purpose of a linear analysis [26].

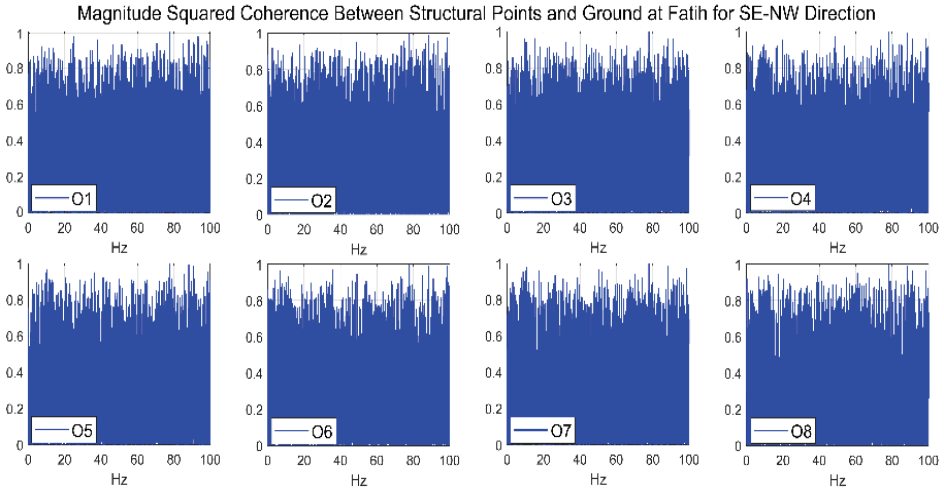

Fig. 12 - Magnitude squared coherences between the structural responses and the input motion (defined by the expression in Eq. (2)) for SE-NW direction.

As a last application, short time Fourier transform (STFT) was performed to compute a time-varying spectrum by applying FT to a windowed section of the data. STFT provides time-localized changes in frequency with limited precision and somehow reduces the non-stationarity but the *window size* influences the temporal or *frequency resolution* of the analysis. Selection of the window length is subjective and needs many trials dependent on features of interest. STFT spectra are estimated in Fig. 13, applying Kaiser window for smoothing. In smoothing, the energy in the main lobe of the window is maximized relative to total energy. As seen in T-F plot, nonstationary characteristic can be observed on all observation points. However, at stations O_1 and O_3, two sharp spikes at 24Hz and 38Hz are developed exceptionally and they almost keep the linearity throughout. Key block failure at O_3 and partial damage at O_1 may cause high frequency peaks indicating local damages. Due to poor redundancy, damage may destabilize the adjacent members in the SE- NW direction. This is seen globally on some neighbor members such as at O_2 and O_7 strongly and at O_6 slightly. Results of the conventional approaches are summarized for this section, as follows:

although there are small individual differences in the amplitudes of the transfer functions, for SE-NW direction, global spectral peaks are observed at ~2.5, 3.5, 4.3, and 5.3Hz as seen from Fig. 11. It is obvious that station O_3 with superior amplitudes and station

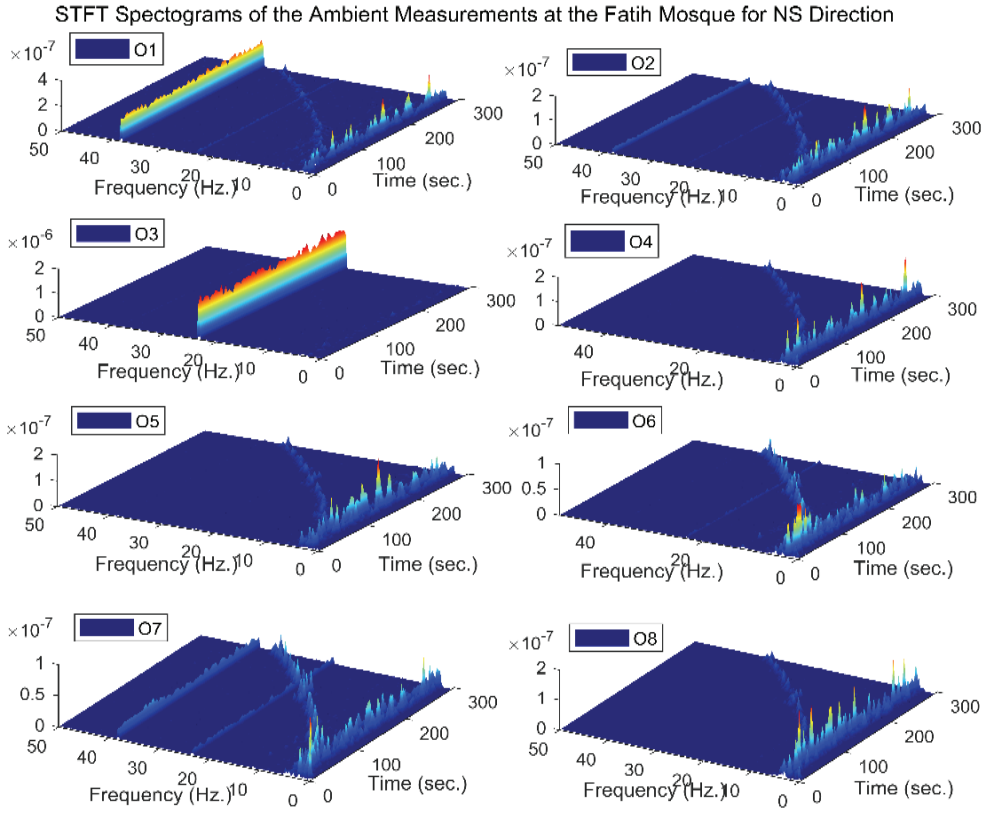

Fig. 13 - STFT of the records at the eight observation stations for SE-NW direction.

O_1 with relatively large amplitudes behave differently in both low and high frequency regions when compared within the group of other similar observation points. Such inconsistencies can be considered as signs of damage and may be explained only by the damage that occurred during the August 17, 1999 Kocaeli earthquake. For instance, close inspection at the crown station O_3 verified the damage by large cracks around the key point of the arch and above as seen in Fig. 2. In general, the response spectrum or Fourier based transfer functions provide average information such as influence of the input motion on structure with different frequencies, which the structure have different sensitiities. From such spectrait is impossible to determine which factors or features of the motion contribute most to damage. Therefore, transfer functions or response spectra based measures are essentially just an alternative representation of Fourier spectra.

6.2. Parametric Analysis

OKID-ERA technique [44, 45] was adopted for single input-multi output pairs (SIMO) and multiple excitations and responses (MIMO) in this experimental modal identification study. As seen from transfer functions for SE-NW direction in Fig. 14, different levels of distinguishable peaks are derived from SIMO and MIMO models. SIMO model captures the important peak frequencies with sufficient accuracy, but magnitudes are arguably small. Responses at the stations O_1, O_2, and O_4, located at the crowns of the main arches, display almost the same peak magnitudes at the same frequency of 2.5Hz for the SE-NW direction; station O_3 (which possesses several peak amplitudes at smaller frequencies, 0.4Hz, 1.2Hz, 1.8Hz and 2Hz) is exceptional and indicative of an anomaly. Dominant frequencies of the structure estimated by SIMO and MIMO systems are close to each other although peaks of the MIMO with closely spaced modes spread over broader bands. In the MIMO model, similar to the SIMO model, O_3 yields an early peak at 1.2Hz before the first global modal frequency. Same peak frequencies with different TF amplitudes for the SE-NW direction are also concluded from spectral analyses as seen in Fig. 11. Furthermore, station 3 among the crown stations exceptionally yields several early peaks as observed in parametric TFs of Fig. 14. These techniques may not always produce similar results because MIMO is more suitable for large complicated structures. However, this bisymmetrical structure yields very close results when comparing the extracted modal parameters from these techniques. All analyses up to now, namely, spectral, parametric SIMO and MIMO models yield almost consistent results for station O_3 alarming serious structural damage in SE-NW direction. Similarly, station O_1 also has damage susceptibility in SE-NW direction. Only minor peak shifts to lower frequencies show poor damage detection results. It is shown that non-parametric estimation qualified quite well with the results of the parametric model. From the discussion, it is evident that both estimation techniques provide valuable insight and represent the underlying dynamics of the structure. Using several validation data sets, identified model was tested in this part to investigate the inherent differences and similarities in dynamic response of the identical members of the structure. However, most frequency and time domain filters are linear, if the waveforms in the data were distorted by nonlinear progression; the band pass type operations could only pick up the fundamental characteristic and exclude all the necessary different waveforms, which can be important components to reconstruct the full waveforms. This drawback may cause poor results and incorrect interpretations for the damage detection.

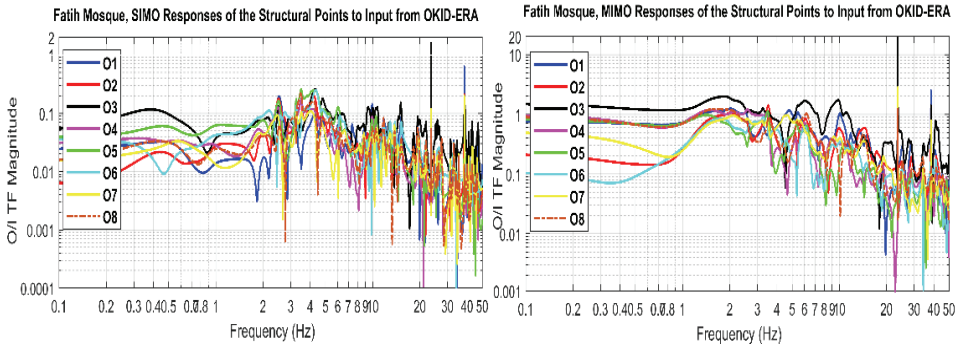

Fig. 14 - Transfer functions of the structural observation points estimated from SIMO (left) and MIMO (right) systems for SE-NW component.

6.3. Time-Frequency (T-F) Analysis

For the ambient data that was only low-pass filtered at Nyquist frequency, T-F spectra are estimated using wavelet theory for each direction. There is no unique wavelet-base form, which can satisfy the requirements in such an analysis. A number of different wavelet families are tested to extract the recognizable features for damage detection. It was found that the so-called bump and Mexican hat wavelet bases [47] are the most successful at identifying the damage at a similar level of performance; finally, the bump wavelet is decided for this study. It is decided that local jump in the wavelet coefficients points out the location of the damage. Cross-examination of the T-F spectra among the stations can reveal localized similarities otherwise local increases in the absolute value of the wavelet coefficients may show nonstationary power in T-F plane. When the zone has become full of high wavelet coefficients, nonlinear behavior becomes practical due to the interferences of the broken sides at the damage point and interactions between the adjacent components. Crown station O_3 in Fig. 15 shows linearity throughout the recording with complete high power at around 24Hz in broadband characteristic. Severe damage at O_3 causes such linearity and loosens the bonds between the stones around the key block. Other stations that generate almost similar energy distributions in T-F domain exhibit nonlinearity-non-stationarity and this tendency increases as the time and frequency progress. T-F spectra with energies as scaled in the color bar manifests that the energy flows from low to high frequencies. Transverse cracks and openings developed around the key block form the third hinge disrupting *monolithic behavior and* responding individually at its local frequency of 24Hz throughout the recording. Another crown station O_1 also shows close non-monolithic behavior at the local frequency of 38Hz (stiffer therefore slight damage). Other structural members of this low redundant system display nonstationary-nonlinear behavior under the effect of the accumulated damages. For example, station 2 is affected strongly by the anomalies of both forms, namely, stationary-linear and non-stationary-nonlinear appearances as seen at stations 1 and 3, due to opening dome base (see Figures 3). Especially neighbor stations O_6 and O_7 located at the springing points of the arch (O_3) and other neighbor stations O_5 and O_6 located at the springing points of the arch (O_2) are strongly affected due to tension rod connection (providing horizontal bracing as a diaphragm) failure causing the dome base to open outwards (see Figure 5,6 and 7). Records of the stations 4 and 8 reflect only low-level nonstationary features manifesting little effects from neighbors in touch. Another characteristic of the T-F spectra is that the wavelet coefficient peaks increasing continuously by the time and reaching their maxima at the end of the recording correlate with each other as well. Many types of signals in practice may be non-sparse in the Fourier-based analysis became detectable in T-F domain as seen in Fig. 15 and 16. It is well known that coherence on a scale from 0 to 1 is a current practice for evaluating the linear correlation between two stationary processes in frequency domain to detect any pattern in the signals in relation with each other. Similarly, wavelet-based coherence provides time-varying correlation as a function of frequency. By using the wavelet coherence (WTC), ambient measurement data set is examined for the structure-basement (ground) system to extract regions in T-F space where the two time histories co-vary (but does not necessarily have high power). The WTC results based on the structural vibration and ground data have maxima around 1 (i.e., nearly perfect agreement) approximately after 50Hz. Additional maxima, characterized by several broadband peaks, close to 1 are distributed pretty equally between the band of 20Hz-40Hz for the station 3, $\boldsymbol{O_3}$.

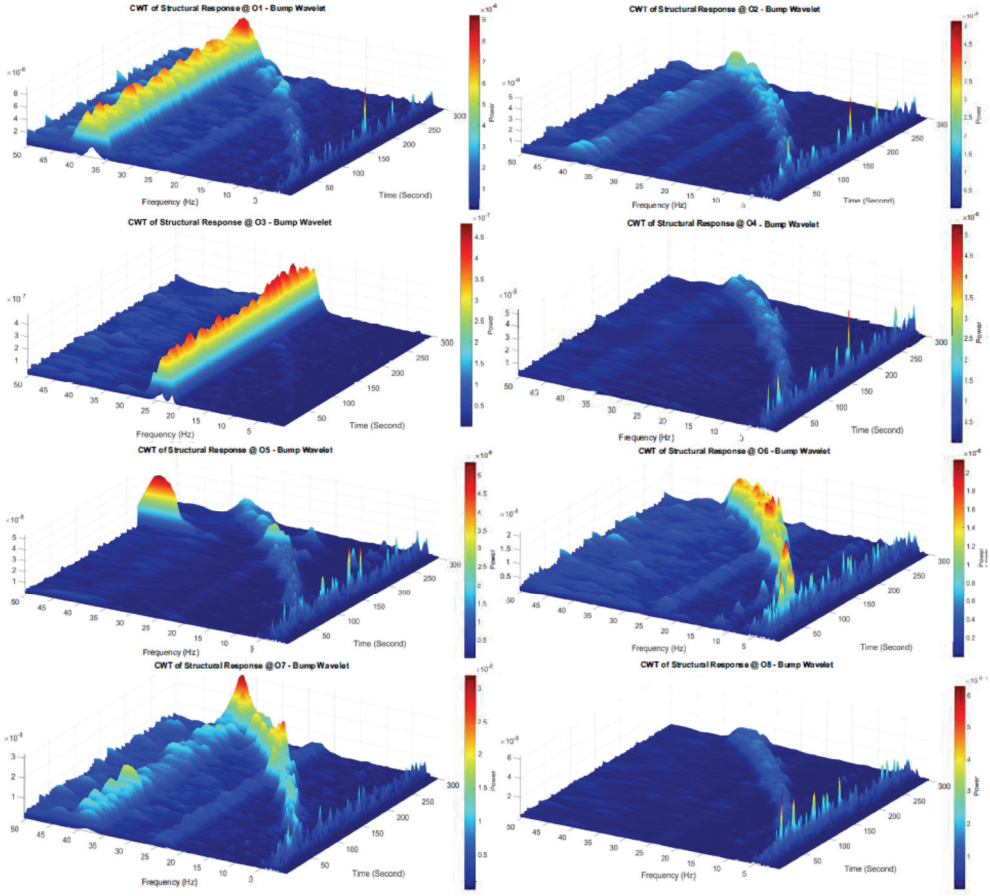

Fig. 15 - Continuous Wavelet Time-Frequency spectra of the structural observation points of the structure estimated for SE-NW component.

The dominant maxima corridor that can be easily recognized, corresponding to the linearity as indicated by the WT spectra in Fig. 15, keeps the highest coherence monotonically for all the recording time while almost the other stations in the considered part show many brief increases in coherence accompanying by significantly high values of 0.7.

On the other hand, cross wavelet transform (XWT) finds regions in T-F space where the time series show high common power. It is intensely seen from Fig. 17 that the cross correlation of the wavelet coefficients for SE-NW direction have high common power practically in a linear fashion between the free field microtremor (as a reference data for linearity) and stations $\boldsymbol{O_1}$ and $\boldsymbol{O_3}$. Comparison of cross correlation and coherence results differed intensely and cross correlation recognizes the relationship to a significant statistical degree whereas the coherence method showed weakness in recognizing the linear association.

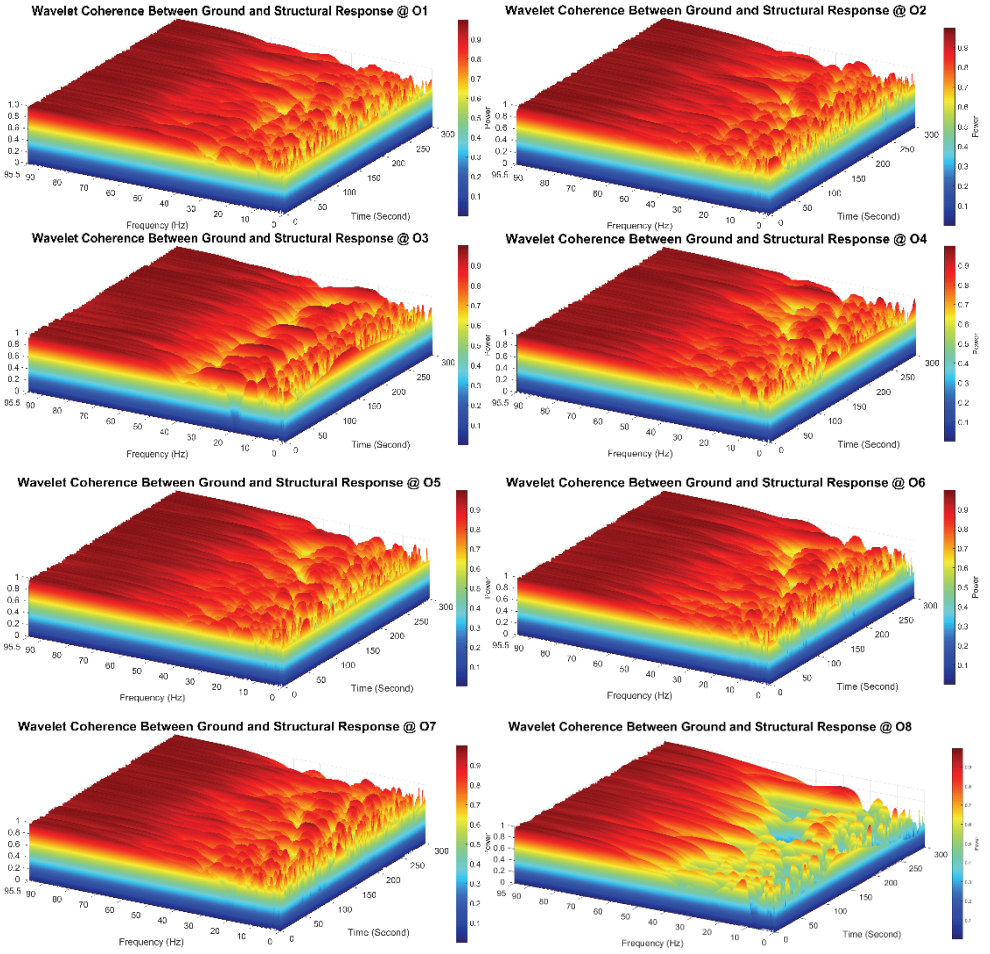

Fig. 16 - Wavelet coherence in Time-Frequency space for the structural responses and basement input motion for SE-NW component.

A survey of Hilbert Huang analysis as well as their suitability in T-F mapping will be presented in this last part. A comparative study carried out to show the performance and accuracy of the two recent methods of T-F analysis for damage assessment. Conventional data preprocessing techniques might hide valuable information or distort the recordings. In contrast, a new method, which prevents the degradation, namely EMD is adopted here. The EMD technique leads to physically meaningful decompositions. As we shall see from Fig. 18, EMD can extract valuable characteristics of the vibrations with just a few IMF components. IMF with higher frequency content could be identified as being generated by a local instability. After member capacity exceedance or dislocations of the stones around the key block of the arch, localized plastic hinge is developed that reduces the level of redundancy and weakens the structural rigidity. As a result of this, flexibility of the

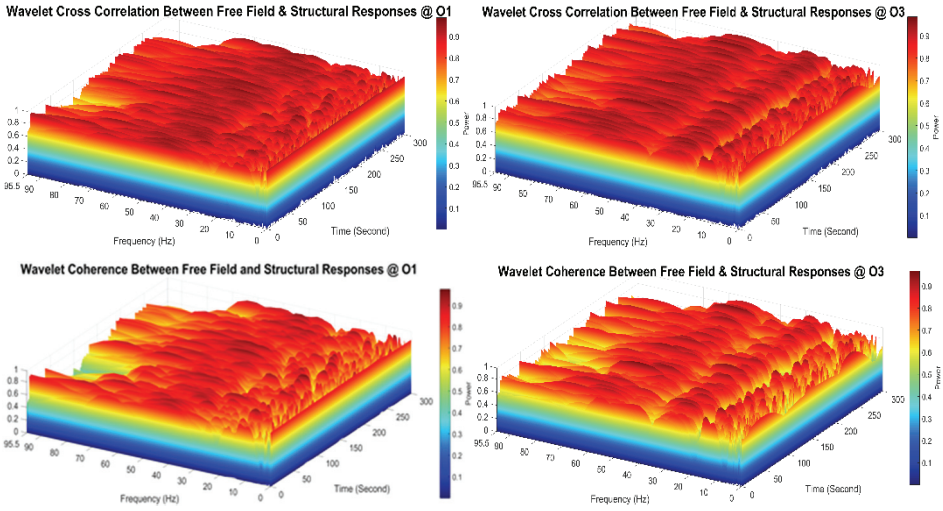

Fig. 17 - Top row, cross correlation of the WT coefficients; second row coherences of the WT coefficients for the free field microtremor and the stations 1 and 3 for SE-NW component.

structural system will be increased in a reverse manner and this lowers the vibration frequency. As seen in Fig. 18, IMFs start with the highest vibrations and slow down to the small frequency oscillations. Vibrations developed around the average dominant frequency starting from 38Hz, down to 24Hz, 19Hz, 12Hz, 4Hz, 2.5Hz, 1.5Hz and 1Hz for the first 8 IMFs respectively. Instant T-F spectra of the HHTs for the entire ambient vibrations recorded at the 8 stations are plotted with the peak points in Fig. 19. The color scales next to the T-F plots illustrate the level of spectral power. Contribution of each frequency component in the instantaneous frequency vectors of the IMFs is clearly seen for top four for arch stations (O_1, O_2, O_3, O_4), lower four for column stations (O_5, O_6, O_7, O_8). all the time stations. As distinguished from Fig. 19, some frequencies are never reached in some IMFs. Therefore, zero contribution to the system dynamics from some frequencies can be noticeable. Comparison of individual CWT spectra of the identical stations from Fig. 15 and 16, and likewise comparison of the corresponding HHS of the IMFs extracted from lightly damaged station O_1 in Fig. 20 clearly show that the presence of nonlinearity adds considerable complexity to the frequency response characteristics of the system. Measures of this complexity relative to the undamaged or lightly damaged structural response can be visible signs of failure at its onset as proposed in an earlier study of Beyen [26]. Furthermore, for nonstationary and nonlinear nature of a low redundant structure with serious damage, Fourier based response spectrum cannot represent accurate low frequency energy particularly when the signal is highly nonstationary because superposition of the linear Fourier decomposition with endless energy generates artificial high frequency harmonics. Therefore, energy spectra obtained from both techniques reveal such differences. However, when the FT is applied on to the IMFs, which were decomposed based on Huang [48], nonstationary-nonlinear characteristics, if they exist, become very distinguishable from FAS plots. As a typical example, such information for the station 8 (O_8) can be easily inferred from Fig. 21 when

compared first four FAS of the IMFs. Nonstationary-nonlinear characteristics strongly manifest the existences in the first and second IMFs. Non-stationarity in the IMF-1 starts after 150sec. and increases continuously through the recording in high frequency region between 20Hz and 40Hz. Same behavior is also seen in the IMF-2 but amplitudes decrease as the time increases. IMF-3 and IMF-4 show somehow linear time frequency variations. Based on this coherence, in order to compensate the lack of non-stationarity in Fourier transformation, it is recommended to decompose the signal based on Huang [48] before applying Fourier Transform for particularly nonstationary dynamics.

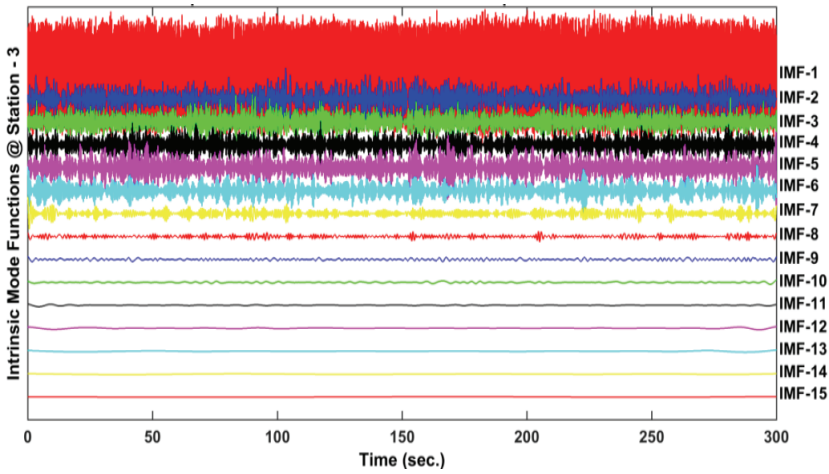

Fig. 18 - IMFs of the station - 3 (O_3) responses for SE-NW component based on EMD with adaptive noise.

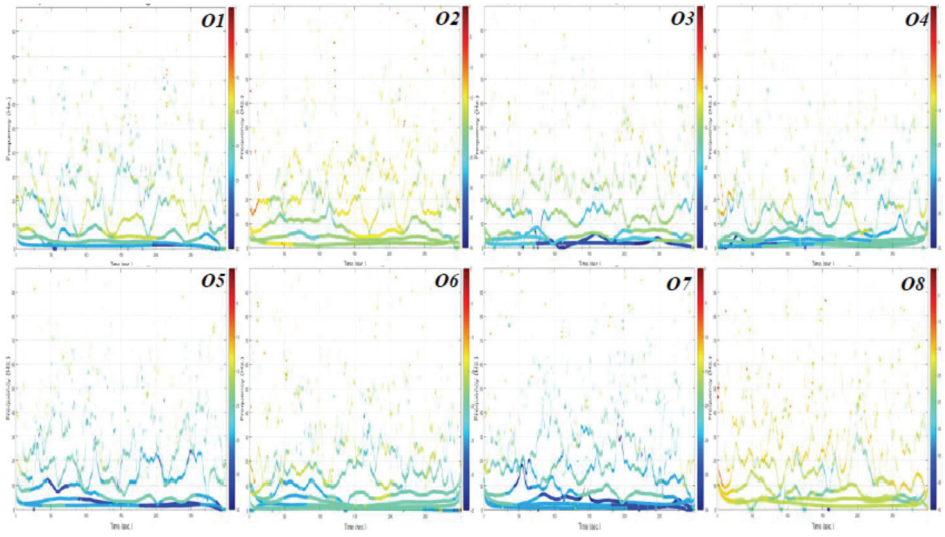

Fig. 19 - HS peak points of all the IMFs decomposed from 8 stations for SE-NW component.

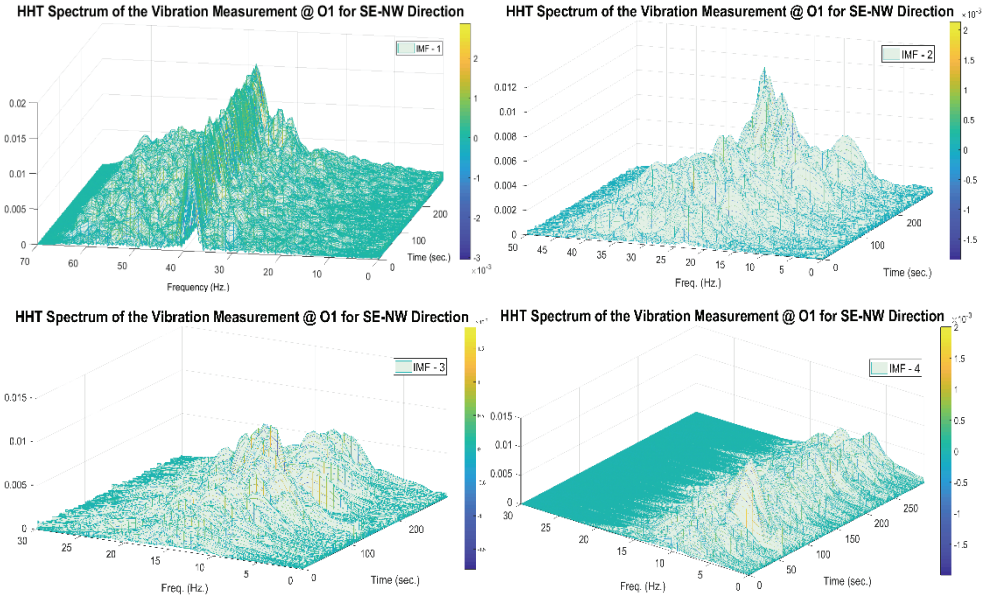

Fig. 20 - Hilbert Spectra of the first four IMFs decomposed from recording at the station O_1.

Contribution of each frequency component in the instantaneous frequency vectors of the IMFs is summed for all the time locations. Depending on frequency resolution (i.e., unit frequency increment), values of the instantaneous frequencies are counted as the same frequency, if the frequencies are nearly close in one frequency step and amplitudes related to each frequency are summed as if they belong to the same frequency value. Adopting such approach, marginal Hilbert spectrum (MHS) is estimated for each IMF at the all observation stations. Summation will also produce smoothed MHS as seen in Fig. 22. Another important point in the instantaneous approach naturally coming from either decomposition technique or system dynamics is that some values are never reached in the instantaneous frequency vectors of the IMFs. Therefore, some frequency stations do not appear in the spectrum as having zero contribution in the global behavior. As a typical example, MHS of the arch stations O_1, O_2, O_3 and O_4 are given in Fig. 22. Contribution of each IMF and the analytical function for SE-NW direction can be easily distinguished when compared the amplitudes of the MHSs. From MHS of O_3, decomposed signal IMF-1 has the highest oscillatory characteristic with a broadband frequencies (i.e., over the frequency region between 10Hz and 40Hz) but centered at about 19Hz-21Hz while IMF-2 has the peak at 24Hz as the highest frequency signal with an amplitude, which is three times greater than IMF-1's. IMF-1 can be identified as the global characteristic and IMF-2 with extraordinary sharp peak and narrow band frequency characteristic may be produced by the local failure at the station-3 (O_3). MHS of the analytical function also shows same peak at 24Hz. Other small frequency peaks certainly belong to the global behaviors.

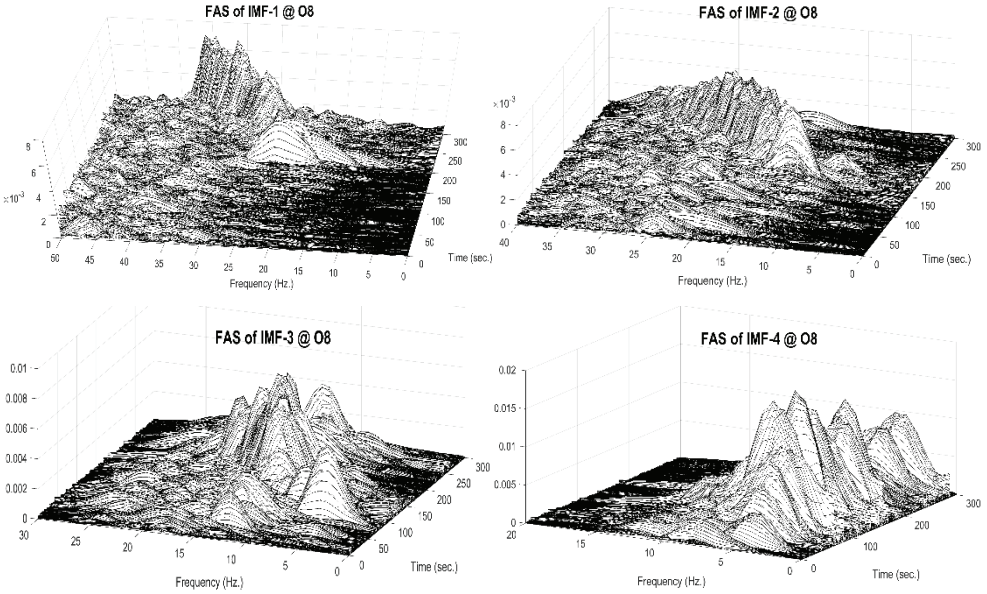

Fig. 21 - FAS of the first four IMFs decomposed from recording at the station O_8.

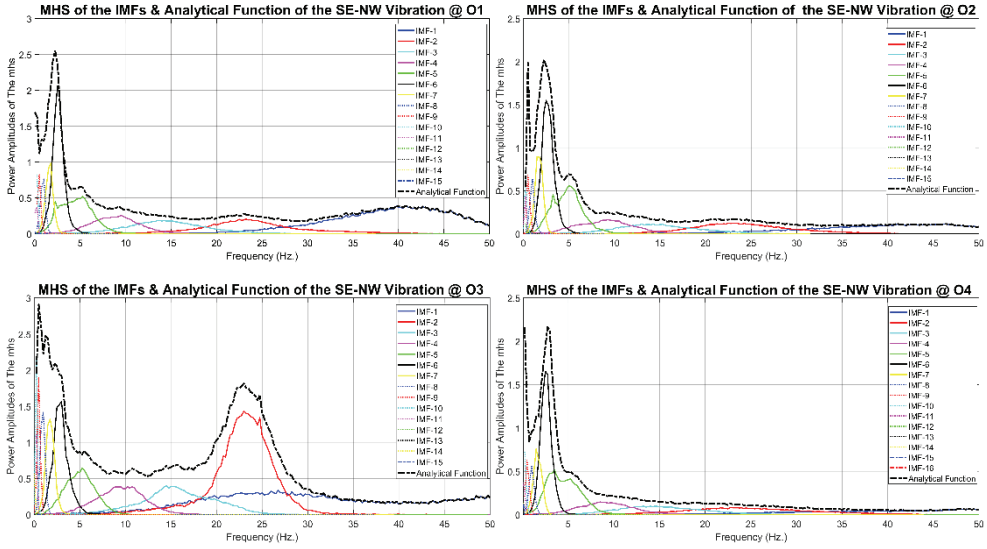

Fig. 22 - MHS of the IMFs decomposed from SE-NW ambient vibrations of the arch stations O_1, O_2, O_3 and O_4 and MHS of the analytical functions in dot-dash black line.

7. CONCLUSIONS

This paper, as a state of the art and practice in the damage detection, presents a brief review of different damage identification methods and their applications to a historical structure, Fatih Mosque, damaged during the 1999 Kocaeli Earthquake. Spectral analysis of the structure yields average peak frequencies, respectively at around 2.5, 3.5, 4.3, 5.3 Hz for SE-NW direction. Similarly, for the SW-NE direction, they are at around 2.6, 3.2, 4.5-5.0 Hz with a broadband characteristic. From spectral and parametric results, Northwest arch (O_3) that is expected to move in harmony with other structural components will not display such a consistent behavior and produces additional local frequency at 24Hz due to loose bonds between the stone masonry blocks around the crown. Southeast arch (O_1) also has roughly comparable damage producing another locality at 38Hz. On a global scale, damage additionally generates significant source of the non-stationarity on the neighbors in touch. Northeast arch (O_2) is affected strongly by the anomalies appeared at stations O_3 and O_1. Especially the neighbor stations O_6 and O_7 located at the springing points of the arch (O_3) and others O_5 and O_6 located at the springing points of the arch (O_2) are strongly affected due to tension rod failure causing the dome base to open outwards. Nonlinear behavior and strong nonstationary characteristics under the effect of accumulated damages are observed all neighbor components. It is seen that the progressive damage and partial failure destabilized the adjacent members. Analyses were extended to T-F decomposition in order (1) to describe how the spectral content of the signal changes with time; (2) to verify the effectiveness of the T-F analysis in damage identification in case of ambient vibration recordings and (3) to discuss comparably well sides and significant doubts on the suitability of the techniques in damage identification studies. STFT, WT and HHT utilized as different vehicles were discussed to reexamine superior performance of the suitable one with some advantageous. Finally, useful quantitative information that was extracted from WT and HHT has achieved very close results about the damage and time varying spectral characteristics. On the other hand, since structural damages do not allow the structure to behave in a monotonic fashion, results of the different analysis methods in either way yield similar results but negligibly small differences in frequency content. In order to compensate the FT leakage artifacts (i.e., non-stationarity, zero end conditions), it is recommended to decompose the signal based on Huang before applying Fourier Transform for particularly nonstationary dynamics. Simulations show that the proposed algorithm has better performance in component extraction from complex nature as well as provides more time-frequency details than conventional Fourier Transform method. For historical masonry structures with vulnerable components like large central dome and arches that have low redundancy, there is a need to develop automatic signal/image processing to identify anomaly through image processing, machine vision, and pattern recognition. Ambient measurement data has enough sensitivity for advanced damage identification and adequately captures nonlinear nonstationary characteristics, if exist in the structural behavior.

Acknowledgements

To Prof. Dr. Feridun Çılı (İTÜ) for sharing his own photograph archive and co-author Haluk Yıldız (VGM) for providing the technical details and drawings. To the Yılmaz Construction and Restoration Com. Yusuf Yılmaz and architect Mrs. Gülşah Altun for their help and availability.

References

[1] Goodwin, Godfrey (1971), *Gaspare Fossati Di Morcote and His Brother Giuseppe, A history of Ottoman Architecture*, London.

[2] Hrvoje Smoljanović, Nikolina Živaljić, Željana Nikolić, Overview of the methods for the modelling of historical masonry structures, GRAĐEVINAR **65** (2013) 7, 603-618.

[3] Lourenço, P.B. 1998. Experimental and numerical issues in the modelling of the mechanical behavior of masonry. In: P. Roca et al. (Ed) *Structural Analysis of Historical Constructions*, p. 57-91, Barcelona: CIMNE.

[4] Allemang, R.J. 1984: Experimental Modal Analysis Bibliography. *Proceedings of the 2nd International Modal Analysis Conference*, Orlando, Florida, 1085–1097.

[5] Doebling, S. W., Farrar, C. R., Prime, M B. and D W. Shevitz (1996), Damage identification and health monitoring of structural and mechanical systems from changes in their vibration characteristics: a literature review, *Los Alamos National Loboratory report LA-13070-MS.*

[6] Aktan, A. E., Hunt, V. J., Lally, M. J., Stillmaker, R. B.,Brown, D. L., and Shelley, S.J., (1995), "Field Laboratory for Modal Analysis and Condition Assessment of Highway Bridges', Proceedings of International Modal Analysis Conference XV, Honolulu, Hi., Pages 718–727.

[7] Straser, E.G. and Kiremijdian, A.S. (1996), A Modular Visual Approach to Damage Monitoring for Civil Structures. Proceedings of SPIE Smart Structures and Materials, 2719, 112-122.

[8] P.B. Lourenço, Computations on historic masonry structures, Prog. Struct. Eng. Mater. 4 (2002) 301–319.

[9] E. Quagliarini, G. Maracchini, F. Clementi, Uses and limits of the equivalent frame model on existing unreinforced masonry buildings for assessing their seismic risk: a review, J. Build. Eng. 10 (2017) 166–182.

[10] Daniele Pellegrini, Maria Girardi, Paulo B. Lourenço, Maria Giovanna Masciotta, Nuno Mendes, Cristina Padovani, Luis F. Ramos, Modal analysis of historical masonry structures: Linear perturbation and software benchmarking, Construction and Building Materials 189 (2018) 1232–1250

[11] A. Cabboi, C. Gentile, A. Saisi, From continuous vibration monitoring to FEM-based damage assessment: application on a stone-masonry tower, Constr. Build. Mater. 156 (2017) 252–265.

[12] B. Conde, L.F. Ramos, D.V. Oliveira, B. Riveiro, M. Solla, Structural assessment of masonry arch bridges by combination of non-destructive testing techniques and three-dimensional numerical modelling: application to Vilanova bridge, Eng. Struct. 148 (2017) 621–638.

[13] L.F. Ramos, L. Marques, P.B. Lourenço, G. De Roeck, A. Campos-Costa, J. Roque, Monitoring historical masonry structures with operational modal analysis: two case studies, Mech. Syst. Signal Process. 24 (2010) 1291–1305.

[14] P. Pineda, Collapse and upgrading mechanisms associated to the structural materials of a deteriorated masonry tower. Nonlinear assessment under different damage and loading levels, Eng. Fail. Anal. 63 (2016) 72–93. Elsevier.

[15] Alemdar Bayraktar, Ahmet Can Altunisik, Baris Sevim, Temel Türker, Seismic response of a historical masonry minaret using a finite element model updated with operational modal testing, J. Vib. Control 17 (1) (2011) 129–149.

[16] Dascotte, E. (2007), "Modal Updating for Structural Dynamics; Past, Present and Future Outlook", *Int. Conf. on Engee. Dynamics (ICED)*, Algarve, Portugal.

[17] E. Bassoli, L. Vincenzi, A.M. D'Altri, S. De Miranda, M. Forghieri, G. Castellazzi, Ambient vibration-based finite element model updating of an earthquake-damaged masonry tower, Struct. Control Health Monit. 25 (5) (2018) e2150.

[18] M. Mistler, C. Butenweg, K. Meskouris, Modelling methods of historic masonry buildings under seismic excitation, J. Seismol. 10 (2006) 497–510.

[19] W. Torres, J.L. Almazán, C. Sandoval, R. Boroschek, Operational modal analysis and FE model updating of the Metropolitan Cathedral of Santiago, Chile, Eng. Struct. 143 (2017) 169–188.

[20] M.G. Masciotta, L.F. Ramos, P.B. Lourenço, The importance of structural monitoring as a diagnosis and control tool in the restoration process of heritage structures: a case study in Portugal, J. Cultral Heritage 27 (2017) 36–47.

[21] M.G. Masciotta, L.F. Ramos, P.B. Lourenço, M. Vasta, Damage identification and seismic vulnerability assessment of a historic masonry chimney, Ann. Geophys. 60 (4) (2017) 2017, https://doi.org/10.4401/ag-7126.

[22] B. Pantò, F. Cannizzaro, I. Caliò, P.B. Lourenço, Numerical and experimental validation of a 3D macro-model for the in-plane and out-of-plane behavior of unreinforced masonry walls, Int. J. Archit. Heritage 11 (7) (2017) 946–964.

[23] Ewins, D. J. (2000), *Adjustment or Updating of Models, International Winter School on Optimum Dynamic Design Using Modal Testing and Structural Dynamic Modification*, Indian Academy Sciences, 235-245.

[24] Beyen, K., 2005, 'Fatih Camii Yapısal Davranışının Ve Dinamik Özelliklerinin Çevrel Ölçümler Işığında Tanımlanması', T.C. İstanbul Büyük Şehir Belediyesi İski Genel Müd., Mimtaş ile T.C. Boğaziçi Ü., T.C. Yıldız Teknik Ü. arasında İstanbul Fatih Camii ve Külliyesi Alt ve Üst Yapı Onarım – Restorasyon Projesi, İstanbul (in Turkish).

[25] Ceylan, Oğuz, Ocakcan, Tuğba Keleş, Fatih Camii 2007-2012 Restorasyonu Uygulamaları - *The Restoration of Fatih Mosque Between 2007-2012,* Vakıf Restorasyon Yıllığı, Yıl: 2013, Sayı: 7, (in Turkish).

[26] Beyen, K. (2008), "Structural Identification for Post-Earthquake Safety Analysis of the Fatih Mosque after the 17 August 1999 Kocaeli Earthquake", Engineering Structures, 30.

[27] Farrar, C. R., Doebling S. W., Cornwell, P. J., and E. G. Straser (1997), "Variability of modal parameters measured on the Alamosa Canyon Bridge", in Proc., *15th Int. Modal Analysis Conf.,* Orlando, FL.

[28] Goodwin, Godfrey (1997), *A History of Ottoman Architecture*, Thames and Hudson, London, 121-131.

[29] Ayverdi, Ekrem Hakki (1973), *Fatih Era in Ottoman Architecture - Osmanli Mimarisinde Fatih Devri: (1451-1481)*, Volume III, Baha Matbaasi, Istanbul, 356-387 (Turkish).

[30] Sakin, Orhan (2002), "Tarihsel kaynaklarıyla İstanbul Depremleri", İstanbul, referenced Gregoras Nikephoros Historia, 2, p. 694.

[31] William S. Ginell and E. Leroy Tolles (2000), "Seismic Stabilization of Historic Adobe Structures", JAIC, Vol. 39, No: 1, 147-163.

[32] Bariola, J. B. (1991), "Dynamic stability of adobe walls", Ph.D. dissertation, University of Illinois, Urbana, Ill.

[33] Çılı, F. and Yıldız, H., 2013, 'Fatih Camii ve I. Mahmut Kütüphanesi Güçlendirme Çalışmaları – Strengthening Works of The Fatih Mosque and Mahmut I. Library', Vakıf Restorasyon Yıllığı, No: 7, pgs: 66 – 84.

[34] Yılmaz Yapı Taah. Ve Tic. Ltd. Şti. Özel Fatih Camii Restorasyon Arşivi, 2019.

[35] Fatih Sultan Mehmet Camii ve Sultan I. Mahmut Kütüphanesi Restorasyonu (2008-2012), 2019, Yılmaz Yapı Taah. Ve Tic. Ltd. Şti. Yayınları, (baskıya hazırlanıyor in press).

[36] Durukal, E., Cimilli, S. and Erdik, M. (2003), "Dynamic Response of Two Historical Monuments in Istanbul Deduced from the Recordings of Kocaeli and Düzce Earthquakes", *BSSA,* Vol. 93, no. 2, 694-712.

[37] Rahmatalla, S., Eun, Hee-Chang, Lee, Eun_Taik (2012), "Damage detection from the variation of parameter matrices estimated by incomplete FRF data", Smart Structures and Systems, Vol. 9, No. 1, 55-70.

[38] Lus, H., De Angelis M, Betti, R., and Longman, R.W. (2003), "Obtaining Physical Parameters of Mechanical Systems from Identified State Space Models", ASCE, Journal of Engineering Mechanics, V. 129 (5), 477-488.

[39] Inman, D. J. and Minas, C. (1986), "Matching analytical models with experimental modal data in mechanical systems", Control and Dynamics Systems, Vol. 37, 327-363.

[40] Liu, S. C. and Yao, J. T. P. (1978), "Structural Identification Concept", ASCE Journal of the Structural Division, Vol. 104, No. ST12, 1845-1858.

[41] Law, S. and Li, X. (1993), "Structural damage detection based on higher order analysis", *Procedings of Asia Pacific Vibration Conference*, 640/3, Japan.

[42] Lim, T. W. (1990), "Submatrix approach to stiffness matrix correction using modal test data", AIAA Journal, Vol. 28, No.6, 1123-1130.

[43] Bendat, J. S. and Piersol, A. G. (2004), *Random Data, Analysis and Measurement Procedures*, JW, USA.

[44] Juang, J. N. (1994), "Applied System Identification", Prentice Hall, Englewood Cliffs, New Jersey.

[45] Juang, J. N., Pappa, R. S. (1985), "An Eigen system Realization Algorithm for Modal Parameter Identification and Model Reduction", J. of Guidance, Control and Dynamics, 8, No.5.

[46] Bendat, J. S. (1990), *Nonlinear System Analysis and Identification from Random Dat*a, Wiley-Interscience, USA.

[47] Mathworks (2013), *Signal Processing Toolbox for Matlab, Release 2012b*, The MathWorks Inc., Natick, MA.

[48] Huang, N. E., Zheng, S., Long, S. R., Wu, M. C., Shih, H. H., Zheng, Q., Yen, N.-C., Tung, C. C., and Liu, H. H. (1998), ''The empirical mode decomposition and Hilbert spectrum for nonlinear And nonstationary time series analysis.'' *Proc. R. Soc. London, Ser. A,* 454.

Teknik Dergi, 2021 10611-10628, Paper 605

Determination of Important Building Construction Adverse Impacts Creating Nuisances in Residential Areas on Neighbouring Community

Cenk BUDAYAN[1]
Tolga CELIK[2]

ABSTRACT

The construction industry is criticized due to poor stakeholder management. Whereas, the stakeholders play important roles in the completion of construction projects in line with their concerns and needs. Therefore, it is crucial to identify and incorporate the needs and concerns of the stakeholders during management applications for the commercial success of a construction project. For that purpose, in this study, the adverse impacts of the building constructions in residential areas which create nuisances on one of the external stakeholders, namely neighbouring community, are aimed to be identified. Thus, a questionnaire survey is performed with 266 respondents neighbouring building constructions in different cities of Northern Cyprus. A model based on the adverse impacts of building constructions and their categories is proposed, and this model is analysed using structural equation modelling (SEM). The results of the participants reveal that the entire adverse impacts are perceived as contributing causes for a disturbance on the neighbouring community. Last but not least, conducted research highlights that the social and cultural manners of the society which shows variations from region to region plays a significant role in the way community absorbs and experiences these adverse impacts.

Keywords: Construction projects, neighbouring community, nuisances, stakeholder management, structural equation modelling.

1. INTRODUCTION

Many different contributing parties have power and ability to influence or change a managerial decision of construction projects. Therefore, performance of these parties during a project life cycle is a determining factor for the success of a construction project. For instance, the

Note:
- This paper has been received on November 22, 2018 and accepted for publication by the Editorial Board on October 23, 2019.
- Discussions on this paper will be accepted by May 31, 2021.
- https://dx.doi.org/10.18400/tekderg.486628

1 Yildiz Technical University, Department of Civil Engineering, İstanbul, Turkey - budayan@yildiz.edu.tr https://orcid.org/0000-0002-8433-2824

2 Eastern Mediterranean University, Department of Civil Engineering, Famagusta, North Cyprus, - tolga.celik@emu.edu.tr - https://orcid.org/0000-0002-2513-6735

neighbouring community of construction projects is one of the important contributing parties for the success of construction projects as they are highly involved with the unavoidable nuisances generated from the execution of construction activities which create immense alterations in their daily routine. Consequently, comprehending the existence of neighbouring communities and in a format, incorporating their opinions during the decision-making process is a critical issue in the success of the construction projects [1]. This is why researchers of this study suggest consideration of neighbouring communities as stakeholders.

PMI [2] defines a stakeholder as any party which may affect, be affected by, or perceives itself to be affected by the processes conducted throughout the project. PMI [2] also considers stakeholder management as one of the knowledge areas of project management and emphasizes the importance of stakeholder management in project management. Even, some of the researchers [3] concluded that most of the unsuccessful projects are due to inappropriate social interactions between the project stakeholders rather than lack and ineffective project management practices. Unfortunately, the stakeholder management is poorly applied in the construction industry [4], since the stakeholder management is a difficult process due to high complexity, uncertainty, and equivocality of the project environment [5].

All of the parties involved in the construction internally and externally should be pondered to manage stakeholders effectively. However, most of the contractors and owners overlook the external stakeholders, especially neighbouring community. Therefore, the contractors generally prepare their bids by ignoring the costs required for compensating adverse impacts of the construction activities on the community and indirect costs emerged due to the conflicts and controversies [6]. Whereas, in urban areas, members of the community, who are integrally residents and businesses in the neighbourhood of a construction site, are exposed to wide range of construction causative adverse impacts [7], in terms of ecology, sociology and economy [8, 9]. Especially in urban areas, due to high density of population, construction practices can cause serious environmental nuisances for the adjacent residents and businesses, which will eventually transform into economic loss [10, 11]. Due to these economic losses, these parties may demand compensations from the contractors. Besides, the contractors can face conflicts and controversies due to the nuisances caused by the construction. For instance, the community and non-governmental organizations can protest and litigate the contractors. Also, they can exercise pressures on the governmental agencies, which in turn may lead to strict inspections. These can cause an increase in the likelihood of failures, delays, and economic losses.

Due to the importance of stakeholder management, there are many studies concerning the stakeholder management, however, most of these studies generally focus on three themes, namely identifying the nature of stakeholders, examining under which circumstances and how stakeholders influence organizational decisions and operations and identifying different strategies to deal with stakeholders [12]. On the other hand, there is a limited number of studies about how the stakeholders are affected by the construction processes. Whereas, the contractors can manage their stakeholders more effectively by obtaining an indication of the stakeholder groups' concerns, the problems of the project team faces and stakeholders' requirements of the projects [13]. If these various concerns and needs are not analysed thoroughly and managed properly, severe conflicts and controversies can be expected, which may lead to cost and time overruns [14]. In addition, most of the studies related to stakeholder management generally focus on owner, subcontractor, and suppliers, however, neighbouring community is generally overlooked in these researches.

In the literature, there are also some attempts about the adverse impacts of the construction projects creating nuisances, however, all these studies tried to quantify the adverse impacts. For instance, Gilchrist and Allouche [15] proposed a framework to quantify the adverse impacts for infrastructure construction projects in urban areas. Liu, Huo [6] developed a decision model by using an intuitionistic fuzzy group for bid evaluation of urban infrastructure projects including adverse impacts. Matthews, Allouche [16] quantified the disruptions emerged during pipeline infrastructure projects. Although these studies tried to identify the adverse impacts of construction projects, they did not determine which adverse impacts leading to more severe nuisances on the neighbouring community. In other words, they assumed that all these adverse impacts affect the neighbouring community at the same level. Therefore, they calculated the amount of compensation cost by considering all those adverse impacts at the same intensity. This causes to obtain either higher or smaller compensation costs than the actual one incurred by the stakeholders. In addition, since they just considered the quantification of the compensation cost and ignored the effectiveness level of these adverse impacts, the management of these adverse impacts was overlooked. Consequently, in the literature, there is a gap about the identification of the most important adverse impacts which create nuisances on the neighbouring community and development of a systematic roadmap for managing these nuisances.

This paper concentrates on the identification of the most important needs and concerns of the stakeholders, namely neighbouring community. For that purpose, the most severe adverse impacts of building constructions which lead to the nuisances on the neighbouring community in the residential areas are aimed to be identified based on a questionnaire survey conducted in Northern Cyprus, therefore, more effective neighbouring community management systems can be developed by focusing on these important adverse impacts principally and eliminating the unnecessary costs. Therefore, the conflicts and controversies which emerge between the neighbouring community and contractors can be eliminated or mitigated applying this system.

2. DEVELOPMENT OF A THEORETICAL FRAMEWORK

2.1. Determination of Main Categories of Adverse Impacts

In the development of a generic model, firstly a literature survey is conducted to determine the main categories of adverse impacts emerged due to the execution of construction activities. The studies related to the determination of adverse impacts are generally conducted for specific construction types. For instance, one of the first efforts performed by Read and Vickridge [17] focused on public utility projects and identified eleven adverse impact categories. Similarly, Gilchrist and Allouche [15] mentioned about four categories of adverse impacts of infrastructure projects in urban environments. These categories are traffic, economic activities, pollution, and ecological/social/health. Xueqing, Bingsheng [18] developed a bid evaluation method by considering the social impact of infrastructure projects in urban areas. According to them, adverse impacts of these projects can be categorized into four groups, namely natural environment, public property, local economy, and human society. Liu, Huo [6] developed a decision model for urban infrastructure projects and used similar impact categories proposed by Xueqing, Bingsheng [18]. Ormsby [19] developed a framework for estimating the total cost of buried municipal infrastructure renewal projects. In this study, the external impacts of the projects are considered under three categories, namely social, economic and environmental impacts. Yuan, Cui [20] conducted a study for green building projects and classified the adverse impacts in four main

categories, namely impact on the community, impact on the economy, impact on the environment and public property. Xue, Zhang [21] focused on urban subway construction and determined four impact factors which can affect the satisfaction of a community negatively based on environmental, social impact, and stakeholder theory. These impact factors are the impact on residents' travel, transportation, environment and daily life. Matthews, Allouche [22] considered eight adverse impacts of pipeline infrastructure projects to assess the social cost of these projects. The adverse impacts in this study were stated as travel delay, vehicle operating costs, decreased road surface value, lost business revenue, loss of parking revenues, cost of dust control, noise pollution costs and safety. Similarly, Nunes Vasconcelos [23] conducted another study for pipeline infrastructure projects and determined four impact areas, namely economy, traffic, damage to environment and health, and pollution. Çelik, Arayici [24] tried to monetize the social costs of housing projects on the built environment and classified the adverse impacts of these projects under three main categories, namely damage to natural and built environment, pollution and traffic problems.

Although most of the studies related to adverse impacts of construction projects considered specific construction types, there are also some studies which proposed that all construction projects cause same adverse impacts. They also asserted that the intenseness of these impacts can vary with the construction type [25]. For instance, Yu and Lo [26] developed quantification of the adverse impacts of construction operation on local areas by considering traffic impacts, environmental impacts, and business impacts. Similarly, Wang, Han [27] investigated the reaction of the public to social impacts of construction projects and considered three types of negative project impacts in their study, namely negative impacts on the environment, income and living standards.

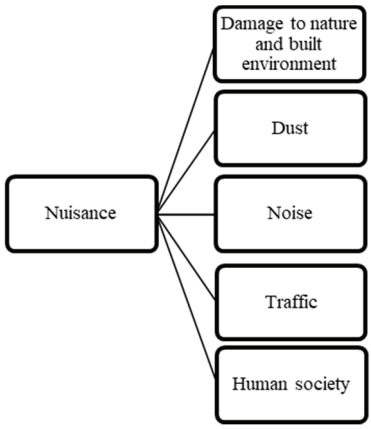

Figure 1 - The proposed model used in this study

In this study, considering the literature, four categories for adverse impacts are identified. These categories are damage to nature and built environment, pollution, traffic, and human society. However, the pollution created by dust and noise is considered separately, since they create different nuisances on the neighbouring community. Besides, in the literature, most of the studies about nuisances are conducted by considering infrastructure projects, therefore the local economy is considered as an important impact category in these studies. However, the aim of this study is

identifying the nuisances of the residents who do not perform economic activities, therefore the negative impacts of construction projects on economic activities performed within the facility of the construction site are considered as out of the scope of this study. Consequently, in harmony with the past studies, categories of building construction-borne adverse impacts have been determined as shown in Figure 1.

2.2. Determination of Adverse Impacts

At the second step of the development of a theoretical framework, a literature survey is conducted. Then, 18 adverse impacts of construction projects are determined by considering the studies of [15, 22, 24, 25], these adverse impacts are categorized under five adverse impact categories stated before. The following sections present detailed information about these adverse impacts and their categories.

2.2.1. Damage to Nature and Built Environment

The impacts of the construction projects in urban areas on ecology are considered as limited since the environment has already been damaged by years of urbanization. However, if the project is conducted in or near recreational areas, this effect can be more intense. Especially, when the number of recreational areas in the neighbourhood is limited, then the reaction of the community can be very drastic [15].

2.2.1.1. Loss in Serviceability of Playfield and Parks

Due to the formation of various impacts because of the on-going construction activities in the neighbourhood, access to some of the recreation facilities in the area may be temporarily unavailable or serviceability standards of those facilities may decrease due to the impacts created by the construction project.

2.2.1.2. Loss of Habitats and Parks

In order to prevent fragmentation, lessening and/or loss in the existing parks and habitat in the area/neighbourhood, land management concerning habitat conservation is necessary for the construction projects. However, due to probable deficiencies of the contractor in land management, habitats/parks of the area may be damaged.

2.2.1.3. Loss of Landscape Standards

Another effect of activities of construction projects on the environment which can be considered as an important nuisance is a loss of landscape standards. The construction activities can change the landscape in the neighbourhood by replacing or removing trash barrels, street furniture, street lights, phone boxes, street post boxes, street signboards, street flower pots etc. The society is affected from this landscape transformation, since the natural view is an important criteria and the society is ready to pay more money for a nice natural view [28].

2.2.2. Dust

One of the adverse effects of construction of buildings on the environment is the dust since there are many dusty activities which produce airborne particles and dust in the construction areas. Therefore, throughout the construction activities, high amount of dust can be observed on the construction site, and the dust in the construction area can be carried to the neighbourhood

community by the breezes [29]. The dust can cause damage to the electronic and mechanical equipment. In addition, it can lead to health problems due to some chemical materials within the dust. Consequently, the neighbourhood community can suffer from the dust in their houses, cars, living environments and backyards.

2.2.3. Noise

Noise is defined as any sound that has potential to cause psychological or physiological symptoms [15]. Bein [30] stated that noise can affect social behavioural, the mental and physical health of people. Unfortunately, construction is one of the main sources of noise. Noise will be generated by site operations including heavy earthmoving and paving equipment, operator pumps, generators, and vehicle traffic and demolition activities. The effects of noise are not limited only with psychological and physiological symptoms, but also the economic effects of noise to the neighbouring community are also observed. For instance, the value of real estates in noisy environments tends to be lower than in quieter environments. Based on this discussion, three adverse impacts of noise are proposed in this study, namely loss of peace and quietude of the neighbourhood, degradation of ambient conditions and prevention of usage of the outdoor areas of the house.

2.2.4. Traffic

The negative effects of construction projects on the traffic were stated widely in the literature [31, 32] as given below.

2.2.4.1. Prolonged Closure of Road Space

Although most of the construction activities are performed within the border of the construction site, some of the activities of the construction can require space outside the construction site, such as movement of machineries while performing the construction activities and entry/exit corridors. Especially, in urban areas, the entry/exist corridors can affect the traffic flow intensely since the manoeuvre capacity of the construction vehicles is so limited when compared with the vehicles used in daily life. These could lead to time delay costs, extra oil combustion, an increase in the number of traffic accidents, vehicle loss cost and environmental pollutions [33].

2.2.4.2. Detours

Due to the construction activities such as utilization of mobilized crane and entry of trucks to the construction site, the roads can be closed for a while, therefore the vehicles can be diverted to the secondary roads designed for light traffic loads in order to avoid excessive delays. This can create problems related to deterioration of road pavement due to overloading which decrease the economic life of the pavement structure, therefore the travel comfort of the drivers will be affected. In addition, the detours can cause nuisances to the drivers in terms of increased fuel consumption and time.

2.2.4.3. Loss of Parking Space

The loss of parking space is another nuisance for the travellers since they have to park farther away and spend more time walking which can be used for more productive purposes [16]. As a result of this, there can be a time delay, extra oil combustion, an increase in the number of traffic accidents, vehicle loss cost, and environmental pollutions [33].

2.2.4.4. Utility Cuts

The utility cuts are considered as one of the adverse impacts of construction projects on traffic by Gilchrist and Allouche [15]. The construction activities can involve the cutting and restoration of paved structures, in addition, the loading trucks can cause damage to the pavement surfaces due to the settlement [15].

2.2.5. Human Society

Although there are tremendous positive impacts of the construction industry on the society, it also affects the life of the human society negatively; in addition, some of these effects are irreversible.

2.2.5.1. Road Safety

The probability of enhanced accident risks due to construction machinery circulating in the neighbourhood/area, spillage of construction materials on the roads during transportation of materials into/out of the construction site, other construction wastes/residuals and etc. may cause traffic congestion, closure of the road, and detours due to probably lessened road safety standards. On the other hand, excess traffic on minor residential area roads may reduce the safety standards of the roads.

2.2.5.2. Human Health Hazards

The adverse impacts created throughout the construction can lead to serious health problems to the environment. For instance, the high concentration of dust in the air can lead to declination in lung function, increase in respiratory hospitalization and increase in mortality from respiratory and cardiovascular causes [34]. As stated before, the noise also can cause health problems such as high blood pressure, cardiovascular disease, anxiety, restlessness, irritability, sleep disturbances and difficulty in concentrating [15, 35].

2.2.5.3. Living Quality Decline

With the newly adverse impacts, the neighbouring communities confront with the decline in their quality living standards. For instance, time spending outside can decrease drastically due to the pollution.

2.2.5.4. Safety Hazards in the Area

The construction sites are dangerous places for the workers, and this is also valid for the neighbouring community, especially when the area of the construction site is limited and it is close to the public areas. Some of the risks occurring due to construction in the area such as; the probability of enhanced accident risks caused by construction machineries being in neighbourhood traffic, spill of construction related material on the roads during transportation of materials into/out of the construction site, additional hazards that are possibly to occur during the actual construction which may result in injuries of the residents, construction wastes/residuals forming threats on the residents' health, possible crime incidents of construction workers, etc., traffic jam in the area and etc.

3. RESEARCH METHODOLOGY

This study is about the identification of adverse impacts emerged due to the execution of construction activities in residential areas. For that purpose, a questionnaire which consists of two

parts is designed and applied to 266 respondents in the three largest cities of Northern Cyprus, namely Famagusta, Kyrenia, and Nicosia. The target population is selected from the people who reside within a 150 m radius of the construction site so that all of the respondents are selected from the people exposed to the adverse impacts at the same degree. The first part is designed to illustrate the demographic structure of the respondents. In this part, the gender, age group and level of education are asked to verify whether there is a heterogeneity among the respondents or not. A community normally has a heterogeneous structure in terms of lifestyle. Individuals of the community have different views and perspectives in giving reaction to any alterations in their daily routine, therefore, more heterogeneity in the sample leads to capturing the different perspectives from different groups. Table 1 shows the demographic structure of the respondents, according to this table, all age groups are included in this research equally; besides, the opinions of people who have different education level are also obtained. Consequently, it can be said that the heterogeneity of the respondents is satisfied and the perception of the respondents who have different demographical background can be captured.

Table 1 - Demographic structure of the respondents

Gender	
Male	52.26%
Female	47.74%
Age Groups	
18-24	22.56%
25-33	24.06%
34-44	21.43%
45-54	15.04%
55-65	12.41%
66 and over	4.51%
Level of Education	
Literate	0.38%
Primary school	16.17%
Secondary school	7.89%
High school	34.59%
2-year college degree	0.38%
4-year college degree	25.94%
Master's degree	3.01%
Doctoral degree	11.65%

The second part is about measuring how intense participants experience the adverse impacts of building construction projects. For this section, 18 pre-identified adverse impacts which are

illustrated in Figure 2 are examined through measuring the experience level of participants. In this part, the respondents evaluated the way they experience adverse impacts based on 10 points Likert scale, according to this scale; 1, 5 and 10 indicate "none", "moderate" and "very high", respectively. In other words, if the respondent considers that the on-going building construction affects its life in terms of any criterion intensively, they will assign this criterion with a high value. On the other hand, if this effect is limited, then the respondent can prefer different values than 10 based on the severity of this effect.

4. ANALYSIS

One of the important steps of the analysis is the selection of the analysis method by considering some or all of the criteria such as; accuracy, sensitivity, selectivity, robustness, time and availability of equipment. In this study, the analysis method is selected by comparing the features of the analysis methods. Although traditional statistical analysis methods can provide valuable information about the severity of these adverse impacts, they may not reflect the real situation since they do not consider the interrelationships between the adverse impacts. Whereas, there are interrelationships between the adverse impacts. In other words, the emergence of one of the adverse impacts can lead to the creation of another adverse impact, or the existence of two adverse impacts at the same time can increase the perceived nuisance level. For instance, cleanliness of the house is one of the important adverse impacts of dust, however, it can also lead to problems in human health, which in turn, may lead to human health hazards, and therefore cleanliness of the house can have a more disturbing effect on the neighbouring community than assigned by the respondents. Therefore, to reveal the real nuisance levels of these adverse impacts on the neighbouring community, a more complex analysis method which can estimate the model which consists of interrelationships between the adverse impacts should be selected. Therefore, a different method, namely structural equation modelling (SEM) which is capable of dealing with the numerous numbers of dependent variables and examining direct and indirect relationships between one or more independent variables and one or more dependent variables, is decided to be used. The SEM analysis is performed by using EQS 6.4, a software program used for performing SEM analyses. Based on the developed theoretical framework, a model consisting of 18 indicators, 5 latent exogenous variables, and 1 latent endogenous variable is used in the analyses. Indicators are the variables whose effects can be measured. Indicators can be considered as independent variables in SEM. Latent variables cannot be measured directly, therefore they should be estimated by measuring the effects of indicators representing latent variables' effect. Latent variables can be considered as dependent variables in SEM. There are two types of latent variables. These are latent exogenous variables, which are determined based on indicators and affect other variables in the model, and latent endogenous variables which are influenced by the exogenous latent variables in the model, directly or indirectly.

Before application of the SEM, some of the factors should be considered to check the appropriateness of the dataset for SEM analysis. Firstly, the internal reliability of the data set is examined by performing reliability analysis with the alpha model via SPSS 22. Since, in this survey, different social groups who have different social backgrounds are considered in the research, the reliability of the data should be examined prudently. According to the reliability analysis, the Cronbach alpha is calculated as 0.903 which is higher than the threshold value (0.7) recommended by Nunnally [36] for internal reliability. In addition, the reliability coefficient rho,

the square of the multiple correlation coefficient is determined as 0.910. Consequently, the dataset obtained for this research is concluded as internally stable.

The sample size is another important factor which should be considered. In SEM, the larger sample size is required to estimate the weights and fit indices accurately. There are different recommendations about the required sample size for SEM applications, for instance, Ding, Velicer [37] determined that the minimum satisfactory sample size should be between 100 to 150 subjects. On the other hand, some authors recommended a minimum ratio of parameters to the sample size instead of a minimum sample size. Rule of 10 requiring the choosing of 10 observations per indicator in setting a lower bound for the adequacy of sample sizes is widely accepted and used in the literature [38]. In this research, the number of observations is 266; therefore, the dataset is adequate for conducting a SEM analysis, since a total number of indicators is 18.

In the next step, the model shown in Figure 2 should be estimated. Firstly, the estimator method should be selected. Maximum Likelihood (ML) method is the default and widely used method in the literature due to its advantages [39]. However, this method provides an accurate fit indices when the normality exists in the data set [39]. Whereas, it can yield distorted outcomes about model adequacy when the multivariate normality assumption violates. Consequently, in order to decide which method is used in the analysis, the multivariate normality of the data set is examined by checking Mardia's coefficient. In this study, this coefficient is calculated as 73.925. This value is far beyond the accepted range of -3 to 3 to declare that the dataset is multivariate normal. Thus, the robust method with ML recommended for the non-normal data set [39] is used for analyses to obtain robust statistics.

The obtained model should be evaluated in two aspects, namely the overall fit of the model and the significance of particular parameters of the model for verifying the reliability of the proposed model [40]. There are different fit indices developed for evaluating the overall fit of the model, however, there is no golden rule for best fit index. On the other hand, reporting a variety of indices is necessary for reflecting different aspects of model fit [41]. One of the indices is essential to state is the model Chi-square along its degree of freedom and associated p-value [42]. In this study, Satorra - Bentler chi-square is calculated as 7.739 based on 4 degrees of freedom. This information is used to test the significance of the difference between the estimated population covariance matrix and the sample covariance matrix [40]. The probability value for chi-square statistics is 0.102 which is higher than 0.05. This indicates that the model fits the data. Although some of the researchers, such as McIntosh [43], Hayduk, Cummings [42], asserted that Chi-square is enough for evaluating the overall fit of the model, the other fit indices are considered in the model evaluation, since the small differences create significant chi-squares when the sample size is large [40]. Hu and Bentler [44] suggested a two-index presentation format. In their study, they recommended the use of both standardized root mean square residual (SRMR) and one of the following indices, Comparative fit index (CFI), Non-Normed Fit Index (NNFI) or Root Mean-Square Error of Approximation (RMSEA). However, SRMR is not calculated for the robust method, therefore SRMR is not available. On the other, Ullman and Bentler [40] used CFI and RMSEA to evaluate the overall fit of their model analyzed by using the robust method. Table 2 shows the fit indices calculated by using the robust method. According to this table, calculated CFI and RMSEA values are placed in the boundary of threshold values, therefore we can conclude that the model fits.

Table 2 - Fit indices of the model

Fit indices	Recommended value	Calculated indices
Bentler-Bonett NNFI	>0.90	0.920
CFI	>0.90	0.935
Bollen's fit index	>0.90	0.936
RMSEA	<0.10	0.067
Lower Limit		0.056
Upper Limit		0.077
X^2/degree of freedom	Bet. 1 and 3	2.182

Secondly, the statistically significant relationships within the model are examined. EQS provides output for evaluating the regression coefficients. Based on this output, all relationships exist between latent exogenous variables and their indicators, and latent exogenous variables and endogenous latent variable shown in the model are identified significant at the 5% level. In addition, a confirmatory factor analysis (CFA) is performed by eliminating the endogenous latent variable for checking the existence of convergent validity based on recommendations of Zainudin [45]. Then, convergent validity can be examined by checking the significance of all factor loadings [46]. All factor loadings obtained at the end of CFA is determined as significant. In addition, to assess the convergent validity, the overall fit of the measurement model, and the magnitude, direction, and statistical significance of the estimated parameters between latent variables and their indicators are examined [47, 48]. Based on these examinations, it is concluded that the convergent validity is verified for this model. Consequently, according to significance levels of the relationships and fit indices, the model used in this research is identified as reliable.

The detailed information about the analysis of the model is shown in Figure 2. The numbers on the light arrows in Figure 2 represent the factor loadings. As stated before, all these factor loadings are determined as significant, therefore all these adverse impacts lead to the formation of nuisances.

Since the path coefficients obtained at the end of the SEM analysis can be used as regression weights, these coefficients are used in determining the effect level of exogenous latent variables on the endogenous latent variable. According to the model, it is observed that all adverse impact categories are very important to create nuisance to the neighbouring community, since "damage to nature and built environment", "human society", "noise", "dust" and "traffic" have significant direct effects on nuisances with path coefficients of 0.998, 0.938, 0.915, 0.987 and 0.925, respectively.

5. DISCUSSION OF FINDINGS

According to the findings of SEM, all of the adverse impact categories are perceived as disturbing by the neighbouring community, and all lead to the creation of the nuisance. Therefore, the contractors should consider all of these categories in stakeholder management and manage them to eliminate the possibility of the emergence of conflicts and disputes.

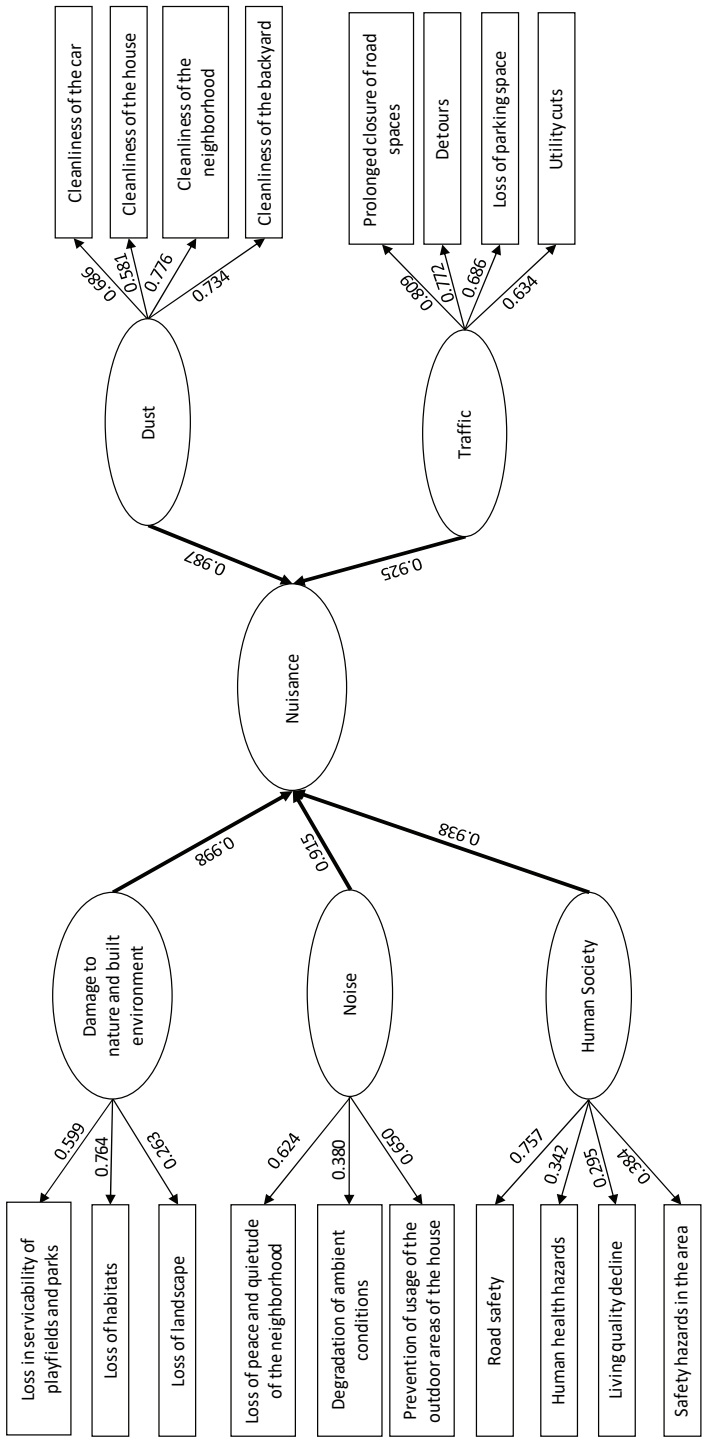

Figure 2 - The proposed model with factor loadings and path coefficients

Although all of the adverse impact categories create nuisances to the neighbouring community intensively, there are two adverse impact categories, namely damage to nature and built environment and dust, which influence the neighbouring community more intensively compared to other nuisances. This shows that the neighbouring community should give importance to nature and built environment, and they should keep in their mind that they will be affected negatively when nature and built environment is impaired due to their construction projects. Shen and Tam [49] acknowledged that the construction industry is known as one of the major contributors to the environment pollution, and with the increasing awareness of the community about nature and built environment, the construction companies can confront with the reactions from the public. Therefore, the environmental management systems can play an important role in the construction companies to manage the neighbouring community. The construction companies can apply ISO 14000 used for standardization of the environmental management system to overcome the problems emerged due to the damage to nature and built environment. In addition, when there will be a damage to nature and built environment, the neighbouring community should be informed about this damage and the agreement between the parties should be reached about methods used for dealing this effect. Hereby, open and trustworthy communication with the media and affected stakeholder, especially on the environmental subjects, is important in the successful implementation of stakeholder management [13, 50]. In addition, this finding shows that the community values the buildings which do not cause damage to nature and built environment, in other words, the sustainability of the constructed buildings is very important for the public. Falkenbach, Lindholm [51] also identified that the contractors can benefit from investing in environmentally sustainable buildings in environmental, social and economic perspective. The significant increase in the number of green buildings constructed annually can be considered as another evidence of this conclusion. Consequently, construction companies can avoid public reactions by developing projects more environment-friendly. Among the adverse impacts of damage to nature and built environment, "loss in serviceability of playfields and parks" is identified as the most significant. On the other hand, "loss of landscape" is determined as the least significant. This shows that people demand more places where they can spend time instead of picturesque sceneries. In other words, demolition of unnatural places is not considered as important as demolition of natural places.

The construction projects produce a high number of airborne particles and dust; therefore, effects of dust are expected to be very disturbing to the neighbouring community. Therefore, dust is identified as one of the most disturbing adverse impact categories in Northern Cyprus. The reason for this finding can be explained by the conditions of Cyprus. Due to the weather conditions of Northern Cyprus, especially high temperature and windy weather, the effects of dust can be more disturbing. Therefore, it can be concluded that dust can be very disturbing in countries where hot and windy weather conditions prevail. Consequently, when considering weights of adverse impact categories, the conditions of the region where the construction projects are conducted should be considered carefully.

When the adverse impacts of the noise are considered, the "prevention of usage of the outdoor areas" is observed as the most significant. Due to the weather conditions and cultural heritage of Northern Cyprus, spending time outside is one of the important rituals of Cypriot people and visiting neighbours is an important tradition, therefore anything which prevents them spending time outside is considered as disturbing. Consequently, the contractors should be aware that due to different cultural background, different adverse impacts can create different level nuisances in different countries. Therefore, they should develop different strategies for stakeholders from

different countries. This also verifies the importance of the conditions of the region in the determination of the important adverse impacts.

In addition, the contractors should conceive the culture parameter when managing the stakeholders. Rowlinson and Cheung [52] also emphasize the importance of culture in stakeholder management and propose that different management approaches are required in different locations.

When the human society is discussed, most of the adverse impacts stated under this category, namely "human health hazards", "living quality decline" and "safety hazards in the area", are perceived as less disturbing compared to other adverse impacts. These adverse impacts are not observed immediately, in other words, these effects occur in the long period time, even some of these effects, such as human health hazards, can emerge many years later after completion of the project. In addition, all neighbouring community is not affected by these adverse impacts at the same degree. This shows that the construction companies should focus on the management of adverse impacts which affect the community immediately and widely to reduce complains of the neighbours.

The results of SEM suggest that "prolonged closure of road spaces" and "detours" are the most significant adverse impacts under "traffic" category. This shows that the neighbouring community is affected intensively by the nuisances which cause them time loss and affect their daily routine negatively.

6. CONCLUSION

The building construction projects lead to many adverse impacts on the neighbouring community who is one of the external stakeholders. However, these adverse impacts are generally overlooked, in which turn may lead to conflicts and controversies. Therefore, the construction projects can confront with many problems, such as delays and cost overruns. This shows that development of a management system for neighbouring community is crucial. The first step of development of this system is the determination of the most important adverse impacts creating the nuisances on the neighbouring community. Consequently, in this study, a theoretical framework is developed based on adverse impacts of building construction and their categories.

The theoretical framework consists of five adverse impact categories, namely "damage to nature and built environment", "dust", "noise", "traffic" and "human society", and a total of 18 adverse impacts placed under these adverse impact categories. It is hypothesized that these five categories lead to nuisance. This framework is evaluated by using SEM analysis with a total of 266 questionnaires obtained from Northern Cyprus. This analysis verifies that these five categories have significant role in creation of nuisance.

Among these five categories, "damage to nature and built environment" is perceived as the most disturbing adverse impact category by the neighbouring community. Therefore, the construction companies should be aware of the public's concerns about the nature.

The other interesting finding of this study is the role of cultural heritage and conditions of the region in establishing of nuisances. The construction companies should establish different strategies in management of neighbouring community, since their concerns and demands can vary high among the different regions.

This study has some limitations as other studies. Firstly, although the model developed in this study can be used in different countries, the findings of this study should be considered as country specific. In order to identify the effects of adverse impacts in different countries, a comparative study should be conducted. Furthermore, the parameters identified in this study can be used as a benchmark to conduct similar studies in other project-based industries.

References

[1] Yang, J., Shen, G.Q., Ho, M., Drew, D.S., Xue, X., Stakeholder Management in Construction: An Empirical Study to Address Research Gaps in Previous Studies. International Journal of Project Management, 29(7), 900-910, 2011.

[2] PMI, A Guide to the Project Management Body of Knowledge (Pmbok® Guide), Newtown Square, Pennsylvania. Project Management Institute, 2013.

[3] Missonier, S., Loufrani-Fedida, S., Stakeholder Analysis and Engagement in Projects: From Stakeholder Relational Perspective to Stakeholder Relational Ontology. International Journal of Project Management, 32(7), 1108-1122, 2014.

[4] Loosemore, M., Managing Project Risks. The Management of Complex Projects: A Relationship Approach, S. Pryke and H. Smyth, Editors, Oxford, UK. John Wiley & Sons, 187-204, 2012.

[5] Burton, R.M., Obel, B., Strategic Organizational Diagnosis and Design: Developing Theory for Application, Massachusetts, USA. Springer Science & Business Media, 1998.

[6] Liu, B., Huo, T., Wang, X., Shen, Q., Chen, Y., The Decision Model of the Intuitionistic Fuzzy Group Bid Evaluation for Urban Infrastructure Projects Considering Social Costs. Canadian Journal of Civil Engineering, 40(3), 263-273, 2013.

[7] Communities and Local Government, A Plain English Guide to the Localism Act. 2011, Department for Communities and Local Government: London.

[8] Sev, A., How Can the Construction Industry Contribute to Sustainable Development? A Conceptual Framework. Sustainable Development, 17(3), 161-173, 2009.

[9] Balaban, O., The Negative Effects of Construction Boom on Urban Planning and Environment in Turkey: Unraveling the Role of the Public Sector. Habitat International, 36(1), 26-35, 2012.

[10] Ferguson, A., Qualitative Evaluation of Transportation Construction Related Social Costs and Their Impacts on the Local Community, M.Sc. Thesis,Department of Civil Engineering, 2012.

[11] Gangolells, M., Casals, M., Gassó, S., Forcada, N., Roca, X., Fuertes, A., A Methodology for Predicting the Severity of Environmental Impacts Related to the Construction Process of Residential Buildings. Building and Environment, 44(3), 558-571, 2009.

[12] Kolk, A., Pinkse, J., Stakeholder Mismanagement and Corporate Social Responsibility Crises. European Management Journal, 24(1), 59-72, 2006.

[13] Yang, J., Shen, G.Q., Ho, M., Drew, D.S., Chan, A.P.C., Exploring Critical Success Factors for Stakeholder Management in Construction Projects. Journal of Civil Engineering and Management, 15(4), 337-348, 2009.

[14] Li, T.H.Y., Ng, S.T., Skitmore, M., Conflict or Consensus: An Investigation of Stakeholder Concerns During the Participation Process of Major Infrastructure and Construction Projects in Hong Kong. Habitat International, 36(2), 333-342, 2012.

[15] Gilchrist, A., Allouche, E.N., Quantification of Social Costs Associated with Construction Projects: State-of-the-Art Review. Tunnelling and Underground Space Technology, 20(1), 89-104, 2005.

[16] Matthews, J.C., Allouche, E.N., Sterling, R.L., Social Cost Impact Assessment of Pipeline Infrastructure Projects. Environmental Impact Assessment Review, 50, 196202, 2015.

[17] Read, G.F., Vickridge, I., Social or Indirect Costs of Public Utility Works. Sewers: Replacement and New Construction: Replacement and New Construction, G.F. Read, Editor, Oxford. Elsevier, 339, 2004.

[18] Xueqing, W., Bingsheng, L., Allouche, E.N., Xiaoyan, L., Practical Bid Evaluation Method Considering Social Costs in Urban Infrastructure Projects. Management of Innovation and Technology, 2008. ICMIT 2008. 4th IEEE International Conference on. IEEE, 2008.

[19] Ormsby, C., A Framework for Estimating the Total Cost of Buried Municipal Infrastructure Renewal Projects Ms. ,Department of Civil Engineering and Applied Mechanics, 2009.

[20] Yuan, Q.-M., Cui, D.-J., Jiang, W., Study on Evaluation Methods of the Social Cost of Green Building Projects. Advances in Industrial Engineering, Information and Water Resources, Wang Jun, et al., Editors, Southampton. WIT press, 11, 2013.

[21] Xue, X., Zhang, R., Zhang, X., Yang, R.J., Li, H., Environmental and Social Challenges for Urban Subway Construction: An Empirical Study in China. International Journal of Project Management, 33(3), 576-588, 2015.

[22] Matthews, J.C., Allouche, E.N., Sterling, R.L., Social Cost Impact Assessment of Pipeline Infrastructure Projects. Environmental Impact Assessment Review, 50, 196-202, 2015.

[23] Nunes Vasconcelos, C., Development of a Decision Support Model for the Social Costs of Pipelines Renovation Projects, 2017.

[24] Çelik, T., Arayici, Y., Budayan, C., Assessing the Social Cost of Housing Projects on the Built Environment: Analysis and Monetization of the Adverse Impacts Incurred on the Neighbouring Communities. Environmental Impact Assessment Review, 77, 1-10, 2019.

[25] Çelik, T., Kamali, S., Arayici, Y., Social Cost in Construction Projects. Environmental Impact Assessment Review, 64, 77-86, 2017.

[26] Yu, W.D., Lo, S.S., Time-Dependent Construction Social Costs Model. Construction Management and Economics, 23(3), 327-337, 2005.

[27] Wang, Y., Han, Q., de Vries, B., Zuo, J., How the Public Reacts to Social Impacts in Construction Projects? A Structural Equation Modeling Study. International Journal of Project Management, 34(8), 1433-1448, 2016.

[28] Bianchini, F., Hewage, K., Probabilistic Social Cost-Benefit Analysis for Green Roofs: A Lifecycle Approach. Building and Environment, 58, 152-162, 2012.

[29] Watkins, L.H., Some Research into the Environmental Impact of Roads and Traffic. Transport Research for Social and Economic Progress. Proceedings of the Second World Conference on Transport Research. London, England, Gower Publishing Company, 1981.

[30] Bein, P., Monetization of Environmental Impacts of Roads, Victoria, British Columbia. Ministry of Transportation and Highways, 1997.

[31] Lee, E., Ibbs, C., Thomas, D., Minimizing Total Cost for Urban Freeway Reconstruction with Integrated Construction/Traffic Analysis. Journal of Infrastructure Systems, 11(4), 250-257, 2005.

[32] Jiang, Y., A Model for Estimating Excess User Costs at Highway Work Zones. Transportation Research Record: Journal of the Transportation Research Board, 1657(-1), 31-41, 1999.

[33] Mao, L.-Z., Zhu, H.-G., Duan, L.-R., The Social Cost of Traffic Congestion and Countermeasures in Beijing. Sustainable Transportation Systems@ sPlan, Design, Build, Manage, and Maintain. ASCE, 2012.

[34] Woskie, S.R., Kalil, A., Bello, D., Virji, M.A., Exposures to Quartz, Diesel, Dust, and Welding Fumes During Heavy and Highway Construction. AIHA Journal, 63(4), 447-457, 2002.

[35] Akan, Z., Yilmaz, A., Özdemir, O., Selvi, Y., Korpinar, M.A., P-436 - Noise Pollution, Psychiatric Symptoms and Quality of Life: Noise Problem in the East Region of Turkey. European Psychiatry, 27, Supplement 1, 1, 2012.

[36] Nunnally, J.C., Psychometric Theory, 2nd ed, New York. McGraw-Hill, 1978.

[37] Ding, L., Velicer, W.F., Harlow, L.L., Effects of Estimation Methods, Number of Indicators Per Factor, and Improper Solutions on Structural Equation Modeling Fit Indices. Structural Equation Modeling: A Multidisciplinary Journal, 2(2), 119-143, 1995.

[38] Westland, J.C., Lower Bounds on Sample Size in Structural Equation Modeling. Electronic Commerce Research and Applications, 9(6), 476-487, 2010.

[39] Bentler, P.M., Eqs 6 Structural Equation Program Manual, Encino, CA. Multivariate Software Inc., 2006.

[40] Ullman, J.B., Bentler, P.M., Structural Equation Modeling. Handbook of Psychology, 607-634, 2003.

[41] Hooper, D., Coughlan, J., Mullen, M.R., Structural Equation Modeling: Guidelines for Determining Model Fit. Electronic Journal of Business Research Methods, 6(1), 53-60, 2008.

[42] Hayduk, L., Cummings, G., Boadu, K., Pazderka-Robinson, H., Boulianne, S., Testing! Testing! One, Two, Three – Testing the Theory in Structural Equation Models! Personality and Individual Differences, 42(5), 841-850, 2007.

[43] McIntosh, C.N., Improving the Evaluation of Model Fit in Confirmatory Factor Analysis: A Commentary on Gundy, C.M., Fayers, P.M., Groenvold, M., Petersen, M. Aa., Scott, N.W., Sprangers, M.A.J., Velikov, G., Aaronson, N.K. (2011). Comparing Higher-Order Models for the Eortc Qlq-C30. Quality of Life Research, Doi:10.1007/S11136-011-0082-6. Quality of Life Research, 21(9), 1619-1621, 2012.

[44] Hu, L.-t., Bentler, P.M., Fit Indices in Covariance Structure Modeling: Sensitivity to Underparameterized Model Misspecification. Psychological methods, 3(4), 424, 1998.

[45] Zainudin, A., A Handbook on Sem: Structural Equation Model- Ling Using Amos Graphics 4th Edition ed, Kelantan. University Technology MARA Press, 2012.

[46] Dunn, S.C., Seaker, R.F., Waller, M.A., Latent Variables in Business Logistics Research: Scale Development and Validation. Journal of business logistics, 15(2), 145, 1994.

[47] Steenkamp, J.-B.E., Van Trijp, H.C., The Use of Lisrel in Validating Marketing Constructs. International Journal of Research in marketing, 8(4), 283-299, 1991.

[48] Garver, M.S., Mentzer, J.T., Logistics Research Methods: Employing Structural Equation Modeling to Test for Construct Validity. Journal of business logistics, 20(1), 33, 1999.

[49] Shen, L.Y., Tam, V.W.Y., Implementation of Environmental Management in the Hong Kong Construction Industry. International Journal of Project Management, 20(7), 535-543, 2002.

[50] Olander, S., Landin, A., Evaluation of Stakeholder Influence in the Implementation of Construction Projects. International Journal of Project Management, 23(4), 321-328, 2005.

[51] Falkenbach, H., Lindholm, A.-L., Schleich, H., Review Articles: Environmental Sustainability: Drivers for the Real Estate Investor. Journal of Real Estate Literature, 18(2), 201-223, 2010.

[52] Rowlinson, S., Cheung, Y.K.F., Stakeholder Management through Empowerment: Modelling Project Success. Construction Management and Economics, 26(6), 611-623, 2008.

Teknik Dergi, 2021 10629-10643, Paper 606

Acceleration Displacement Response Spectra for Design of Seismic Isolation Systems in Turkey

Aslıhan YOLCU[1]
Gülüm TANIRCAN[2]
Cüneyt TÜZÜN[3]

ABSTRACT

In this study, base shear and inelastic displacement limits of seismic isolation systems are presented through acceleration-displacement response spectra considering the ground motion and design provisions of the Turkish Building Seismic Design Code. A series of nonlinear response history analyses are performed using a combination of eight site-specific design spectra, six isolation systems having six different periods and five yield levels. As a result, eight spectra presented herein can be used for the preliminary design stage of seismic isolation systems in Turkey.

Keywords: Seismic isolation, non-linear response history analysis, acceleration-displacement response spectrum.

1. INTRODUCTION

The impact of two devastating earthquakes in Turkey in 1999 has revealed not only the existence of many structures that are not in compliance with seismic regulations but also nationwide belated implementation of advanced technologies for earthquake resistant design. Until 1999, application of isolation systems was limited to a few viaducts in Turkey. Istanbul Airport terminal building is the first building that has been reinforced by using isolators (friction pendulum bearings) at the time of the 1999 earthquakes. Over the past 19 years the number of applications has increased both for reinforcement of existing structures and for design of new structures. According to the database of Turkish Association for Seismic Isolation, as of 2018, number of base isolated structures including airports, hospitals, industrial structures as well as residential buildings are over 125 [1]. As the use of seismic

Note:
- This paper has been received on January 11, 2019 and accepted for publication by the Editorial Board on December 4, 2019.
- Discussions on this paper will be accepted by May 31, 2021.
- https://dx.doi.org/10.18400/tekderg.511798

1 Bogazici University, Kandilli Observatory and Earthquake Research Institute, Istanbul, Turkey - aslihanyolcu@hotmail.com - https://orcid.org/0000-0002-4096-1215

2 Bogazici University, Kandilli Observatory and Earthquake Research Institute, Istanbul, Turkey - birgore@boun.edu.tr - https://orcid.org/0000-0002-0535-5658

3 Gebze Technical University, Department of Civil Engineering, Kocaeli, Turkey - ctuzun@gmail.com https://orcid.org/0000-0003-2489-2640

isolation has become more widespread, seismic design criteria of isolation systems/isolated buildings have been accorded a separate chapter of the most recent Turkish Building Seismic Design Code (hereafter; TBSDR-2018) [2].

According to the provision in the most current seismic design codes (*e.g*. [2, 3]) isolation systems should be designed considering their nonlinear characteristics under maximum considered earthquake ground motion. Hysteretic behaviour of the seismic isolation systems can be defined in accordance with an equivalent linear system with secant stiffness and an equivalent viscous damping approach (*e.g.* [4, 5]). Effective stiffness, effective period and effective damping ratio are the major properties of an equivalent linear system. The major obstacle in implementing force-displacement hysteresis during the preliminary design of the seismic isolation system is that those properties are response displacement amplitude dependent and hence determining the acceptable displacement response values for the design requires an iterative procedure. In this context, as an alternative to equivalent linear analysis method, time history analysis method has also been practiced by many researchers for the design of isolation systems.

Looking through research in this direction, Park and Otsuka [6] applied the nonlinear response spectrum approach to investigate the optimal yield level of isolation systems for bridges. Tena-Colunga [7] proposed inelastic capacity design spectra of isolation systems for fixed yield strength and post yield stiffness. Ryan and Chopra [8] offered an alternative procedure for the iterative equivalent linear methods by reducing the parameters of equation of motion as presented in the next section. Whittaker and Jones [9, 10] proposed the concept of acceleration-displacement response spectra (ADRS). The concept is based on time history analyses of inelastic single degree of freedom (SDOF) oscillator to represent the nonlinear behaviour of the isolation systems. Properties of seismic isolation systems are independent of amplitude and can be selected by designers in the preliminary design process. Hence, the concept helps designers to develop quickly an estimate of the inelastic seismic demands of seismically isolated systems [11]. The concept has been applied to Christchurch-New Zealand, Vancouver-Canada, San Francisco Bay area-USA and Chile based on relevant codes [11] [12]. This concept has also been performed for two specific structures in Istanbul and Erzurum–Turkey following ASCE 7-10 [13] provisions [14]. However, none of the above studies considers different seismic input levels and site classes.

The main objective of this paper is to calculate and present the ADRS graphs considering the ground motion and building seismic design provisions of Turkey [2]. The ADRS approach is applied to high and moderate seismic zones of Turkey using different combinations of two earthquake ground motion levels (maximum considered earthquake: DD1 and design basis earthquake: DD2) and two site categories (stiff sites: ZC, and soil sites: ZD). For each category eleven pairs of ground motion recordings are selected from PEER-West2 [15] worldwide earthquake catalogue and linearly scaled to fit the pre-defined design spectra. A wide range of period (2-5 seconds) and yield strength ratio (5% -15% of W) are used to represent a broad envelope which includes not only the practical and applicable period and strength ratio levels but also extreme values of them for an isolation system. Results are discussed in the following parts of the paper. Finally, conclusions are drawn based on the obtained results. Hence, this study can be evaluated as a general approach for preliminary design of seismic isolation systems proposed for Turkey for the first time.

2. METHODOLOGY

Seismic isolation system can be idealized as a SDOF oscillator with a rigid mass on a single isolator. A bi-linear characterization of force-displacement hysteresis curve which can be considered as the envelope of isolation system response, is used for more practice-oriented representation of the nonlinear behaviour of a typical seismic isolation system in a horizontal direction as given in Fig. 1. In the figure, zero displacement force intercept (Q_d) expresses characteristic strength of a seismic isolator. F_y is the yield force. First and second slopes of the force-displacement graph are the elastic stiffness (k_1) and characteristic stiffness (k_2) of the seismic isolation system, respectively. In general applications, k_2 is taken as a fraction of k_1 [16]. Effective stiffness (k_e) is the secant slope of the simplified maximum response and is a function of maximum displacement.

Among all parameters defining the hysteresis loop, k_2 and Q_d are dependent only on material properties (*e.g.* shear modulus of rubber and yield shear stress of lead for lead rubber bearings) and geometric features (*e.g.* radius of friction pendulum systems, cross section area and thickness of lead rubber bearings) of isolation systems. Ryan and Chopra [8] simplified calculation of the equation of motion by utilizing $\omega = \sqrt{k_2 / m_t}$ and yield (or characteristic) strength ratio (Q_d /W), where W is the weight acting on the system.

The deformation history of the isolator $u(t)$, subjected to ground acceleration $\ddot{u}_g(t)$, is governed by the Equation 1;

$$\ddot{u}(t) + \omega^2 u(t) + (Qd\ /W)\ g\ z(t, k, u, \dot{u}) = -\ddot{u}_g(t), \tag{1}$$

where g is acceleration due to gravity and z represents the yielding history. Also, $\ddot{u}(t)$ shows isolator acceleration when m_t represents the mass. Moreover t, k, u and $\dot{u}$ are time, stiffness, displacement and velocity, respectively.

Computation of the ADRS graphs consists of two major steps: Preparation of horizontal ground motion excitations in compliance with TBSDR-2018 [2] and calculation of deformation history of a nonlinear SDOF system for various ground motion pairs with predefined hysteretic model parameters. Nonlinear time history analyses are performed for various post yield stiffness period of the isolation system (T), Q_d /W and k_2 combinations to obtain the displacement response. Finally, base shear transmitted to superstructure can be found out;

$$V_M = \frac{S_{ae}^{DD1}(T_M) W \eta_M}{R} \tag{2}$$

In the Equation 2, S_{ae}^{DD1} is 5% damped spectral acceleration parameter at effective vibration period (T_M) of the isolation system under DD1 ground motion level. T_M corresponds to the period where the maximum displacement of the isolation system is obtained. Earthquake force reduction factors (R) are tabulated in design codes for desired performance levels. Damping scaling coefficient (η_M) can be calculated by the following equation [2, 17, 18];

$$\eta = \sqrt{\frac{10}{5+\xi}} \tag{3}$$

where ξ is effective damping ratio and it shows the damping ratio as a percent. Parameters for calculation of ξ, vary depending on the type of the isolation system. In this research calculations follow straightforward design concept of friction type isolator.

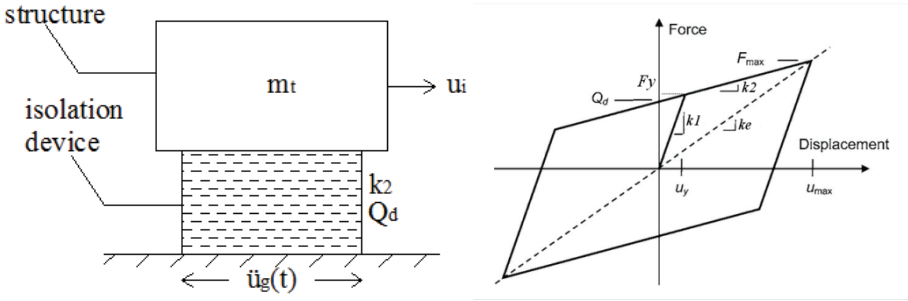

Figure 1 - (left) Seismic isolation system representation (adapted from Ryan and Chopra [8]); (right) Idealized bi-linear hysteretic response of isolators

3. GROUND MOTION REPRESENTATION

3.1. Selection of Hazard Levels

The capacity of an isolation system should be larger than strength and displacement demands of maximum considered earthquake ground motion (*e.g.* [2, 13]). Hence, in accordance with this performance expectation, nationwide distribution of the 5% damped spectral acceleration parameters at 1 s period (S_{a1}) is investigated. DD1 and DD2 (levels are provided from revised seismic hazard maps of Turkey [19, 20]. In order not to use the earthquake records which may contain near-field effects, the average values of S_{a1} are estimated in the regions at least 15 km from the fault. For the reference site condition, maximum S_{a1} value reaches 1.4 g at zero distance to major active faults and sharply decrease to 0.6 g at approximately 15-20 km away from the fault lines. It further decreases to 0.4 g at 45-50 km epicentral distance (see Fig. 2). For those regions, the hazard is diversified into two levels; moderate hazard level (MH) (0.4 g≤ S_{a1} (DD1) <0.5 g) and high hazard level (HH) (0.5 g≤ S_{a1} (DD1) <0.6 g). Aritmetic mean values of these ranges are used as representative values for calculating elastic response spectra. DD2 performance level is also required by the TBSDR-2018 [2] for calculating maximum shear forces transferred to structure above the isolator. Therefore, corresponding representative average S_{a1} values at DD2 level are chosen compatible with S_{a1} values at DD1 level as 0.30 g and 0.25 g for high and moderate hazard regions, respectively. Case numbers are assigned to eight hazard levels for easy follow-up of the results (Table 1).

Table 1 - Cases for ground motion levels formed by the combination of design, hazard and site categories

	Case1	Case2	Case3	Case4	Case5	Case6	Case7	Case8
Hazard Level	DD1	DD1	DD2	DD2	DD1	DD1	DD2	DD2
	MH	MH	MH	MH	HH	HH	HH	HH
Site Type	ZC	ZD	ZC	ZD	ZC	ZD	ZC	ZD

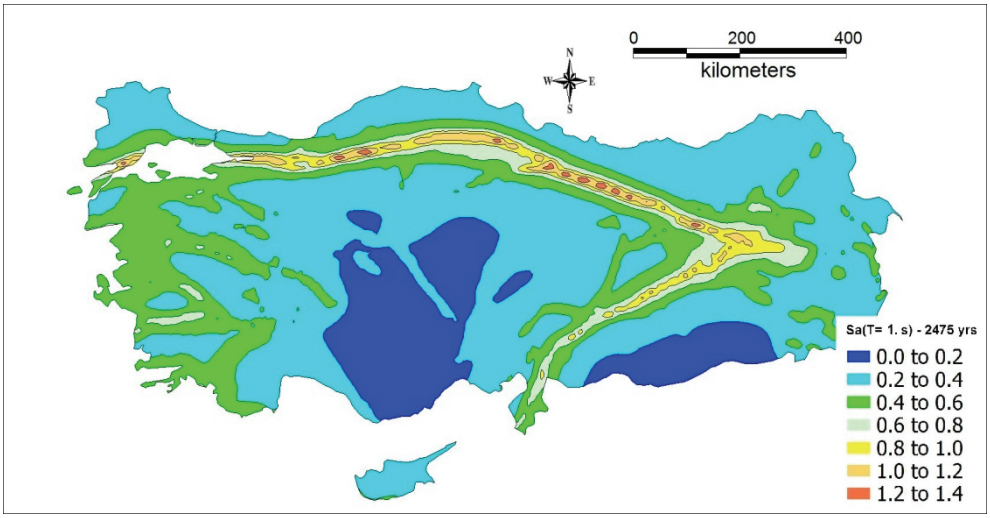

Figure 2 - Sa1 contour map at reference site conditions (Vs_{30}=760 m/s) for 2% probability of exceedance in 50 years exposure time (DD1 level) (redrawn after [19]).

3.2. Selection and Scaling of Strong Motion Recordings

30 strong motion recordings are selected from Pacific Earthquake Engineering Research (PEER) Center database [15]. The magnitude (Mw) range is assigned as 6.0 to 7.28 and style of faulting is strike slip considering the two major faulting zones exhibiting the highest seismic hazard in Turkey, the North Anatolian and the East Anatolian Fault Zone. The Distance (R_{jb}) between recording station and vertical projection of fault plane is chosen between 15 km - 60 km. List of earthquake ground motion pairs are tabulated in Table 2. 15 km distance is assumed to be the sufficient distance to neglect near field effects. Pulse-like recordings are ignored. Soil types belong to ZC (360 m/s $\leq V_{s30}<$ 760 m/s) and ZD (180 m/s $\leq V_{s30} <$ 360 m/s) categories. Eleven horizontal ground motion pairs are selected for each of eight groups which are formed by the combination of design, hazard and site categories. Maximum number of ground motion recordings from the same event for each of eight groups is three.

Following the provisions given in TBSDR-2018 [2] ground motion pairs are scaled linearly to match the 5% damped elastic horizontal design spectra. Geometric mean spectrum of selected ground motion pairs fit the horizontal elastic spectra between 1.4-7 s. period range. The same scaling factor is used for each horizontal component of a ground motion recording. The majority of scale factors takes values between 1-9. Two out of eleven scaling factors used for DD1/MH /ZC spectrum are as high as 14. Even though small scale values are recommended for linearly scaled ground motions, the effect of scaling factor and magnitude-distance bins on median nonlinear structural response for long period structures (T≤4 s) is found to be small and scale results are unbiased [21]. 5% damped elastic design spectra for DD1 and DD2 design levels are given together with elastic response spectra of selected and scaled recordings in Fig. 3.

3.3. Nonlinear SDOF Time History Analyses

Considering the bilinear hysteric model in Fig. 1, nonlinear time history analyses are performed for each scaled horizontal component of ground motions. PRISM software [22] is employed for the calculations. Assumptions and parameters for the calculation are as follows. Average k_2/k_1 is taken as 0.1 which is a common value for design purposes, provided by the manufacturers and obtained by prototype test results [17, 23]. Elastic damping ratio of bilinear oscillation is omitted, six periods of vibration (T = 2.0, 2.5, 3.0, 3.5, 4.0, 5.0 s) and five Q_d /W (5%, 7.5%, 10%, 12.5%, 15%) values are used. A total of 5280 nonlinear analyses are performed using 30 different bilinear hysteretic curves under the excitation of 11 different ground motion pairs produced for eight cases. Square root of the sum of the squares (SRSS) of two response displacements at period corresponding to the largest response displacement in horizontal direction, is calculated. The largest of the SRSS is considered as the maximum response displacement of the system excited with the scaled ground motion pair and averages of 11 ground motions pair are calculated.

4. RESULTS AND COMPARISON

The analyses results are presented as eight ADRS graphs which are shown in the following pages, in Figures. 4-7. ADRS graphs provide the base shear and displacement demands for the seismic isolation systems in the region under DD1 and DD2 design levels.

In general, base shear ratios change between 3.4 % -40% and maximum level is reached at DD1 level (Case 6). Furthermore, there is almost eight times difference in displacement (755 mm / 91 mm) among all cases. The shortest period (T=2 s) and the smallest yield ratio (5%) combination gives the maximum base shear ratio of the system. For the same yield level, system has the highest displacement capacity at the longest period. High deformation and high base shear values at above 4 s period (as in Case 5 and Case 6) are considered infeasible. ADRS graphs indicate that optimum isolation system period should be kept between 2.5-4 s considering the fact that the isolation system with a period of 2 s is not effective in terms of spectral acceleration reduction in the superstructure. Regarding the long period range, 5 s period may cause re-centering problems and may result in unfeasible displacement demands. Upper and lower bounds of displacement and base shear values are tabulated in Table 3.

Case 3 (Fig. 4) and Case 6 (Fig. 7) show the response of the system under two extreme ground motion levels and is worth comparing. Maximum base shear ratio is 40% and 12% under the excitation of the highest (Case 6) and the lowest levels (Case 3) of ground motion, respectively. Displacement range is between 217 mm and 755 mm with an average value of 190 mm between 2.5 and 4 s. for the Case 6. Displacement range is limited to 92 mm - 237 mm for Case 3. There is a similar proportional reduction in minimum base shear ratios, from 10% to 3.5%. There is almost 3.3 times difference between the maximum base shears of Case 3 and Case 6. The maximum displacement value of Case 3 is nearly equal to the minimum displacement of Case 6. The effect of yield levels which are above 10% is not significant on ADRS chart in Case 3 when the period is 3 s.

Case 5 and Case 6 portray the change in the response of the system when the soil type switches from ZC to ZD. At the stiff site, (Case 5) maximum and minimum base shear values are 25% less than those at softer soil site (Case 6). When period becomes longer at the stiff site, the effect of yield level increases and horizontal displacement lines are elongated. When

the soil is stiffer the effect of period and yield level both diminish. Displacement demand at soil site is 170 mm larger than it is at the stiff site. Similarly, difference in maximum displacement demand is not less than 100 mm at ADRS graphs under moderate hazard conditions (Case 3 and Case 4) as well. Consequently, at soft soil, seismic isolation systems with high fundamental period necessitate very high displacement capacity.

Table 2. Earthquake ground motion used in this study.

#	Event	Mw	Station	Rjb (km)	Soil Type
1	Düzce, Turkey 1999	7.14	LAMONT 362	23.41	ZC
2	Hector Mine 1999	7.13	ABY	41.81	ZC
3			JNT	50.42	ZC
4			29P	42.06	ZC
5	Chi-Chi, Taiwan-04	6.2	CHY024	19.67	ZC
6			CHY006	24.58	ZC
7			CHY029	25.75	ZC
8			CHY101	21.61	ZD
9			CHY030	30.46	ZD
10			CHY028	17.63	ZC
11	Darfield, New Zealand 2010	7	HVSCS	24.36	ZC
12			CSHS	43.6	ZC
13			OXZ	30.63	ZC
14			PPHS	18.73	ZD
15			CHHC	18.40	ZD
16			PRPC	24.55	ZD
17			HVS	24.36	ZC
18			CCCC	19.89	ZD
19			PRPC	24.55	ZD
20	Landers 1992	7.28	FVR	25.02	ZC
21			FHS	26.84	ZD
22	El Mayor-Cucapah, Mexico 2010	7.2	CISWSHN	31.79	ZC
23			E11	15.36	ZD
24			TAM	25.32	ZD
25			CHI	18.21	ZD
26			CXO	19.12	ZD
27	Imperial Valley-06 1979	6.53	DLT	22.03	ZD
28			E12	17.94	ZD
29	Superstition Hills-02 1987	6.54	ICC	18.20	ZD
30	Victoria, Mexico 1980	6.33	CHI	18.53	ZD

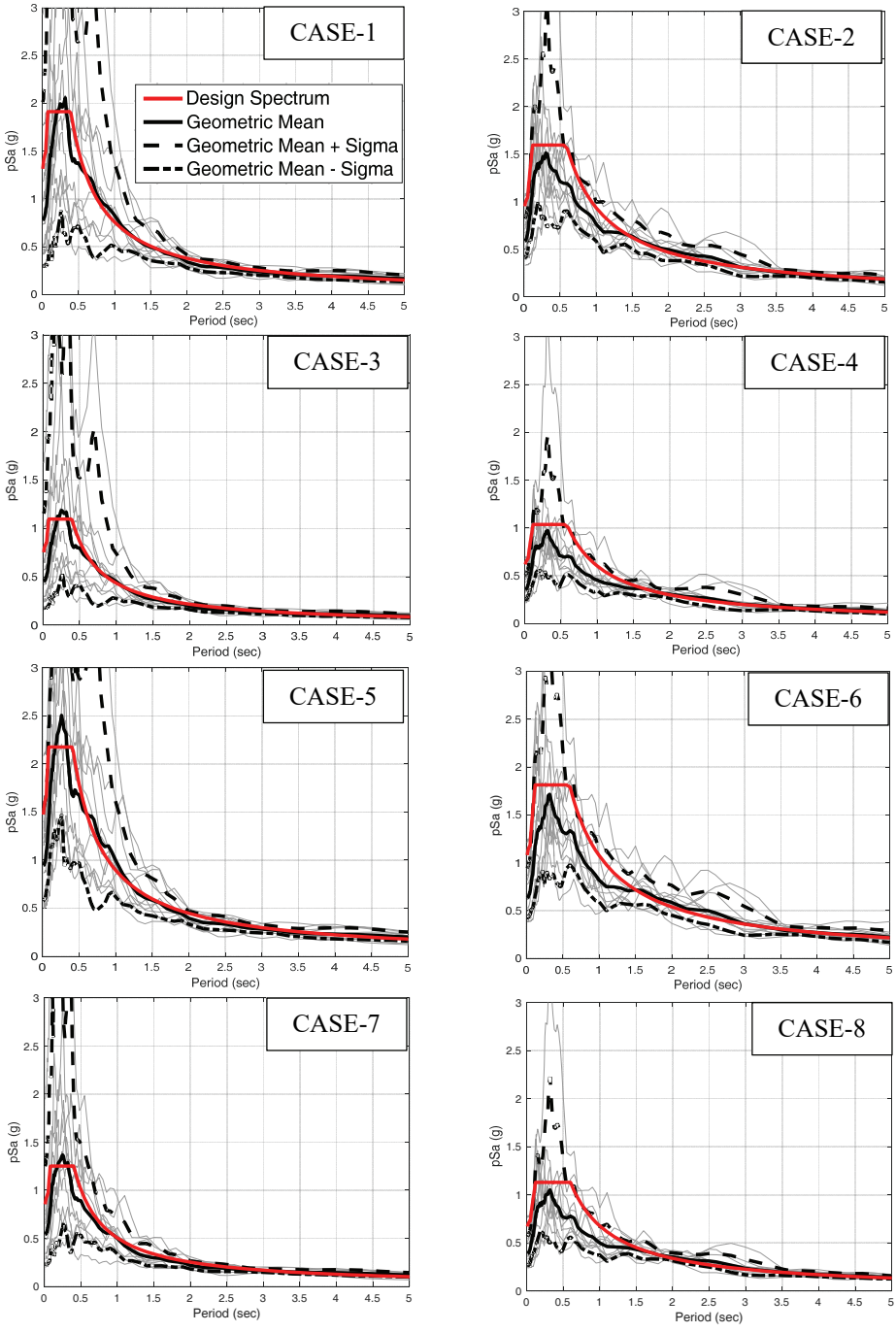

Figure 3 - Target design spectrum and spectra for scaled ground motions for Case 1-8

Fig. 7 shows the response of system for the Case 8. Base shear is around 20% and 5.7% for the smallest and largest period and yield ratio pairs, respectively. Displacements are between 105 mm and 409 mm. The effect of yield levels which are above 12.5% is not significant on ADRS chart when the period is 4 s. On the other hand, difference in yield level dominates the responses of the system at lower periods; 2.5 and 3 s.

Comparison of ADRS graphs for Case 6 and Case 8 reveals that, for the same soil condition, base shear imposed to superstructure under DD2 level is approximately half of that is imposed by DD1 level.

Table 3 - Upper and lower bounds of displacement and base shear

CASE #	**1**	**2**	**3**	**4**	**5**	**6**	**7**	**8**
Max. Displacement (mm)	494	647	237	341	595	**755**	274	409
Min. Displacement (mm)	166	176	92	95	226	217	91	105
Max. Base Shear (V/W)	0.25	0.33	0.12	0.18	0.31	**0.40**	0.14	0.21
Min. Base Shear (V/W)	0.07	0.09	0.03	0.05	0.08	0.11	0.04	0.06

Isolation system parameters of Sabiha Gökçen International Airport (SGIA) Terminal building and of two seismically isolated hospital buildings which are Okmeydanı Training and Research Hospital (OTRH) and Marmara University Başıbüyük Training and Research Hospital (BTRH) in Istanbul are compared with those calculated in this study. Triple-friction pendulum devices are used in SGIA Terminal building [24] and OTRH. Lead rubber bearings, sliding bearings and the pot bearing units are used in BTRH [17]. Implementation techniques of the isolators, main parameters which are taken into consideration and the other information for BTRH explained in related references [17, 25, 26].

Table 4 - Design parameters of seismically isolated structures in Istanbul, Turkey. Design parameters for hospitals (OTRH and BTRH) are provided from Bahadır Şadan (personal communication, 2018) and Sabiha Gökçen International Airport (SGIA) design parameters are provided from Zekioglu et al[19]

		OTRH	BTRH	SGIA
Distance to Fault (km)		>15	>15	>15
ADRS Chart		Case 2	Case 6	Case 5
Yield Strength Ratio (%)		10	15	13
Isolation Period (s.)		4	3	3
Displacement Demand (cm)	actual design	45	38	27-30
	this study	40	34	29

Comparison is tabulated in Table 4. For the given period and yield strength ratio the displacement values of ADRS graphs are consistent with the values used in the actual design, however a slight underestimation by ADRS graphs is observed. The boundary conditions which restrict structural design may sometimes lead to the extreme solutions of optimum area given in ADRS graphs. For instance, displacement demand needs to be increased due to the criterion of keeping the base shear force below a certain value. In this respect, it should be emphasized that the main argument in this research is not to precisely estimate the displacement demand but rather to determine the design solution envelope more quickly and effectively for preliminary phase.

5. CONCLUSION

In this paper, a parametric study is performed to determine the ideal parameters of seismic isolation systems at preliminary design phase. As generally accepted, bilinear force-displacement hysteresis curve is assumed to represent nonlinear behaviour of a typical seismic isolation system in a horizontal direction. A series of nonlinear time history analyses are performed for six post-elastic periods and five yield strength ratios of seismic isolation systems under the excitation of eleven ground motion pairs produced for eight cases. Each case is formed by the combination of design, hazard and site categories. Base shear is calculated through the average maximum displacement response. Finally, for the given yield strength ratio and isolation period, weight independent base shear versus displacement relationship is represented in ADRS graphs to provide optimal area for the preliminary design of the isolation systems. Graphs can be used for all typical seismic isolation systems since the calculations are solely based on post-elastic periods and yield levels.

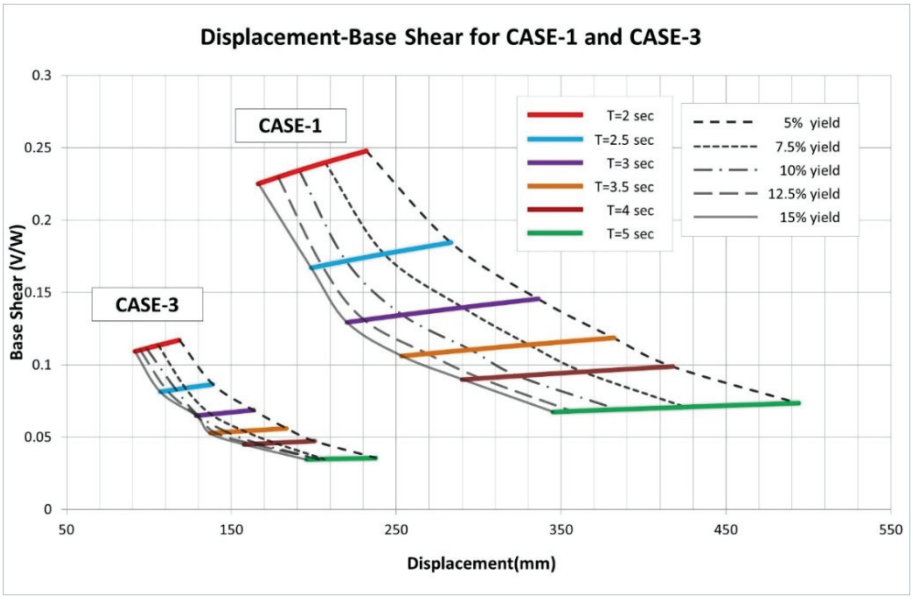

Figure 4 - Acceleration Displacement Response spectra for the Case1 and Case3

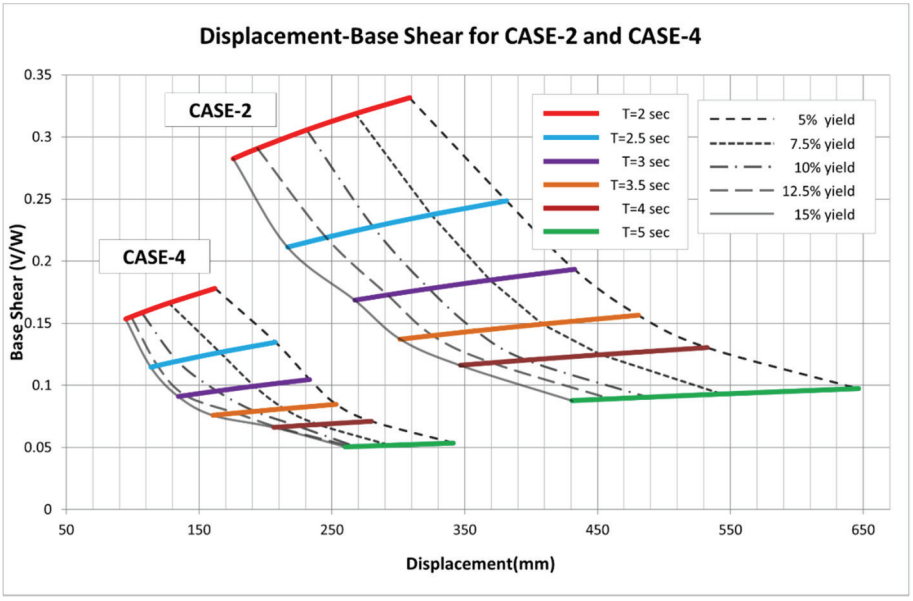

Figure 5 - Acceleration Displacement Response spectra for the Case2 and Case4

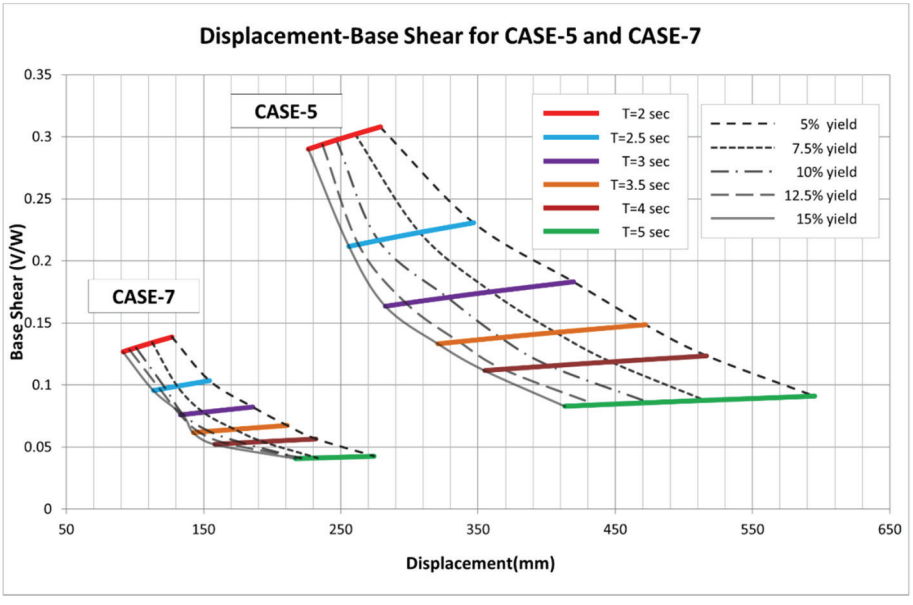

Figure 6 - Acceleration Displacement Response spectra for the Case5 and Case7

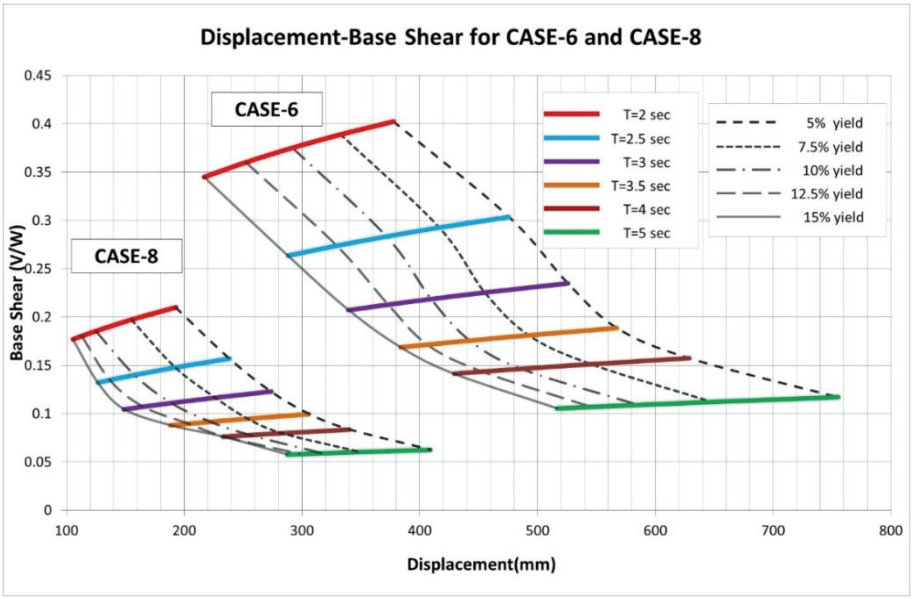

Figure 7 - Acceleration Displacement Response spectra for the Case6 and Case8.

It is worth noting that, only for Case 2; at T=3 s period, displacement responses are almost constant when yield levels are equal to or higher than 10%. In further studies, analyses might be repeated using different ground motion data set to see if such an issue is raised by the excitation characteristics of the ground motion.

Furthermore, it should also be kept in mind that, ADRS graphs presented in this study are valid under non-pulse far field ground motion excitation and may not be realistic at sites very close to active faults, particulary when the directionality effect is dominant in the ground motion recordings. Hence, this study can be expanded considering pulse-like ground motion sets.

Further studies can be focused on more detailed analysis with specific type of isolators such as high damping rubber bearing (HDRB), lead rubber bearing (LRB) and friction pendulum system (FPS) types.

Symbols

F_y Yield force

g Acceleration of gravity

k Stiffness

k_1 Elastic stiffness

k_2 Post-elastic stiffness

k_e	Effective stiffness
m_t	The total mass above the isolation device
M_w	Moment magnitude
Q_d	Strength on yield force
R	Earthquake force reduction factor
R_{jb}	Joyner and Boore distance
S_{ae}^{DD1}	Lateral spectral acceleration for 5% damping at maximum ground motion level (g)
S_{a1}	Hazard map spectral acceleration coefficient for 1 second period
T	Period
t	Time
T_M	The effective vibration period of seismically isolated building at maximum displacements
u	Displacement
u_{max}	Maximum deformation
u_y	Yield deformation
$u(t)$	Deformation of seismic isolation system
ü$_g(t)$	Ground acceleration
$\dot{u}$	Velocity of seismic isolation system
V_M	Base shear which is transmitted to superstructure
V_{s30}	The average shear wave velocity of top 30 meter depth.
W	System weight
z	Yielding history
η_M	Damping scaling coefficient
ξ	Damping ratio
ω	Circular frequency
ADRS	Acceleration-Displacement Response Spectra
DD1	Maximum Considered Earthquake
DD2	Design Basis Earthquake
HH	High hazard
MH	Moderate hazard
SDOF	Single degree of freedom
SRSS	Square root of the sum of the squares
TBSDC	Turkish Building Seismic Design Code
PEER	Pacific Earthquake Engineering Research

Acknowledgements

This study is supported by Boğaziçi University Research Fund Grant Number 13144. The subject matter is the MSc thesis of the first author. We thank to Mine B. Demircioğlu-Tümsa for preparing Fig.2.

References

[1] TASI, Turkish Association for Seismic Isolation. https://did.org.tr/, 2018.

[2] TBSDC-2018, Turkish Building Seismic Design Code, Disaster and Emergency Management Authority, Ankara, 2018.

[3] IBC 2015, International Building Code, International Code Council (ISBN: 978-1-60983-468-5), 2015.

[4] Anderson, E., and Mahin S. A., Displacement-based design of seismically isolated bridges, Proc. of the Sixth U.S. National Conference of Earthquake Engineering, Earthquake Engineering Research Institute, Oakland, California, 1998.

[5] Dicleli, M., Buddaram S., Comprehensive evaluation of equivalent linear analysis method for seismic-isolated structures represented by SDOF systems, Engineering Structures, Vol.29, 1653-1663, 2007.

[6] Park, J., and Otsuka, H., Optimal Yield Level of Bilinear Seismic Isolation Devices, Earthquake Engineering and Structural Dynamics, Vol. 28:941-955, 1999.

[7] Tena-Colugna A., A new method for the seismic design of structures with bilinear isolators using inelastic spectra, 12th World Conference on Earthquake Engineering, Auckland, New Zealand, 2000.

[8] Ryan, K. L., and Chopra A. K., Estimation of Seismic Demands on Isolators Based on Nonlinear Analysis, Journal of Structural Engineering,130 (3):392-402, ASCE, 2004.

[9] Whittaker, D., Jones, L., Design spectra for seismic isolation systems in Christchurch, New Zealand, NZSEE Conference, New Zealand, 2013.

[10] Whittaker, D., Jones, L., Displacement and acceleration design spectra for seismic isolation systems in Christchurch, New Zealand, NZSEE Conference, New Zealand, 2014.

[11] Jones, L., Aiken, I., Black, C., Whittaker, D., Design displacement and acceleration spectra for seismic isolation systems: New Zealand, San Francisco and Vancouver, 14th World Conference on Seismic Isolation, Energy Dissipation and Active Vibration Control of Structures, San Diego, CA USA, 2015.

[12] Jones, L., Aiken, I., Black, C., Whittaker, D., Ratemales, R., Boroschek, R., An improved design methodology for seismic isolation systems using nonlinear response spectra, 16th World Conference on Earthquake Engineering, Santiago, Chile, 2017.

[13] ASCE 7-10. Minimum design loads for buildings and other structures, American Society of Civil Engineers, Reston, 2010.

[14] Jones, L., Aiken, I., Black, C., Whittaker, D., Şadan, B., Nonlinear response spectra for isolation system design: case studies in Turkey, California and New Zealand, 3 TDMSK, Izmir, Turkey, 2015.

[15] NGA-West 2 Database (NGA-West2, 2015). Pacific Earthquake Engineering Research Center (PEER), University of California, Berkeley, USA(http://peer.berkeley.edu/ngawest2/).

[16] Naeim, F., and Kelly J. M., Design of Seismic Isolated Structures: From Theory to Practice, John Wiley & Sons, Chichester, UK, 1999.

[17] Erdik. M., Ülker, Ö., Şadan, B., Tüzün, C., Seismic isolation code developments and significant applications in Turkey, Soil Dynamics and Earthquake Engineering 115, 413-437, 2018.

[18] Eurocode 8, Design provisions for earthquake resistance of structures, ENV-2003, CEN, Brussels, 2003.

[19] Akkar, S., Azak T., Çan T., Çeken U., Demircioğlu Tümsa M. B., Duman, T. Y., Erdik, M., Ergintay, S., Kadirioğlu, F. T., Kalafat, D., Kale, Ö., Kartal R. F., Kekovalı K., Kılıç T. S., Zülfikar Ö., Evolution of seismic hazard maps in Turkey, Bulletin of Earthquake Engineering, Vol.16, Issue 8, pp 3567-3570, 2018.

[20] New Probabilistic Seismic Hazard Map of Turkey (TDTH, 2016) (https://tdth.afad.gov.tr/).

[21] Luco, N., and Bazzurro P. Does amplitude scaling of ground motion records result in biased nonlinear structural drift responses?, Earthquake Engineering and Structural Dynamics; 36 Issue13: 1813–35., 2007.

[22] Prism for Earthquake Engineering Software 2.0.1 (PRISM) 2018, Earthquake Engineering Research Group, Department of Architectural Engineering, INHA University, Incheon, South Korea, 2018.

[23] Erdik M., Seismic Isolation for Buildings, 6th National Conference on Earthquake Engineering, Istanbul, 16-20 October 2007.

[24] Zekioglu, A., Darama, H., Erkuş, B. Performance-based seismic design of a large seismically isolated structure: Istanbul Sabiha Gokcen International Airport Terminal Building., Proc. of the SEAOC 2009 Convention, San Diego, California, September 23-26, 2009.

[25] Sucuoğlu, H., Kubin, J., Kubin, D., Özmen, A., Şadan, B., Eroğlu, E., Seismic retrofit of an existing multi-block hospital by seismic isolators, 15WCEE Lisboa, Portugal, 2012.

[26] Sartori, M., Maraston, S., Zivanovic, I., Seismic retrofitting of the Marmara Başibüyük University Hospital in Istanbul, 16WCEE, Santiago Chile, 9-13 January 2017.

Teknik Dergi, 2021 10645-10673, Paper 607

An Effective Improved Multi-objective Evolutionary Algorithm (IMOEA) for Solving Constraint Civil Engineering Optimization Problems

Ali MAHALLATI RAYENI[1]
Hamed GHOHANI ARAB[2]
Mohammad Reza GHASEMI[3]

ABSTRACT

This paper introduces a new metaheuristic optimization method based on evolutionary algorithms to solve single-objective engineering optimization problems faster and more efficient. By considering constraints as a new objective function, problems turned to multi objective optimization problems. To avoid regular local optimum, different mutations and crossovers are studied and the best operators due their performances are selected as main operators of algorithm. Moreover, certain infeasible solutions can provide useful information about the direction which lead to best solution, so these infeasible solutions are defined on basic concepts of optimization and uses their feature to guide convergence of algorithm to global optimum. Dynamic interference of mutation and crossover are considered to prevent unnecessary calculation and also a selection strategy for choosing optimal solution is introduced. To verify the performance of the proposed algorithm, some CEC 2006 optimization problems which prevalently used in the literatures, are inspected. After satisfaction of acquired result by proposed algorithm on mathematical problems, four popular engineering optimization problems are solved. Comparison of results obtained by proposed algorithm with other optimization algorithms show that the suggested method has a powerful approach in finding the optimal solutions and exhibits significance accuracy and appropriate convergence in reaching the global optimum.

Keywords: Evolutionary algorithm, single objective optimization problem, multi objective optimization algorithm, constraint handling, constraint optimization, civil optimization problem.

Note:
- This paper has been received on March 18, 2019 and accepted for publication by the Editorial Board on October 22, 2019.
- Discussions on this paper will be accepted by May 31, 2021.
- https://dx.doi.org/10.18400/tekderg.541640

1 University of Sistan and Baluchestan, Civil Engineering Department, Zahedan, Iran - a.mahallati.r@pgs.usb.ac.ir - https://orcid.org/0000-0002-0259-8849

2 University of Sistan and Baluchestan, Civil Engineering Department, Zahedan, Iran - ghohani@eng.usb.ac.ir - https://orcid.org/0000-0001-9808-4596

3 University of Sistan and Baluchestan, Civil Engineering Department, Zahedan, Iran - mrghasemi@eng.usb.ac.ir - https://orcid.org/0000-0002-7014-6668

1. INTRODUCTION

Optimization is one of the most practical mathematical methods in all fields of science, especially engineering and industrial problems. Regarding the wide range of optimization issues, various categories have been made to divide them into certain divisions, linear and nonlinear, constrained and unconstrained, convex and concave, single-objective and multi-objective categories and so on.[1]. Among them, nonlinear constrained problems are the most difficult issues to tackle and several methods have been proposed for dealing with them. In single-objective optimization problems, designers' goal is finding a vector of design variables that will provide the best possible design. This vector is meant to give global minimum or maximum response to the designer's problem.

Researchers always have been curios to find an appropriate method to detect the best solutions for optimization problems, an accurate method with an acceptable speed. Although gradient-based methods often provide acceptable responses, they may easily trapped in a local optimum point [2]. Thus, after introducing heuristic and metaheuristic methods by researchers, they were greatly welcomed by scientists due to their high speed and convenient accuracy in finding optimal solutions against gradient methods. Extensive activities have been undertaken to solve optimization problems by metaheuristic methods, and so, various methods have been proposed. After the introduction of the genetic algorithm by Holland in 60's, the use of heuristic and metaheuristic methods for solving optimization problems flourished [3]. Kennedy and Eberhart in 1995, by proposing Particle Swarm Optimization (PSO) algorithms, solved some continuous optimization problems [4]. Atashpaz and Lucas also introduced the Imperialist Competitive Algorithm in 2007 by modeling the performance of the imperialists against their Colonies in real world [5]. Among recent optimization algorithms introduced, the Teaching-Learning Based Optimization Algorithm, built bassed on teacher and student behavior in classroom, was presented by Rao and Patel in 2012 [6]. One can also refer to the Ghaemi and Feizi researches that introduced the Forest Optimization Algorithm to solve continuous nonlinear optimization problems [7]. In 2015, Rezaee proposed the Brainstorm optimization algorithm based on the human brain's ability to search for solutions for everyday life issues [8]. Also in the same year, Dai et al. proposed a modified genetic algorithm to optimize Stiffness optimization of coupled shear wall structure[9]. Mirjalili and Lewis adapted Whale Optimization Algorithm in 2016 inspired by the social behavior of the humpback whales and solved various optimization problems [10]. Varaee and Ghasemi introduced a new algorithm based on ideal gas molecular movement[11] .Tabari and Ahmad also proposed the Electro-Search Algorithm in 2017 based on the movement of electrons through the orbits around the nucleus of an atom [12]. And many other researchers focused their attention to introduce new algorithms[13-15].

Many scholars have focused their research on improving the performance of heuristic and metaheuristic algorithm methods in dealing with constrained problems. generally, modification of optimization methods are divided into five main categories, including the penalty function, combining of algorithms, separation of constraints and goals, using special operators, and repairing the algorithm. For modification by combination of many algorithms, researchers attempted to combine different features of existing algorithms and use the strengths of each one to improve the overall performance of the method [16]. The proposed technique was then used in a research by the Zhang and Kucukkoc combines Artificial Intelligence and parallel computing [17]. Also research by Chou et al., Tosta et al., Araghi et al., all utilizing the combination of genetic algorithm and fuzzy logic [18-20]. As well as Li et al. used hybrid algorithm which is achieved

by combination of genetic algorithm and particle swarm optimization. And many other researchers modified existed algorithms by this technique.

The second popular task which extensively used to enhance the performance of heuristic and metaheuristic algorithms is the Penalty Functions. It is claimed that by applying various methods of penalizing such as static, dynamic or adaptive penalties and etc., this technique eliminates constraint violated samples from the procedure, thereby increases the efficiency of the method by reducing the computational cost [16]. Yang et al., embedded a weighted penalty function to sequential optimization method in order to improve the performance of the algorithm in the estimation of set density [21]. Dong and Zhu optimize the search pattern in an algorithm in a scattered space by combining an accelerated iteration hard thresholding (AIHT) with analytical penalty methodology[22]. In 2016, Kia used e-exact penalty function to solve problems with inequality constraints [23].

One of the most practical techniques been used for improving the performance of optimization algorithms predominantly, is the separation of objectives and constraints, in which the problem is solved by examining the constraints situation and also limitations of the problem. Due to the particular action given to equations and constraints, this method is also called constraint control, has a huge impact on the performance of the algorithm, especially increasing the speed of computing and reducing its volume [16]. Tang et al. at the selection stage in the Genetic Algorithm, with the ranking of individuals based on the frequency of violations in constraint problems, succeeded in increasing the efficiency of the genetic algorithm [24]. Long in order to solve multi-objective constraint problems, at first divided them into several sub-problems, then prioritized them with a multi-objective genetic algorithm [25]. Garcia et al. investigated the effects of conventional constraints control on a genetic algorithm [26].

With the progress of technology and exploration of new fields in science, scientists also encountered new optimization problems in which they had more than one objective function. Therefore, in order to optimize these problems which contain several objective functions; multi-objective optimization algorithms were developed. Multi-objective optimization methods trying to find values of design variables that are applicable in the constraints and optimize the objective function at the same time. Generally, it is not possible to obtain the best value for all objectives simultaneously, and there will be no definite answer which all the objective functions be satisfied. In multi-objective optimization problems, unlike single-objective problems, generally a unique vector of design variables cannot be suggested because an absolute optimal solution does not exist in such issues. In some cases, these objective functions are opposite to each other, so by minimizing one of them, the other one will deteriorate. Therefore, there is no certain optimal answer that optimizes all the objective functions simultaneously, and generally facing many optimal responses which satisfy problem constraints with no superiority against each other. In multi-objective problems, always there are a number of optimal answers that are known as Pareto optimal solutions or Pareto Front, which are the main difference of single-objective and multi-objective optimization problems. Once the Pareto answers is determined for a problem, the user is able to decide on choosing the best answer based on his preferences and needs. Meanwhile, evolutionary algorithms with their proper function in finding solution of optimization problem were considered more than other methods. Many of the optimization problems in the engineering field are multi-objective optimization problems in which there are several objective functions that needed to be optimized simultaneously[27].

Over the past decades, several heuristic and metaheuristic methods have been proposed for solving multi-objective optimization problems. The primary reason, is to find better Pareto-optimal solutions with least runs. Using stochastic techniques made it much easier to find local optima avoidance and gradient-free mechanism that made them applicable to real world problems[28]. Some of the well-known optimization techniques are: Non-dominated Sorting Genetic Algorithm 2 (NSGA-2) [29-32], Multi-objective Particle Swarm Optimization (MOPSO)[33, 34]., and Multi-objective Evolutionary Algorithm based on Decomposition (MOEA/D)[35].

As mentioned, constraint handling method is one of the applicable methods for improving the performance of evolutionary algorithms. In 2000, Coello Coello by considering the constraints of constraint optimization problem as an objective function, solved the optimal solution using multi-objective evolutionary algorithms [36]. In 2016, Segura et al. also categorized two-objective optimization methods for solving single-objective problems [37].

In this paper, by using the concepts of objectives and constraints separation, multi-objective evolutionary algorithms, efficient selection strategy and elitism, an effective improved multi-objective evolutionary algorithm (IMOEA) is introduced for solving constraint industrial single-objective problems. In order to evaluate the performance of this method, some benchmark problems of the CEC2006 were solved and compared with other methods. Also, in order to innovate and enhance the function of the proposed method, normal mutation and uniform crossover operators are selected for producing the next generation and their performance is also examined by other known methods. Due to the direct effect of mutation and crossover operators on the performance of evolutionary algorithms, the percentage of interference of these two operators is considered dynamically according to the number of iterations carried. Thus, regarding the feasible solutions, a certain percentage of those individuals (elites) are also stored and transferred to the next iteration. After achieving acceptable result for mathematical problems, some popular engineering benchmark problems which is the main contribution of this research is solved and compare to previous studies.

2. BASIC DEFINITIONS IN MULTI-OBJECTIVE OPTIMIZATION

In multi-objective optimization, several objective functions are treated simultaneously and defined in the general model as follows:

$$\begin{aligned} &\text{Minimize } \mathrm{F}(X) = (\mathrm{f}_1(X), \mathrm{f}_2(X), \mathrm{f}_3(X), \dots) \\ &\text{Subject to: } \begin{cases} \mathrm{h}_\mathrm{i}(X) = 0, & \mathrm{I} = 1, 2, \dots, \mathrm{m}_1 \\ \mathrm{g}_\mathrm{j}(X) \leq 0, & \mathrm{j} = 1, 2, \dots, \mathrm{m}_2 \end{cases} \end{aligned} \tag{1}$$

where $\boldsymbol{X}$ is an n-dimensional vector of design variables and $f_i(X)$ are the objective functions. $g_j(X)$ and $h_i(X)$ are the design constraints known as the inequality and equality constraints, respectively. m_1 and m_2 are, in order, the number of equality and inequality constraints.

Generally, multi-objective optimization problems are converted to a single-objective optimization problem by a scalar function, in particular when objectives are in conflict with each other. They will be then solved by single-objective optimization algorithms. After introducing of Multi-Objective Genetic Algorithm (MOGA) in 1993 by Fonseca and Fleming, based on genetic

algorithm, multi-objective optimization algorithms were used for solving multi-objective problems. This algorithm gains premature convergence due to the adoption of a very large answer space in its process [38]. So, in 1994, Srinivas and Deb improved the MOGA algorithm by ranking the answers and introduced the Non-dominated Sorting Genetic algorithm (NSGA) [39]. Since then, Deb et al. in 2000, introduced the second version of the NSGA, which obviated the problems in the first version (NSGA-I) which was including high computational complexity, lack of elitism, and the need to specify the subscription parameter [40]. In each multi-objective optimization problem, finding a set of trade-offs optimal solutions is very important. These solutions practically are the answer to the multi-objective optimization in a variety of situations called the Pareto solution set or Pareto Front, named after Vilferedo Pareto[41]. The goal of multi-objective optimization algorithms is to find the Pareto Front, which enables user to extract the optimal answer according to existing situation. The main feature of The Pareto Front is that there is no better answer than this Pareto solution points set in the problem and in other word Pareto Front solutions are not dominated by any other answer. Thus, the Pareto front uses the non-dominated concept to form the solutions of any problem. In other word, A dominates B, if A has at least one objective function better than B and is not worse in other objectives. The non-dominant answer is called Pareto-optimal.

3. METHOD

Before explaining the method outlined in this paper, several basic descriptions that have been used to solve problems are introduced.

3.1. Basic Definitions

The general form of the single-objective optimization problem with equality and inequality constraints is shown as:

$$Minimize\ f(X)$$

$$Subject\ to: \quad \begin{cases} h_i(X) = 0, & i = 1, 2, \dots, m_1 \\ g_j(X) \leq 0, & j = 1, 2, \dots, m_2 \\ L_k \leq x_k \leq U_k, & k = 1,2, \dots m_3 \end{cases} \tag{2}$$

where X is a n-dimensional vector of design variables and $f(X)$ is the objective function which in this case minimization of $f(X)$ is the objective of optimization. $g_j(X)$ and $h_i(X)$ are constraints of optimization problem and also known as inequality and equality constraints, respectively.

To reduce the complexity for solving single-objective problems, due to increase the accuracy and speed of solving such problems, following equation for transforming constraints to objectives are considered.

For equality constraints:

$$v_{1i}(x) = max(|h_i(x) - \sigma|, 0) \quad i = 1,2,3 \dots, m_1 \tag{3}$$

And for inequality constraints:

$$v_{2i}(x) = max(g_i(x), 0) \quad i = 1,2,3 \dots, m_2 \tag{4}$$

Finally, the objective function derived from the constraints is the sum of above-mentioned objectives:

$$v = \sum_{1}^{m_1} v_{1i}(x) + \sum_{1}^{m_2} v_{2i}(x) \tag{5}$$

where, σ is a positive value used for equal constraints in order to convert them to inequality constraints. Now, any constrained single-objective problem can be easily turned into an unconstrained bi-objective optimization.

$$F(X) = \big(f(x), v(x)\big) \tag{6}$$

Now, by above definitions a Pareto Front can be depicted and optimum answer can be easily chosen by this diagram. This procedure will explain in 3.2.2.

3.2. Design of the Proposed Algorithm

The proposed algorithm (IMOEA) is categorized as an evolutionary algorithm. As well as a major novelty in answer selection, it includes effective crossover and mutation which are the two main operators of evolutionary algorithms. In addition to the aforementioned features, further steps are proposed in detail as follows.

3.2.1. Pseudocode of Algorithm

In table 1, the pseudocode of the introduced algorithm is presented.

Table 1 - Pseudo code of the IMOEA

Initialize the first population randomly and set the initial parameters
Calculate the objective functions of individuals ($f(x), v(x)$)
Sort non-feasible individuals by $v(x)$ and feasible individuals by $f(x)$
Find the best individuals and choose determined elites of feasible and non-feasible solution
Create the next generation by crossover and mutation
Until reach the convergence or the end of maximum iterations set
Update the position of individuals
Calculate the fitness of individuals
Sort non-feasible individuals by $v(x)$ and feasible individuals by $f(x)$
Find the best individuals and choose determined elites of feasible and non-feasible solution
Update elite if individuals become fitter than the elite
Return

3.2.2. Optimal Answer Selection Method

During optimization process and drawing Pareto Front, the Pareto answers will be sorted according to the second objective function (constraints ($v(x)$) which defied in 3.1.). Naturally, the best answer will be in the possible minimum violation (without any violation ($v(x) = 0$)), which is the global answer of optimization problem. By this way, when the obtained values arranged by $v(x)$, it is completely obvious that the values with $v(x) = 0$ are placed at the beginning of these ordered answers. Therefore, according to the mentioned procedure, answers in which the value of the second objective function is zero ($v(x) = 0$) are located in the feasible area and acquired needed qualification to be an acceptable answer for the problem. While the other solutions with the second objective function (constraint) value is not equal to zero (definitely a positive number due to the mentioned definition ($v(x) > 0$)), has violated the initial constraints of the main problem and are not in feasible space. Thus, by selecting an appropriate answer, the speed of algorithm is guaranteed by limiting the search space, due to removing many individuals in the search space and also local optimums which can mislead the optimization process to reach the global optimum. Generally, the researchers are trying to draw the Pareto Front to introduce the existing answers and provide the possibility of choosing appropriate answer by the user. But in this method, depending on the particular approach, which is applied to the constraints, the selection of the answer is already done ($v(x) = 0$) and there is no need to draw other answers or Pareto Front anymore. Therefore, the Pareto front drawing is luxury in this algorithm, and according to the explanation, the answer is a point on the $f(x)$ axis and has the lowest possible value of $f(x)$. In this process, feasible individuals are in the first priority of selection and then for reaching the desired number of individuals of each iteration, remaining individuals are selected between infeasible individuals. This concept is shown in Fig. 1.

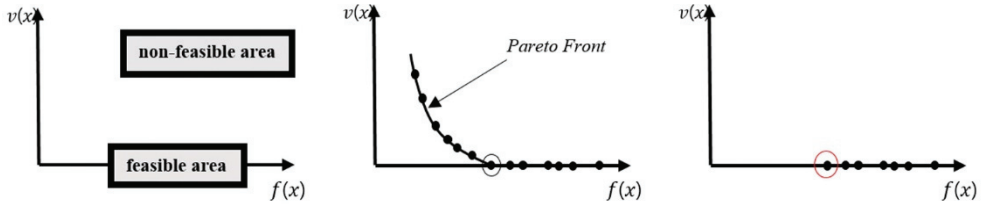

(a) feasible and non-feasible area *(b) Pareto Front* *(c) place of global optimum*

Fig. 1 - Global optimum position in this method

3.2.3. Infeasible Space Controller

To avoid any additional searches in the infeasible space, as well as increasing the efficiency of the algorithm and make faster convergence, some regulation for constraints is employed. Owe to the existence of multiple constraints in constraint optimization problems, and since it is obvious that even if one of these constraints violated, then the answer is not acceptable because this answer is not in the feasible space, so by specifying an allowed value for violation of constraints, producing new generations are focused on the immediate vicinity of the optimum answer which are definitely without any violations. The choice of this value is also considered rationally, and the main definitions of the problem are used in its selection. This value is the maximum violation among all the constraints of the problem. Clearly, in each iteration, this amount can change and

reduce the production interval for offspring so that it makes it easier for algorithm to reach the global response of the problem faster and with no violation. It should be noted that the value of v_{max} is specified in the ith iteration and bounds the scope of the second-objective function in the $i^{th} + 1^{st}$ iteration.

$$v_{max} = \max(v_{1i}(x), v_{2i}(x)) \tag{7}$$

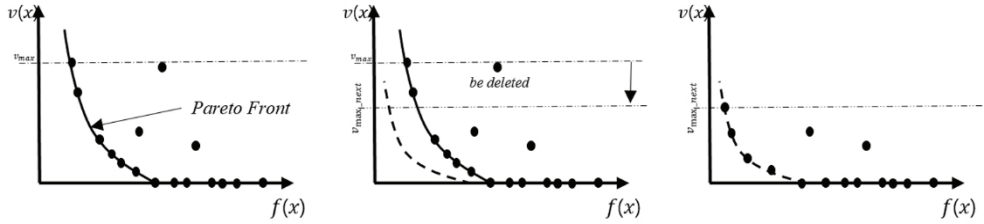

(a) whole infeasible answer space *(b) reducing infeasible space* *(c) reduced infeasible space*

Fig. 2 - Procedure of Infeasible space controller. v_{max} is the maximum value of $v(x)$ in the current population. v_{max_next} is the maximum violation for the next population

3.2.4. Mutation Operator

The mutation operator has always been one of the most influential operators in evolutionary algorithms. Many methods are developed to achieve better Mutation, including basic methods such as swap, inversion and etc., as well as more sophisticated methods such as uniform, normal [42] and so on. Swap mutation attempts to select two genes from a chromosome and replaces them with each other [43]. In the inversion mutation, several genes are selected from the chromosome and the order of the selected genes is reversed inversion [44]. For continuous problems, the use of more complicated mutations is more prevalent. The general form of the mutation operator in continuous problems is in the form of the given equation:

$$x_i' = x_i + (u_i - l_i)\overline{\delta_i} \tag{8}$$

where x_i' is the mutated gene (child), x_i is the primary gene (parent), u_i is the upper limit, l_i is lower limit and $\overline{\delta_i}$ is the distribution function. Now, if the uniform distribution function is chosen, that is, random numbers in the range of -1 to 1 is generated as new generation, then the uniform mutation is formed [45]. In the case of the use of a standard normal distribution that normally distributes a set of random numbers, in $\overline{\delta_i}$, the mutation is called normal [46]. In this research, the performance of these four types of mutations was investigated on all test subject on 50 independent runs and 100 iterations. Since G02 is a harder problem against other problems due to its many variables, the average of 50 result is depict in Fig. 3. According to this figure, normal distribution shows proper function to find the optimal point, and this mutation was used as the

mutation of the algorithm. It is important to note that this comparison was carried out for problems selected from CEC2006 [47].

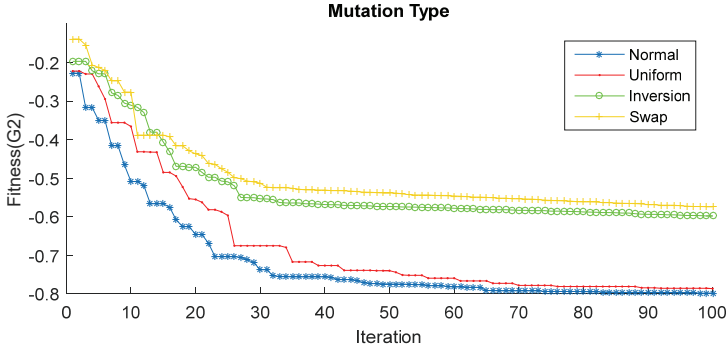

Fig. 3 - Comparing role of mutation operators

3.2.5. Crossover Operator

Another influential operator in the evolutionary algorithms is the crossover operator. This operator, like the mutation operator, includes many methods like single-point, arithmetic, Uniform, heuristic and etc. A single-point crossover is that two parent genes are cut from a random location and then two genes are combined, and children are created [48-50]. In Uniform crossover also a completely randomized gene is produced as the size of parents' genes. In case of having a value of 0 in a randomized gene, the corresponding strand should be found in the first parent and poured into a new gene. In case of having the value of 1 in a randomized gene, corresponding value of the second gene will assign to the new gene. The Uniform crossover is also known as Mask crossover. The schematic of Uniform crossover is shown in Fig. 4. The Uniform function in this research provided good results.

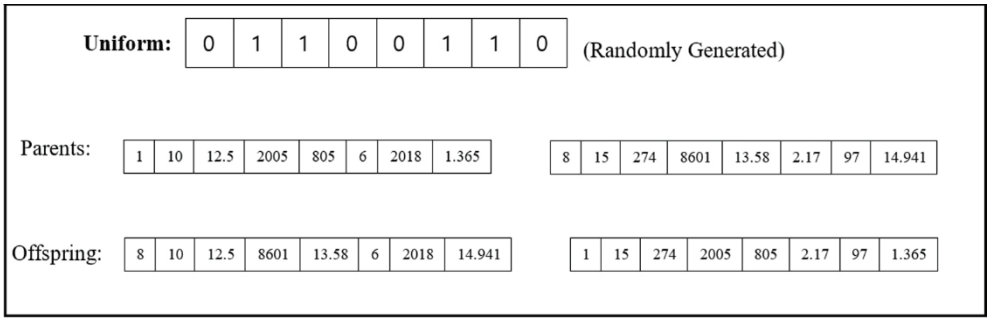

Fig. 4 - Schematic of Uniform crossover

In the arithmetic crossover, a weighted average between the two parents also produces a new generation. Thus, between the two parents, the one which has a better value is selected as an

observer, and a random number is multiplied by the difference between the other two parents, adding to the observer's value, and the new generation is generated by the heuristic crossover. Also, the performance of these four types of crossover was investigated on all test subject on 50 independent runs. Since G02 is a harder problem against other problems, the average of 50 result is depict in Fig. 5, the Uniform crossover was selected as the main crossover of the algorithm, because of its relatively better performance. This comparison was carried out for the problems selected from CEC2006 [47].

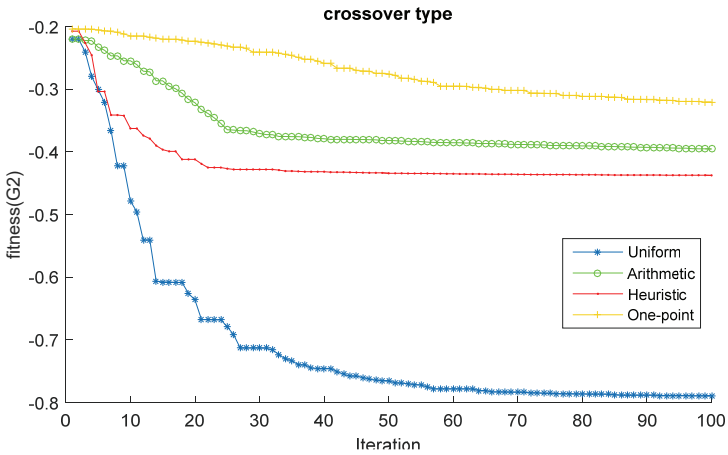

Fig. 5 - comparison function of crossover operators

3.2.6. Interference of Operators

As mentioned in other studies, evolutionary algorithms are used to find the optimal solution by mutation and crossover operator functions [51, 52]. For a reasonable moving toward the global optimum, the impact percentage of these two operators is very important for the production of each new generations. Generally, in the initial iterations, the crossover operator makes a better convergence of the algorithm, and in the final iterations, the Mutation operator prevents individuals from being captured at local optima. Therefore, in order to consider this feature in the proposed algorithm and also to avoid additional calculations, the coefficients of impact of these two operators are considered dynamically and it is related to momentary iteration of the procedure. In Crossover operator it is linearly reduced and for the Mutation operator is linearly increased. This means that in the initial iterations, the Crossover operator has its maximum value and in the final iterations the Mutation operator produce majority of breeds than Crossover. The formulation of this feature of IMOEA shown in equation 9 and 10.

For mutation:

$$M_p = \frac{M_{max} - M_{min}}{it_{max} - 1} \times (it - 1) + M_{min} \tag{9}$$

and for crossover:

$$C_p = \frac{C_{max} - C_{min}}{1 - it_{max}} \times (it - 1) + C_{min} \tag{10}$$

where M_p and C_p are mutation and crossover percentage of current iteration, respectively. M_{max} is maximum allowable mutation, M_{min} is minimum allowable mutation, C_{max} is maximum allowable crossover, C_{min} is minimum allowable crossover and it_{max} is maximum allowable iteration which all of these parameters are defined in the beginning of optimization process. it represent current iteration of algorithm. Due to the above definitions M_p and C_p update in every iteration and their values are completely depends on current iteration of process.

3.2.7. The Importance of Individuals without Violation (Feasible Elites)

Crossover and Mutation operators use individuals of each iteration to search the solution space to achieve optimal points. If they are chosen among violated individuals (parents), there would be very little chance to find a point in the feasible area. So due to the specific performance of the proposed algorithm and also many points that could be in the infeasible area, a certain percentage of the feasible solution in each iteration are selected called feasible elites. Now crossover and Mutation certainly can select individuals in the feasible area and combine them with other individuals which will increase the probability of finding global answer. There is also a special way to prioritize these individuals. Since these individuals have no constraints violation ($v(x) = 0$), these individuals are arranged according to the value of the main objective function of the problem ($f(x)$) in an ascending order, which is clear that the smallest value of $f(x)$ of these individuals is the optimal answer of the problem, and then the rest of the individuals with higher $f(x)$ are arranged. It should be noted that if the number of existed individuals without any violation is less than a selected specified percentage which set at the beginning of optimization process, the algorithm fills the population with other individuals without violation, and if the present individuals with no violation is greater than is needed, the algorithm chooses the individuals as much as the elite number and does not consider the rest.

4. NUMERICAL VERIFICATION

In order to evaluate the performance of the proposed algorithm, ten mathematical benchmark functions were solved and compared to the some existing algorithms to demonstrate the efficiency of IMOEA. After that by using IMOEA features four benchmark engineering problems have been solved.

4.1. Mathematical Constraint Problems

In this subsection, benchmark problems from the CEC2006 competitions are chosen to test the performance of IMOEA. The solutions and properties of the benchmark functions to the following constrained functional problems can be found in [47] and also demonstrated in Table 2. ρ is the ratio of feasible region to decision region and a is the number of active constraints. Li represents

the number of linear inequalities constraints. NI is the number of nonlinear inequalities constraints. LE is the number of linear equality constraints. NE is the number of nonlinear equality constraints.

Table 2 - Details of the test benchmark problems (Liang, et al., 2006)

Function	Optimal value	n	Type of function	(%)ρ	Li	NI	LE	NE	α
G01	15.0000000000	13	Quadratic	0.0111	9	0	0	0	6
G02	-0.8036191042	20	Nonlinear	99.9971	1	1	0	0	1
G03	-1.0005001000	10	Nonlinear	0.0000	0	0	0	1	1
G04	-30665.53867178	5	Quadratic	52.1230	0	6	0	0	2
G05	5126.4967140071	4	Cubic	0.0000	2	2	0	3	3
G06	-6961.813875580	2	Cubic	0.0066	0	5	0	0	2
G07	24.3062090681	10	Quadratic	0.0003	3	2	0	0	6
G08	-0.0958250414	2	Nonlinear	0.8560	0	4	0	0	0
G09	680.6300573744	7	Nonlinear	0.5121	0	3	0	0	2
G10	7046.2480205287	8	Linear	0.0010	3	0	0	0	3

Table 3 - Robustness of IMOEA

No. samples	Percent of Elites	No. Elites	Best answer
60	10	6	-0.2382
	20	12	-0.3699
	30	18	-0.4098
110	10	11	-0.3756
	20	22	-0.7989
	30	33	-0.4376
160	10	16	-0.6174
	20	32	-0.4609
	30	48	-0.0465

Table 3 represent the robustness of IMOEA and sensitivity to its parameters for G02. G02 selected because is a harder problem against other problems due to its many variables. As it can be seen in the table, with increasing population better answer is acquired. But number of elites have a crucial role. If number of elites chosen is low, IMOEA may stuck in local optimum. And if this number acquired is too high, IMOEA lose its way toward global optimum due to the large number of elites. So, number of elites should be chosen as a moderate number according to population. Also, maximum and minimum crossover and mutation selected based on their abilities to combine answers to find better solution and escape from local optimums after some experiment. The maximum possible Crossover and Mutation are 0.9 and minimum are 0.3 of the whole population.

Table 4 shows the performance of the proposed algorithm in finding the optimal solution. The number of individuals is kept constant as 110 for all problems. The maximum possible Crossover and Mutation are 0.9 and their minimum are 0.3 of population. Also, if there are more than one individual without violation, 20% of all individuals can be allocated to feasible elites. For each problem, 50 independent runs have taken place and the values of the best, average, and worst answers have been reported. It is important to note that the maximum allowable iteration for all problems is considered 100 iterations and final answer is reported in Table 4.

Table 4 – Comparison of optimum results for the proposed algorithm with literature

function	metrics	PSO[55]	ASCHEA[54]	BBO[53]	IMOEA
G1	Best	-15	-15	-14.97	**-15**
	Mean	-13	-14.84	-14.58	**-14.8418**
	Worst	-14.71	-14.555	-14.67	**-14.7207**
	Std.	N/A	N/A	N/A	0.14006
	No. Analyses	350000	155000	240000	11000
G2	Best	-0.66	-0.785	-0.78	**-0.7989**
	Mean	-0.29	-0.59	-0.73	**-0.7794**
	Worst	-0.41	-0.0792412	-0.76	-0.69522
	Std.	N/A	N/A	N/A	0.04497
	No. Analyses	350000	155000	240000	11000
G3	Best	-0.99	**-1**	**-1**	**-1**
	Mean	-0.76	**-1**	-0.04	**-0.99336**
	Worst	0.46	**-1**	-0.39	-0.97104
	Std.	N/A	N/A	N/A	0.01237
	No. Analyses	350000	155000	240000	11000
G4	Best	**-30665.539**	**-30665.539**	**-30665.539**	**-30665.539**
	Mean	-30665.539	-30665.539	-30411.86	**-30665.539**
	Worst	-30665.539	-30665.539	-29942.3	**-30665.539**
	Std.	N/A	N/A	N/A	0
	No. Analyses	350000	155000	240000	11000
G5	Best	5126.5	**5126.484**	5134.2749	5130.3417
	Mean	5249.825	5185.714	7899.2756	**5185.648**
	Worst	**5135.973**	5438.387	6130.5289	5198.481
	Std.	N/A	N/A	N/A	29.5642
	No. Analyses	350000	155000	240000	11000

Table 4 – Comparison of optimum results for the proposed algorithm with literature (continue)

G6	Best	**-6961.814**	**-6961.814**	**-6961.8139**	**-6961.4498**
	Mean	**-6961.814**	-6961.805	-5404.4941	-6716.7997
	Worst	**-6961.814**	-6961.813	-6181.7461	-6412.0801
	Std.	N/A	N/A	N/A	224.7254
	No. Analyses	350000	155000	240000	11000
G7	Best	24.37	**24.33**	25.6645	24.3594
	Mean	32.407	**24.66**	29.829	26.0917
	Worst	56.055	**25.19**	37.6912	30.3007
	Std.	N/A	N/A	N/A	2.4944
	No. Analyses	350000	155000	240000	11000
G8	Best	**-0.095825**	**-0.095825**	**-0.095825**	**-0.095825**
	Mean	-0.095825	**-0.095825**	-0.095817	-0.075487
	Worst	-0.095825	**-0.095825**	-0.095824	-0.069144
	Std.	N/A	N/A	N/A	0.01134
	No. Analyses	350000	155000	240000	11000
G9	Best	680.63	680.63	**680.63**	681.6552
	Mean	**680.33**	680.64	692.7162	687.739
	Worst	**680.33**	680.653	721.0795	690.3995
	Std.	N/A	N/A	N/A	3.6598
	No. Analyses	350000	155000	240000	11000
G10	Best	**7049.548**	7061.13	7679.0681	7052.0911
	Mean	7147.334	7497.434	9570.5714	**7136.2836**
	Worst	9264.886	7224.407	8764.9864	**7164.5763**
	Std.	N/A	N/A	N/A	47.7742
	No. Analyses	350000	155000	240000	11000

As it can be seen, the proposed algorithm in most of cases finds better answer rather than other algorithms with lower number of calculations which shows fast convergence of IMOEA. The main superiority of IMOEA is that in most of the cases, the standard deviation of answer is very low which guaranteed the acceptable performance and obtaining good result of algorithm in each run. It is obvious that if the number of iterations or individuals increases, IMOEA is completely able to acquire better result and find global optimum.

4.2. Real Engineering Design Problems

Since evolutionary algorithms are very popular for solving engineering problems [56-65], in this section, 4 well-known engineering benchmark problems have been solved and compared with the literature. Number of individuals is equal to 120 and the number of permitted iterations is 100. So

the maximum amount of required processing is 12,000. Also, the maximum crossover and mutation are 0.9 and their minimum are 0.3. Also, if there are more than one individual without violation, 30% of all individuals can be allocated to feasible elites. For each problem, 50 independent runs have been taken, the values of the best, average, worst responses and standard deviation and also, the number of analyzes needed to reach the final answer have been reported.

4.2.1. Optimum Design of a Pressure Vessel

The objective is to minimize the total fabrication cost of a cylindrical pressure vessel, as shown in Fig. 6

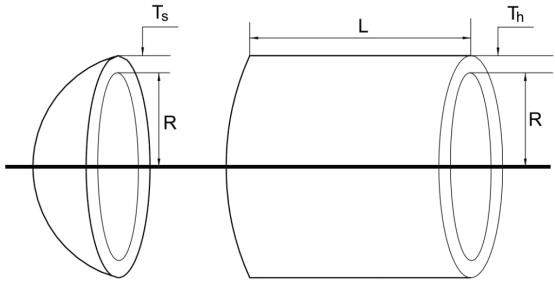

Fig. 6 - Pressure vessel design problem with four design variables

This problem has also been popular among researchers. Many heuristic techniques have been used to optimize this problem, such as GA [66], CPSO [67], DE [68], PSO [67], and GWO [69]. The problem involves two discrete and two continuous variables and four inequality constraints. The design variables are the shell thickness ($\boldsymbol{T_s}$), the spherical head thickness ($\boldsymbol{T_h}$), the radius of cylindrical shell (R), and the shell length (L). The shell and head thicknesses should be multiples of 0.0625 in and within the range 1 × 0.0625 and 99 × 0.0625 in. The radius of cylindrical shell and the shell length are limited between 10 and 200 in. The mathematical model for the problem can be stated as follows:

$$
\begin{aligned}
&\min f(T_s, T_h, R, L) = 0.6224\,T_s RL + 1.7781 T_h R^2 \;\; + 3.1661 T_s^2 L + 19.84 T_s^2 R. \\
&\text{Subject to:} \\
&g_1 = -T_s + 0.0193R \le 0, \\
&g_2 = -T_h + 0.0095R \le 0, \\
&g_3 = -\pi R^2 L + \frac{4}{3}\pi R^3 + 1296000 \le 0, \\
&g_4 = L - 240 \le 0.
\end{aligned}
\tag{11}
$$

The optimal solution and constraint values obtained by the suggested method were compared with those in the literature and are presented in Table 5. As shown in Table 5, IMOEA achieved better

results for the pressure vessel design problem compared to those based on GA, CPSO, DE, and PSO. The statistical data on various independent runs compared with the results by others in the literature are listed in Table 6.

Table 5 - Comparison of the best solution for pressure vessel design problem

	GA[66]	CPSO[67]	DE[68]	PSO[67]	GWO[69]	IMOEA
T_s	0.812	0.812	0.812	0.812	0.812	0.812
T_h	0.4375	0.4375	0.4375	0.4375	0.4345	0.4345
R	42.0974	42.0913	40.3239	42.0984	42.0892	42.0509
L	176.6540	176.7465	200.00	176.6366	176.759	177.2305
g_1	-0.00002	-1.37E−06	-0.03425	-8.80E−07	-1.788E−04	-9.1666499e-04
g_2	-0.035	-.0036	-0.054	-0.036	-0.038	-0.035
g_3	-27.886	-118.768	-304.4	*3.122*	-40.616	-24.819
g_4	-63.346	-63.253	-40	-63.363	-63.241	-62.769
f_{min}	6059.9463	6061.077	6288.744	6059.714	6051.5639	6056.179
No. Analyses	80,000	240,000	900000	60,000	NA	12000

Table 6 - Statistical results of different approaches for pressure vessel design problem

	Best	Mean	Worst	Std.	No. Analyses
Coello and Montes [68]	6059.946	6177.253	6469.322	130.9267	80,000
He and Wang [67]	6061.078	6147.133	6363.804	86.4545	240,000
Mirjalili et al. [69]	6051.5939	NA	NA	NA	NA
Kaveh and Talatahari [70]	6059.73	6081.78	6150.13	67.2418	NA
IMOEA	6056.179	6060.769	6069.978	4.348555	12000

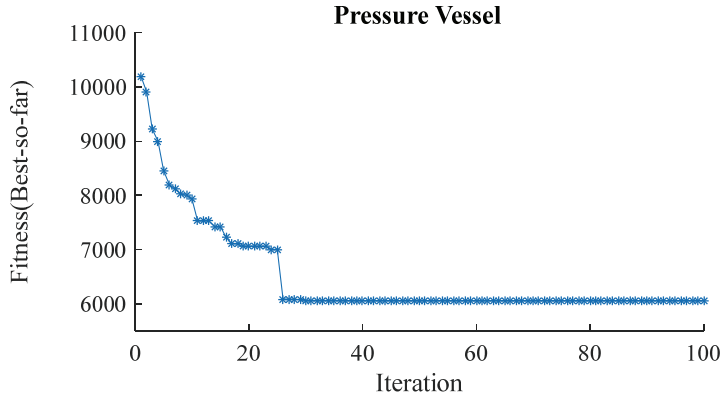

Fig. 7 - Convergence history for the pressure vessel design problem

Fig. 7 illustrates the convergence history for the pressure vessel design problem using proposed algorithm. As is clear from Fig.7, after almost 25 iterations the global optimum is found but since the maximum searching iteration is meant 100, it continuous to that end.

4.2.2. Optimum Design of a Tension/Compression Spring

The tension/compression spring problem was first introduced by Belegundu [71] and Arora [72] as shown in Fig. 7. The aim for this problem is to minimize the weight of the tension/compression spring subject to surge frequency, shear stress, and minimum deflection. There are three design variables in this problem: wire diameter (d), mean coil diameter (w), and the number of active coils (N). The problem can be stated as follows:

$$\min f(w,d,N) = (N+2)w^2 d.$$

Subject to:

$$\begin{aligned} g_1 &= 1 - \frac{d^3 N}{71785 w^4} \le 0, \\ g_2 &= \frac{d(4d-w)}{12566 w^3 (d-w)} + \frac{1}{5108 w^2} - 1 \le 0, \\ g_3 &= 1 - \frac{140.45 w}{d^2 N} \le 0, \\ g_4 &= \frac{2(w+d)}{3} - 1 \le 0. \end{aligned} \tag{12}$$

The bounds on the design variables are:

$$0.05 \le w \le 2.0, 0.25 \le d \le 1.3, 2.0 \le N \le 15.0. \tag{13}$$

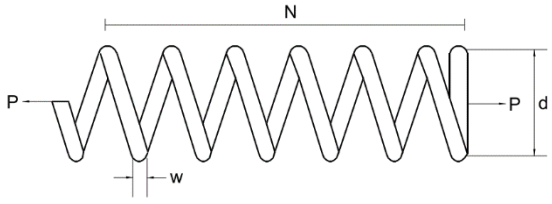

Fig. 8 - Tension/compression spring design problem indicating also the design variables

Belegundu [71] attempted the problem using eight different mathematical optimization methods. Arora [72] also found the optimum results using a numerical optimization approach with a constraint correction at the constant cost. Coello and Montes [68] utilized a GA-based method. In addition, He and Wang [67] solved this problem using a co-evolutionary particle swarm

optimization (CPSO). Recently, Eskandar et al. [73] and Kaveh and Talatahari [74] used water iteration algorithm (WCA) and the charged system search (CSS) to find the optimum results. Tables 7 and 8 compare the best results obtained by proposed method with those recorded by others. The standard deviations of optimum costs reported in Table 8 prove the consistency of the proposed method with those in the literature.

Table 7 - Comparing the best solutions for the tension/compression spring design problem using different approaches

	MPM [71]	GA [68]	WCA [73]	CC [72]	CPSO [67]	IMOEA
w	0.50	0.051989	0.051689	0.053396	0.051728	0.0518449
d	0.3159	0.363965	0.356522	0.399180	0.357644	0.360472
L	14.25	10.890522	11.30041	9.185400	11.244543	11.0726
g_1	- 0.000014	-0.000013	-1.65E−13	-0.053396	-0.000845	-1.462237433758062e-05
g_2	- 0.003782	-0.000021	-7.90E−14	-0.000018	-1.26E−05	-1.4317270180419e-05
g_3	- 3.938302	-1.061338	-4.053399	-4.123832	-4.051300	-4.060985594960838
g_4	- 0.756067	-0.722698	-0.727864	-0.698283	-0.727090	-0.725122066666667
f_{min}	0.0128334	0.0126810	0.012665	0.0127303	0.0126747	0.012666178120783
No. Analyses	NA	80,000	11,750	NA	NA	12000

Table 8 - Statistical results of different methods for tension/compression spring optimum design problem

	Best	Mean	Worst	Std.	No. Analyses
Belegundu and Arora [71]	0.0128334	NA	NA	NA	NA
Coello and Montes [68]	0.012681	0.012742	0.012973	5.90E−05	80,000
Eskandar et al. [73]	0.012665	0.012746	0.012952	8.06E−05	11,750
Arora [72]	0.0127303	NA	NA	NA	NA
He and Wang[67]	0.0126747	0.01273	0.012924	5.20E−05	200,000
Kaveh and Mahdavi [75]	0.0126697	0.0127296	0.128808	5.0038E−05	4000
IMOEA	0.012666178120783	0.012732	0.012986	0.000102	12000

Fig. 9 illustrates the convergence history for the tension/compression spring design problem using the new approach. As is clear from Fig. 9, after almost 60 iteration the global optimum is found but since the maximum iteration of search is 100, searching continuous to reach this number. It is important to note that in the first iteration of this problem, proposed algorithm could not find any individuals in feasible area but its procedure did not stop and continue processing until find an answer which suits problem constraints.

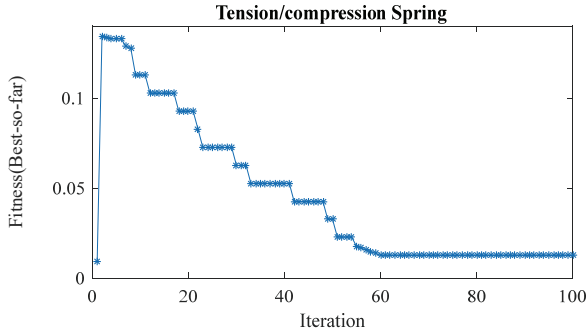

Fig. 9 - Convergence history for the tension/compression spring

4.2.3. Cantilever Beam Design Problem

Fig. 10 shows a cantilever beam consisting of five hollow square blocks. There is also a vertical load applied to the free end of the beam while the other side of the beam is rigidly supported. The aim is to minimize the weight of the beam, while the vertical displacement is defined as a constraint that should not be violated by the final optimal design. The design variables are the heights (or widths) of the different hollow blocks with fixed thickness (t = 2/3).

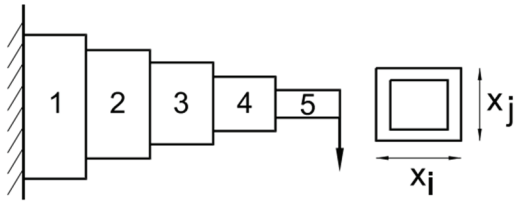

Fig. 10 - Cantilever beam design problem also indicating the design variables

Based on the discretization of five elements, the optimization problem was formulated by Svanberg [76] in a closed form:

$$\min f(x) = 0.0624(x_1 + x_2 + x_3 + x_4 + x_5).$$
Subject to:
$$g(x) = \frac{61}{{x_1}^3} + \frac{37}{{x_2}^3} + \frac{19}{{x_3}^3} + \frac{7}{{x_4}^3} + \frac{1}{{x_5}^3} \leq 1. \quad (14)$$

The bounds on the design variables are:

$$0.01 \leq x_1, x_2, x_3, x_4, x_5 \leq 15.0. \quad (15)$$

Having solved the problem using proposed method, the results were recorded in Table 8, where a comparison is made between method of moving asymptotes (MMA) [77], generalized convex approximation (GCA_I) [77], GCA_II [77], moth-flame optimization (MFO) algorithm [78], and symbiotic organisms search (SOS) [79]. It shows that the proposed algorithm exhibits a better performance compared to other algorithms. The statistical data on various independent runs compared with the results obtained by others in the literature are listed in Table 10.

Table 9 - Comparison of results for cantilever beam design problem

	SOS [79]	MMA [77]	GCA-I [77]	GCA-II [78]	MFO [78]	IMOEA
x_1	6.01878	6.0100	6.0100	6.0100	5.98487	6.0367
x_2	5.30344	5.3000	5.3040	5.3000	5.31673	5.2859
x_3	4.49587	4.4900	4.4900	4.4900	4.49733	4.5067
x_4	3.49896	3.4900	3.4980	3.4900	3.51362	3.4858
x_5	2.15564	2.1500	2.1500	2.1500	2.16162	2.1592
g	*0.000139*	NA	NA	NA	NA	-6.251037278692806e-06
f_{min}	1.33996	1.3400	1.3400	1.3400	1.339988	1.339996320000000
No. Analyses	15000	NA	NA	NA	30,000	12000

Table 10 - Statistical results using different approaches for cantilever beam design problem

	Best	Mean	Worst	Std.	No. Analyses
Cheng and Prayogo [79]	1.33996	NA	NA	NA	15,000
Chickermane and Gea [77]	1.34	NA	NA	NA	NA
Mirjalili et al. [78]	1.33998	NA	NA	NA	30,000
Mirjalili et al. [78]	1.33996	NA	NA	NA	15,000
IMOEA	1.339996320000000	1.340907	1.3458	0.001643	12000

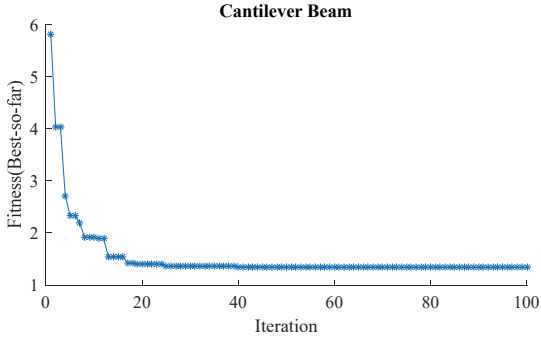

Fig. 11 - Convergence history for the Cantilever beam design problem

Fig. 11 illustrated the convergence history for the cantilever design problem using proposed algorithm. As is clear from Fig. 11, before reaching 20 iteration proposed algorithm almost found the global optimum but the process continuous until reach the maximum iteration of 100.

4.2.4. Three-Bar Truss Design Problems

This case considers a three-bar truss design problem, as shown in Fig. 11. The objective of this case is to minimize the volume of a statistically loaded three-bar truss subject to stress (σ) constraints. The problem involves two decision variables: cross sectional areas x_1 and x_2.

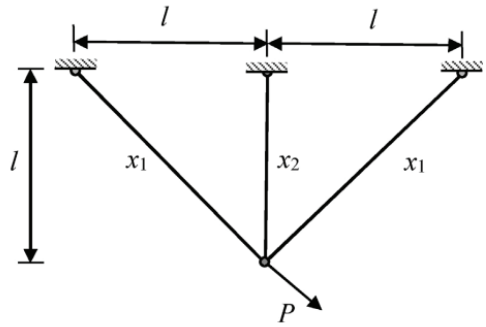

Fig. 12 - Schematic view of the three-bar truss indicating the design variables

The design variables are bounded as:

$$0 \leq x_1 \leq 1, 0 \leq x_2 \leq 1. \tag{16}$$

where $l = 100$ and $P = 2\ KN$ and $\sigma = 2\ {}^{KN}/_{cm^2}$.

This design is a nonlinear fractional programming problem. This problem has been solved by a hybrid method based on PSO and differential evolution (PSO-DE)[80], Society and Civilization optimization algorithm[81] and PSO-SA algorithm[82]. The results are given in Table 11 and 12 showing that the results of the proposed algorithm are very competitive with less function evaluation numbers.

Table 11 - Comparison of results for three-bar truss design problems

	PSO-DE[80]	SAC[81]	PSO-SA[82]	IMOEA
x_1	NA	NA	NA	0.78883
x_2	NA	NA	NA	0.40781
f_{min}	263.895843	263.895846	263.895918	263.8958168813538
No. Analyses	17,600	17,610	12,530	12000

Table 12 - Statistical results using different approaches for three-bar truss design problem

	Best	Mean	Worst	Std.	No. Analyses
Liu et al.[80]	263.89584338	263.89584338	263.89584338	4.5E-10	17,600
Ray & Liew[81]	263.89584654	263.90335672	263.96975638	1.3E-02	17,610
Javidrad &Nazari[82]	263.89591830	263.89656630	263.89699970	9.8E-08	12,530
IMOEA	263.895816881	263.895816881	263.89584338	1.3 E-07	12000

It is noted that although the IMOEA method has better objective function values than the other algorithms with minimum number of iterations required. The stability of solution was 100%. The overall results confirm that the IMOEA can have the substantial capability in handling constrained optimization problems.

Fig. 13 shows the convergence history for the three-bar truss design problem using proposed algorithm. As is clear from Fig. 13, before reaching 10 iteration proposed algorithm almost found the global optimum but the process continuous until reach the maximum iteration of 100. It is important to note that in the first iteration of this problem, proposed algorithm could not find any individuals in feasible area but its procedure continued and until find an answer which suits problem constraints.

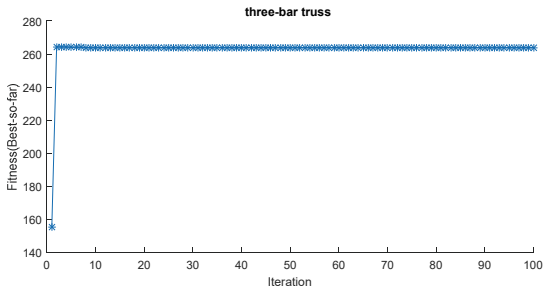

Fig. 13 - Convergence history for the three-bar truss design problem

5. DISCUSSION

In this paper, to evaluate efficiency of IMOEA, different kind of problems, including linear, nonlinear, Quadratic, Cubic, unconstrained, constrained and continuous single objective problems are solved. According to the results in Table 4, IMOEA finds better answer rather than other algorithms in most of cases with lower number of calculations. Also, low standard deviation which is reported in Table 4 almost guarantee the acceptable performance and obtaining good result of algorithm in each run. It is obvious that if the number of iterations or individuals increases, IMOEA has a better chance to acquire better result and find global optimum. In case of engineering design problems, Table 5-12 showing results of IMOEA compare with other studies with reporting important data. In these tables low standard deviation and also finding better solution with less calculation can be observed. In fig. 7,9,11 and 13 convergence history of IMOEA for solving engineering problems is depicted. These figures reflects the fast convergence speed of IMOEA in its process. So, after interpretation of results, acceptable Performance and

efficiency of IMOEA is proven. But it should be noted that correct selection of operators is very crucial. Like other optimization algorithms (c_1, c_2 and ω in PSO, α and β in ACO and etc.), IMOEA is very sensitive to its parameters in a way that with incorrect assignment, the algorithm cannot find the global optimum and deviate to a local optimum [16, 83-85]. So, finding appropriate parameters for operators depends on the skills of user of the algorithm. IMOEA will converge to an optimum because of its process in case of large number of design variables, it may face some difficulties in finding the global answer. Though, this problem can easily be solved by selecting appropriate parameters it is still a restriction of IMOEA similar to all other meta-heuristic algorithms [5-7]. On the other hand, in case of enormous search space, finding global optimum is hard and time-consuming for IMOEA. For solving mentioned problems, considering special operators which is designed for these purpose is highly recommended[86, 87].

6. CONCLUSION

To address the issue of the trade-off between the convergence and speed, this paper proposes a method which converts a SOP into an equivalent MOP with two objectives by basic definition which used in optimizations algorithm. Then an effective improved multi-objective evolutionary algorithm (IMOEA) is applied to the MOP, thus the SOP is solved. Comparison between different Mutation and Crossover leads to wise selection of these two important operators. The dynamic environment of gradually increasing mutation and decreasing crossover drives the trade-off between the convergence and the diversity through the whole evolutionary process. Also considering feasible elites for the crossover and mutation operators produced better offspring. Furthermore, new selection strategy enhances the search ability of the algorithm and provide faster convergence by including non-feasible individuals. The proposed method has been validated by optimization of various benchmark functions. The results show that, in general, the proposed method has good stability together with reasonable speed in finding global optimum point. Moreover, the performance of IMOEA is statistically better than that of the other state-of-the-art algorithms. Furthermore, the IMOEA resulted in the best mean solution, solution, and standard deviation and the least function evaluations compared to that of all of the algorithms tested in the civil engineering design problems. In overall, it is concluded that the proposed method can effectively and reliably be used for constraint optimization purposes especially for complex civil-engineering optimization problems

References

[1] Rao, S.S., *Engineering optimization: theory and practice*. 2009: John Wiley & Sons.

[2] Bazaraa, M.S., J.J. Jarvis, and H.D. Sherali, *Linear programming and network flows*. 2011: John Wiley & Sons.

[3] Holland, J.H.J.S.a., *Genetic algorithms.* 1992. **267**(1): p. 66-73.

[4] Eberhart, R. and J. Kennedy. *A new optimizer using particle swarm theory*. in *Micro Machine and Human Science, 1995. MHS'95., Proceedings of the Sixth International Symposium on*. 1995. IEEE.

[5] Atashpaz-Gargari, E. and C. Lucas. *Imperialist competitive algorithm: an algorithm for optimization inspired by imperialistic competition*. in *Evolutionary computation, 2007. CEC 2007. IEEE Congress on*. 2007. IEEE.

[6] Rao, R. and V. Patel, *An elitist teaching-learning-based optimization algorithm for solving complex constrained optimization problems.* International Journal of Industrial Engineering Computations, 2012. **3**(4): p. 535-560.

[7] Ghaemi, M. and M.-R. Feizi-Derakhshi, *Forest optimization algorithm.* Expert Systems with Applications, 2014. **41**(15): p. 6676-6687.

[8] Jordehi, A.R., *Brainstorm optimisation algorithm (BSOA): An efficient algorithm for finding optimal location and setting of FACTS devices in electric power systems.* International Journal of Electrical Power & Energy Systems, 2015. **69**: p. 48-57.

[9] Dai, T., et al., *Stiffness optimisation of coupled shear wall structure by modified genetic algorithm.* 2016. **20**(8): p. 861-876.

[10] Mirjalili, S. and A. Lewis, *The whale optimization algorithm.* Advances in Engineering Software, 2016. **95**: p. 51-67.

[11] Varaee, H. and M.R. Ghasemi, *Engineering optimization based on ideal gas molecular movement algorithm.* Engineering with Computers, 2017. **33**(1): p. 71-93.

[12] Tabari, A. and A. Ahmad, *A new optimization method: Electro-Search algorithm.* Computers & Chemical Engineering, 2017. **103**: p. 1-11.

[13] TOĞAN, V. and M.A.J.T.D. EIRGASH, *Time-Cost Trade-Off Optimization with a New Initial Population Approach.* 2018. **30**(6).

[14] Muhammad, A.A., et al., *Adoption of Virtual Reality (VR) for Site Layout Optimization of Construction Projects.* 2019. **31**(2).

[15] AZAD, S.K. and A.J.T.D. Ebru, *Cost Efficient Design of Mechanically Stabilized Earth Walls Using Adaptive Dimensional Search Algorithm.* **31**(4).

[16] Coello, C.A.C., *Theoretical and numerical constraint-handling techniques used with evolutionary algorithms: a survey of the state of the art.* Computer methods in applied mechanics and engineering, 2002. **191**(11): p. 1245-1287.

[17] Kucukkoc, I. and D.Z. Zhang, *Balancing of parallel U-shaped assembly lines.* Computers & Operations Research, 2015. **64**: p. 233-244.

[18] Chou, C.-H., S.-C. Hsieh, and C.-J. Qiu, *Hybrid genetic algorithm and fuzzy clustering for bankruptcy prediction.* Applied Soft Computing, 2017. **56**: p. 298-316.

[19] Araghi, S., et al., *Influence of meta-heuristic optimization on the performance of adaptive interval type2-fuzzy traffic signal controllers.* Expert Systems with Applications, 2017. **71**: p. 493-503.

[20] Tosta, T.A.A., et al., *Computational method for unsupervised segmentation of lymphoma histological images based on fuzzy 3-partition entropy and genetic algorithm.* Expert Systems with Applications, 2017. **81**: p. 223-243.

[21] Yang, G., Y. Wang, and L. Guo, *A sparser reduced set density estimator by introducing weighted l 1 penalty term.* Pattern Recognition Letters, 2015. **58**: p. 15-22.

[22] Dong, Z. and W. Zhu, *An improvement of the penalty decomposition method for sparse approximation.* Signal Processing, 2015. **113**: p. 52-60.

[23] Kia, S.S., *Distributed optimal resource allocation over networked systems and use of an e-exact penalty function.* IFAC-PapersOnLine, 2016. **49**(4): p. 13-18.

[24] Tang, K.-Z., T.-K. Sun, and J.-Y. Yang, *An improved genetic algorithm based on a novel selection strategy for nonlinear programming problems.* Computers & Chemical Engineering, 2011. **35**(4): p. 615-621.

[25] Long, Q., *A constraint handling technique for constrained multi-objective genetic algorithm.* Swarm and Evolutionary Computation, 2014. **15**: p. 66-79.

[26] de Paula Garcia, R., et al., *A rank-based constraint handling technique for engineering design optimization problems solved by genetic algorithms.* Computers & Structures, 2017. **187**: p. 77-87.

[27] Coello, C.A.C., G.B. Lamont, and D.A. Van Veldhuizen, *Evolutionary algorithms for solving multi-objective problems*. Vol. 5. 2007: Springer.

[28] Dhiman, G. and V.J.K.-B.S. Kumar, *Multi-objective spotted hyena optimizer: A Multi-objective optimization algorithm for engineering problems.* 2018. **150**: p. 175-197.

[29] Deb, K., et al., *A fast and elitist multiobjective genetic algorithm: NSGA-II.* IEEE transactions on evolutionary computation, 2002. **6**(2): p. 182-197.

[30] Monfared, S.A.H., et al., *Water Quality Planning in Rivers: Assimilative Capacity and Dilution Flow.* Bulletin of environmental contamination and toxicology, 2017. **99**(5): p. 531-541.

[31] Hashemi Monfared, S. and M. Dehghani Darmian, *Evaluation of Appropriate Advective Transport Function for One-Dimensional Pollutant Simulation in Rivers.* International Journal of Environmental Research, 2016. **10**(1): p. 77-84.

[32] Noura, A. and F.J.A.M.S. Saljooghi, *Determining feasible solution in imprecise linear inequality systems.* 2008. **2**(36): p. 1789-1797.

[33] Mostaghim, S. and J. Teich. *Strategies for finding good local guides in multi-objective particle swarm optimization (MOPSO)*. in *Swarm Intelligence Symposium, 2003. SIS'03. Proceedings of the 2003 IEEE*. 2003. IEEE.

[34] Coello Coello, C. and M. Lechuga. *MOPSO: a proposal for multiple objective particle swarm optimization*. in *Proc., Evolutionary Computation, 2002. CEC'02. Proceedings of the 2002 Congress on*.

[35] Zhang, Q. and H.J.I.T.o.e.c. Li, *MOEA/D: A multiobjective evolutionary algorithm based on decomposition.* 2007. **11**(6): p. 712-731.

[36] Coello, C.A.C., *Use of a self-adaptive penalty approach for engineering optimization problems.* Computers in Industry, 2000. **41**(2): p. 113-127.

[37] Segura, C., et al., *Using multi-objective evolutionary algorithms for single-objective constrained and unconstrained optimization.* Annals of Operations Research, 2016. **240**(1): p. 217-250.

[38] Fonseca, C.M. and P.J. Fleming. *Genetic Algorithms for Multiobjective Optimization: FormulationDiscussion and Generalization*. in *Icga*. 1993.

[39] Srinivas, N. and K. Deb, *Muiltiobjective optimization using nondominated sorting in genetic algorithms.* Evolutionary computation, 1994. **2**(3): p. 221-248.

[40] Deb, K., et al. *A fast elitist non-dominated sorting genetic algorithm for multi-objective optimization: NSGA-II*. in *International Conference on Parallel Problem Solving From Nature*. 2000. Springer.

[41] Ngatchou, P., A. Zarei, and A. El-Sharkawi. *Pareto multi objective optimization*. in *Intelligent systems application to power systems, 2005. Proceedings of the 13th international conference on*. 2005. IEEE.

[42] Smith, J. and T.C. Fogarty. *Self adaptation of mutation rates in a steady state genetic algorithm*. in *Evolutionary Computation, 1996., Proceedings of IEEE International Conference on*. 1996. IEEE.

[43] Moon, C., et al., *An efficient genetic algorithm for the traveling salesman problem with precedence constraints.* European Journal of Operational Research, 2002. **140**(3): p. 606-617.

[44] Ho, W., et al., *A hybrid genetic algorithm for the multi-depot vehicle routing problem.* Engineering Applications of Artificial Intelligence, 2008. **21**(4): p. 548-557.

[45] Juang, C.-F., *A hybrid of genetic algorithm and particle swarm optimization for recurrent network design.* IEEE Transactions on Systems, Man, and Cybernetics, Part B (Cybernetics), 2004. **34**(2): p. 997-1006.

[46] Mühlenbein, H. and D. Schlierkamp-Voosen, *Predictive models for the breeder genetic algorithm i. continuous parameter optimization.* Evolutionary computation, 1993. **1**(1): p. 25-49.

[47] Liang, J., et al., *Problem definitions and evaluation criteria for the CEC 2006 special session on constrained real-parameter optimization.* Journal of Applied Mechanics, 2006. **41**(8).

[48] Horn, J., N. Nafpliotis, and D.E. Goldberg. *A niched Pareto genetic algorithm for multiobjective optimization*. in *Evolutionary Computation, 1994. IEEE World Congress on Computational Intelligence., Proceedings of the First IEEE Conference on*. 1994. Ieee.

[49] Deep, K. and M. Thakur, *A new crossover operator for real coded genetic algorithms.* Applied mathematics and computation, 2007. **188**(1): p. 895-911.

[50] Herrera, F., M. Lozano, and A.M. Sánchez, *A taxonomy for the crossover operator for real-coded genetic algorithms: An experimental study.* International Journal of Intelligent Systems, 2003. **18**(3): p. 309-338.

[51] Weile, D.S. and E. Michielssen, *Genetic algorithm optimization applied to electromagnetics: A review.* IEEE Transactions on Antennas and Propagation, 1997. **45**(3): p. 343-353.

[52] Schott, J.R., *Fault Tolerant Design Using Single and Multicriteria Genetic Algorithm Optimization*. 1995, AIR FORCE INST OF TECH WRIGHT-PATTERSON AFB OH.

[53] Patel, V.K. and V.J. Savsani, *Heat transfer search (HTS): a novel optimization algorithm.* Information Sciences, 2015. **324**: p. 217-246.

[54] Hamida, S.B. and M. Schoenauer. *ASCHEA: New results using adaptive segregational constraint handling*. in *Evolutionary Computation, 2002. CEC'02. Proceedings of the 2002 Congress on*. 2002. IEEE.

[55] Karaboga, D. and B. Akay, *A modified artificial bee colony (ABC) algorithm for constrained optimization problems.* Applied soft computing, 2011. **11**(3): p. 3021-3031.

[56] Topal, U., et al., *Buckling load optimization of laminated plates resting on Pasternak foundation using TLBO.* J Structural Engineering and Mechanics, 2018. **67**(6): p. 617-628.

[57] Zhiyi, Y., Z. Kemin, and Q. Shengfang, *Topology optimization of reinforced concrete structure using composite truss-like model.* J Structural Engineering and Mechanics, 2018. **67**(1): p. 79-85.

[58] Noura, A. and F. Saljooghi, *Ranking decision making units in Fuzzy-DEA Using entropy.* Applied Mathematical Sciences, 2009. **3**(6): p. 287-295.

[59] Saljooghi, F.H. and M.M.J.A.J.o.A.S. Rayeni, *Distinguishing congestion and technical inefficiency in presence undesirable output.* 2011. **8**(9): p. 903.

[60] Artar, M. and A.J.T.D. Daloglu, *The Optimization of Multi-Storey Composite Steel Frames with Genetic Algorithm Including Dynamic Constraints.* 2015. **26**(2): p. 7077-7098.

[61] Mustafa, O., et al., *Construction Site Layout Planning: Application of Multi-Objective Particle Swarm Optimization.* **29**(6).

[62] Rayeni, M.M., F.H.J.I.J.o.S. Saljooghi, and O. Management, *Ranking and measuring efficiency using secondary goals of cross-efficiency evaluation–a study of railway efficiency in Iran.* 2014. **17**(1): p. 1-16.

[63] Bulut, B. and M.T.J.T.D. Yilmaz, *Analysis of the 2007 and 2013 Droughts in Turkey by NOAH Hydrological Model.* 2016. **27**(4): p. 7619-7634.

[64] Mahallati, M. and F.J.J.o.A.S. Saljooghi, *Performance assessment of education institutions through interval DEA.* 2010. **10**: p. 2945-2949.

[65] Tözer, K.D., T. Çelik, and G.E.J.T.D. Gürcanlı, *Classification of Construction Accidents in Northern Cyprus.* 2018. **29**(2): p. 8295-8316.

[66] Coello, C.A.C. and C.S.P. Zacatenco, *List of references on constraint-handling techniques used with evolutionary algorithms.* Information Sciences, 2012. **191**: p. 146-168.

[67] He, Q. and L. Wang, *An effective co-evolutionary particle swarm optimization for constrained engineering design problems.* Engineering Applications of Artificial Intelligence, 2007. **20**(1): p. 89-99.

[68] Mezura-Montes, E. and C.A.C. Coello, *An empirical study about the usefulness of evolution strategies to solve constrained optimization problems.* International Journal of General Systems, 2008. **37**(4): p. 443-473.

[69] Mirjalili, S., S.M. Mirjalili, and A. Lewis, *Grey wolf optimizer.* Advances in Engineering Software, 2014. **69**: p. 46-61.

[70] Kaveh, A. and S. Talatahari, *An improved ant colony optimization for constrained engineering design problems.* Engineering Computations, 2010. **27**(1): p. 155-182.

[71] Belegundu, A.D. and J.S. Arora, *A study of mathematical programming methods for structural optimization. Part I: Theory.* International Journal for Numerical Methods in Engineering, 1985. **21**(9): p. 1583-1599.

[72] Arora, J., *Introduction to optimum design*. 2004: Academic Press.

[73] Eskandar, H., et al., *Water cycle algorithm–A novel metaheuristic optimization method for solving constrained engineering optimization problems.* Computers & Structures, 2012. **110**: p. 151-166.

[74] Kaveh, A. and S. Talatahari, *A novel heuristic optimization method: charged system search.* Acta Mechanica, 2010. **213**(3): p. 267-289.

[75] Kaveh, A. and V. Mahdavi, *Colliding bodies optimization: a novel meta-heuristic method.* Computers & Structures, 2014. **139**: p. 18-27.

[76] Svanberg, K., *The method of moving asymptotes—a new method for structural optimization.* International journal for numerical methods in engineering, 1987. **24**(2): p. 359-373.

[77] Chickermane, H. and H. Gea, *Structural optimization using a new local approximation method.* International journal for numerical methods in engineering, 1996. **39**(5): p. 829-846.

[78] Mirjalili, S., *Moth-flame optimization algorithm: A novel nature-inspired heuristic paradigm.* Knowledge-Based Systems, 2015. **89**: p. 228-249.

[79] Cheng, M.-Y. and D. Prayogo, *Symbiotic organisms search: a new metaheuristic optimization algorithm.* Computers & Structures, 2014. **139**: p. 98-112.

[80] Liu, H., Z. Cai, and Y. Wang, *Hybridizing particle swarm optimization with differential evolution for constrained numerical and engineering optimization.* Applied Soft Computing, 2010. **10**(2): p. 629-640.

[81] Ray, T. and K.M. Liew, *Society and civilization: An optimization algorithm based on the simulation of social behavior.* IEEE Transactions on Evolutionary Computation, 2003. **7**(4): p. 386-396.

[82] Javidrad, F. and M. Nazari, *A new hybrid particle swarm and simulated annealing stochastic optimization method.* Applied Soft Computing, 2017. **60**: p. 634-654.

[83] Yılmaz, M., et al., *Uydu Kaynaklı Yağmur Verilerinin Hata Oranlarının Deniz Kıyılarına Olan Uzaklığa Bağlı Analizi.* 2017. **28**(3): p. 7993-8005.

[84] Dorigo, M. and G. Di Caro. *Ant colony optimization: a new meta-heuristic*. in *Proceedings of the 1999 congress on evolutionary computation-CEC99 (Cat. No. 99TH8406)*. 1999. IEEE.

[85] Shafigh, P., S.Y. Hadi, and E.J.I.s. Sohrab, *Gravitation based classification.* 2013. **220**: p. 319-330.

[86] Lin, Y., et al., *A hybrid differential evolution algorithm for mixed-variable optimization problems.* 2018. **466**: p. 170-188.

[87] Deng, H., et al., *Ranking-based biased learning swarm optimizer for large-scale optimization.* 2019. **493**: p. 120-137.

Teknik Dergi, 2021 10675-10694, Paper 608

Consolidated Undrained Monotonic Shearing Response of Hydrophobic Kızılırmak Sand

Hüseyin Melih TATAR[1]
Kemal Önder ÇETİN[2]

ABSTRACT

Geotechnical properties of hydrophilic (wettable) sands have been widely discussed in the literature. However, sands may gain hydrophobic (non-wettable) properties after being exposed to a hydrophobic agent in the nature. The number of available studies regarding the response of hydrophobic sands is very limited, and mostly focus on their environmental and hydrological aspects. To close this gap, a controlled laboratory testing program, consisting of 18 monotonic strain-controlled consolidated undrained triaxial shear tests, was designed. Tests were performed on fully saturated hydrophilic and hydrophobic re-constituted Kızılırmak sand samples of different relative densities with pore water measurements. Hydrophobic samples were prepared by using 1 and 2 % WD-40 lubricant by mass. The effect of hydrophobic agent was assessed by comparing the stress – excess pore water pressure - strain responses of hydrophobic sand samples with those of conventional (hydrophilic) sand samples. Test results revealed that addition of hydrophobic agent increases the dilatancy of sands at low confining stresses (~100kPa) by decreasing the excess pore water pressure generation. At higher confining stresses (~400kPa) this effect is less pronounced. Moreover, the addition of hydrophobic agent up to 2% by mass does not systematically and significantly change the effective angle of shearing resistance of sand samples, independent of their initial relative density and confining stress levels.

Keywords: Kızılırmak sand, CU triaxial shear test, hydrophobicity, WD-40 lubricant, dilatancy, density, effective stress, critical state, stress-strain response.

1. INTRODUCTION

In the literature, there exist numerous studies regarding the engineering properties and straining responses of hydrophilic (wettable) sands. Their shear strength parameters, drained and undrained shearing responses at relatively dense or loose states can be conveniently

Note:
- This paper has been received on March 22, 2019 and accepted for publication by the Editorial Board on October 22, 2019.
- Discussions on this paper will be accepted by May 31, 2021.
- https://dx.doi.org/10.18400/tekderg.543306

1 KOBA Engineering and Consulting Co. Ltd., Ankara, Turkey - melihtatar2@gmail.com https://orcid.org/0000-0003-0120-5991

2 Middle East Technical University, Civil Engineering Department, Ankara, Turkey - kemalondercetin@gmail.com - https://orcid.org/0000-0003-0540-2247

assessed [1, 2, 3, 4, 5, 6, 7, 8, etc.]. However, sands are not always available in the nature as a wettable material, and may exhibit hydrophobic (non-wettable) properties after being exposed to a hydrophobic agent. Figure 1 shows a water drop lying on a handful of hydrophobic sand, which illustrates visually the difference in their response as compared to a hydrophilic sand. In the literature, unlike hydrophilic sands, there exists only a handful research studies, which mostly focus on the environmental and hydrological aspects of hydrophobic soils.

Figure 1 - Hydrophobic Sand

There are only two research studies (to the knowledge of authors) that investigated the stress-strain response of hydrophobic sands with emphasis on their geotechnical properties. These experimental studies were performed by Byun and Lee [9] and Kim et al. [10], and will be discussed next.

Byun and Lee investigated the effect of hydrophobicity on shear strength. Hydrophobicity was achieved by silica salinization reaction. By using angular and sharp particles, particle shape – hydrophobicity – shear strength response was studied. For the purpose, direct shear tests were performed on glass beads (GB) and crushed sands (CS), and peak and ultimate shear strengths were determined. It was concluded that hydrophobicity reduced the peak angle of shearing resistance by 4 and 2 degrees for GB and CS samples, respectively, independent of the particle shape. Hydrophobicity modestly reduced the ultimate angle of shearing resistance of CS samples, which is reported to be only 2 degrees. No reduction in the ultimate angle of shearing resistance was observed for the GB sample.

Kim et al. [10] also performed direct shear tests on hydrophilic and hydrophobic Jumunjin sands. Hydrophobic samples were prepared by a chemical treatment. Tests were performed under naturally dried conditions. Due to hydrophobic treatment, up to 8 degrees of a reduction in angle of shearing resistance was reported. The decrease in shear strength was attributed to surface modification of sand grains due to hydrophobic treatment.

As concluded by the results of these limited number of research studies, there exists a lack of consensus on the effects of hydrophobicity on drained shearing response of sandy soils. Additionally, and more dramatically, there exists actually no study for the assessment of

undrained response of hydrophobic sands. To attempt to close this gap and contribute to the state of available geotechnical literature regarding the effects of hydrophobicity, this research study aims to investigate the effects of addition of hydrophobic agent on the stress - strain - excess pore water pressure responses of "loose" and "dense" Kızılırmak sand samples, which are tested at confining stresses of 100, 200, and 400 kPa. For this purpose, a laboratory monotonic testing program was designed consisting of 18 monotonic strain-controlled consolidated undrained triaxial shear tests, with pore water measurements (i.e.: C$\overline{U}$ tests). Due to lack of undrained test results available in the literature, the responses of hydrophilic and hydrophobic Kızılırmak sand samples will only be comparatively discussed on the basis of results presented herein.

2. LABORATORY TESTING PROGRAM AND TESTING PROCEDURE

The index properties of re-constituted poorly graded Kızılırmak sand samples were determined. The average specific gravity(G_S), minimum and maximum void ratios (e_{min}) and (e_{max}) are determined as 2.66, 0.534 and 0.857, respectively. Similarly, the uniformity coefficient and coefficient of curvature are estimated as 2.36 and 2.88, respectively. Table 1 presents a summary of these test results.

Table 1 - Index Properties of Kızılırmak Sand Used in This Study

USCS Type:	SP
% Gravel:	0,00
% Sand:	99.31
% Fines:	0.69
D_{10} (mm):	0.22
D_{30} (mm):	0.33
D_{60} (mm):	0.52
C_u:	2.36
C_c:	2.88

Hydrophobic treatment of samples was performed by exposing the sand to WD-40 lubricant, 1% and 2 % by mass. Some engineering properties of WD-40 are given in Table 2.

Table 2 - Engineering Properties of the WD-40 Lubricant Used in This Study

Color:	Light (or pale) amber
Specific Gravity:	0.80 – 0.82
Freezing Temperature:	-63 °C
Boiling Temperature:	183 – 187 °C
Kinematic Viscosity:	2.79 – 2.96 cSt (0.00000279 – 0.00000296 m^2/sn)

Testing program is summarized in Table 3. A total of 9 tests were performed on 80 % relative density specimens. Similarly, additional 9 tests were performed on 40 % relative density specimens. For comparison purposes, 6 of 18 tests were performed on hydrophilic sand samples (i.e.: with no WD-40 treatment). In order to test the effects of the level of hydrophobicity, 6 of 18 tests were performed on specimens prepared with 1% WD-40 treatment by mass, and 6 tests were performed on specimens with 2% WD-40 treatment.

Table 3 - Triaxial Testing Program

D_R = 80%	STXD_01 / 100kPa / 0%	STXD_02 / 200kPa / 0%	STXD_03 / 400kPa / 0%
	STXD_04 / 100kPa / 1%	STXD_05 / 200kPa / 1%	STXD_06 / 400kPa / 1%
	STXD_07 / 100kPa / 2%	STXD_08 / 200kPa / 2%	STXD_09 / 400kPa / 2%
D_R = 40%	STXL_01 / 100kPa / 0%	STXL_02 / 200kPa / 0%	STXL_03 / 400kPa / 0%
	STXL_04 / 100kPa / 1%	STXL_05 / 200kPa / 1%	STXL_06 / 400kPa / 1%
	STXL_07 / 100kPa / 2%	STXL_08 / 200kPa / 2%	STXL_09 / 400kPa / 2%

* Test Name / Consolidation Pressure / WD-40 by mass

Samples were prepared by wet tamping method. In order to avoid non-homogeneous layering, sand sample with 5 % moisture content is placed into the mould in 10 layers. By using a tamping device of 25 mm in diameter, 3 to 13 tamps, depending on the target relative density, were applied to each layer. During sample preparation stage, the utmost attention was given to produce a homogenous soil sample with constant compaction energy delivered to each layer. Specimens at 40% relative density were re-constituted by applying 3 tamps/layer in wet tamping method. Similarly, to achieve 80% relative density, 15-20 tamps per each layer were applied with a 15 mm diameter tool. All static triaxial tests were performed by using the VJ TECH triaxial testing system, shown in Figure 2. The system includes the following components:

- A triaxial cell to mould the specimen and apply cell pressure
- A cell pressure unit with pressure transducer to apply and measure the cell pressure throughout the test
- A back pressure unit with to apply back pressure and pressure transducers to measure the back pressure and volume change of the specimen throughout the test
- A load cell to measure the deviator load acting on the specimen
- A linear variable displacement transducer (LVDT) to measure the axial deformation of the specimen
- A data logger to monitor the deviator load and axial deformation
- A loading unit
- A computer

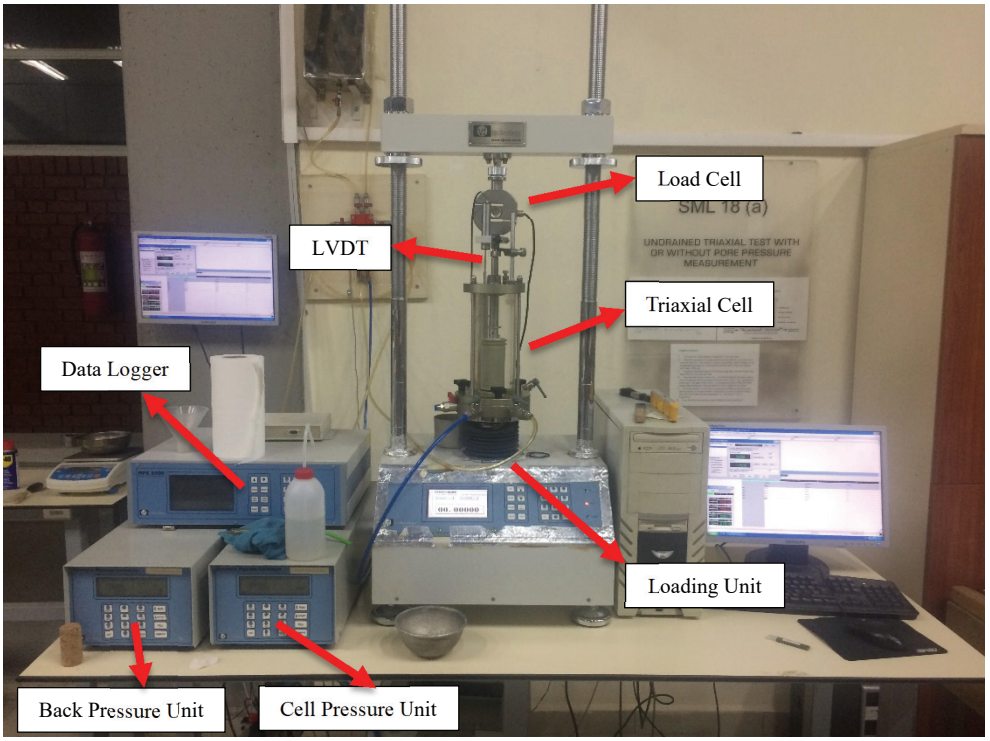

Figure 2 - Triaxial testing system used in this study

Before the beginning of each test, triaxial cell was thoroughly cleaned to eliminate remaining sand particles from earlier tests to improve water tightness. Additionally, cell pressure, back pressure, pore pressure and top cap valves were also controlled against clogging. The tests were performed following closely relevant ASTM standards [11] and due to page limitations details of these ASTM testing procedures will not be repeated herein.

The saturation of the sand specimen was achieved by back pressure saturation. The degree of saturation of the specimen was confirmed by calculating the B value, which is defined as the ratio of pore pressure increase to cell pressure increase:

$$B = \frac{\Delta u}{\Delta \sigma_3} \tag{3.5}$$

In each test, back pressure saturation phase usually started with $B \approx 0.6$. At the end of back pressure saturation stage, $B \geq 0.96$ was usually obtained at a maximum of 500kPa back pressure level. The consolidation phase followed the back pressure saturation, during which volume and pore pressure changes were monitored. After the completion of the consolidation phase, specimens were loaded axially with a 0.1mm/min strain rate under undrained loading conditions. The applied deviator load, axial deformation, pore water pressure and cell

pressure levels were monitored during monotonic loading. Tests were stopped at about 20% axial strain level.

The consolidation (confining) pressure (σ_c), amount of WD-40 used during specimen preparation, void ratio and corresponding relative density before consolidation ($e_{initial}$, $D_{R,initial}$) and monotonic shearing phases (e_{final}), axial strain levels at failure ($\varepsilon_{a,\ failure}$) and estimated effective angle of shearing resistance (ϕ') values are summarized in Table 4:

Table 4 - Summary of Triaxial Test Results

Test	σ_c (kPa)	WD-40 (%) by mass	$e_{initial}$	$D_{R,\ initial}$ (%)	ΔV (ml)	e_{final}	$\varepsilon_{a,\ failure}$ (%)	ϕ' (°)
STXD_01	100	0	0,602	78,9	0,26	0,597	3,3	40,0
STXD_02	200	0	0,601	79,2	0,53	0,592	3,1	40,0
STXD_03	400	0	0,604	78,4	1,03	0,585	4,2	39,0
STXD_04	100	1	0,590	82,8	0,31	0,584	3,9	39,6
STXD_05	200	1	0,593	81,8	0,60	0,582	2,6	40,4
STXD_06	400	1	0,598	80,4	0,95	0,580	3,4	39,1
STXD_07	100	2	0,596	80,9	0,35	0,589	2,4	40,5
STXD_08	200	2	0,606	77,7	0,53	0,596	3,3	40,0
STXD_09	400	2	0,603	78,7	0,84	0,588	3,8	38,7
STXL_01	100	0	0,719	42,9	0,43	0,710	4,6	35,3
STXL_02	200	0	0,732	38,9	1,03	0,711	5,5	32,5
STXL_03	400	0	0,731	38,9	1,54	0,701	9,8	33,8
STXL_04	100	1	0,730	39,4	0,39	0,722	8,9	34,2
STXL_05	200	1	0,726	40,7	0,76	0,710	5,7	35,0
STXL_06	400	1	0,732	38,9	1,30	0,706	10,3	33,8
STXL_07	100	2	0,728	40,1	0,35	0,721	8,5	34,5
STXL_08	200	2	0,730	39,3	0,81	0,714	5,8	34,0
STXL_09	400	2	0,727	40,3	1,50	0,697	10,2	32,8

Major and minor effective stresses, excess pore water pressure and strain levels at the time of failure are determined on the basis of maximum stress obliquity criterion. Triaxial test results are presented in the form of four-way plots as given in Figures 3 through 20. Four-way plots enable to consistently follow the deviator stress - mean effective stress - strain variations throughout the test, along with the failure surface and Mohr circle corresponding to the failure state. A complete presentation of test results is also available in Tatar [12], and will not be repeated herein.

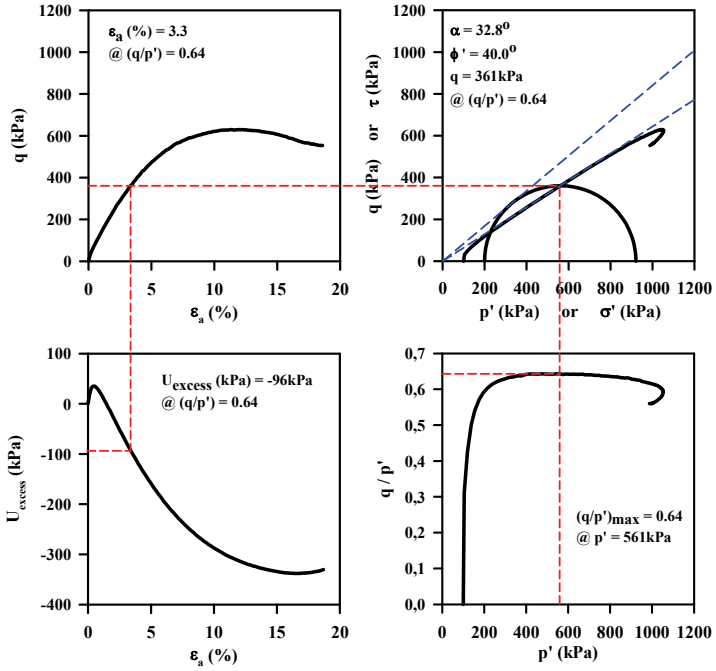

Figure 3 - Four way plots of test STXD_01

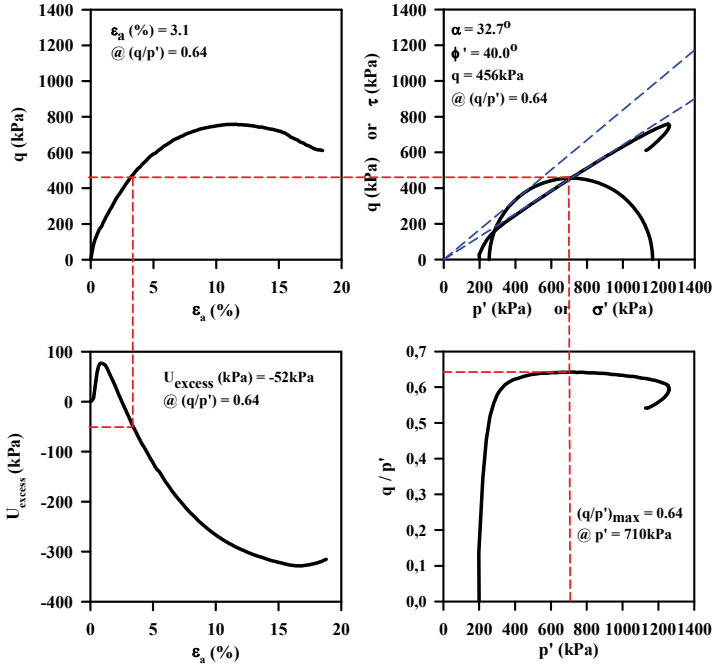

Figure 4 - Four Way plots of test STXD_02

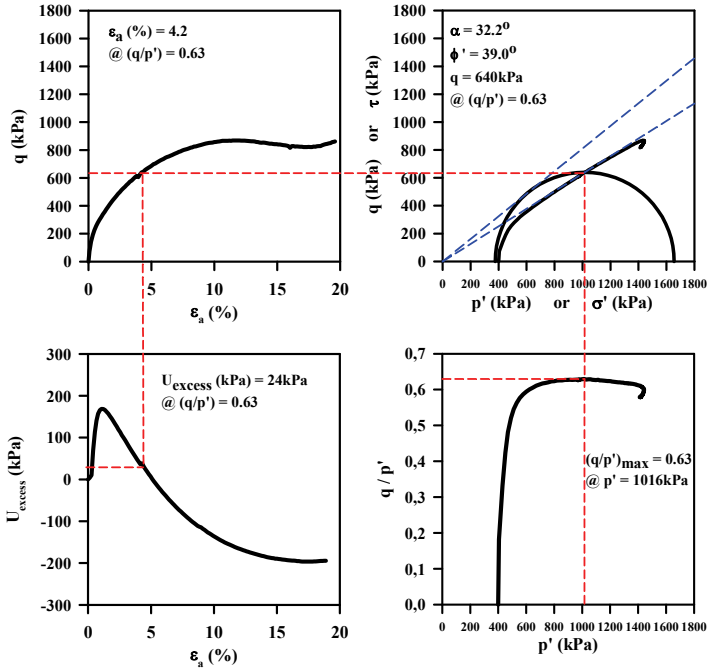

Figure 5 - Four way plots of test STXD_03

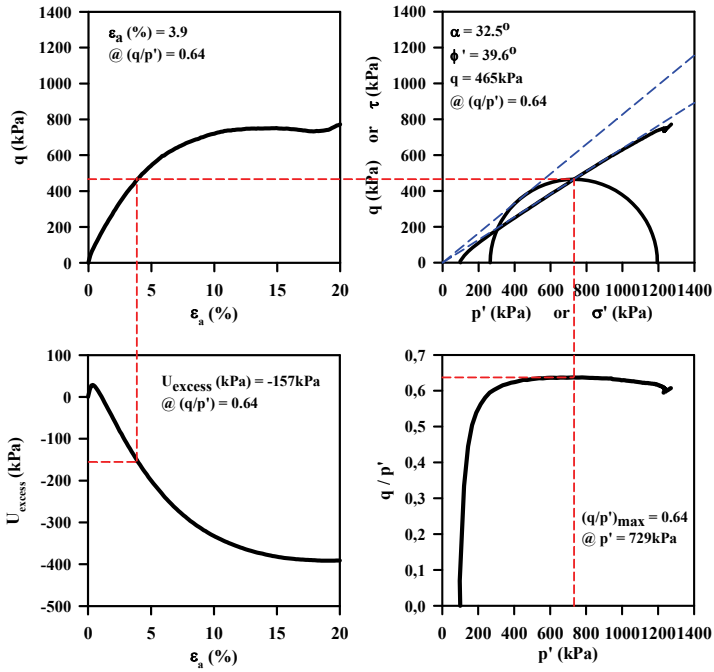

Figure 6 - Four way plots of test STXD_04

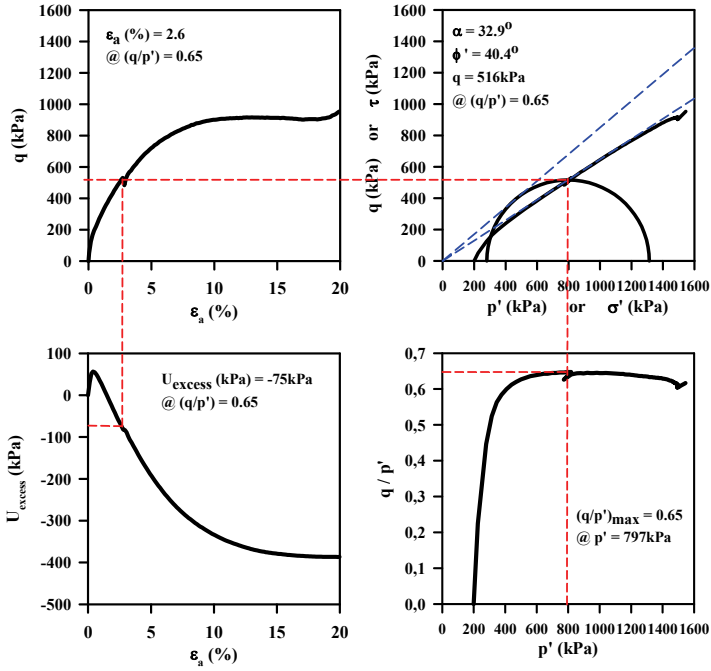

Figure 7 - Four way plots of test STXD_05

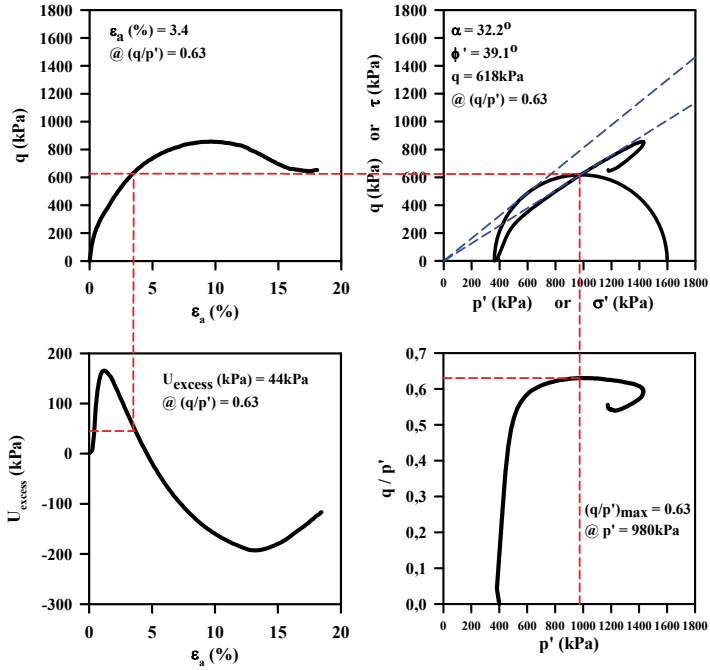

Figure 8 - Four way plots of test STXD_06

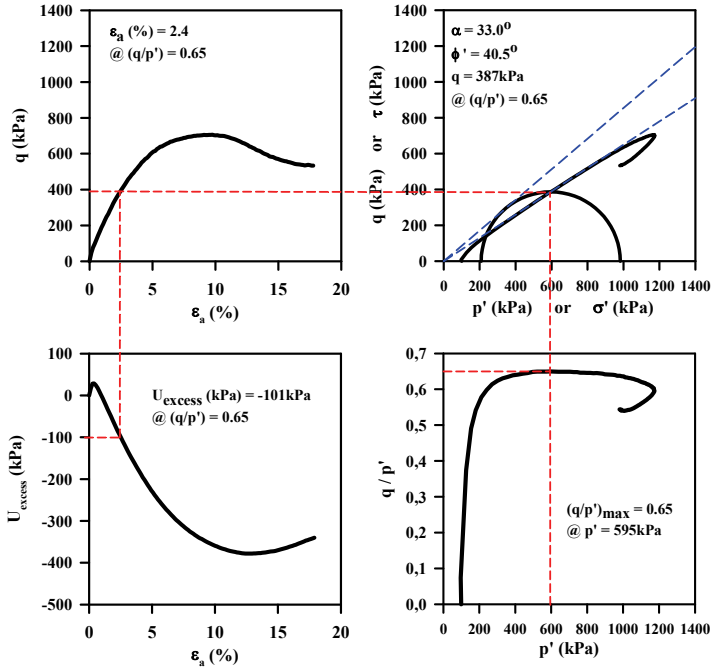

Figure 9 - Four way plots of test STXD_07

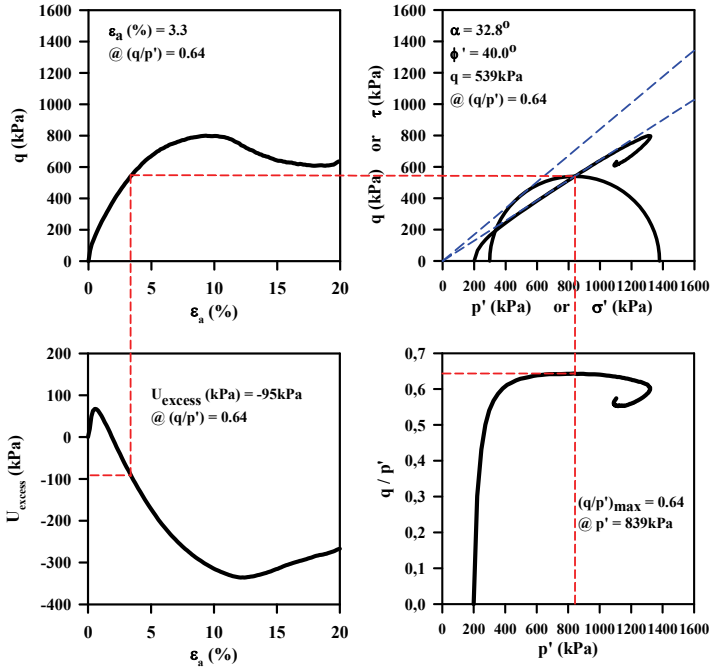

Figure 10 - Four way plots of test STXD_08

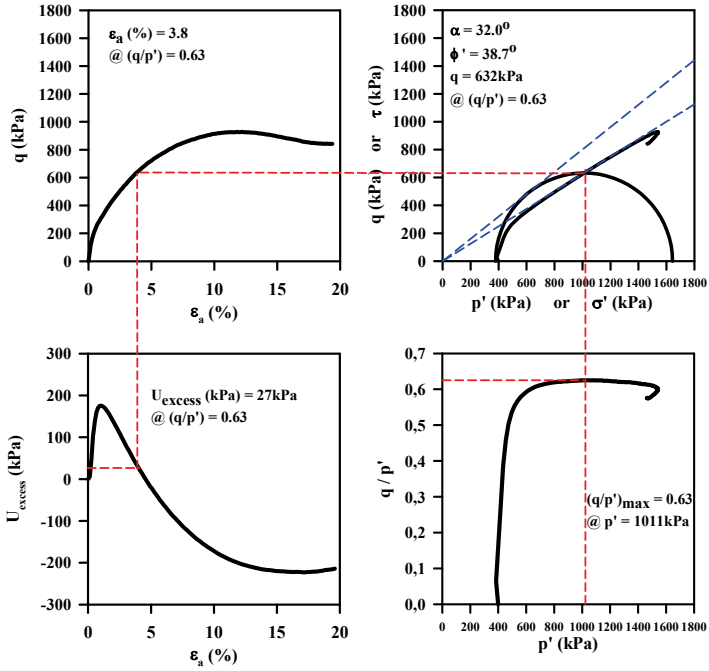

Figure 11 - Four way plots of test STXD_09

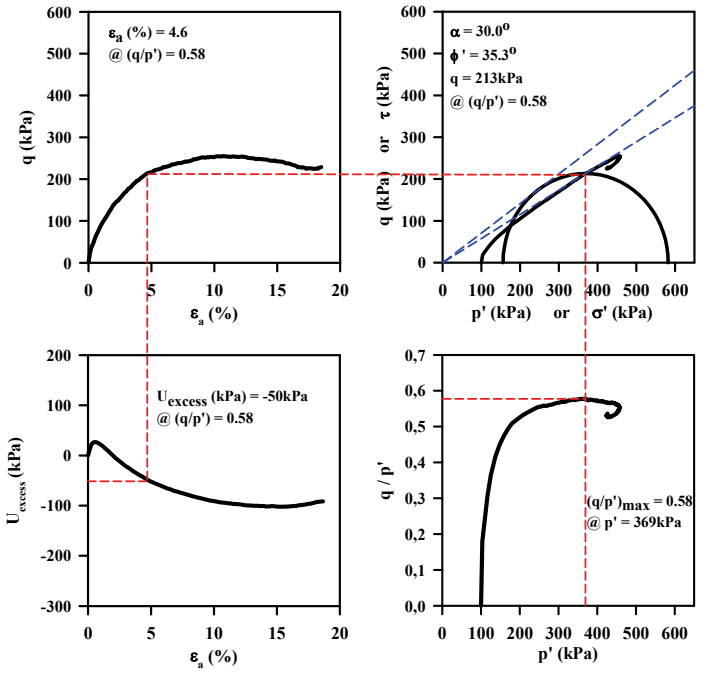

Figure 12 - Four way plots of test STXL_01

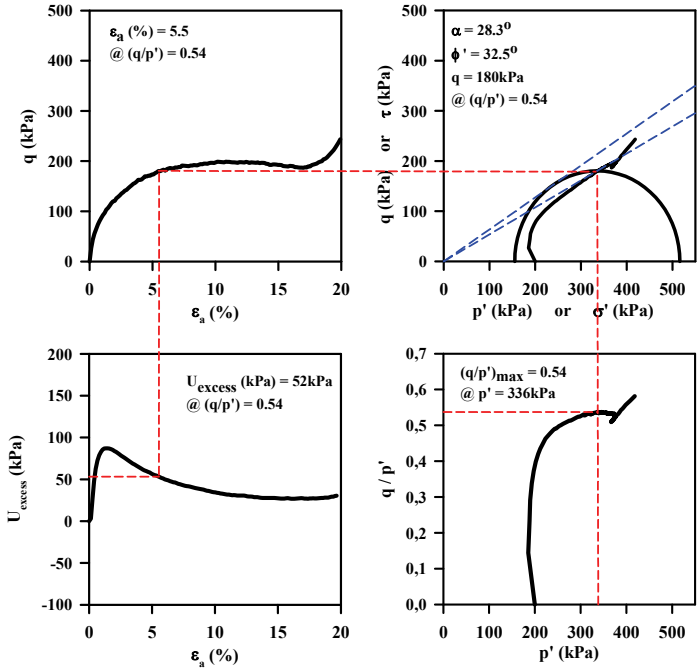

Figure 13 - Four way plots of test STXL_02

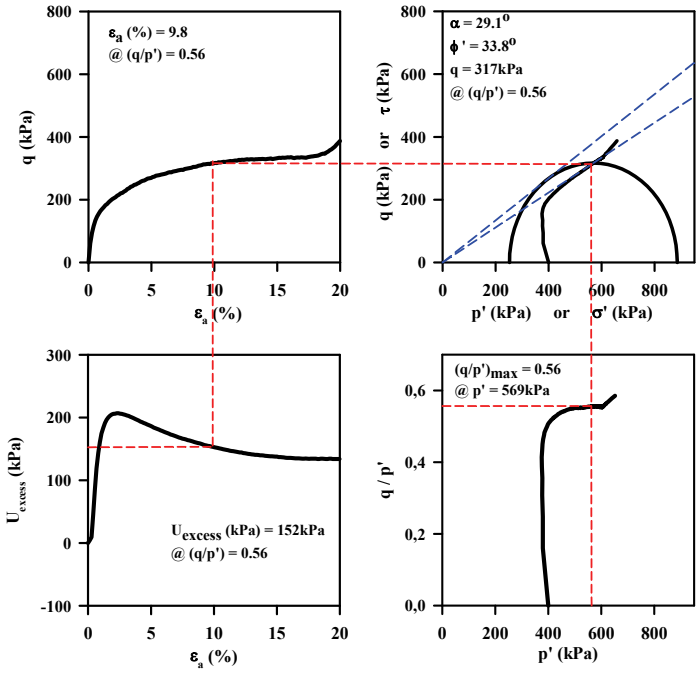

Figure 14 - Four way plots of test STXL_03

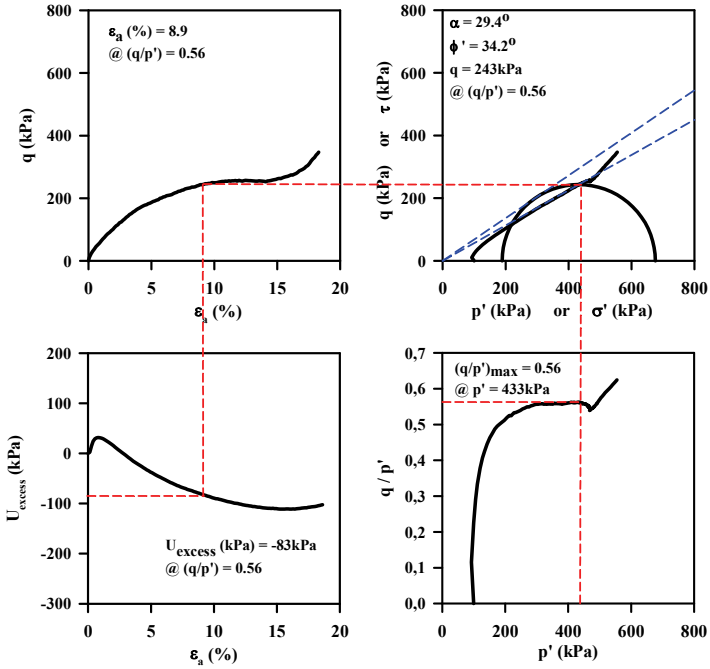

Figure 15 - Four way plots of test STXL_04

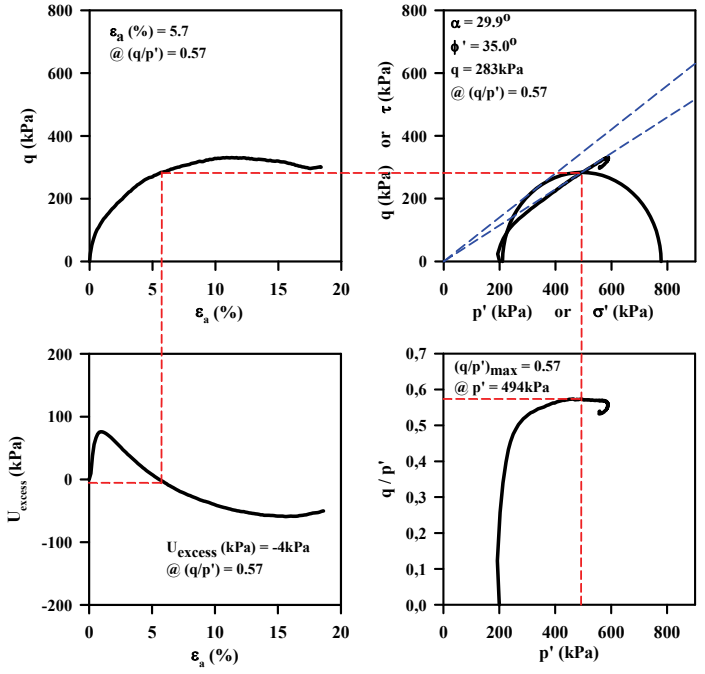

Figure 16 - Four way plots of test STXL_05

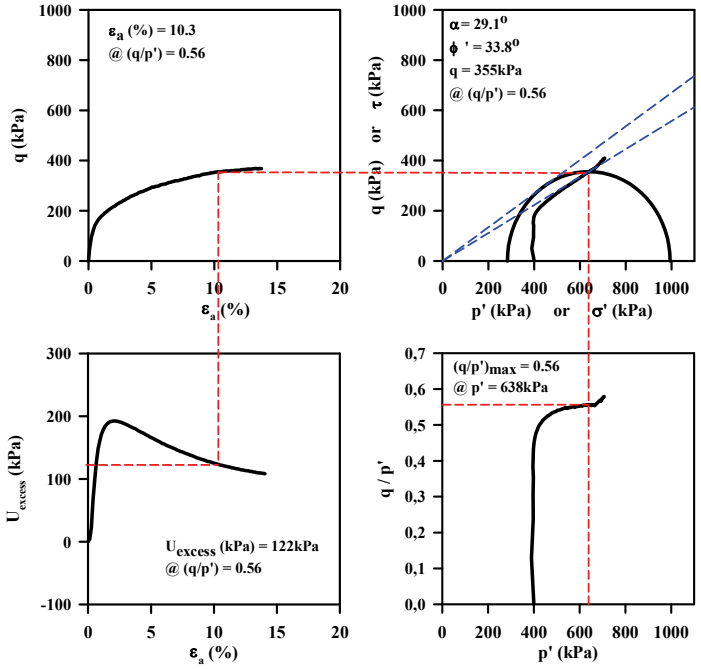

Figure 17 - Four way plots of test STXL_06

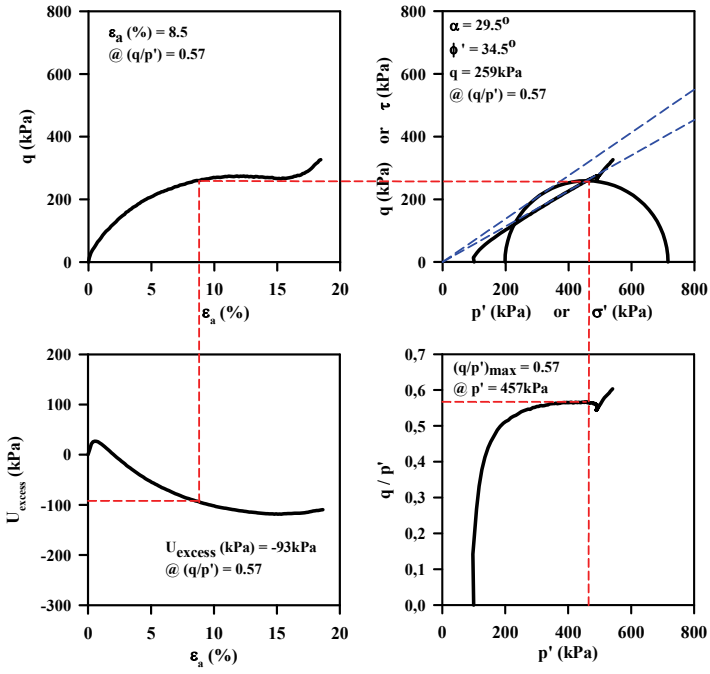

Figure 18 - Four way plots of test STXL_07

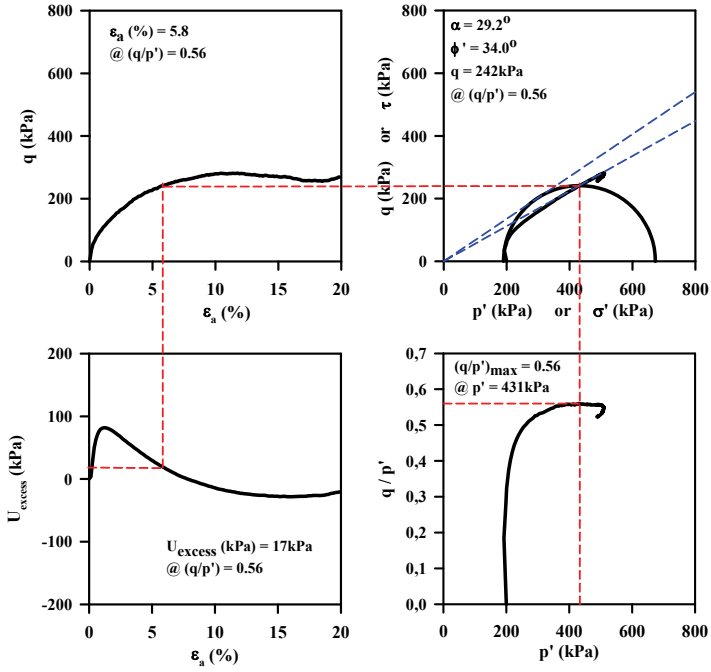

Figure 19 - Four way plots of test STXL_08

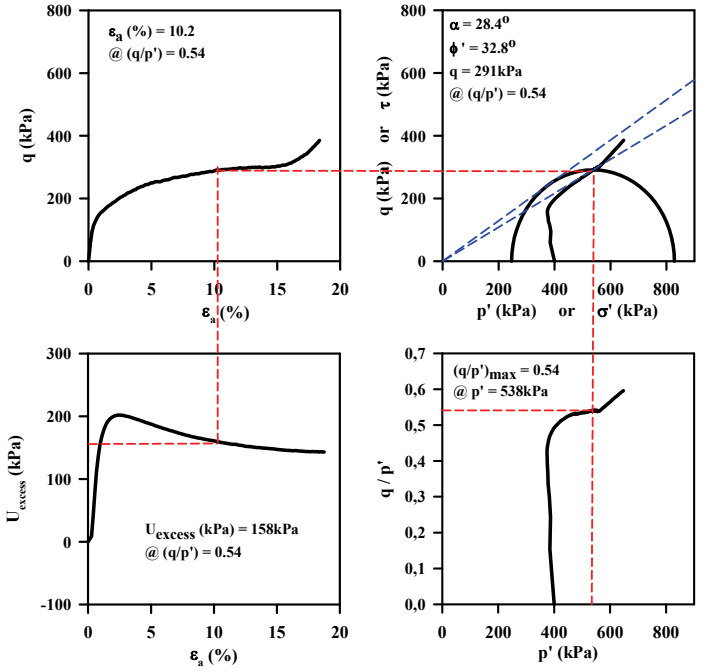

Figure 20 - Four way plots of test STXL_09

3. DISCUSSION OF RESULTS AND CONCLUSION

The interpretation and discussion of triaxial test results will be presented separately for hydrophilic and hydrophobic sands to enable comparisons with available literature and cross-comparison with each other. In addition to test results presented in Figures 3 through 20, Figures 21 and 22 will be used as the basis of the discussion and conclusion. Figures 21 and 22 present respectively the variations of i) angle of shearing resistance, ii) excess pore pressure coefficient A_f, defined as the ratio of excess pore pressure normalized with deviator stress corresponding to the time of failure; with confining stress, relative density and degree of hydrophobicity.

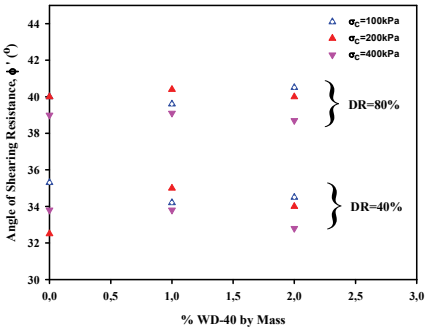

Figure 21 - The variation of angle of shearing resistance with confining stress, relative density and degree of hydrophobicity.

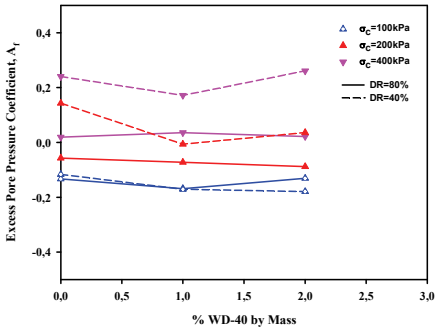

Figure 22 - The variation of excess pore pressure coefficient A_f with confining stress, relative density and degree of hydrophobicity.

Following observations and conclusions were made for the hydrophilic sand samples:

Relatively dense sand samples (i.e.: $D_R \approx 80$ %) fail at axial strains falling in the range of 2-4 %, and effective angles of shearing resistance were estimated to vary in the range of 39 to 41°. However, relatively loose sand samples (i.e.: $D_R \approx 40$ %) fail at axial strains falling in the range of 5-10 %, and effective angle of shearing resistance values were estimated to vary in between 33 to 35°. The angles of shearing resistances decrease by 1 to 2 degrees with increase in confining stress from 100 kPa to 400 kPa.

In the literature, the failure strain levels for “dense” and “loose” sand samples were reported to vary in the range of 2-5 and 4-10 %, which are in conformance with the test results presented herein [13]. Additionally, the effective angles of shearing resistance values were also reported to vary in the range of 34-36° and 39-44° again conforming with the triaxial test results presented herein [3,5]. The decrease in angles of shearing resistance with increasing confining stress is an indication of suppression of dilatancy with increasing confining stress and is consistent with critical state soil mechanics principles. Hence, in general the tested responses of hydrophilic Kızılırmak sands are in close agreement with available literature and are concluded to provide a suitable basis of comparison with the test results of hydrophilic sands.

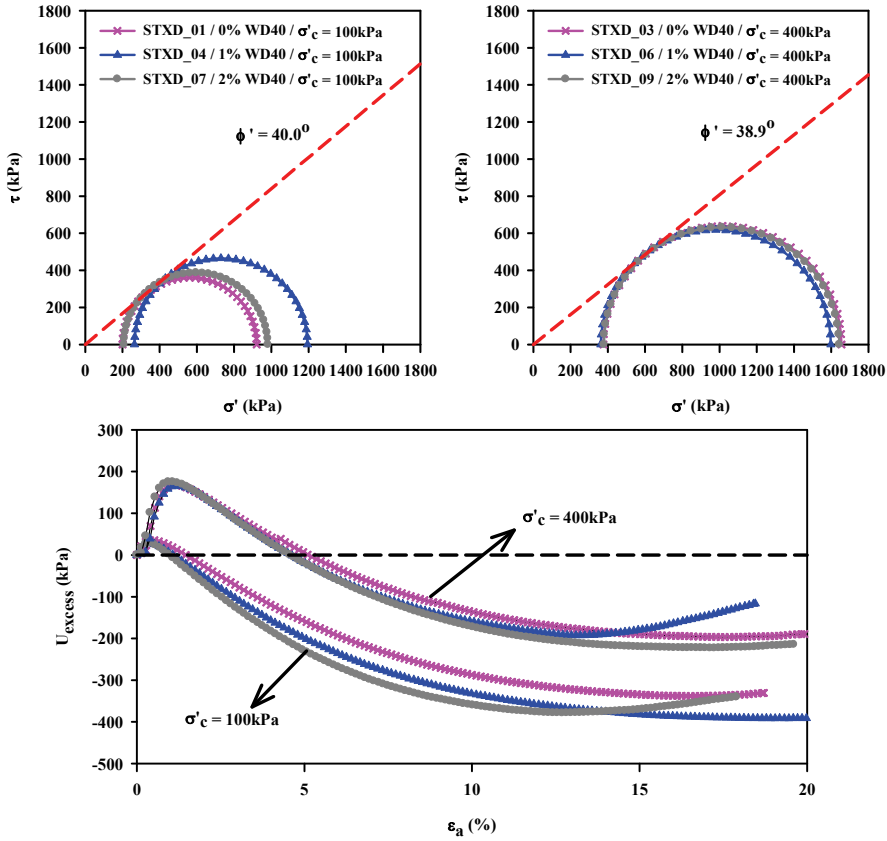

Figure 23 - Comparison of responses of tests STXD_01, STXD_04, STXD_07 and STXD_03, STXD_06, STXD_09 (DR ≅ 80%)

To determine the effect of hydrophobicity, test results of hydrophilic sands, as well as of samples prepared with 1 and 2 % hydrophobic agent (i.e.: WD 40), were used. Following observations and conclusions were made for the hydrophilic sand samples, which are only valid for the sand type, confining stress level, hydrophobic agent and the amount of hydrophobic agent used in this study:

Relatively dense hydrophobic sand samples (i.e.: $D_R \approx 80$ %) fail at axial strains falling in the range of 2-4 %, and effective angle of shearing resistance values were estimated to vary in between 39 to 41°. However, relatively loose sand samples (i.e.: $D_R \approx 40$ %) fail at axial strains falling in the range of 5-10 %, and effective angle of shearing resistance values were estimated to vary in between 33 to 35°. These strain and effective angle of shearing resistances are not significantly different than those of hydrophilic sand samples. Hence, it is concluded that the addition of 1 to 2 % hydrophobic agent by mass does not significantly affect the failure strain levels or effective angle of shearing resistances, independent of the relative density states. This conclusion, especially the angle of shearing resistance not to be significantly affected by hydrophobic treatment, contradicts with the conclusions of Kim et

al. [10] and supports Byun and Lee [9] argument suggesting a small to no reduction in angle of shearing resistance due to hydrophobicity. It should be noted that direct comparisons with these earlier studies may not be accurate due to differences in the type of sand, test apparatus, drainage conditions and hydrophobic agent used.

To eliminate the uncontrolled test variables among earlier studies and this study, to provide a fair basis of comparison to assess the effects of hydrophobic agent on the overall response, interpretation of test results on the basis of comparisons between hydrophilic and hydrophobic Kızılırmak sand samples herein, will be presented next.

As shown in Figure 23, when excess pore water pressure responses of $D_R \approx 80$ % hydrophobic Kızılırmak sands were compared with that of hydrophilic sands, a more pronounced dilative response was observed with increasing hydrophobicity. As shown in Figure 24, a similar trend is also observed in $D_R \approx 40$ % samples. The addition of hydrophobic agent (especially at 1 % WD-40 by mass) increases dilative response, which is supressed with increasing confining stresses.

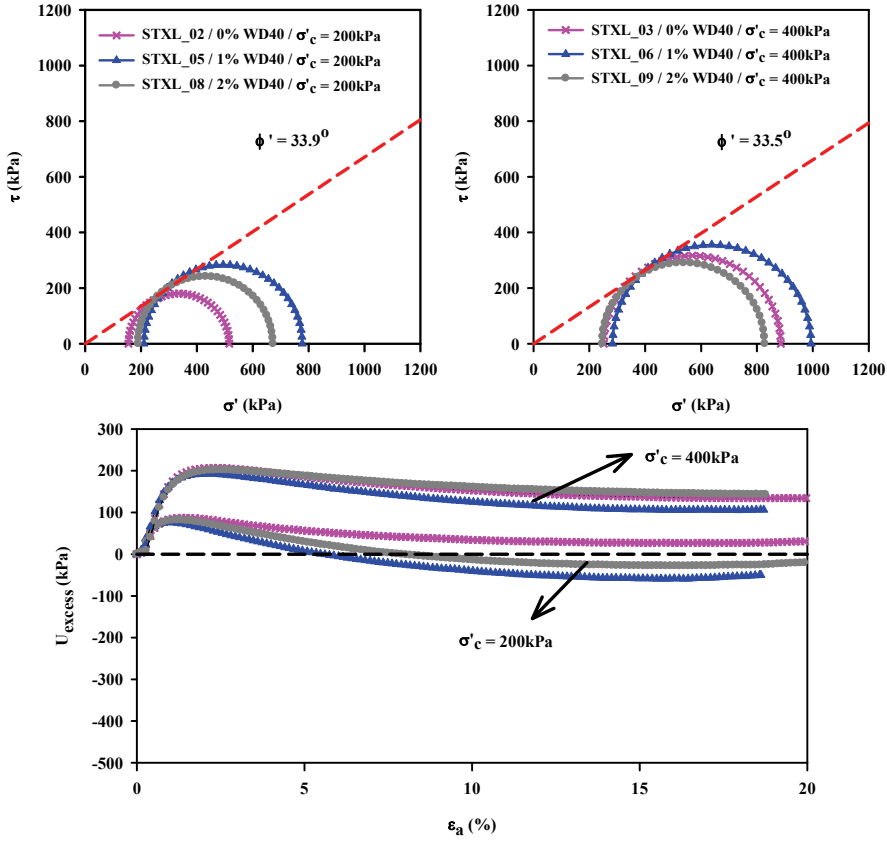

Figure 24 - Comparison of responses of tests STXL_02, STXD_05, STXD_08 and STXL_03, STXD_06, STXD_09 ($D_R \cong 40\%$)

Due to increased dilatancy with increased hydrophobicity, the stress paths are observed to steer towards higher effective stresses, which in turn lead to an increased shear strength levels under undrained loading. In simpler terms, if one studies the Mohr-Coulomb shear strength relationship presented in Equation 1, with decreased excess pore pressures (or increased negative pore pressures due to dilational trends) shear strength is expected to increase, which is consistent with the triaxial test results of hydrophobic sands.

$$\tau_{ff} = \sigma'_{ff}.tan\Phi' = (\sigma_{ff} - u_f).tan\Phi' \quad (1)$$

Note that in Equation 1, τ_{ff} and σ'_{ff}, respectively, are the shear and normal effective stresses acting on the failure plane at the time of failure, u_f and Φ are the pore pressure at the time failure and effective angle of shearing resistance, respectively. Also, it should be noted that the addition of 1 % WD-40 produces the optimum dilatancy effects, considering the overall shearing response of hydrophobic Kızılırmak sand samples.

As a summary, within the confines of this manuscript, it is shown that hydrophobic sand response is more dilative than that of hydrophilic sands, under undrained loading conditions. Additionally, and favourably, failure shear strain levels and effective angle of shearing resistances are not significantly affected by the addition of hydrophobic agent WD-40 up to 2 % by mass. As also supported by the test data, exposure to 1 % WD-40 by mass produced optimum improvement. These increased dilative response and corollary increased undrained shear strength encourage the use of hydrophobic agents for the prevention of major geotechnical shear failure problems, including but not limited to seismic soil liquefaction, during which undrained shear strength capacity is significantly reduced due to contractive nature of fully saturated sandy soils subjected to cyclic shearing. However, before practical and feasible use of hydrophobic treatment in geotechnical practice, it is necessary to extend the current state of research to in-situ and laboratory testing of hydrophobic sands with emphasis to cover a wider range of sand type, hydrophobic agent, stress and density levels, along with the assessment of durability and environmental effects of the hydrophobic agent. This humble study is hoped to contribute to fulfil this need as much of a sand particle in an ocean.

References

[1] Roscoe, K. H., Schofield, A. N., Wroth, C. P., On the Yielding of Soils. Géotechnique, 8(1), 22–53, 1958.

[2] Schofield, A. N., Wroth, C. P., Critical State Soil Mechanics, Cambridge, 1968.

[3] Schmertmann, J. H., Guidelines for Cone Penetration Test, Performance and Design, Washington, 1978.

[4] NAVFAC Design Manual, Naval Facilities Engineering Command, DM-7.01, 1986.

[5] Bolton, M. D., The Strength and Dilatancy of Sands. Géotechnique, 36(1), 65–78, 1986.

[6] Houlsby, G. T., How the dilatancy of soils affects their behaviour. Proceedings of the 10th European Conference on Soil Mechanics and Foundation Engineering, Florence, Italy, 1991.

[7] Terzaghi, K., Peck, R. B., Mesri, G., Soil Mechanics in Engineering Practice, New York, 1996.

[8] Andersen, K. H., Schjetne, K., Database of Friction Angles of Sand and Consolidation Characteristics of Sand, Silt, and Clay. Journal of Geotechnical and Geoenvironmental Engineering, 139(7), 1140–1155, 2013.

[9] Byun, Y., Lee, J., Influence of Particle Shape of Hydrophobic Granular Materials on Shear Strength. Advances in Civil, Environmental, and Materials Research, Seoul, Korea, 2012.

[10] Kim D., Yang H.-J., Yun T. S., Kim B., Kato S., Park S.-W., Characterization of Geomechanical and Hydraulic Properties of Non-Wettable Sands. Proceedings of the 18th International Conference on Soil Mechanics and Geotechnical Engineering, Paris, France, 2013.

[11] Standard Test Method for Consolidated Undrained Triaxial Compression Test for Cohesive Soils, ASTM, D-4767, 2011.

[12] Tatar, H. M., Consolidated Undrained Shearing Response of Hydrophobic Sands, M.Sc., Middle East Technical University, 2018.

[13] Jefferies, M., Been, K., Soil Liquefaction, A Critical State Approach, Abingdon, New York, 2006.

Teknik Dergi, 2021 10695-10716, Paper 609

Snap-through Buckling of Shallow Spherical Shells under Ring Loads

Esra Eylem KARATAŞ[1]
Receb Faruk YÜKSELER[2]

ABSTRACT

Snap-through buckling behaviour of rigid vinyl polyethylene shallow spherical shells, undergoing large displacements, subjected to static ring loads is investigated by using finite difference and the Newton-Raphson Method. The load-deflection diagrams corresponding to various values of thickness, depth and ring diameter of the shell with simply supported and clamped edges are sketched and compared. The accuracy of the used algorithm and the prepared computer program are tested by comparing some of the numerical results obtained in this study with those obtained by an experimental study, available in the relevant literature. Further steps on the concerning subject are achieved.

Keywords: Shallow spherical shell, nonlinear behaviour, large deflection, snap-through buckling, upper-limit point, rigid vinyl polyethylene, stability.

1. INTRODUCTION

For determining the load carrying capacities of structures the stability criterion, as well as the strength and stiffness criteria, must be considered especially for structures having thin-walled members. There are, mainly, two types instability: namely, bifurcation of equilibrium [1-11], and snap-buckling. Snap-through behaviour of structural elements (especially; shallow spherical shells, shallow arches and initially imperfect rods which have been used in many engineering, biological, industrial and scientific systems and have been subjected to severe external effects) is a very important physical phenomenon, not only for engineers but also for the scientists dealing with various structural systems. Although the snap-through behaviour of the relevant c structural elements resemble each other generally, the details of the concerning phenomenon (which is different for different structural elements, dimensional characteristics, materials used) can be crucially important from the point of design and

Note:
- This paper has been received on May 14, 2019 and accepted for publication by the Editorial Board on December 4, 2019.
- Discussions on this paper will be accepted by May 31, 2021.

• https://doi.org/10.18400/tekderg.565095

1 Yildiz Technical University, Department of Civil Engineering, İstanbul, Turkey - ekaratas@yildiz.edu.tr- https://orcid.org/0000-0003-1396-2463

2 Yildiz Technical University, Department of Civil Engineering, İstanbul, Turkey - yukselerfaruk@gmail.com - https://orcid.org/0000-0002-2733-580X

analysis of such systems. Therefore, it is not a surprise to observe publications on this subject receiving much attention for many years, including those in recent years [12-28].

Rigid vinyl polyethylene is a special material having appealing mechanical properties [https://www.aeplastics.com/rpvc/] used in many engineering systems (e.g. doorways, windows, waste water pipes, home plumbing pipes, profiles, extruded wire coverings, etc.). It was chosen to be used in the experimental study of Evan-Iwanowski et al [29] on the snap-through behaviour of shallow, clamped, simply-supported, and free edge spherical shells and arches subjected to the ring loads and concentrated loads for various values of thickness, ring diameter, depth and other dimensions related with the details of their experiments. They concluded, importantly, that there was no snap-buckling for a clamped shallow spherical shell, subjected to the ring loads, having a ring diameter below a certain value depending on the dimensions of the shell. They made a similar comment for the simply-supported spherical shells, disregarding the second summit in their load-deflection diagrams. No comment was made, in their very rigorous study, about the probability of snap-buckling free situation via the appropriate choice of the thickness higher than a certain value depending on the chosen values of the ring diameter and dimensions of the shell. To the best of the authors' knowledge of the current study, there has been no other experimental study performed on this subject, using the same material.

Second study on the snap-through behaviour of spherical shells, using the same material, under the ring loads belonged to Cagan and Taber [30]. They considered deep as well as the shallow spherical shells with clamped edges only, and used a Newton-Raphson technique on discretized nonlinear shell equations. Comparing their numerical results with those of the experimental results of Evan-Iwanowski et al [29], they achieved good agreement generally. The results, they obtained, showed that (i) if the ring diameter was smaller than a certain value, no buckling occurred, similar to what had been stated by Evan-Iwanowski et al [29]; (ii) if the ring diameter was between two prescribed values, the buckling occurred as gradual formation of a dimple of reversed curvature; (iii) if the ring diameter was between a certain value and the diameter of the shell, then the buckling occurred with an abrupt change in shape. No comment was made about the probability of no-buckling via the appropriate choice of the thickness higher than a certain value depending on a set of values for the ring diameter and other dimensions of the shell.

The present study has been the third examination of this subject. The snap-through buckling behaviour of rigid vinyl polyethylene shallow simply-supported and clamped spherical shells subjected to the static ring loads is investigated numerically. The finite difference and Newton-Raphson Method are used. The load-deflection diagrams corresponding to various values of thickness, depth and ring diameter of the shell with simply supported and clamped edges are drawn and interpreted. The main contributions of this study to the relevant literature are: (i) extension of the range of the apical deflections whereby further characteristics of the load-deflection diagrams are revealed; (ii) determination of a certain value of thickness, depending on chosen ring diameter and depth of the shell, above which no snap-buckling occurs for a clamped spherical shell, the load-deflection diagram of which generally contains only one summit (upper-limit point), (iii) determination of a certain value of thickness of a simply-supported spherical shell, above which the first summit of the load-deflection diagram (which generally contains two summits) disappears, (accordingly; the appropriate choice of the thickness can change the snap-buckling loads and deflections considerably and,

therefore, design criteria of such structures in a significant way.), (iv) the variations of the stress resultants, displacements along a meridian of the shell and deformed shapes of the shell corresponding to the various stages of the deformation (before, during and after the snap-through buckling), which are essential for engineers dealing with the design of such structures, and which have not been encountered in the relevant literature.

In Section 2, the geometrical details, definitions of stress-resultants, equations of equilibrium, kinematic equations, constitutive relations and reduced form of the governing equations are given. The discretization of the governing equations by using the finite difference and the application of the Newton-Raphson Method are presented in Section 3. In Section 4, the effect of the variations of the ring diameter, thickness and depth of the shallow spherical shells, subjected to the ring loads, to the snap-through behaviour are investigated via the load-deflection diagrams for both of the support conditions. The concluding remarks are presented in Section 5.

2. GEOMETRY AND GOVERNING EQUATIONS OF SHELL OF REVOLUTION

The geometry of a shell element of revolution before the deformation is represented in Figure (1a,1b) [31]. In the figure, the two basic curvatures are specified ($1/r_1$ and $1/r_2$) where r_1 is meridional radius of curvature and r_2 is circumferential radius of curvature, respectively. r and y are the radial and vertical coordinates of a point on the surface; s is the meridional arc length; ϕ and θ are the meridional and parallel central angles, respectively.

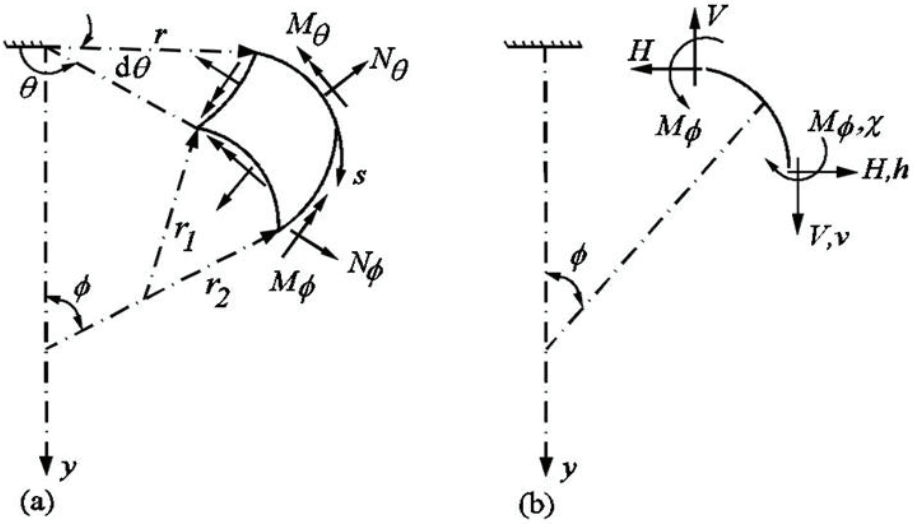

Figure 1 - The geometry of a shell element of revolution before the deformation.

The following basic relations are established [32]:

$$ds = r_1 d\phi,\ r_2 = \frac{r}{sin\phi},\ ds^2 = dr^2 + dy^2,\ \frac{dy}{dr} = tan\phi. \tag{1}$$

2.1. Stress Resultants

The stress resultants per unit length of the undeformed midsurface are defined by

$$N_\phi = \int_{-t/2}^{+t/2} \sigma_{\phi\phi}\left(1+\frac{z}{r_2}\right)\mathrm{d}z,\ N_\theta = \int_{-t/2}^{+t/2} \sigma_{\theta\theta}\left(1+\frac{z}{r_1}\right)\mathrm{d}z,\ \ Q = \int_{-t/2}^{+t/2} \sigma_{\phi z}\left(1+\frac{z}{r_2}\right)\mathrm{d}z,$$

$$M_\phi = \int_{-t/2}^{+t/2} \sigma_{\phi\phi}\left(1+\frac{z}{r_2}\right)z\mathrm{d}z,\ M_\theta = \int_{-t/2}^{+t/2} \sigma_{\theta\theta}\left(1+\frac{z}{r_1}\right)z\mathrm{d}z \tag{2}$$

where $\sigma_{\phi\phi}$, $\sigma_{\theta\theta}$, σ_{zz} and $\sigma_{\phi z}$ are meridional stress, circumferential stress, transverse normal stress and transverse shear stress components, respectively; N_ϕ andN_θ are the meridional and circumferential forces, respectively; Q is the transverse shear force; M_ϕ and M_θ are meridional and circumferential bending moments, respectively; z is the normal distance from the midsurface and t is the thickness of the undeformed shell. The positive signs of the stress resultants are shown in Figure (1b).

It is generally more convenient to study horizontal and vertical components; H and V, respectively. The corresponding relations are as follows:

$$V = N_\phi sin\phi - Qcos\phi,\ H = N_\phi cos\phi + Qsin\phi. \tag{3}$$

where V and H are vertical and horizontal force resultants acting per unit length of the midsurface curve, respectively [32].

2.2. Equilibrium Equations

The equilibrium equations for axisymmetric deformation of a shell of revolution are as follows [30, 32]:

$$\frac{\mathrm{d}}{\mathrm{d}s}(rV) = -rP_V, \qquad \frac{\mathrm{d}}{\mathrm{d}s}(rH) = N_\theta - rP_H,$$

$$\frac{d}{\mathrm{d}s}\left(rM_\phi\right) = rM_\theta cos\phi + rHsin\phi - rVcos\phi. \tag{4}$$

where P_V and P_H are vertical and horizontal surface loads acting per unit midsurface area of the undeformed shell, respectively [32].

2.3. Kinematic Equations

Displacements occurring at a point on the midsurface of the shell can be defined with the radial and vertical displacement components, h and v respectively, shown in Figure (1b). Meridional and circumferential strains (e_ϕ, e_θ) in distance z from the midsurface, respectively, are

$$e_\phi = \frac{\varepsilon_\phi + z\kappa_\phi}{1+\frac{z}{r_1}},\ e_\theta = \frac{\varepsilon_\theta + z\kappa_\theta}{1+\frac{z}{r_2}}. \tag{5}$$

where ε_ϕ and ε_θ are meridional and circumferential midsurface strain measures, respectively; κ_ϕ and κ_θ meridional and circumferential curvature change measures, respectively. Equations (5) are valid for small strains. The linear measures used in equations (5) are:

$$\varepsilon_\phi = \frac{\mathrm{d}h}{\mathrm{d}s}cos\phi + \frac{\mathrm{d}v}{\mathrm{d}s}sin\phi,\ \varepsilon_\theta = \frac{h}{r},\ \kappa_\phi = \frac{\mathrm{d}\chi}{\mathrm{d}s}, \kappa_\theta = \frac{\chi cos\phi}{r}. \tag{6}$$

On the assumption that transverse shear deformation can be neglected, the rotation of the normal to the midsurface is equal to χ.

2.4. Constitutive Equations

The stress component normal to the shell surface σ_{zz} is assumed to be small compared to the stresses tangent to the surface $\left(\sigma_{zz} \ll \sigma_{\phi\phi}, \sigma_{\theta\theta}\right)$. Three dimensional constitutive equations for an isotropic, elastic shell after neglection of the transverse shear stress are written as follows:

$$Ee_z = -\vartheta\left(\sigma_{\phi\phi} + \sigma_{\theta\theta}\right),\ \sigma_{\phi\phi} = \frac{E}{1-\vartheta^2}\left(e_\phi + \vartheta e_\theta\right),\ \sigma_{\theta\theta} = \frac{E}{1-\vartheta^2}\left(e_\theta + \vartheta e_\phi\right). \tag{7}$$

A thin shell assumption is used $\left(\frac{t}{r_1} \ll 1,\ \frac{t}{r_2} \ll 1\right)$, therefore the terms including $\frac{z}{r_i}$ are considered to be negligibly small in comparison with unity in Eqs. (2) [23]. The corresponding two dimensional constitutive equations are

$$N_\phi = \frac{Et}{1-\vartheta^2}\left(\varepsilon_\phi + \vartheta\varepsilon_\theta\right), \qquad N_\theta = \frac{Et}{1-\vartheta^2}\left(\varepsilon_\theta + \vartheta\varepsilon_\phi\right),$$

$$M_\phi = Etc^2\left(\kappa_\phi + \vartheta\kappa_\theta\right),\ M_\theta = Etc^2\left(\kappa_\theta + \vartheta\kappa_\phi\right). \tag{8}$$

where E and υ are the elastic modulus and Poisson's ratio, respectively, and

$$c^2 = \frac{t^2}{12(1-\vartheta^2)}. \tag{9}$$

2.5. Fundamental Equations of a Shell of Revolution

The fundamental differential equations for a shell of revolution are reduced to a first order matrix system [32]. The general form of these equations is

$$\left\{\frac{\mathrm{df}}{\mathrm{d}s}\right\} = [\mathrm{A}]\{\mathrm{f}\} + \{N(\mathrm{f})\} + \{\mu\} \tag{10}$$

where

{f}: the vector that contains the stress-resultants and displacements which is described as

$$\{\mathrm{f}\}^T = \left[rM_\phi \;\; rH \;\; rV \;\; \chi \;\; h \;\; v\right], \tag{11}$$

$[A]$: the coefficient matrix which is described as

$$[A] = \begin{bmatrix} \frac{\vartheta cos\phi}{r} & sin\phi & -cos\phi & \frac{Et^3cos^2\phi}{12r} & 0 & 0 \\ 0 & \frac{\vartheta cos\phi}{r} & \frac{\vartheta sin\phi}{r} & 0 & \frac{Et}{r} & 0 \\ 0 & 0 & 0 & 0 & 0 & 0 \\ (rEtc^2)^{-1} & 0 & 0 & \frac{-\vartheta cos\phi}{r} & 0 & 0 \\ 0 & \frac{1-\vartheta^2}{rEt}cos^2\phi & \frac{1-\vartheta^2}{rEt}cos\phi sin\phi & -sin\phi & \frac{-\vartheta cos\phi}{r} & 0 \\ 0 & \frac{1-\vartheta^2}{rEt}cos\phi sin\phi & \frac{1-\vartheta^2}{rEt}sin^2\phi & -cos\phi & \frac{-\vartheta sin\phi}{r} & 0 \end{bmatrix} \tag{12}$$

$\{N(\mathrm{f})\}$: the vector that contains non-linear terms which is described as

$$\{N(\mathrm{f})\} = \begin{bmatrix} \chi(rHcos\phi + rVsin\phi) \\ 0 \\ 0 \\ 0 \\ -\chi^2 cos\phi/2 \\ -\chi^2 sin\phi/2 \end{bmatrix}, \tag{13}$$

{μ}: the vector of loading terms which is described as

$$\{\mu\}^T = [0 \quad -rP_H \quad -rP_V \quad 0 \quad 0 \quad 0]. \tag{14}$$

The terms (11), (12), (13) and (14) are inserted into equation (10) and expressed explicitly as follows [30]:

$$\left(rM_\phi\right)_{,s} = \left(\frac{\vartheta cos\phi}{r}\right)rM_\phi + sin\phi rH - cos\phi rV + \frac{Et^3cos^2\phi}{12r}\chi$$

$$+\chi(rHcos\phi + rVsin\phi), \tag{15}$$

$$(rH)_{,s} = \left(\frac{\vartheta cos\phi}{r}\right)rH + \left(\frac{\vartheta sin\phi}{r}\right)rV + \frac{Et}{r}h, \tag{16}$$

$$(rV)_{,s} = 0, \tag{17}$$

$$\chi_{,s} = \frac{M_\phi}{Etc^2} - \frac{\vartheta cos\phi}{r}\chi, \tag{18}$$

$$h_{,s} = \frac{1-\vartheta^2}{rEt}cos^2\phi rH + \frac{1-\vartheta^2}{rEt}sin\phi cos\phi rV - sin\phi\chi - \frac{\vartheta cos\phi}{r}h - \frac{\chi^2 cos\phi}{2}, \tag{19}$$

$$v_{,s} = \frac{1-\vartheta^2}{rEt} sin\phi cos\phi rH + \frac{1-\vartheta^2}{rEt} sin^2\phi rV + cos\phi\chi - \frac{\vartheta sin\phi}{r} h - \frac{\chi^2 sin\phi}{2}. \quad (20)$$

In this study, for the mathematical structure of the manuscript, Reference [32] has been used which was one of the pioneering works on this field. There are, of course, new studies providing improvements on this subject by relaxing the restrictions on rotations and deformations (e.g. by taking into account the transverse normal and transverse shear strains) and by using higher order constitutive relations. If a rubber-like material, for example, which can undergo very large elastic strains, had been considered, then it would have been inevitable to deal with an advanced shell theory, developed recently.

3. SOLUTION METHOD

In this section, the fundamental differential equations for a shell of revolution, given in the previous section, are applied for the shallow spherical shell. If the ratio of the rise of the midsurface of the shell at the centre to the base diameter is smaller than $1/8$, the concerning spherical shell is called ‘‘shallow’’[33]:

$$\eta = \frac{B}{2a} \leq \frac{1}{8} \quad (21)$$

where η, B and a are the parameter of depth, the rise of the midsurface of the shell at the centre and the base radius, respectively, as shown in Figure 2. The spherical shell subjected to a static ring load, shown in Figure 2, is divided into $(nn-1)$ finite segments, corresponding to nn nodes where the first node is located at a clamped support or a simple support while the final node is located at the apex, with the step length of Δs. There is a uniformly distributed ring load with the resultant P at the point $\ell\ell$ of the shell where r_0 is the radius of the ring before the deformation. R is the radius of the undeformed shell. ϕ_0 and ϕ_m are the meridional angles at the application point of the ring load and at the support, respectively.

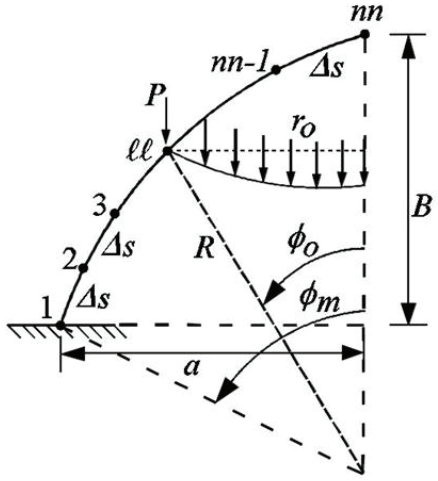

Figure 2 - Shell divided into finite segments.

The derivatives seen in Eqs. (15)-(20) are expressed by using the forward difference formulas for any point (i) and the following nonlinear algebraic equations are obtained:

$$-M_{i+1}+M_i\left(1+\frac{\Delta\vartheta cos\phi_i}{r_i}-\frac{\Delta cos\phi_i}{r_i}\right)+\Delta sin\phi_i H_i-\Delta V_i cos\phi_i+\frac{\Delta Et^3 cos^2\phi_i}{12r_i^2}\chi_i+$$
$$\Delta\chi_i(H_i cos\phi_i+V_i sin\phi_i)=0, \tag{22}$$

$$-H_{i+1}+H_i\left(1+\frac{\Delta\vartheta cos\phi_i}{r_i}-\frac{\Delta cos\phi_i}{r_i}\right)+\frac{\Delta\vartheta sin\phi_i}{r_i}V_i+\frac{\Delta Et}{r_i^2}h_i=0, \tag{23}$$

$$-V_{i+1}+V_i\left(1-\frac{\Delta cos\phi_i}{r_i}\right)=0, \tag{24}$$

$$-\chi_{i+1}+\chi_i\left(1-\frac{\Delta\vartheta cos\phi_i}{r_i}\right)+\frac{\Delta M_i}{Etc^2}=0, \tag{25}$$

$$-h_{i+1}+h_i\left(1-\frac{\Delta\vartheta cos\phi_i}{r_i}\right)+\frac{\Delta(1-\vartheta^2)cos^2\phi_i}{Et}H_i+\frac{\Delta(1-\vartheta^2)cos\phi_i sin\phi_i}{Et}V_i-\Delta sin\phi_i\chi_i-$$
$$\Delta\chi_i^2\frac{cos\phi_i}{2}=0, \tag{26}$$

$$-v_{i+1}+v_i+\frac{\Delta(1-\vartheta^2)sin\phi_i cos\phi_i}{Et}H_i+\frac{\Delta(1-\vartheta^2)sin^2\phi_i}{Et}V_i-\Delta cos\phi_i\chi_i\frac{\Delta\vartheta sin\phi_i}{r_i}h_i-$$
$$\Delta\chi_i^2\frac{cos\phi_i}{2}=0. \tag{27}$$

Equations (22)-(27) are employed between the points $(1,\ell\ell-2)$ of the shell. At the point $(\ell\ell-1)$, on the other hand, the equation related to the vertical force resultant, Eq.(24), is omitted in order to exclude the external force P from the list of the unknows. Therefore, 5 equations are written for this point. Moreover, 5 equations are written at each node between the points $(\ell\ell, nn-1)$ including the point $(nn-1)$ due to the fact that the vertical force resultant is equal zero for these points which may easily be obtained from the equilibrium of the concerning segment. The numerical solution is derived by the Newton-Raphson method. In order not to encounter a problem of convergence in the vicinity of the region where the slope of the force-deflection curve is zero, the apical vertical displacement v_{nn} is used in the input data instead of the ring load P.† The initial guess of the state vector is taken to be zero vector ($\{f\}=\{0\}$), corresponding to the zero value of v_{nn}. As a criteria for the convergence of the successive approximations of the Newton-Raphson method, a vector corresponding to the energy level at the (k) th iteration is defined as follows [30]:

$$\left\|f^{(k)}(s)\right\|_E=\left(\left|rM_\phi\cdot\chi\right|+\left|rH.h\right|+\left|rV.v\right|\right) \tag{28}$$

† There have been advanced techniques, proposed by Memon and Su [34], Riks [35,36], Wempner [37], Polat and Calayır [38], Polat [39] to treat the convergence problem in the vicinity of the limit points of the force-deflection curves, which may unavoidably be used for relatively more complex problems than the one considered in the current study.

The convergence at any iteration is considered to be achieved, if the relative difference Ω, defined as

$$\Omega = \frac{\|f^{(k+1)}(s)\|_E - \|f^{(k)}(s)\|_E}{\|f^{(k+1)}(s)\|_E}, \tag{29}$$

is smaller than a prescribed value. The boundary conditions at the apex (nn) are

$$\chi_{nn} = h_{nn} = 0. \tag{30}$$

The boundary conditions for a clamped edge are

$$\chi_1 = h_1 = v_1 = 0, \tag{31}$$

while the boundary conditions for a simply supported edge are

$$M_1 = h_1 = v_1 = 0. \tag{32}$$

$(5nn + \ell\ell - 7)$ equations written between the points $(1, nn - 1)$ and 3 boundary conditions at the support represent a total equal to $(5nn + \ell\ell - 4)$ equations which is equal to the number of unknowns. The external force P which is absent in the state vector can be computed by the help of the vertical equilibrium equation of the whole of the shell after the numerical solution of the unknowns at each level of the loading is obtained:

$$P2\pi r_0 + V_1 2\pi a = 0. \tag{33}$$

where

$$r_0 = Rsin\phi_0, \quad a = Rsin\phi_m. \tag{34}$$

where R, r_0, ϕ_0 and ϕ_m denote the radius of the spherical shell, the radius of the ring load, the meridional angle at the application point of the ring load and the meridional angle at the support, respectively.

4. NUMERICAL EXPERIMENTS

The effect of the variation of the diameter of the ring load, thickness and depth of the shell on the axially symmetrical ring load versus the deflection curves at the point of application of the load for two types of supports (clamped edge and simply supported edge) are investigated by several numerical experiments. Additionally, the variations of the stress-resultants and deformed shapes are investigated corresponding to various stages of the loading; before, during and after the snap-through buckling (where the slope of the load-deflection curve is zero).

Computer program used in the numerical study has been coded by the authors in the package FTN90.

In this study, a non-dimensional load P^*, the resultant of the distributed ring load, acting at any height of the shell, and a nondimensional deflection v^* at the application point of the ring load are defined as follows:

$$P^* = \frac{PR}{Et^3}, \quad v^* = \frac{v_i}{t}. \tag{35}$$

where v_i is the deflection at the application point of the ring load.

In order to demonstrate the accuracy of the prepared computer program, the numerical results obtained by using the computer program prepared in the present study are compared with those obtained by Evan-Iwanowski et al. [29] via an experimental study on die-pressed plastic shallow shells made of rigid vinyl polyethylene (rigid PVC) with radii of $254\ mm$. The results of the comparison are shown in Figure 3. A sufficient agreement is observed.

The curves of the non-dimensional load P^* versus the non-dimensional deflection v^* obtained in the numerical experiments for various values of the diameter of the ring load, the shell thickness and the parameter of the depth for clamped edge and simply supported edge are shown in Figures (3-8).

It can be seen from Figure 3 that there is no snap-buckling for $d \leq 15.0492\ mm$. The curve corresponding to *d=15.0492* is indicated by a solid red line. The curves indicated by blue lines are for $d = 12.7\ mm$ and those indicated by black lines are for $d = 25.4\ mm$. As the ring diameter d is increased, both of the buckling load and buckling deflection increase, as well

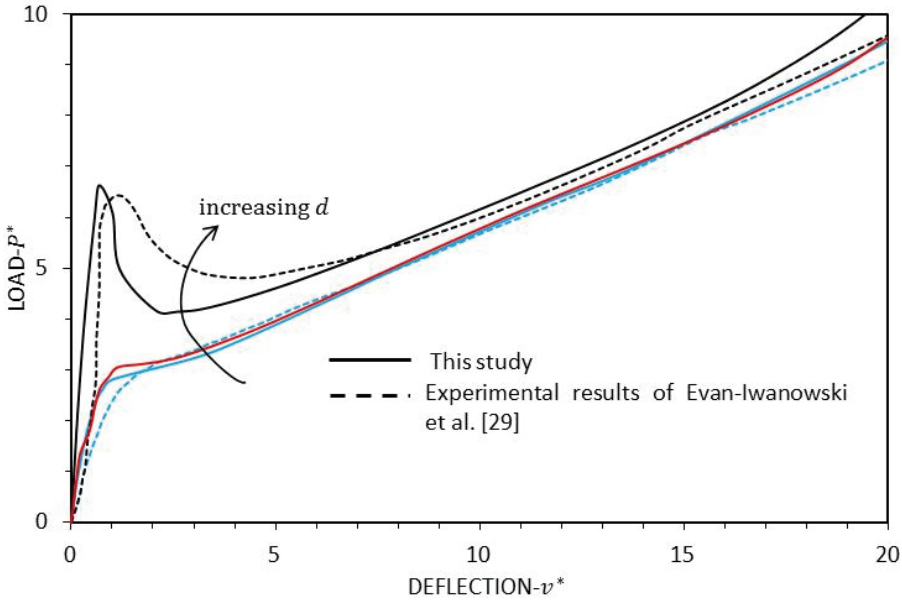

Figure 3 - Comparison of the load-deflection curves obtained in this study with those corresponding to the experiments performed by Evan-Iwanowski et al. [29] for clamped edge shallow shell for $\eta = 0.0618, t = 0.3810\ mm, d = 12.7; 15.0492; 25.4\ mm.$

Figure 4 shows the load-deflection curves of the clamped shallow spherical shells for various values of t, corresponding to the given values of d and η. Accordingly; for (i) $t = 0.3810\ mm$, the load-deflection curve has two peaks (upper limit points) the first of which controls the buckling; (ii) $t = 0.7620\ mm$, the second summit is seen to disappear, leaving a unique summit; (iii) $t = 1.0660\ mm$, there is no summit, meaning that no snap-buckling occurs for this value of the thickness and those greater than this value. As the thickness t is decreased, both of the buckling load and buckling deflection are increased, as well. Therefore; an appropriate choice of the thickness, depending on the values d and η, can prevent the likelihood of snap-buckling completely.

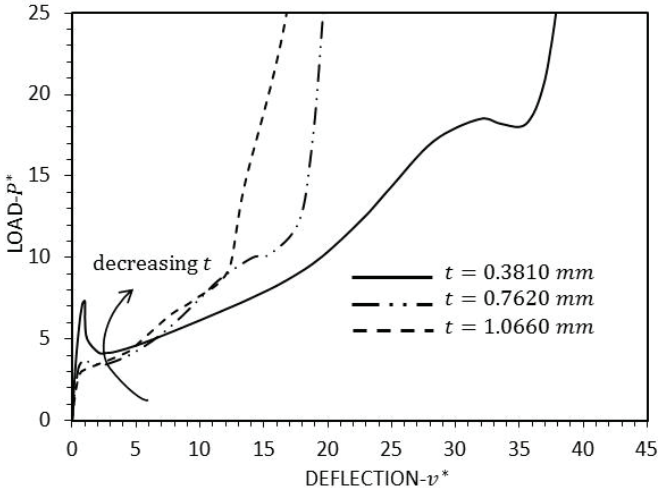

Figure 4 - Load-deflection curves for different values of t *for clamped edge shallow shell for* $\eta = 0.0618, d = 25.4\ mm$.

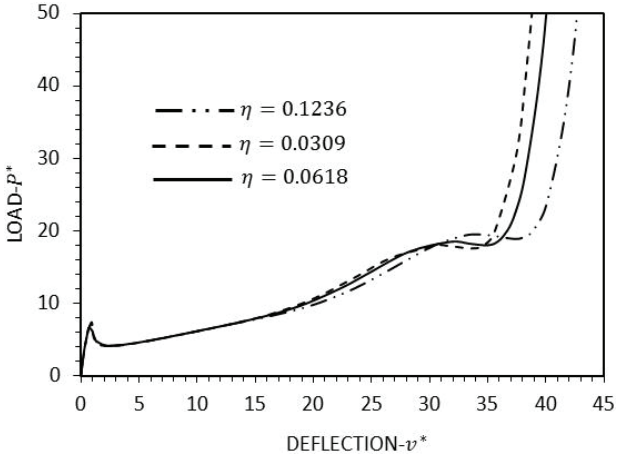

Figure 5 - Load-deflection curves for various values of η *for clamped edge shallow shell for* $d = 25.4\ mm, t = 0.3810\ mm$.

Figure 5 illustrates the effect of η on the concerning behaviour of the clamped shallow spherical shells for the given values of t and d. Extending the range of the values of v^*, second summits in the load-deflection diagrams are observed at about $30 < v^* < 35$, which were not seen in the previous studies. The first summits, therefore the buckling loads and buckling deflections, are observed to be unaffected by the variation of η .

The load-deflection curves, shown in Figure 6, of the simply supported shallow spherical shells for various values of d, corresponding to the given values of t and η, have two summits for $d > 14.9314\ mm$, in which cases the first summit dominate the buckling. For any curve corresponding to $d \leq 14.9314\ mm$, there is only one summit. This phenomenon yields that a choice of the ring diameter d smaller than or equal to $14.9314\ mm$, corresponding to the given values of t and η, increases the buckling loads and buckling deflections remarkably.

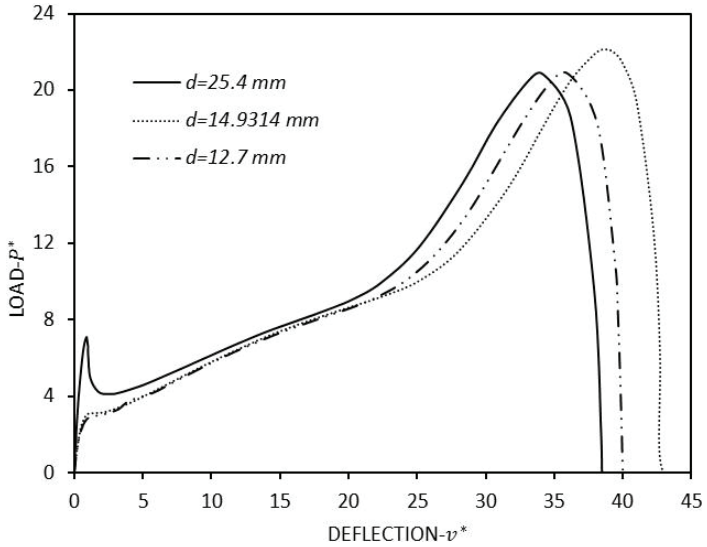

Figure 6 - Load-deflection curves for various values of d for simply supported shallow shell for $t = 0.3810\ mm, \eta = 0.0668$.

The load-deflection curves, shown in Figure 7, of the simply supported shallow spherical shells for various values of t, corresponding to the given values of d and η, have two peaks, except the one belonging to $t = 1.1307\ mm$ (in which case, there is only one summit), similar to what was observed in Evan-Iwanowski et al. [29] . This phenomenon suggests that a choice of the thickness t greater than or equal to $1.1307\ mm$, corresponding to the given values of d and η, increases the buckling loads and buckling deflections remarkably.

The load-deflection curves, shown in Figure 8, of the simply supported shallow spherical shells for various values of η, corresponding to the given values of t and d, have two summits. Increasing the values of η is seen to cause increase in the coordinates of the second summits considerably, but this has almost no effect on the first summit, which controls the buckling load and buckling deflection.

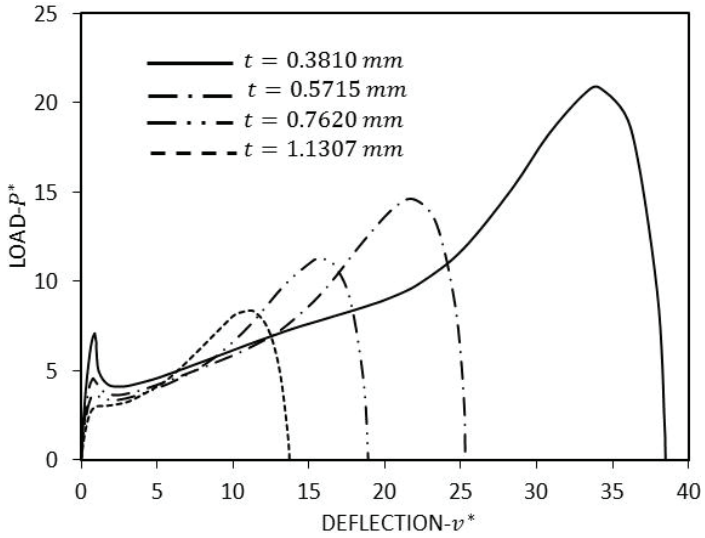

Figure 7 - Load-deflection curves for various values of t *for simply supported shallow shell for* $\eta = 0.0668, d = 25.4\ mm.$

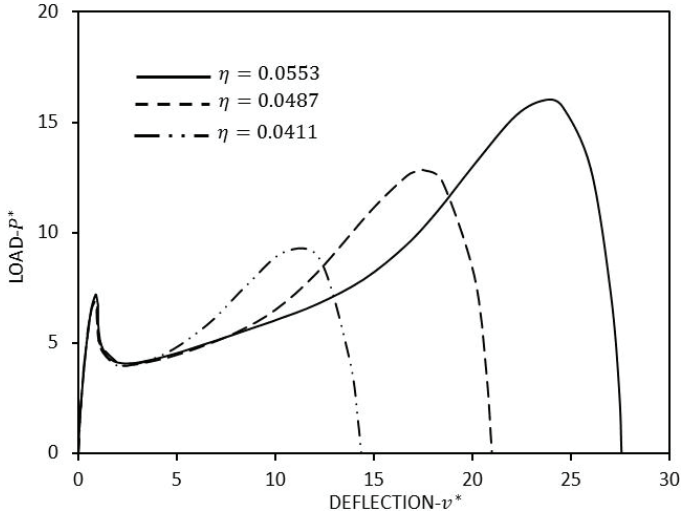

Figure 8 - Load-deflection curves for various values of η *for simply supported shallow shell for* $t = 0.6350\ mm, d = 25.4\ mm.$

Comparison of some of the load-deflection curves corresponding to the simply supported and clamped shallow shells are shown in Figure 9 and Figure 10, by varying $d$and t, respectively. Interestingly, the load-deflection curves corresponding to the concerning supports almost coincide in the neighbourhood of the first summits. The load-deflection diagrams corresponding to the simply supported shallow spherical shells are seen to, generally, contain

two summits, the first of which can disappear via the appropriate choices of t, d and η, as mentioned. The second summits in the load-deflection diagrams corresponding to the clamped shallow spherical shells are observed to be realized only at relatively high values of the deflection. For the values of $d = 12.7\ mm, t = 0.3810\ mm$ and $\eta = 0.0668$, the first summit disappears, seen in Figure 9.

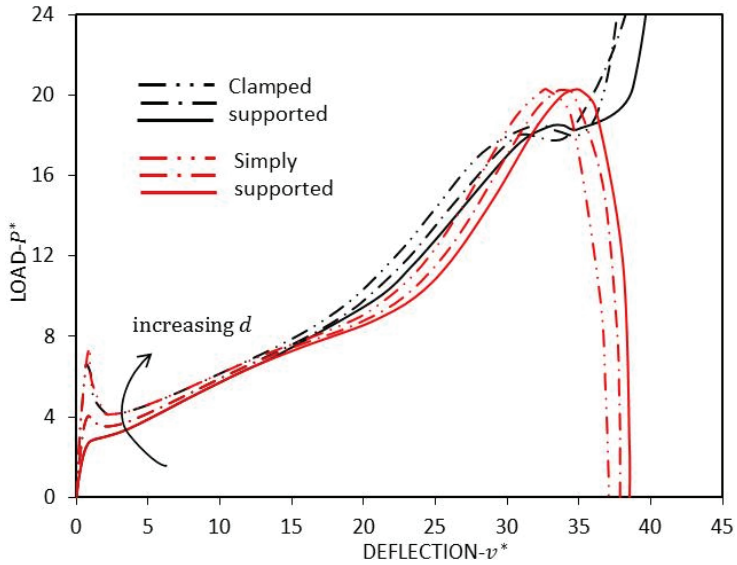

Figure 9 - Comparison of the results corresponding to clamped and simply supported for different values of d for $\eta = 0.0618, t = 0.3810\ mm, d = 12.7; 19.1; 25.4\ mm$.

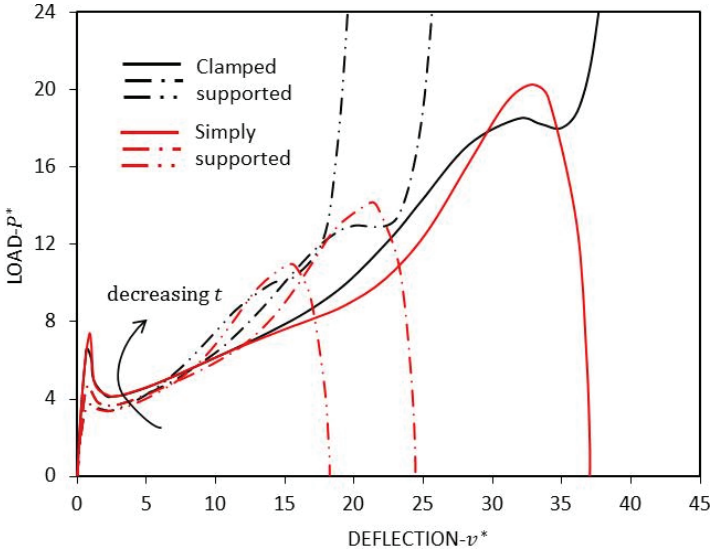

Figure 10 - Comparison of the results corresponding to clamped and simply supported for different values of t for $\eta = 0.0618, d = 25.4, t = 0.3810; 0.5715; 0.7620\ mm$.

In order to see the variations of the stress-resultants, displacements and the deformed shapes of a clamped shallow spherical shell along the arc length s during the various stages of the loading, the graphs of the stress-resultants and the deformed shapes of the shell corresponding to various values of v^* (before the buckling, during the buckling and after the buckling corresponding to the load-deflection diagram seen in Figure 3 for $d = 25.4\ mm, t = 0.3810\ mm, \eta = 0.0618$) are shown in Figures 11-16. v_{cr}^* is the deflection of the shell (at the level of the ring) when the buckling occurs[‡]. s^*, seen in Figures 11-16, is the non-dimensional meridian length such that s^* is taken to be zero at the apex and equal to 1 at the support. The value of s^* at any point i of the meridian can be checked to be determined as

$$s^* = \frac{1}{(nn-1)}[(nn-1)-(i-1)]. \tag{36}$$

In Figure 11; the diagrams of the meridional bending moment M along a meridian corresponding to the various stages of the deformation (namely; before the buckling, during the buckling and after the buckling) are shown for a given set of values of d, t and η. An abrubt change in the magnitude and sign of M due to the buckling is observed clearly. The apical moment (at $s^* = 0$) should be considered primarily for the design of such a structure.

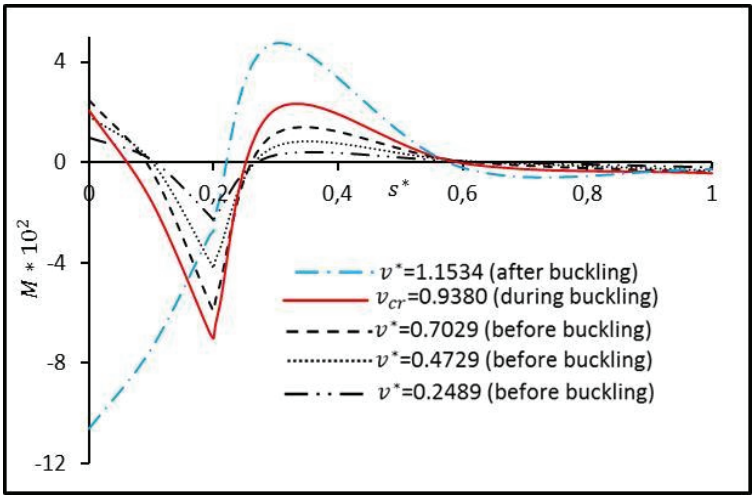

Figure 11 - The variation of the meridional moment M along the meridian for various values of v^* for $\eta = 0.0618, d = 25.4\ mm, t = 0.3810\ mm$.

The diagrams of the horizontal force resultant H along a meridian corresponding to the various stages of the deformation are shown for a given set of values of d, t and η in Figure 12. The values of H are seen to be increasing drastically during and after the buckling. The apical H value should be considered to be most essential value.

[‡] In other words, v_{cr}^* is the deflection where the slope of the load-deflection diagram vanishes.

The diagrams of the vertical force resultant V along a meridian corresponding to the various stages of the deformation are shown for a given set of values of d, t and η in Figure 13. V is seen to vanish between the apex and the ring, as expected. It attains its highest values in the neighbourhood of the ring.

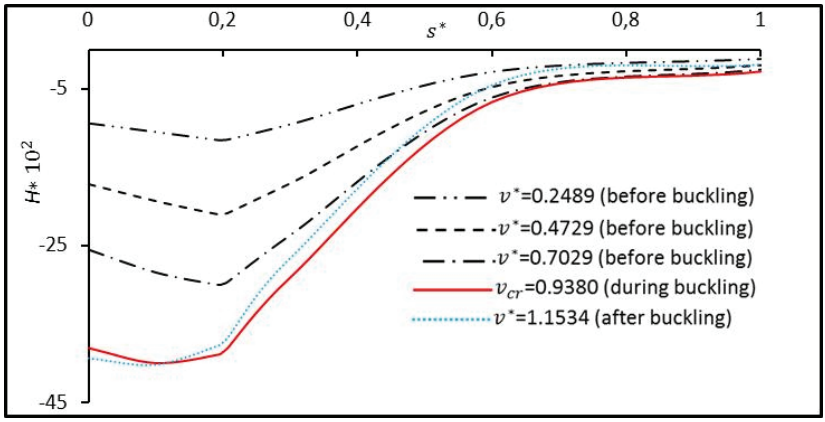

Figure 12 - The variation of the horizontal force resultant H along the meridian for various values of v^* for $\eta = 0.0618, d = 25.4\ mm, t = 0.3810\ mm$.

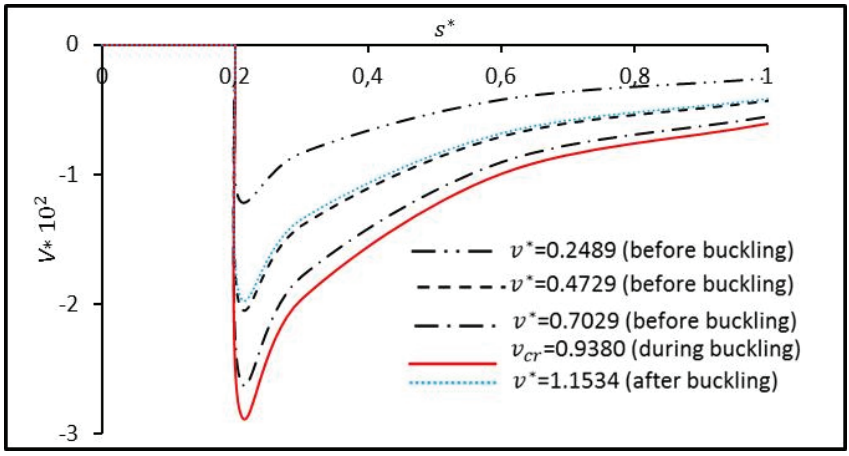

Figure 13 - The variation of the vertical force resultant V along the meridian for various values of v^* for $\eta = 0.0618, d = 25.4\ mm, t = 0.3810\ mm$.

The diagrams of the rotation angle χ corresponding to the various stages of the deformation are shown in Figure 14 for a given set of values of d, t and η. The rotation angle is zero at the apex, as a boundary condition. It reaches its maximum value in the neighbourhood of the ring, especially after the buckling.

The diagrams of the horizontal displacement h corresponding to the various stages of the deformation are shown in Figure 15 for a given set of values of d, t and η. h is zero at the apex, as expected. It reaches its highest values in the region of $0.5 \leq s^* \geq 0.6$.

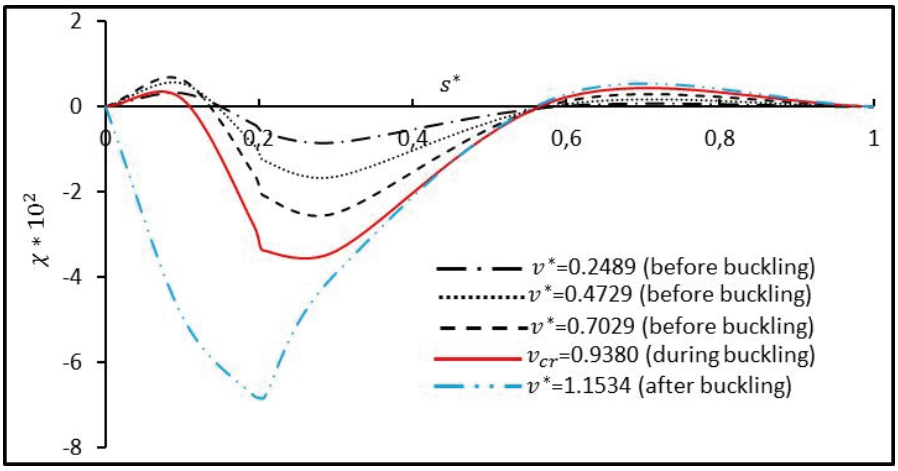

Figure 14 - The variation of the rotation χ of the normal to the midsurface for various values of v^* for $\eta = 0.0618, d = 25.4\ mm, t = 0.3810\ mm$.

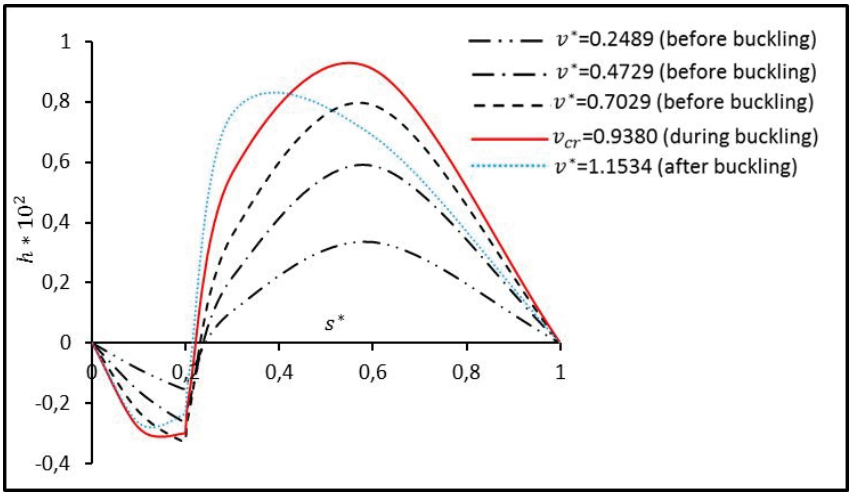

Figure 15 - The variation of the horizontal displacement h for various values of v^* for $\eta = 0.0618, d = 25.4\ mm, t = 0.3810\ mm$.

The diagrams of the vertical displacement v corresponding to the various stages of the deformation are shown in Figure 16 for a given set of values of d, t and η. The vertical

displacement is seen to obtain its highest values at the apex. An abrupt increase in the values of v is observed in the figure due to the buckling.

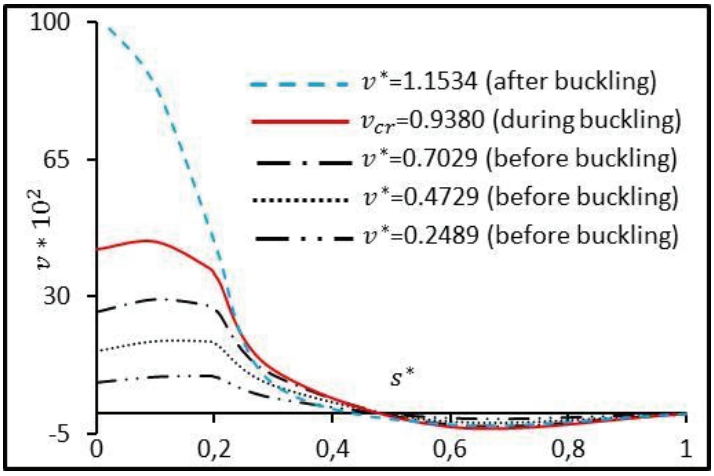

Figure 16 - The variation of the vertical displacement v for various values of v^* for $\eta = 0.0618, d = 25.4\ mm, t = 0.3810\ mm$.

Deformed shapes of a clamped shallow shell corresponding to various stages of load, namely those corresponding to before the buckling ($v^* < v_{cr}$), during the buckling ($v^* = v_{cr}$) and after the buckling ($v^* > v_{cr}$) are shown in Figure 17. The auxiliary expressions are presented in Appendix A and Appendix B. A very drastic deformation can be observed after buckling.

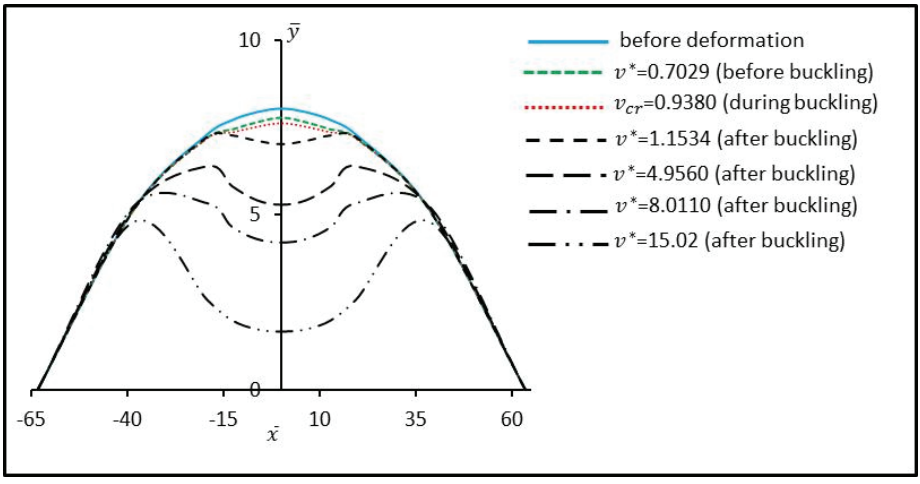

Figure 17 - Geometries of shallow spherical shell before, during and after deformation for clamped shell for $\eta = 0.0618, d = 25.4\ mm, t = 0.3810\ mm$.

5. CONCLUSIONS

According to the numerical results obtained for the rigid vinyl polyethylene shallow spherical shells subjected to the static ring loads, the following main conclusions can be drawn:

- The numerical results obtained in this study are sufficiently compatible with the results of the experimental study conducted by Evan-Iwanowski et al. [29].
- It is possible to prevent the probability of the snap-buckling of a clamped shallow spherical shell through the appropriate choices of the ring diameter, thickness and depth of the shell.
- It is possible to increase the snap-buckling loads and deflections considerably for a simply supported shallow spherical shell through the appropriate choices of the ring diameter, thickness and depth of the shell.
- As the thickness of a shell is decreased and/or the ring diameter is increased, both of the snap-buckling load and the snap-buckling deflection are increased.
- The snap-buckling loads and the snap-buckling deflections of the shallow spherical shells are not significantly affected by the variation of the depth of the shell.
- The second summits of the load-deflection diagrams of the clamped shallow spherical shells are revealed by extending the range of the apical deflections.
- For the design and/or analysis of such a structure; (i) the apical values of the deflection (vertical displacement), bending moment and the horizontal force, (ii) the values of the vertical force and the rotation angle in the neighbourhood of the ring should be considered primarily.

Appendix A

The coordinates x and y of a point of the midsurface of the shell before the deformation can be checked to be expressed as in terms of R, ϕ and ϕ_m as

$$x = R\sin\phi, \tag{A1}$$

$$y = R(\cos\phi - \cos\phi_m), \tag{A2}$$

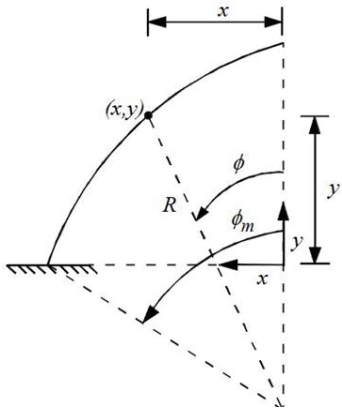

Figure 18 - Geometry of shell before deformation.

Appendix B

Using the displacement components h and v, the coordinates $\bar{x}$ and $\bar{y}$ of a point of the midsurface of the shell after the deformation can be checked to be expressed as

$$\bar{x} = Rsin\phi + h, \tag{B1}$$

$$\bar{y} = R(cos\phi - cos\phi_m) - v. \tag{B2}$$

References

[1] Labisch, F. K., On the Axisymmetric Buckling Behavior of Incompressible Nonlinearly Elastic Spherical Shells. Z. Angew. Math. Mech., 86(7), 572-583, 2006.

[2] Pi, Y. L., Bradford, M. A. and Tin-Loi, F., Nonlinear Analysis and Buckling of Elastically Supported Circular Shallow Arches. International Journal of Solids and Structures, 44, 2401-2425, 2007.

[3] Guana, F. and Pastrone, F., Axisymmetric Instabilities for Elastic Conical Shells under Compressive End Loadings. Mathematics and Mechanics of Solids, 12, 164-182, 2007.

[4] Pi, Y. L., Bradford, M. A. and Tin-Loi, F., Non-linear In-plane Buckling of Rotationally Restrained Shallow Arches under a Central Concentrated Load. International Journal of Non-Linear Mechanics, 43, 1-17, 2008.

[5] Cai, J. and Feng, J., Buckling of Parabolic Shallow Arches When Support Stiffens under Compression. Mechanics Research Communications, 37, 767-471, 2010.

[6] Coman, C. D., Bifurcation Instabilities in Finite Bending of Circular Cylindrical Shells. International Journal of Engineering Science, 119, 249-264, 2017.

[7] Hutchinson, J. W., Buckling of Spherical Shells Revisited, Proceedings of the Royal Society A: Mathematical, Physical and Engineering Sciences, 472 (2195), 2016. DOI:https://doi.org/10.1098/rspa.2016.0577.

[8] Yükseler, R. F., The Strain Energy Density of Compressible, Rubber-Like Shells of Revolution, ASME Journal of Applied Mechanics, 63, 419 – 423, 1996.

[9] Yükseler, R. F., On the Definition of the Deformed Reference Surface of Rubber-Like Shells of Revolution, ASME Journal of Applied Mechanics, 63, 424 – 428, 1996.

[10] Yükseler, R. F., A Theory for Rubber-Like Rods, International Journal of Solids and Structures, 69-70, 350–359, 2015.

[11] Yükseler, R. F., Local and Nonlocal Buckling of Mooney-Rivlin Rods, European Journal of Mechanics - A/ Solids, Volume 78, November-December 2019, (https://doi.org/10.1016/j.euromechsol.2019.103816)

[12] Moon, J., Yoon, K. Y., Lee, T. H., et al. In-plane Elastic Buckling of Pin-ended Shallow Parabolic Arches. Engineering Structures, 29:2611-2617, 2017.

[13] Altekin, M. and Yükseler, R. F., A Parametric Study on Geometrically Nonlinear Analysis of Initially Imperfect Shallow Spherical Shells, Journal of Elastomers and Plastics, 40. DOI: 10.1177/0095244307084907, 2008.

[14] Yıldırım, B. and Yükseler, R. F., Effect of Compressibility on Nonlinear Buckling of Simply Supported Polyurethane Spherical Shells Subjected to an Apical Load, Journal Of Elastomers And Plastics, 43. DOI: 10.1177/0095244310393930, 2011.

[15] Pi, Y. L. and Bradford, M. A., Non-linear Buckling and postbuckling Analysis of Arches with unequal Rotational End Restraints under a Central Concentrated Load. International Journal of Solids and Structures, 49:3762-3773, 2012.

[16] Chen, X. and Meguid, S. A., On the Parameters Which Govern the Symmetric Snap-through Buckling Behavior of an Initially Curved Microbeam. International Journal of Solids and Structures, 66:77-87, 2015.

[17] Plaut, R. H., Snap-through of Shallow Reticulated Domes under Unilateral Displacement Control. International Journal of Solids and Structures, 148-149:24-34, 2018.

[18] Tsiatas, G. C. and Babouskos, N. G., Linear and Geometrically Nonlinear Analysis of Non-uniform Shallow Arches under a Central Concentrated Force. International Journal of Non-Linear Mechanics, 92:92-101, 2017.

[19] Virgin, L. N., Wiebe, R., Spottswood, S. M., et al. Sensitivity in the Structural Behavior of Shallow Arches. International Journal of Non-Linear Mechanics, 58:212-221, 2014.

[20] Ma, H., Fan, F., Wen, P., et al. Experimental and Numerical Studies on a Single-layer Cylindrical Reticulated Shell with Semi-rigid Joints. Thin-Walled Structures, 86:1-9, 2015.

[21] Cui, Z., Bhattacharyya, D., Moltschaniwskyj, G., Experimental and Numerical Study of Buckling Response of Composite Shells Compressed Transversely Between Rigid Platens. Composites: Part B., 36:478-486, 2005.

[22] Ko1odziej, S. and Marcinowski, J., Experimental and Numerical Analyses of the Buckling of Steel, Pressurized, Spherical Shells. Advances in Structural Engineering, 21(16):2416-2432, 2018.

[23] Made, A. M., Mirmiran, A. and Nelsen, D., Stability Tests of Sandwich Composite Elastica Arches. Journal Of Structural Engıneerıng, 128(5):683-686, 2002.

[24] Erdölen, A. and Yükseler, R. F., An Approach for Finite Strains and Rotations of Shells of Revolution with Application to a Spherical Shell under a Uniformly Distributed Pressure. Journal of Elastomers and Plastics, 35 (4), 357-365, October 2003, DOI:10.1177/009524403038015.

[25] Altekin, M. and Yükseler, R. F., Geometrically Nonlinear Analysis of Clamped Shallow Spherical Shells, 8th Int. Congress on Advances in Civil Engineering, Eastern, Mediterranean University, Famagusta, North Cyprus, 2008.

[26] Yıldırım, B. and Yükseler, R. F., Combined Effect of Compressibility, Height and Thickness on the Nonlinear Behaviour of Polyurethane, Simply-Supported Spherical Shells under Apical Loads, Bitlis Eren Univ J Sci & Technol, 4 (1), 12-19, 2014.

[27] Koçak, A. and Yükseler, R. F., Finite Axisymmetric Strains and Rotations of Shells of Revolution with Application to the Problem of a Spherical Shell under a Point Load. Sixth Annual International Conference on Composites Engineering, Orlando, Florida, 1999.

[28] Altekin, M. and Yükseler, R. F., Geometrically Nonlinear Axisymmetric Buckling Analysis of Shallow Spherical Shells. International Civil Engineering & Arcitecture Symposium for Academicians, Side-Antalya, Turkey, 2014.

[29] Evan-Iwanowski, R. M., Loo, T. C. and Tierney, D. W., Local Buckling of Shells. Developments in Mechanics, 2:221-251, 1963.

[30] Cagan, J. and Taber, L. A., Large Deflection Stability of Spherical Shells with Ring Loads. J. Appl. Mech., 53:897-901, 1986.

[31] Ranjan, G. V., Edge Zone Expansions for Thin Shells with Application to (1) Torispherical Pressure Vessel and (2) Large Deflection of Sphere with Point Load, PhD Thesis, Stanford University, USA, 1976.

[32] Parnell, T. K., Numerical Improvement of Asymptotic Solutions and Nonlinear Shell Analysis. PhD Thesis, Stanford University, USA, 1984.

[33] Huang, N., Unsymmetrical Buckling of Thin Shallow Spherical Shells, J. Appl. Mech., 31, 447-457, 1964.

[34] Memon, B. A. and Su, X. Z., Arc-Length Technique for Nonlinear Finite Element Analysis. Journal of Zhejiang University, 5(5), 618-628, 2004.

[35] Riks, E., The Application of Newton's Method to the Problem of Elastic Stability. Journal of Applied Mechanics, 39, 1060-1065, 1972.

[36] Riks, E., An Incremental Approach to the Solution of Snapping and Buckling Problems. International Journal of Solids and Structures, 15(7), 529-551, 1979.

[37] Wempner, G. A., Discrete Approximation Related to Nonlinear Theories of Solids. International Journal of Solids and Structures, 7(11), 1581-1599, 1971.

[38] Polat, C., and Calayır Y., Lineer Olmayan Yapı Sistemlerinin Analizi İçin Yay-Boyu Metodu. FÜ Fen ve Mühendislik Bilimleri Dergisi 19.4, 525-530, 2007.

[39] Polat, C., Co-rotational Formulation of a Solid-shell Element Utilizing the ANS and EAS Methods. Journal of Theoretical and Applied Mechanics 48.3, 771-788, 2010.

Teknik Dergi, 2021 10717-10737, Paper 610

Structural Equation Model of the Factors Affecting Construction Industry Innovation Success

Gökhan DEMIRDÖĞEN[1]
Zeynep IŞIK[2]

ABSTRACT

Innovation is seen as one of the major factors to improve construction industry despite conventional structure of the industry impede implementation of its practices. A convenient solution to promote innovation or force the companies to adopt it, is the legal regulations that can be set forth by the decision makers of whom aware and prevailed of the macro benefits of innovation practices. However, the impact of innovation practices on industry indicators was not defined adequately to understand those benefits. This study aims to reveal the relationship between company-level innovation success measures and industry-level innovation success indicators. Therefore, a comprehensive literature review was performed to determine those success measures and indicators and the results were validated with an illustrative case study. The outputs of the case study was used to construct structural equation model exhibiting the interdependencies between factors. The study results approved that there is a significant relationship between the innovation practices of construction companies and construction industry innovation. According to the results, increase in competitive advantage among rivals and improved reputation were seen as the two highest indicators in the company-level. Additionally, the study showed that the most important innovation success indicator at the industry-level was found as "employment and new job opportunities".

Keywords: Innovation, structural equation modeling, building information modeling, construction industry.

1. INTRODUCTION

The improvements in process, technology, and organization in the construction industry so-called -construction innovation- accelerate economic growth and productivity [1]. One of the major driving factors behind the development of construction industry is the globalization leading companies to take strategic innovative decisions in terms of -employee, technology,

Note:
- This paper has been received on May 17, 2019 and accepted for publication by the Editorial Board on October 22, 2019.
- Discussions on this paper will be accepted by May 31, 2021.
- https://dx.doi.org/10.18400/tekderg.567272

1 Yildiz Technical University, Department of Civil Engineering, Istanbul, Turkey - gokhand@yildiz.edu.tr https://orcid.org/0000-0002-2929-2399

2 Yildiz Technical University, Department of Civil Engineering, Istanbul, Turkey - zeynep@yildiz.edu.tr https://orcid.org/0000-0002-7849-8633

marketing, knowledge, and relationships- to survive and maintain their competitiveness [2,3]. The construction industry correspondences 15 percentages of gross domestic production (GDP) in the World [7]. Therefore, nation-wide innovation strategies will not only contribute to the profitability of construction companies, but will also increase construction industry figures and indirectly nations' GDP. For example; Utterback and Suarez [8] stated that a couple of firms could dominate the industry with product technology obtained by innovations. Such instances can be especially seen in information technology (IT) industry where high tech companies' annual turnover exceeds many countries' GDP [9].However, construction innovations such as "improvements of construction methods or sequences, application or extension of methods, application of new equipment or tools, and existing methods" have not been reported or recorded explicitly [4-6].

In the literature, construction innovation related studies were performed under five categories such as "construction innovation diffusion", "organizational factors' impact on construction innovation", "the origin of innovation (technology-push or pull)", "commercialization of construction innovations" and "national efforts for construction innovation" [10]. The literature review parallel to Toole [10]'s findings showed that the studies were mainly performed on developments of guidelines, construction innovation drivers, organizational structure and cultural factors, process identification with successful innovations, owner role, manufacturers' role, innovation sources, innovation models, diffusion, root causes for construction innovations, national approaches/government role, academia-industry cooperation, industry level innovation factors, innovations at project level, barriers, innovation management system, development of framework, and case study implementations with successful example [11-37]. . The literature indicated that many authors attempted to determine innovation success indicators on the company or project level, however, construction industry-specific performance studies were rare.

For instance, Lim et al. [38] used annual turnover of construction companies, annual research and development expenditure, the percentage change in construction value-add per person employed, the research and development capacity and the number of responsible personnel, to measure innovation activities and their impact on the construction industry. Also, Zhang et al. [39] not specific to construction industry contended that innovations are essential to enable national competitive advantage, resource optimization, workforce, and social welfare. Furthermore, Bygballe and Ingemansson [40] stated that there was a debate about the compatibility of existing measures for the construction industry that was stated in Lim et al.'s study [38]. According to Zubizarreta et al. [41], these measures were not appropriate for the construction industry. Additionally, Loosemore [5] agreed that measurement of innovation in the construction industry was provided with data adopted from other industries since construction innovations are not identified or detected in the project level [35]. However, Brockmann et al. [42] stated that "innovation in construction is defined as changes leading to an improved input-output relationship for products and processes as well as within the technical, management, or legal organization of a project that can be evaluated monetarily." which in turn have tremendous impacts on cost, time and quality issues inevitable for the construction industries' success.

Moreover, some authors claimed that construction innovation is an added value activity for the construction industry [35]. However, neither more comprehensible innovation success indicators of the construction industry have been identified, nor the relationship between the

measures of construction companies innovation success and the indicators of the construction industry innovation success have been investigated. Therefore, this study aims to fulfill the gap by developing indicators which could be used or employed the boost innovation performance of construction industry and to reveal the relationship between the measures of construction company innovation success and the indicators of construction industry innovation success. From this perspective, first of all a comprehensive literature review was conducted. To validate findings of the literature review and to set hypothesis, an illustrative case study was performed. Finally, a measurement model indicating the innovation-related factors specific to the construction industry and a structural model representing the interrelationships between those factors were proposed to assess the impact of innovation in the construction industry. In this context, data collected from 52 construction companies were analyzed using Structural Equation Modeling (SEM) to verify the proposed measurement and structural model. The findings of the study, and set forth relationships between construction industry indicators and companies' innovation success measures showcased, would reveal a roadmap for new developments that make sense for construction industry professionals and decision makers.

2. RESEARCH METHODOLOGY

The research methodology followed in this study consists of "*identification of model variables with a comprehensive literature review, validation of literature review results with illustrative case study, and questionnaire survey to construct model, analysis of data, and model creation with SEM methodology*". In this study, two research methods were used. Firstly, findings from literature review were verified with an illustrative case study. In the illustrative case study, two type open-ended questions were asked to three high level executive manager interviewees working in the companies placed in Engineering News Record 2018 Top 250. In the first question, it was asked from the respondents to associate identified indicators given under the measures of construction company innovation success with BIM implementations in their companies. Secondly, it was asked, whether they observe the implications of indicators of the construction industry innovation success as the representatives of leading companies in construction industry. After that, the proposed model was verified with SEM to enable the measurement of unobservable parameters by observed parameters. In the questionnaire, the questions -"Please indicate importance level indicators which are given under the measures of construction company innovation success according to your company implementations" and "Please indicate importance level variables which are given under the indicators of the construction industry innovation success according to your companies' innovation results"- were asked to the participants. The proposed model consists of two constructs: the measures of construction companies' innovation success, and the indicators of success in terms of the construction industry. In order to measure these constructs, indicators were evaluated by respondents according to a 1 to 5-point Likert scale. The questionnaire was sent to 141 construction company members of the Turkish Contractors Association (TCA) via e-mail and conducted to 52 companies accepting to perform face-to-face interviews (37% response rate). The respondent companies are specialized mainly on buildings 85%, waterworks 15%, transportation 21%, industrial 23% and infrastructure 17%. The respondents' average experience is approximately eight years.

3. PROPOSED MODEL VARIABLES

The measures of "Construction Company" success such as, "increase in higher perceived value", "decrease in costs", "time savings", "increase in competitive advantage among rivals", "improved reputation/company image", "productivity enhancements", "increase in growth, market share and profit", "improved learning and development process", "increase in satisfaction of customer/consumer"; and indicators of "Construction Industry" such as, "contribution to the development of supporting industries", "employment and new job opportunities", "opening up new markets (exporting construction services)", "increase in turnover and production", and "decrease in material and labour wage" were determined with a comprehensive literature review and presented in Table 1.

Table 1 - Measures and indicators

Factors	Indicators	References
The measures of construction company innovation success	Increase in higher perceived value	[1, 11, 13-15,20, 22-25, 27-28, 33, 37-38, 50, 55, 60-61,63]
	Decrease in costs	[1, 4-5 10-11, 13, 15-17, 21-23, 28, 30, 35, 38, 42-43, 45, 47, 50-52, 54-55, 57, 60-61, 63]
	Time savings	[4-5, 10-11, 13-15, 22, 28-30, 35, 38, 50, 54, 57, 60-61]
	Increase in competitive advantage among rivals	[1, 4, 11, 13, 17, 19, 22-24, 27-28, 30, 33-37, 38, 43-44, 48, 50, 52-54, 58-60, 63-64]
	Improved reputation/ company image	[1, 15, 17-18, 23, 28, 30, 38, 50, 54, 57, 60, 63]
	Productivity enhancements	[1, 10-11, 13, 16-17, 21, 25, 28, 30, 33, 35, 38, 42, 44-45, 47, 50-52, 54, 57, 59-60, 63]
	Increase in growth, market share, and profit	[1, 3, 10-11, 17-18, 20-24, 28-30, 35, 38, 44-45, 50, 52, 56-57, 59-60, 63]
	Improved learning and development process	[3, 13, 27-28, 30, 46, 50, 52, 54, 56-60]
	Increase in satisfaction customer/consumer	[10-11, 15, 20, 23-24, 28, 38, 43-44, 50, 55-57, 60, 63]
The indicators of the construction industry innovation success	Decrease in material and labour wage	[1, 10-11]
	Increase in turnover and production	[1, 21-22, 35, 50]
	Employment and new job opportunities	[1, 3, 11, 15, 17-18, 25, 27, 58]
	Contribution to the development of supporting industries	[10-11, 13, 15-16, 23, 35, 49-50, 53-54, 58, 62-63]
	Opening up new markets (Exporting construction services)	[3, 12-13, 17, 22, 27, 30, 38, 43-44, 48, 63]

4. THE ILLUSTRATIVE CASE STUDY

In this research, an illustrative case study methodology was employed to gain a better understanding of the effect of innovation outcomes on the construction industry. Thus, the validation of literature review results were tested to gather more meaningful results with a practical implementation related to innovation indicators in the construction industry. Gerring [65] defined case study methodology as "the intensive study of a single unit for the purpose of understanding a larger class of (similar) units". Barlish and Sullivan [66] stated that a case study is more beneficial to understand the advantages of innovative information technologies such as Building Information Modeling (BIM) since it highlights the issues that

are difficult to describe based on only empirical data. Eisenhardt [67] stated that collocation of qualitative and quantitative data in the case study method provides an increase in the creativity and the reliability of the study. The qualitative part of the study is to conduct illustrative case study. Results of the case study give insights about reliability of the literature review, hypothesis creation and relationships used in the model. As for the quantitative part of the study, the SEM method was introduced to analyze results of the illustrative case study.

4.1. Building Information Modeling (BIM) as a Disruptive Technology

BIM is an example of radical innovation for the construction industry [67]. The benefits of BIM use in an organization cannot be limited to solely as a technological improvement since it also changes the way how operational processes will be handled [68]. The literature clearly stated a lot of definitions for BIM; Aranda- Mena et al. [69] stated innovative characteristics of BIM as; "a new software application; a process for designing building information; a whole new approach to practice and advancing the profession which requires the implementation of new policies, contracts and relationships amongst project stakeholders". In the construction industry, it is believed that BIM is a remedy for problems because it enables them to be modelled prior to construction. For example, when BIM softwares are used, it is seen that they have the capability of manipulating a geometric representation of building elements and generating locations for these elements due to its parametric object-oriented architecture [70]. This enables realistic calculations and accurate planning in advance. BIM offers companies a variety of opportunities to get better results in their projects. Moreover, some of these opportunities show parallels with the gains from innovation actions that was mentioned in previous sections. Therefore, BIM technology was chosen as a case topic. Also, BIM adoption with different level requirements (Level 0, Level 1, Level 2, and Level 3) introduce new technological applications and challenges to construction companies. Additionally, BIM obligations, BIM utilization mandate for the projects, BIM standards, BIM Guides and different level requirements for BIM utilizations by countries trigger construction companies in terms of innovativeness increasing technology transfer capability [71]. Therefore, BIM is a hot topic to adapt it in the companies. Moreover, Becerik-Berber and Rice [72] stated that construction companies have problems with cost, time, conflicts etc. and they cause loss of 3-4% of total industry turnover. Also, the authors stated that BIM as an innovation can be a remedy of the productivity of construction industry.

In the literature, Papadonikolaki [37] handled BIM as an innovation and the author investigated BIM diffusion in the companies. However, the study was only focused on BIM adoption and its implementation in the companies. In this study, BIM was used to validate indicators comprehended from a literature review. The indicators used in the proposed framework is general and they are applicable to different innovations.

4.2. Illustrative Case Study Implementation

The three companies chosen for the illustrative case study hold a significant market share in the domestic and international market as being placed in Engineering News Record 2018 Top 250 International List. The chosen companies are the leading companies in terms of sustainable construction implementations, energy investments, hotel, hospital, factory,

residential housing, infrastructure, office and shopping mall projects. Another reason for choosing these companies is that they are multinational companies. They deliver service in European and Middle East countries. Furthermore, market leadership of these companies is not limited with national industry, but the companies are also open to new markets, technological advancements, innovations and demonstrate a high capability and adaptability. When conducting the three case studies, face-to-face interviews were performed at the managerial level. The case study was conducted with open-ended questions. The questions asked were designed to find out the impact of the company's innovation success on the company's output since industrial figures are the collective results of a company's performance. Interviewees have top management tasks in their companies and have experience of more than ten years.

BIM technologies have been used actively for five years by Company A. They have preferred Allplan and Revit BIM software in their company. In the project history of Company A, BIM technologies have been implemented in five projects. Furthermore, the company has provided employment for ten white-collar workers in order to perform the BIM-related work. The company has used BIM technologies heavily within the bill of quantities for projects and for mechanical, electrical and plumbing (MEP) coordination. In addition to the bill of quantities and MEP implementations, they have started to use BIM technologies for projects developed in the national market. In Company B, BIM technologies have been used more than ten years. BIM has been used in both facilities management and in the planning phase. Through the BIM technologies, they can perform 3D modeling of the project, detection of clashes, MEP implementation, energy analysis and bill of quantities. Company B has exploited BIM technologies actively through facilities management. Company C had experience of BIM over more than five years and started to use BIM as a project contract necessity. They have used BIM technologies in the design phase and in MEP implementations. They have also benefited from 3D modeling, bill of quantities and detection of clashes.

According to Company A's bill of quantities implementation, BIM has provided opportunities to more accurately control working hours and material quantities. This process helped to reduce "material and labour wage" compared to classical methods in the company process because it was stated that construction sequencing and parametric modeling of building components can be seen easily with BIM. This prevents mishandling of projects and wastage in terms of material. In other words, rework activities can be reduced with BIM by helping design quality improvements [73]. As a common comment from participant companies, BIM, with quality increments and a well-organized operational structure, helps companies achieve "increase in profit and production". For example, Company B used BIM for a project they were awarded in order to increase expected concession periods by virtue of improved quality in minimizing the construction process.

Also BIM implementation in the companies increased workers' qualifications. With the help of BIM, the companies employed more qualified workers for the bill of quantity works. Furthermore, in Company C, the project owner demanded project planning with BIM. Therefore Company C had to launch a BIM department specific to the project. This led to new job vacancies in the company. In contrast to Company C, Company B has a permanent department for BIM due to its facilities management. The capability of BIM utilization with different level of details has led to "increase in competitive advantages between the

companies" within the international market. The quality increments achieved through BIM implementation helped the company to be awarded, and take part, in international projects. For example, in the Middle East countries, BIM has been used as a qualification requirement for contractors because this qualification is the representation of quality in design, construction and operational stages of projects. As stated before, Company C started using BIM as a result of this contract clause.

As stated in Azhar's [74] study, BIM technology helps towards cost savings in projects. In parallel with Azhar's [74] findings, the case studies acknowledged that innovation such as BIM helps to "decrease in costs". Therefore, cost and time wastage are eliminated by the help of BIM. Company A clearly stated that BIM technologies help to monitor and eliminate unnecessary "material and labour wages" in the management of the projects [75]. Also, elimination of the unnecessary costs helps to "industry turnover". Additionally, Company C stated that a clash of MEP designs is a costly problem in conventional project management. However, BIM, with Navisworks tools, helps them to save significant monetary resources in projects. This utilization of BIM directly affects "decrease in costs". Company B also stated that these tools helped them to observe the financial status of the project. If they have to take corrective action, it helps them in the decision-making process. As a common view among the case study companies, "decrease in costs" reflects directly on the "increase in turnover and production" of the companies. Usage of BIM technolgy also leads to an increase in the company's competitive position. For example, Company B benefited from BIM in estimating yearly expenditures and revenue in the operational phase [76]. Therefore, they can use BIM as a competitive tool against their rivals. This provides more accurate historical data when bidding for new projects. All companies agreed that the tools have helped companies to win projects in the international arena since they were able to plan more accurately. According to Company C, the company's BIM competence provided them with the means to participate in the tender process, and provides more advantages to help them win bids. This also helped to protect the company's position in the international market, to provide job vacancies or attract more talented workers and to "increase in industrial turnover and production".

Latiffi et al. [77] stated that BIM applications help to monitor work sequence, equipment and materials in companies. According to their findings, the authors advised their government to develop BIM technology in order to increase their efficiency and effectiveness industry-wide. Following on from the literature review, interviewees were asked to judge what impact "time savings" – by using BIM technologies – had on industrial indicators. In Company A, the impact of "time savings", and of "material and labour wage", was seen as very limited because a subcontracting method was extensively used in their projects. However, an interviewee from Company A stated that BIM-based technologies for MEP projects provided a more effective solution for coordination and production in the projects. Also MEP applications using BIM provided time savings in project planning and execution. In contrast to Company A, the manager of Company B said that BIM technologies helped them reduce change orders [74]. Also, Company C stated that these tools can be used in claims and that they proved their claims with these tools. Therefore some problems can be solved without requiring a court or using arbitration procedures [75]. In addition to these findings, Company C stated that BIM helps to coordinate project partners. This enables efficient and effective communication between project stakeholders. All managers agreed that "time savings" with BIM helps "increase in turnover and production". Therefore, this can help protect their position in international markets.

The findings related to the impact of "reputation and company image" on industrial output in the literature were supported by Qian's [75] study. According to that study, BIM technologies provide them with a better company image, help them make less mistakes and errors and provide strategic competitive advantages. Interestingly, the manager of Company A stated that the reputation and company image gained through implementing BIM helped the company to get more projects in the international market, and the technology helped with the company's international project strategies. In addition to the view of Company A, Company C has used technologies like BIM to improve their company image in order to be a bidder in some tenders, and this helps protect their international market position and "exporting construction services".

"Productivity improvements" with BIM can be observed at the company level. Here, BIM implementations help with project documentation, estimating "cost and time savings" in productivity during the operational phase [74]. The manager of Company A stated that BIM helps to keep employees more satisfied than with classical methods. To explain this, he gave an example of where white-collar workers now called themselves 3D modellers, even though they had already previously been performing the same tasks. This also helps lead to an increase in worker productivity. This impact was also observed in the bill of quantities, which became easier and was more accurate. This has helped with "material and labour wage". Therefore BIM implementation can deliver productivity advantages in the international market arena. It was also stated that integrated project planning with BIM provides the flexibility to easily implement project change orders, using the example of implementing column size changes on an existing project. In parallel to Azhar's [74] study, the manager of Company B stated that BIM helps to effectively document the project. It also helps to decrease architectural expenditure because it minimizes the time for the project design. This reflects directly on a company's profit and production.

The financial benefits of BIM technologies on a company's output attracts lots of companies to use it. As stated in Becerik-Gerber's [72] study, BIM helped staff requirements and enabled changes to be identified and implemented at the design phase, which is cheaper than changes at the construction phase. Interestingly, the manager of Company A stated that being innovative with BIM technologies increases the financial creditability of the company. Therefore the company had a "competitive advantage" in the international market. Moreover, the manager of Company C stated that earnings at the project level helped to sustain the financial status of the company. So Company C can deliver services in the international market and provide" new job opportunities" by way of international projects. Also, they used some construction material from Turkey such as marble etc., which therefore contributed to the development of supporting industries.

The another result obtained from literature review is increase in learning and development with innovation implementations. According to the manager of Company A, BIM cannot be implemented in every company's projects because of customer requirements, profitability of the project and competitiveness of the company awarded the project. Therefore, the company appealed for know-how about BIM technologies to improve their ability to run a BIM-based project. This provided capability for both learning and development of the company and qualification of its workers. Therefore, any acquired know-how and technology can be used when tendering for projects requiring new technologies like BIM. Company B gained an advantage with BIM in the prefabrication of some construction elements. Therefore,

Company B can contribute to the development of supporting industries in the prefabrication phase. However, the process cannot be fully utilized for prefabrication features of BIM when comparing with other international company counterparts. This finding also acknowledged Azhar's [72] study findings about future BIM utilization in prefabrication.

"Increase in satisfaction of customer/consumer" is an important criterion for companies in a project. In this context BIM technology provides promising features for companies. For example, in the literature, it was stated that BIM provides better customer services with visual representation [78]. However, the projects Company A conducted with BIM technology belonged to the company's real estate property, so this question wasn't answered. Company B has actively used BIM in the operational phase. This helps management of facilities by both considering customers' expectations and their numbers.

5. IMPLEMENTATION OF STRUCTURAL EQUATION MODELING (SEM)

The SEM, connecting observable variables to unobservable variables, is a method in which causal relationships between unobservable variables are examined. It consists of a combination of a measurement model (confirmatory factor analysis) and a structural model (regression or path analysis) [79]. In the SEM methodology, various statistical methods are used together to create a validated model. These methods are factor analysis, multiple correlation, regression and path analysis [80]. The distinguishing specialty of the SEM method compared to other statistical methods is that it enables the use of unobservable variables. This allows problem representation to be accurately handled by variance and covariance analysis [81]. Moreover, the SEM method gives researchers an opportunity to research or test whether collected data supports a model designed by the researcher or not. Also SEM is a comprehensive methodology since it considers multiple relationships between factor structures [80]. The SEM methodology contains two steps. In the first step, factor structures are tested with bidirectional impacts to reveal the reality of the relationships between factors [82,83]. The structural model is the second step in which causal relationships between latent variables are investigated. In other words, defined relationship in measurement model is defined in the structural model [83]. In the structural model, every relationship corresponds to a hypothesis. And these relationships are tested to validate asserted model. Basically, in this study, hypothesis that -there is significant relationship between indicators of construction companies' innovation success on the indicators of success of the construction industry- was tested.

Table 2 - Fitness indices for measurement and structural models

		Measurement Model		Structural Model
Fit indices	**Allowable range**	**F1**	**F2**	**Final model**
Non-normed fit index (NNFI)	0 (no fit) to 1(perfect fit)	0.973	0.969	0.848
Comparative fit index (CFI)	0 (no fit)-1(perfect fit)	0.980	0.985	0.873
RMSEA	< 0,1	0.048	0.050	0.090
$\chi 2$/degree of freedom	< 3	1.118	1.1258	1.4088

The Goodness of Fitness Indices (GFI) and construct validity were used to verify the model since it investigates fitness between the model and the collected data. In this study, GFI were chosen to be the non-normed fit index (NNFI), the comparative fit index (CFI), the root mean square error of approximation (RMSEA) and the chi-square model due to their common use in the literature. The measurement and structural model structures (F1- indicators of construction companies' innovation success, and F2- indicators of the success of the construction industry) presented a nearly perfect fit as seen in Table 2.

Table 3 - Latent and observed variables of the model with factor loadings

F1	**The measures of construction company innovation success**	**Factor Loadings**	**F2**	**The indicators of the construction industry innovation success**	**Factor Loadings**
V1	Increase in higher perceived value	0.605	V10	Decrease in material and labour wage	0.632
V2	Decrease in costs	0.770	V11	Increase in turnover and production	0.578
V3	Time savings	0.769	V12	Employment and new job opportunities	0.773
V4	Increase in competitive advantage among rivals	0.784	V13	Contribution to the development of supporting industries	0.519
V5	Improved reputation/company image	0.779	V14	Opening up new markets (Exporting construction services)	0.419
V6	Productivity enhancements	0.718			
V7	Increase in growth, market share and profit	0.567			
V8	Improved learning and development process	0.672			
V9	Increase in satisfaction of customer/consumer	0.595			

Construct validity consists of content validity, scale reliability, convergent validity and discriminant validity. Content validity testing was performed with a literature review without making a statistical analysis. In the study, 14 variables were specified and they were acknowledged with a pilot study. Scale reliability is measured with Cronbach's alpha value, which gives information about the relationship of observed variables to their latent variables. This value must be 0.7 as a minimal condition [84]. According to the analysis of the model, the value was found to be 0.891 for the measurement model of the measures of construction company innovation success. The value for the measurement model of the indicators of the construction industry innovation success was found to be 0.718. As can be understood from these values, this constraint was met. Convergent validity is examined with factor loadings. In order to fulfill convergent validity, observed variables must be statistically significant at $\alpha = 0.05$. As a result of the convergent validity analysis, all variables and factors were found statistically significant. Furthermore, variables that have a value less than 0.3 are eliminated. In our model, the nearest value was 0.419. Therefore, no variable was excluded from the

model. The results are given in Table 3. For discriminant validity, correlation between the variables under the same latent variable is investigated. The correlation value between variables must be less than 0.9 [85]. According to the analysis, all values stayed below 0.9. After the implementation of the structural analysis, the model results gave acceptable values. An interpretation of the findings is presented in the following discussion part.

5.1. Discussion of SEM Results

According to the analysis of the measures of construction company innovation success, and the indicators of construction industry innovation success, the path coefficient is 0.862. This shows that the relationship between the two is very strong. (See Figure 1)

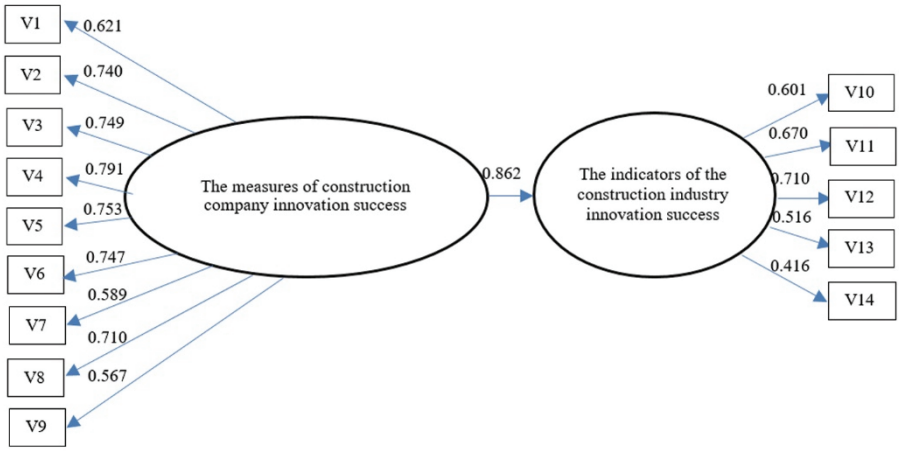

Figure 1 - The measures of construction company innovation success impact on the indicators of construction industry innovation success

5.1.1. The Measures of Construction Company Innovation Success

In the study, nine observed variables were taken into consideration in line with the literature review. All considered variables were found to be significant as a result of the SEM analysis. According to the analysis, factor loadings of the structural model were found to be 0.621 for increase in higher perceived value (quality), 0.740 for decrease in costs, 0.749 for time savings, 0.791 for increase in competitive advantage among rivals, 0.753 for improved reputation/company image, 0.747 for productivity enhancements, 0.589 for increase in growth, market share and profit, 0.710 for improved learning and development and 0.567 for increase in satisfaction of customer/consumer. As the findings were compared with Ozorhon et al.'s study [57], variables show compatibility with their findings – except for quality and competitive advantage among rivals which weren't considered in their study. In contrast, the increase in competitive advantage among rivals was found to be the most significant factor affecting a companies' innovation success. Additionally, this relationship was also confirmed by the study of Lim et al. [38]. Another difference between the studies involved increase in higher perceived perception or quality. Arditi et al. [45] stated that innovative developers in

the construction equipment industry provide advancements in quality when they simultaneously compete for market position. Furthermore, findings showed compatibility with the study by Xiaolong et al. [86]. According to their study, outputs of innovation provide a time savings and decrease in costs, productivity enhancements and improved corporate image. As was mentioned in the definition of indicators of construction companies' innovation success, no surprising results emerged.

5.1.2. The Indicators of the Construction Industry Innovation Success

The indicators of the construction industry innovation success were evaluated in terms of five factors. These factors were chosen according to the relationship between the innovation efforts of companies and the industry. The factor loadings of these variables were found to be 0.601 for decrease in material and wage costs, 0.670 for increase in turnover and production, 0.710 for employment and new job opportunities, 0.516 for contribution to the development of supporting industries and 0.416 for opening up new markets (exporting construction services). According to the data analysis, employment and new job opportunities were found to be the highest variable, followed by decrease in material and wage labour, increase in turnover and production, contribution to the development of supporting industries, and the opening up new markets, respectively.

The study revealed that there is a positive correlation between innovation and employment and new job opportunities. To achieve positive outcomes which are presented in Table 3, the construction companies should recruit new graduates or open new employee positions in the company so that innovation or creative ideas can be enhanced and facilitated within the company. Therefore, the companies contribute an increase in employment rate in the industry [3, 11].

Another important finding from this study is that "decrease in material and wage costs" via innovations was found to be the most critical second indicator. Toole [10] stated that by the help of innovations, building product could be moved from on-site production to off-site production (factories). Slaughter [1] mentioned the intangible benefits of innovations and stated that technological improvements provided achievable construction productions for customers. This demonstrated that competition for equipment and materials, and new methods of innovation, exert pressure to decrease in costs.

The third highest score belonged to an increase in turnover and production. This can be explained by the importance given to innovations by governments [35]. They have constituted new regulations and incentives to attract new developments in the construction industry since the industry represents a significant proportion of the economy. Therefore, industrial savings and production efficiency through new developments benefit government earnings simultaneously. Also, Koellinger [87] investigated relationship between innovation and turnover development, and employment development. The study results approved that there is positive relationship between innovation and turnover and employment growth.

The fourth highest score was found as contributions of innovations to the development of supporting industries. Some authors expressed that the contractor has an intermediary role between manufacturers and clients since the contractors provide adaptation of innovations or new components in the project to meet the requirements [54]. Furthermore, Rundquist et al.

[53] expressed that supporting companies are not represented at the construction sites. Therefore, the problems which arise from site needs to be conveyed to supporting companies such as material companies via contractors. It means that collaboration for new developments between stakeholders are facilitated. In other words, the construction industry directly affects the development of local material industries.

Technological improvements or developments can be used as a leverage to help companies expand abroad. Edum-Fotwe [48] expressed that the competition between companies is not limited to nationwide. To maintain competitive advantage, the companies need to consider foreign companies' competitive advantages (innovations, technologies, etc.) as well [38]. Also, Podmetina et al. [88] performed a study which investigate relationship between innovation activities and exportation activities for all industries. The study results showed that there is a significant relationship between them. Therefore, the result of the SEM analysis acknowledged that innovation activities of the construction companies aid export activities as an industry outcome indicators positively.

Thus, the construction industry success provided with innovation related success of the companies was validated with the SEM model developed, as well as the findings of the literature review and illustrative case study.

6. LIMITATIONS OF THE STUDY

This study involves limitations as summarized below:

1. Though most of the respondents of the questionnaire and all the interviewees of illustrative case study were representatives of leading companies listed in international indexes, the study results represent more the dynamics of companies and industry in developing countries since data were collected from companies located in a developing country. To comprehend the model, the study can be implemented in developed countries' construction industries as well which can give more insight about the innovation process in the construction industry.
2. The study focused on measuring the impact of company related innovation success on industry related innovation success. Therefore, macro-economic related policies, relationships, intra-company, or environmental impact on companies were not considered. Further studies can be extended by considering these factors.
3. Moreover, findings from the study includes the idea for different project types. Therefore, the further studies can be performed by focusing on separate project types.

7. CONCLUSIONS

Technological and innovative advancements open new perspectives for any industry. The technological improvement of companies gain importance also in the construction industry since construction industry significantly affects a country's economy due to its huge share in national income. These improvements are not only restricted to the construction industry, but also impact other supporting industries interacting with the construction industry, such as the material manufacturing industry. Therefore, this study aims to contribute innovation

performance measurement framework for construction industry and its implementation with well-known IT technology to existing innovation literature. In this context, this study tried to measure the effect of the indicators of construction companies' innovation success, and the indicators of success of the construction industry. Accordingly, nine measures for construction company innovation success, and five indicators for the construction industry innovation success, were defined as a result of a comprehensive literature review.

An illustrative case study was performed to validate literature review findings and construct the theoretical structure of the structural equation model. According to the case study findings, BIM provides an opportunity for contractors to keep projects within the approved budget [90]. Also, BIM enables an analysis of the energy performance of a building which provides opportunity for development in the construction material industry in terms of energy saving materials promoting also new sub sectors and employment opportunities in the industry [91]. Additionally, the growing popularity of BIM is likely to lead to an increased number of innovative job opportunities via professional BIM consultancy according to Wong and Fan [92]. Wong and Fan [92] also stated that BIM helps reduce the use of materials and energy, and helps waste reduction. This discourse was also supported by Fernandes [93] since BIM enables easier material and equipment tracking. These requirements also reflect on industrial indicators as positive turnover and production. When Eastman et al. [94] mentioned the future of BIM, they stated that lack of trained professional staff leads to difficulty in implementing BIM. This indicates that BIM requires trained staff providing new job opportunities such as building modeller or model manager in the industry. Experience and de facto rules play an important role in traditional construction and architecture. However, this situation has started to lose its importance since BIM provides opportunities to make sound judgments with analysis tools.

After performing the illustrative case study, SEM methodology was conducted to model relationships between company-level and industrial-level. In this context, the literature findings were tested by a questionnaire conducted to 52 companies. As a result of this modeling method, the proposed model stayed in statistical allowable limits. Furthermore, it enables an important framework for company performance measurement using industrial indicators. According to the SEM results, competitive advantage and reputation as a result of innovation activities were found to be the two highest scores at the company-level. It shows that the construction companies believe that embracing new technologies helps to increase their competitiveness and reputation. It was stated in the illustrative case study, new technologies can open the way for new projects by meeting participation requirements for the tenders. Also, the respondents believed that increasing innovation implementations in their companies helps to eliminate iron-triangle and productivity problems. Additionally, the companies thought that requirements which comes with innovations lead to change either organization or necessity for human resources. Therefore, the highest score was found as "employment and new job opportunities". Besides, they believed that increase in their profitability with innovations also reflect on industry-level turnover and production. Besides, these indicators, the participants believed that innovations aid to "decrease in material and wage costs", "contribution to the development of supporting industries", and "opening up new markets (exporting construction services)".

Main contribution of this study for construction industry professionals is that the government bodies and professional chambers can use identified innovation success factors to measure

and boost innovation performance of the construction industry, since the government bodies use incentive mechanism or new regulations (i.e. BIM technology to participate tender process) to enable productivity increase and eliminate wastes in the construction industry Therefore, the innovations which have positive outcome on the industry are identified with the application of the proposed model and their adaptations or spread of innovation can be facilitated industry-wide. Also, the government side can incentivize by identifying technological implementations which help to increase or improve the factors given in innovation success factors of construction companies by performing pilot projects for special innovations. Another contribution of the study is that the study will be helpful to increase awareness of the construction practitioners about innovation success factors and BIM implementations. It should be noted that the proposed indicators in this study must be measured, analyzed, reported, and stored by the decision makers periodically to implement effectively.

References

[1] Slaughter, E. S., Models of construction innovation, Journal of Construction Engineering and management, 124(3), 226-231, 1998.

[2] Seaden, G., Guolla, M., Doutriaux, J., Nash, J., Strategic decisions and innovation in construction firms, Construction Management and Economics, 21(6), 603-612,2003.

[3] Manley, K., McFallan, S., Kajewski, S.,Relationship between construction firm strategies and innovation outcomes, Journal of construction engineering and management, 135(8), 764-771,2009.

[4] Tatum, C. B.,What prompts construction innovation?. Journal of construction engineering and management, 110(3), 311-323, 1984

[5] Loosemore, M.,Construction innovation: Fifth generation perspective, Journal of management in engineering, 31(6),, 2015.

[6] Loosemore, M., Richard, J., Valuing innovation in construction and infrastructure: Getting clients past a lowest price mentality, Engineering, construction and architectural management, 22(1), 38-53, 2015.

[7] KPMG, Sektörel Bakış, 2018. https://assets.kpmg/content/dam/kpmg/tr/pdf/2018/01/sektorel-bakis-2018-insaat.pdf

[8] Utterback, J. M., Suárez, F. F. Innovation, competition, and industry structure Research policy, 22(1), 1-21, 1993.

[9] Pratap, A. (2018). “Apples’s staff size”. https://notesmatic.com/apples-staff-size/

[10] Toole, T. M.,Technological trajectories of construction innovation, Journal of Architectural Engineering, 7(4), 107-114, 2001.

[11] Laborde, M., Sanvido, V., Introducing new process technologies into construction companies, Journal of Construction Engineering and Management, 120(3), 488-508, 1994.

[12] Tatum, C. B., Potential mechanisms for construction innovation, Journal of Construction Engineering and Management, 112(2), 178-191, 1986.

[13] Tatum, C. B., Organizing to increase innovation in construction firms, Journal of construction engineering and management, 115(4), 602-617, 1989.

[14] Lockwood, W. D., Hensey, M., Managing Civil Engineering Innovation: An Interview, Journal of Management in Engineering, 6(3), 313-322, 1990.

[15] Nam, C. H., Tatum, C. B., Strategies for technology push: Lessons from construction innovations, Journal of construction engineering and management, 118(3), 507-524, 1992.

[16] Slaughter, E. S., Builders as sources of construction innovation, Journal of Construction Engineering and Management, 119(3), 532-549, 1993.

[17] Goodrum, P. M., Haas, C. T. Variables affecting innovations in the US construction industry, In Construction Congress VI: Building Together for a Better Tomorrow in an Increasingly Complex World, 525-533, 2000.

[18] Steele, J., & Murray, M., Creating, supporting and sustaining a culture of innovation, Engineering, construction and architectural Management, 11(5), 316-322, 2004.

[19] Park, M., Nepal, M. P., Dulaimi, M. F., Dynamic modeling for construction innovation, Journal of Management in Engineering, 20(4), 170-177, 2004.

[20] Bossink, B. A., Managing drivers of innovation in construction networks, Journal of construction engineering and management, 130(3), 337-345, 2004.

[21] Abbot, C., Jeong, K., Allen, S., The economic motivation for innovation in small construction companies, Construction Innovation, 6(3), 187-196, 2006.

[22] Na, L. J., Ofori, G., Park, M., Stimulating construction innovation in Singapore through the National System of Innovation, Journal of construction engineering and management, 132(10), 1069-1082, 2006.

[23] Ling, F. Y., Hartmann, A., Kumaraswamy, M., Dulaimi, M., Influences on innovation benefits during implementation: client's perspective. Journal of Construction Engineering and Management, 133(4), 306-315, 2007.

[24] Kale, S., Arditi, D., Innovation diffusion modeling in the construction industry, Journal of Construction Engineering and Management, 136(3), 329-340, 2009.

[25] Shapira, A., Rosenfeld, Y., Achieving construction innovation through academia-industry cooperation—Keys to success, Journal of Professional Issues in Engineering Education & Practice, 137(4), 223-231, 2010.

[26] Esmaeili, B., Hallowell, M. R. Diffusion of safety innovations in the construction industry, Journal of Construction Engineering and Management, 138(8), 955-963, 2011.

[27] Na Lim, J., Peltner, F., Innovation performance of construction enterprises: An empirical assessment of the German and Singapore construction enterprises, Construction Innovation, 11(3), 282-304, 2011.

[28] Ozorhon, B., Analysis of construction innovation process at project level, Journal of management in engineering, 29(4), 455-463, 2012.

[29] Davidson, C., Innovation in construction–before the curtain goes up, Construction Innovation, 13(4), 344-351, 2013.

[30] Ozorhon, B., Abbott, C., Aouad, G., Integration and leadership as enablers of innovation in construction: Case study, Journal of Management in Engineering, 30(2), 256-263, 2013.

[31] Widén, K., Olander, S., Atkin, B., Links between successful innovation diffusion and stakeholder engagement, Journal of management in engineering, 30(5), 2013.

[32] Rundquist, J., Emmitt, S., Halila, F., Hjort, B., Larsson, B., Construction innovation: addressing the project-product gap in the Swedish construction sector, International Journal of Innovation Science, 5(1), 1-10, 2013.

[33] Na Lim, J., The Government as marketer of innovation. Engineering, Construction and Architectural Management, 21(5), 551-570, 2014.

[34] Singh, V. BIM and systemic ICT innovation in AEC: perceived needs and actor's degrees of freedom, Construction Innovation, 14(3), 292-306, 2014.

[35] Yepes, V., Pellicer, E., Alarcón, L. F., Correa, C. L., Creative innovation in Spanish construction firms, Journal of Professional Issues in Engineering Education and Practice, 142(1), 2015.

[36] Gledson, B. J., Greenwood, D., The adoption of 4D BIM in the UK construction industry: an innovation diffusion approach, Engineering, Construction and Architectural Management, 24(6), 950-967, 2017.

[37] Papadonikolaki, E., Loosely Coupled Systems of Innovation: Aligning BIM Adoption with Implementation in Dutch Construction, Journal of Management in Engineering, 34(6), 2018.

[38] Lim, J. N., Schultmann, F., Ofori, G., Tailoring competitive advantages derived from innovation to the needs of construction firms,Journal of construction engineering and management, 136(5), 568-580, 2010.

[39] Zhang, J., Xie, H., Schmidt, K., Li, H., A new systematic approach to vulnerability assessment of innovation capability of construction enterprises, Sustainability, 8(1), 17, 2016.

[40] Bygballe, L. E., Ingemansson, M., The logic of innovation in construction. Industrial Marketing Management, 43(3), 512-524, 2014.

[41] Zubizarreta, M., Cuadrado, J., Iradi, J., García, H., Orbe, A., Innovation evaluation model for macro-construction sector companies: A study in Spain, Evaluation and program planning, 61, 22-37, 2017.

[42] Brockmann, C., Brezinski, H., Erbe, A., Innovation in construction megaprojects, Journal of Construction Engineering and Management, 142(11), 2016.

[43] Tatum, C. B. Process of innovation in construction firm, Journal of Construction Engineering and Management, 113(4), 648-663, 1987.

[44] Tatum, C. B., Managing for increased design and construction innovation, Journal of management in engineering, 5(4), 385-399, 1989.

[45] Arditi, D., Kale, S., Tangkar, M., Innovation in construction equipment and its flow into the construction industry, Journal of Construction Engineering and Management, 123(4), 371-378, 1997.

[46] Vakola, M., Rezgui, Y., Organisational learning and innovation in the construction industry, The Learning Organization, 7(4), 174-184, 2000.

[47] Macomber, J. D., Follow the money: what really drives technology innovation in construction, In Construction Research Congress In Construction- Wind of Change: Integration and Innovation, 2003.

[48] Edum-Fotwe, F. T., Gibb, A. G. F., Benford-Miller, M., Reconciling construction innovation and standardisation on major projects. Engineering, Construction and Architectural Management, 11(5), 366-372, 2004.

[49] Manley, K., Implementation of innovation by manufacturers subcontracting to construction projects, Engineering, Construction and Architectural Management, 15(3), 230-245, 2008.

[50] Rutten, M. E., Dorée, A. G., Halman, J. I., Innovation and interorganizational cooperation: a synthesis of literature, Construction Innovation, 9(3), 285-297, 2009.

[51] Korman, T. M., Lu, N., Innovation and improvements of mechanical, electrical, and plumbing systems for modular construction using building information modeling. In Proceeding of the architectural engineering conference, Oakland, California 448-455, (2011, March)..

[52] Chan, I. Y., Liu, A. M., Fellows, R., Role of leadership in fostering an innovation climate in construction firms, Journal of management in engineering, 30(6), 2013.

[53] Rundquist, J., Emmitt, S., Halila, F., Hjort, B., Larsson, B., Construction innovation: addressing the project-product gap in the Swedish construction sector, International Journal of Innovation Science, 5(1), 1-10, 2013.

[54] Xue, X., Zhang, R., Yang, R., Dai, J., Innovation in construction: a critical review and future research, International Journal of Innovation Science, 6(2), 111-126, 2014.

[55] Murphy, M. E., Implementing innovation: a stakeholder competency-based approach for BIM, Construction Innovation, 14(4), 433-452, 2014.

[56] Pellicer, E., Yepes, V., Correa, C. L., Alarcón, L. F., Model for systematic innovation in construction companies, Journal of Construction Engineering and Management, 140(4), 2014.

[57] Ozorhon, B., Oral, K., Demirkesen, S., Investigating the components of innovation in construction projects, Journal of Management in Engineering, 32(3), 2015.

[58] Suprun, E. V., Stewart, R. A., Construction innovation diffusion in the Russian Federation: Barriers, drivers and coping strategies, Construction Innovation, 15(3), 278-312, 2015.

[59] Liu, A. M., Chan, I. Y., Critical role of the learning transfer climate in fostering innovation in construction, Journal of Management in Engineering, 33(3), 2016.

[60] Ozorhon, B., Oral, K., Drivers of innovation in construction projects, Journal of construction engineering and management, 143(4), 2016.

[61] Noktehdan, M., Shahbazpour, M., Zare, M. R., Wilkinson, S., Innovation Management and Construction Phases in Infrastructure Projects, Journal of Construction Engineering and Management, 145(2), 2018.

[62] Sariola, R., Utilizing the innovation potential of suppliers in construction projects, Construction Innovation, 18(2), 2018.

[63] Meng, X., Brown, A., Innovation in construction firms of different sizes: drivers and strategies, Engineering, Construction and Architectural Management, 25(9), 1210-1225, 2018.

[64] Ulubeyli, S., Kazaz, A., Sahin, S., Survival of construction SMEs in macroeconomic crises: Innovation-based competitive strategies, Journal of Engineering, Design and Technology, 16(4), 654-673, 2018.

[65] Gerring, J., What is a case study and what is it good for?. American political science review, 98(2), 341-354, 2004.

[66] Barlish, K., Sullivan, K., How to measure the benefits of BIM—A case study approach, Automation in construction, 24, 149-159, 2012.

[67] Eisenhardt, K. M., Building theories from case study research, Academy of management review, 14(4), 532-550, 1989.

[68] Liu, H., Ran, Y., Study on BIM technology application prospect in engineering management industry. In 2013 6th International Conference on Information Management, Innovation Management and Industrial Engineering, 3, 278-280, 2013, November.

[69] Aranda-Mena, G., Crawford, J., Chevez, A., Froese, T., Building information modelling demystified: does it make business sense to adopt BIM?. International Journal of managing projects in business, 2(3), 419-434, 2009.

[70] Watson, A., BIM-a driver for change. In Proceedings of the International Conference on Computing in Civil and Building Engineering 30-2. Nottingham University Press Nottingham, 2010, June..

[71] Kassem, M., Succar, B., Dawood, N., Building information modeling: analyzing noteworthy publications of eight countries using a knowledge content taxonomy, American Society of Civil Engineers, 2015, January.

[72] Becerik-Gerber, B., Rice, S., The perceived value of building information modeling in the US building industry, Journal of Information Technology in Construction (ITcon), 15(15), 185-201, 2010.

[73] Chen, L., Luo, H., A BIM-based construction quality management model and its applications, Automation in construction, 46, 64-73, 2014.

[74] Azhar, S. Building information modeling (BIM): Trends, benefits, risks, and challenges for the AEC industry, Leadership and management in engineering, 11(3), 241-252, 2011.

[75] Qian, A. Y., Benefits and ROI of BIM for Multi-disciplinary Project Management, National University of Singapore, Mar, 2012.

[76] Yan, H., Demian, P. Benefits and barriers of building information modelling, 2008.

[77] Latiffi, A. A., Mohd, S., Kasim, N., Fathi, M. S., Building information modeling (BIM) application in Malaysian construction industry, International Journal of Construction Engineering and Management, 2(4A), 1-6, 2013.

[78] Innovation, C. C., Adopting BIM for facilities management: Solutions for managing the Sydney Opera House, Cooperative Research Center for Construction Innovation, Brisbane, Australia, 2007.

[79] Kline, R. B. Structural equation modelling, 1998.

[80] Xiong, B., Skitmore, M., Xia, B., Masrom, M. A., Ye, K., Bridge, A., Examining the influence of participant performance factors on contractor satisfaction: A structural equation model, International Journal of Project Management, 32(3), 482-491, 2014.

[81] Bielby, W. T., Hauser, R. M., Structural equation models, Annual review of sociology, 3(1), 137-161, 1977.

[82] Sohn, S. Y., Kim, H. S., Moon, T. H., Predicting the financial performance index of technology fund for SME using structural equation model, Expert Systems with Applications, 32(3), 890-898, 2017.

[83] Baumgartner, H., & Weijters, B. (2017). Structural equation modeling. In Advanced Methods for Modeling Markets (pp. 335-360). Springer, Cham

[84] Nunnally, J. C., Psychometric theory (2nd edit.) mcgraw-hill. Hillsdale, NJ, 416, 1978.

[85] Hair, J., Anderson, R., Tatham, R., Black, W., Multivariate data analysis4 Prentice-Hall Englewood Cliffs, 1998.

[86] Xiaolong, X., Zhang, R., Yang, R., Dai, J., Innovation in construction: a critical review and future research, International Journal of Innovation Science, 6(2), 111-126, 2014.

[87] Koellinger, P., The relationship between technology, innovation, and firm performance-Empirical evidence from e-business in Europe, Research policy, 37(8), 1317-1328, 2008.

[88] Podmetina, D., Smirnova, M., Väätänen, J., Torkkeli, M., Innovativeness and international operations: case of Russian R&D companies, International Journal of Innovation Management, 13(02), 295-3173 2009.

[89] Sideridis, G., Simos, P., Papanicolaou, A., Fletcher, J., Using structural equation modeling to assess functional connectivity in the brain: Power and sample size considerations, Educational and psychological measurement, 74(5), 733-758, 2014.

[90] Eastman, C., Teicholz, P., Sacks, R., Liston, K., BIM handbook: A guide to building information modeling for owners, managers, designers, engineers and contractors. John Wiley & Sons, 2011.

[91] Grilo, A., Jardim-Goncalves, R., Value proposition on interoperability of BIM and collaborative working environments, Automation in construction, 19(5), 522-530, 2010.

[92] Wong, K. D., Fan, Q., Building information modelling (BIM) for sustainable building design, Facilities, 31(3/4), 138-157, 2013.

[93] Fernandes, R. P. L., Advantages and disadvantages of BIM platforms on construction site, 2013.

[94] Eastman, C., Teicholz, P., Sacks, R., Liston, K., BIM handbook: A guide to building information modeling for owners, managers, designers, engineers and contractors. John Wiley & Sons, 2008.

Teknik Dergi, 2021 10739-10766, Paper 611

Experimental Investigation of Scour Hole Characteristics for Different Shapes of Piers Caused by Flood Hydrograph Succeeding Steady Flow

Aslı BOR[1]
M. Şükrü GÜNEY[2]

ABSTRACT

In this study, the scour depth and dimensions of the scour hole around different shaped piers for the cases of hydrographs succeeding steady flow were studied experimentally. The experiments were carried out by using circular, square, rectangular, lenticular and rectangular with trapezoidal nose to compare the various scour hole geometries at the same flow conditions. Numerous experiments were conducted in a rectangular flume (18.6 m long, 0.80 m wide and 0.75 m deep) with different triangular shaped hydrographs. The flume bed of 26 cm thickness consists of uniform graded material with D_{50} =1.68 mm. The experiments were carried out in clear water conditions. The temporal variations of the equilibrium scour depths in front of the pier and the scour hole dimensions were recorded by two different cameras. The equilibrium scour depths at lateral sides and downstream of the piers were also measured. Regression analysis was performed in order to derive empirical relations to predict temporal variations of the scour depth in the case of unsteady flow. The shape factor values were also investigated based on the experimental findings and the obtained values were compared to those available in literature. The performance of the obtained empirical relation for circular pier was tested by using limited experimental data available in the literature. The smallest scour hole was observed for the rectangular with trapezoidal noses pier. The increase in the scour hole dimensions for other cross-sections was in the following order: rectangular with circular noses, circular, square and rectangular piers.

Keywords: Unsteady flow, local scour, scour hole, pier, shape coefficient.

1. INTRODUCTION

Bridges are an important part of transportation system which carry people and vehicles

Note:
- This paper has been received on July 22, 2019 and accepted for publication by the Editorial Board on December 6, 2019.
- Discussions on this paper will be accepted by May 31, 2021.
- https://doi.org/10.18400/tekderg.595126

1 Izmir University of Economics, Department of Civil Engineering, İzmir, Turkey - asli.turkben@ieu.edu.tr https://orcid.org/0000-0002-1679-5130

2 Izmir University of Economics, Department of Civil Engineering, İzmir, Turkey -sukru.guney@ieu.edu.tr https://orcid.org/0000-0003-1441-4784

across. They are subjected to dynamic loads (wind, earthquake, flood …etc.) more than other transportation structures. Bridge failures bring economic problems nationwide and cause tragic results. The relevant studies show that governments spend millions of dollars to prevent scour related to bridge damages [1].

The scour hole has been widely studied and various empirical equations have been developed over time by researchers [2-21]. These empirical equations are based on the experiments performed under different conditions. [22] showed that the dimensionless scour hole length and width depend on flow shallowness (h/b) for different shape of piers and presented relevant empirical relations. [15] carried out an experimental study to observe the temporal variations of the scour depth and contours around vertical wall and wing wall abutments. He developed a semi empirical model to determine dimensionless scour hole length and width depending on flow shallowness parameter. In the scope of his thesis, [16] studied the scour hole geometries in the case of circular and square piers under steady flow conditions. He proposed an equation for the scour hole volume in terms of the flow depth. [9] suggested an equation involving the flow shallowness in order to calculate the top width of scour holes. [23] carried out experiments with different shape of piers and they observed that all the equilibrium dimensionless parameters depend on the characteristic pier width.

In the literature, there are limited studies about non-circular piers. Although there are many works on local scour around bridge piers aiming to clarify the nonlinear relationship between sediment and flow, only few studies have been performed to interrelate the scour hole geometries and flow characteristics in the case of different types of pier shapes and under unsteady flow conditions.

[24] was the first researcher who used different shapes of the pier in his experiments. He proposed that local changes in flow caused by bridge piers or other obstructions influence the scour depth around the piers and he observed that the maximum scour depth occurred around the rectangular pier. [2] studied time and velocity effects on the clear water and live bed local scouring at bridge piers. They also carried out studies with different pier diameters, shapes, grain sizes and water depths. They showed that the maximum scour depth oscillated around the average depth. [4] studied time dependent scour depth variation both in clear water and live bed conditions by using circular piers. Their experiments aimed to show the effects of the different pier geometry, sediment and flow properties on the scour time. They allowed scour to occur around six-inch circular pier for desired depth and measured velocity distributions with a small Pitot tube in uniform bed materials. They found three types of vortex systems, namely trailing, horseshoe, and wake and explained them in detail. They showed that the geometry of the structure is important in determining the strength of the vortex system. In addition, they developed an empirical equation involving the pier diameter, average velocity and upstream water depth. [25] indicated that [4] study was based on narrow range of flow and sediment conditions, so it was not suitable for practical applications. The study of [4] had a single time scale, however, scour time histories indicate generally multiple time scales. [26] conducted a series of live bed scour experiments with different diameter of piers. They compared their experimental findings with those available in the related literature. They observed that stagnation pressure causes shear layers generated at the surface near the sediment bed. They also found that wake vortices behind the pier were dissipated as they moved downstream, the wake vortices being usually recognized from the small scale eddies. [16] studied different pier shapes with different skew angle under steady flow conditions. He

obtained empirical equations to predict scour depth, scour hole radius and scour hole volume. [17] measured local scour hole contours around bridge piers under unsteady flow conditions. They used Ultrasonic Velocity Profiler (UVP) to measure temporal variation of scour depth by placing the device vertically. [21] investigated experimentally the flow field and the local scour around bridge pier of different shapes. They observed that the plan area of the scour hole in the case of the trapezoidal pier was larger compared to the triangular pier, but on the other hand the triangular pier created larger scour hole volume compared to the trapezoidal pier and a sharp nose with curved body was ideal for a bridge pier because of less scour around the pier.

The main objective of this study is to analyze the scour depth and the scour hole geometry due to various hydrographs in the case of five different pier shapes. The approach was based on the image processing with a video camera during unsteady flow conditions. The dimensions of the scour hole were determined by using the values of the scour contours obtained from the experiments. The experimental findings were evaluated by using the empirical expressions existing in the relevant literature. Although many studies have been conducted with circular piers, it is a matter of vital importance to study also prismatic shaped piers (rectangular with circular nose and rectangular with trapezoidal nose) since they are widely used in practice.

2. EXPERIMENTAL SETUP AND MEASUREMENT PROCEDURE

The experiments were carried out in the rectangular flume of 18.6 m length, 0.80 m width and 0.75 m depth with a bottom slope of 0.006, as shown in Fig. 1. The rectangular flume has transparent side walls made of plexiglass. Water was pumped from the main tank having a volume of 27 m^3. The flume has a platform which is 1 m wide and 1.8 m height with ladder. The main tank and rectangular basin are at the downstream end of the flume. The water levels could be adjusted by means of a tail gate. The test section was 11 m from the flume entrance. Drive Link-C software was used to control pump speed which has a maximum capacity of 100 L/s. The hydrographs were generated by adjusting the pump speed. The uniform graded material with D_{50} =1.68 mm was used. The geometric standard deviation was σ_g =1.33 mm. which implies that the sediment can be assumed as uniform and its specific gravity was 2.65. The bed material and its grain distribution curve are shown in Fig. 2. Sieve analysis was performed with 4 different samples and grain distribution was obtained as given in Table 1. The samples were taken from different locations of the flume. The geometric standard deviation was determined from $\sigma_g = \sqrt{\frac{D_{84.1}}{D_{15.9}}} = \sqrt{\frac{2.15}{1.22}} = 1.33$ mm. Since this value is less than 1.4 the sediment can be assumed as uniform ([27] and [28]).

2.1. Pier Types

The experiments were performed with five different pier shapes; circular (b = 11cm), square (b = 8.5 cm), rectangular (b = 11.5 cm), rectangular with circular nose (lenticular) (b = 12 cm) and rectangular with trapezoidal nose (b = 11cm). The piers were made of plexiglass and fixed into the sediment layer. The used pier shapes and dimensions are given in Fig. 3, together with the measurement points positions. The recording device 2 (camera) was used

to record the time dependent scour depth values in front of the piers (point A). The recording device 1 recorded the temporal evolutions of the scour hole. The equilibrium scour depths at lateral side (point B) and at downstream end of the piers (point C) were determined by means of the laser meter and controlled by the records of the device 1.

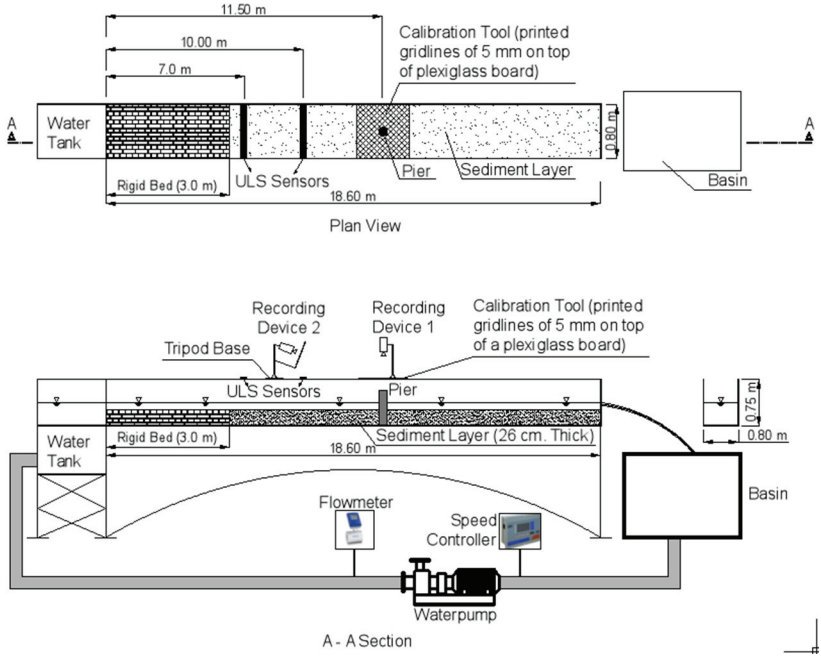

Figure 1 - The scheme of the experimental system [29]

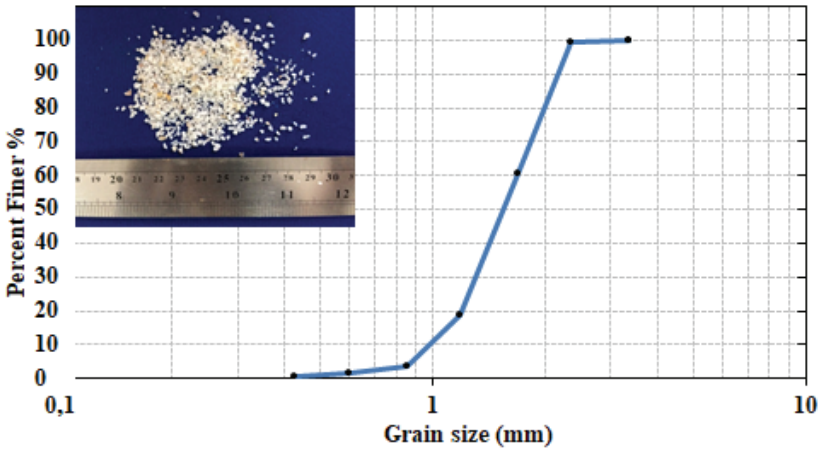

Figure 2 - Sediment sample used in this study [29]

Table 1 - Summary of the sieve analysis

Grain size (mm)	Sample 1	Sample 2	Sample 3	Sample 4
3.35	0.27	0.28	0.04	0.44
2.36	2.16	2.62	1.39	1.97
1.7	277.62	338.81	17.16	707.55
1.17	293.67	381.62	201.5	627.43
0.85	109.98	145.67	81.43	211.9
0.6	14.05	27.77	10.37	37.93
0.425	4.37	12.89	2.45	16.11
Sieve under	5.92	9.02	4.81	9.92
D_{50}	1.69	1.66	1.67	1.71
$D_{84.1}$	2.15	2.14	2.17	2.18
$D_{15.9}$	1.22	1.21	1.22	1.24

2.2. Flow Conditions

All experiments were performed in clear water conditions. Five types of hydrographs were generated by the adjustment of the pump rotational speed. During the first 5 minutes of the experiments the base flow, Q_b (L/s), was kept constant and then it was increased to the peak value, Q_p (L/s), under unsteady flow conditions. The generated triangular hydrographs are described in Table 2 and depicted in Fig. 4. The discharge values were recorded by the magnetic flow meter. The flow depths were measured by ULS, placed at 7th m and 10th m of the flume. The hydrographs (Hid $_{i\,j\,-\,k}$) were described so that the subscripts i and j denote the rising and falling durations in minutes respectively, and the following subscript k indicates the peak discharge of the hydrograph in L/s.

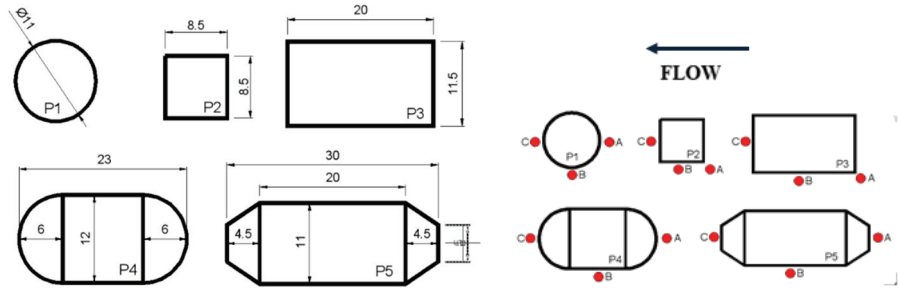

Figure 3 - Pier shapes used in experiments (all dimensions are in cm) and measurement points A, B, and C [29]

In all hydrographs the first part of 5 minutes duration corresponds to the steady flow. The values of the variables characterizing the experimental conditions are summarized in Table

3. In this table, h = approach water depth, u = mean approach velocity, u_c = mean approach critical velocity, I = average flow intensity, $I = \frac{u}{u_c}$ and F_r = Froude number.

Table 2 - Hydrograph characteristics with base flow rates, peak discharges and durations.

Hydrograph Name	Hydrograph Description	Base Flow Rate Q_b (L/s)	Peak Flow Rate Q_p (L/s)	Duration (min)	
				Rising	Falling
Hid1	Hid55-45	8	45	5	5
Hid2	Hid55-63	8	63	5	5
Hid3	Hid55-73	8	73	5	5
Hid4	Hid1010-63	8	63	10	10
Hid5	Hid2020-63	8	63	20	20

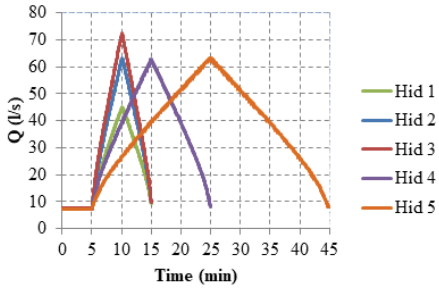

Figure 4 - Hydrographs used in the experiments [29]

Table 3 - Experimental conditions for each experiment

Hydrographs	Total Flow Time	Discharge Q_b - Q_p	Approach Water Depth h_b - h_p	Mean Velocity	Mean Critical Velocity	Flow Intensity Ratio	Froude Number F_{rb} -F_{rp}
				u_b -u_p	u_{cb} -u_{cp}	I_{pb} -I_{pp}	
	min	l/s	cm	m/s	m/s		
Hid1	15	8 - 45	6 - 20.39	0.21-0.28	0.47-0.92	0.45-0.30	0.27-0.20
Hid2	15	8 - 63	6 - 22.61	0.21-0.35	0.47-0.93	0.45-0.38	0.27-0.23
Hid3	15	8 - 73	6 - 23.52	0.21-0.39	0.47-0.94	0.45-0.41	0.27-0.26
Hid4	25	8 - 63	6 - 22.61	0.21-0.35	0.47-0.93	0.45-0.38	0.27-0.23
Hid5	45	8 - 63	6 - 22.61	0.21-0.35	0.47-0.93	0.45-0.38	0.27-0.23

* the subscripts b and p denote base and peak values during hydrographs respectively.

The average flow intensity varied in the range of $0.30 < I < 0.45$ implying that the clear water scouring criterion was satisfied. The mean critical velocities u_c were calculated using the logarithmic average velocity equation Eq. 1.

$$\frac{u_c}{u_{*c}} = 5.75\, log\, 5.53 \frac{h}{D_{50}} \quad (1)$$

where; D_{50} being the median grain size. The critical shear velocity u_{*c} was found for 1 mm≤D_{50}≤100 mm by using the Eq. 2 [30], D_{50} being in mm.

$$u_{*c} = 0.0305\sqrt{D_{50}} - \frac{0.0065}{D_{50}} \quad (2)$$

The Reynolds number varied between 18,300 and 38,300 implying that viscous effects could be overlooked [31].

2.3. Experimental Procedure

25 experiments were conducted with five different types of pier. The temporal variations of the scour depth at the upstream face of the pier, the maximum scour depths at the downstream and lateral faces of the pier were recorded simultaneously. The sediment bed was flattened before each experiment and water was supplied gently without causing any disturbance to the bed material. Before the tests, the bed levels were measured in order to specify the scour depths ds according to these premeasured values.

During the experiments, the cameras recorded the bed elevations allowing the determination of the scour depth at point A and the configuration of the scour hole. The length and width of the scour hole were also measured in the course of the experiments. Measurements were performed with two methods, namely by using a laser meter and by means of a video camera. Laser meter was used only at the end of the experiment, when the water was removed from the flume. Two video cameras were used; one located between 11^{th} m and 12^{th} m of the flume and the other located at 10^{th} m of the flume with an angle of 45° in order to obtain the plan view of the scour hole. The first camera was mounted 41.5 cm above 80 cm × 100 cm plexiglass plate on which 5.0×5.0 mm squares were drawn just like a squared paper. This plate was 54 cm far from the bed. The second camera was mounted 27 cm above 210×297 cm plexiglass plate with meshes of 5.0×5.0 mm. This plate was 120 cm far from the piers. The details of this configuration are given in Fig. 5.

At the end of the experiments, water was removed gently, and the bed topography was measured with laser meter and transmitted to Golden software Surfer program. The maximum scour depths were measured at points B and C, by the laser meter.

The records were analyzed by the image processing technique to determine the time dependent scour depth and the scour hole area. A grid system (1.0×1.0 cm square) was built around the pier and the scour hole contours were identified by surveying with laser meter. The results were plotted as contour lines of the scour hole with the Golden software Surfer program and converted to AutoCAD drawings. Many difficulties were encountered during the measurements. While water was rising during the hydrograph, the images of scour holes

became overestimated due to the optical diffraction. At each time step, as water level above the layer of sediment was different, a calibration became necessary to determine the scoured area. To do so, a grid of one centimeter meshes was printed on a transparent plexiglass. The scour hole dimensions for corresponding times were plotted at AutoCAD.

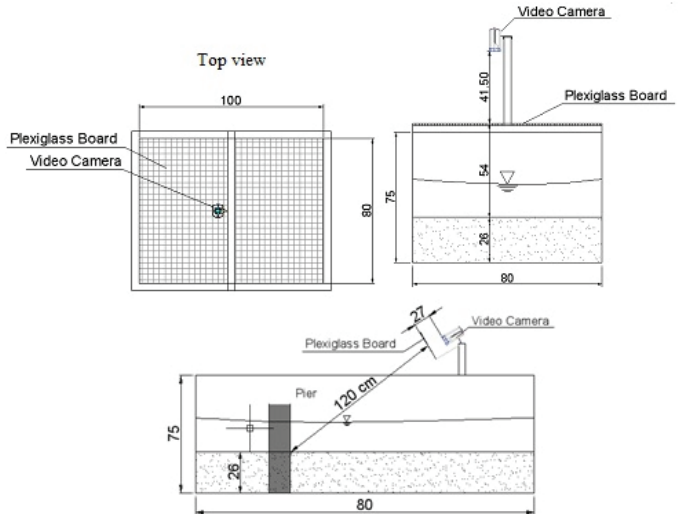

Figure 5 - Sketch to illustrate the measurement procedure by using two cameras [29]

3. RESULTS AND DISCUSSIONS

3.1. Observations of Scour around the Piers of Different Shape

At the end of each experiment, the dimensions of the scour hole were measured. The scouring photographs were taken after removing the water gently. Fig. 6 shows the photographs of the final scour geometries developed around the pier of five different shapes, namely circular (P1), square (P2), rectangular (P3), rectangular with circular nose (P4) and rectangular with trapezoidal nose (P5) at the end of experiments. It was observed that, the shapes of the pier significantly changed the scour holes geometry.

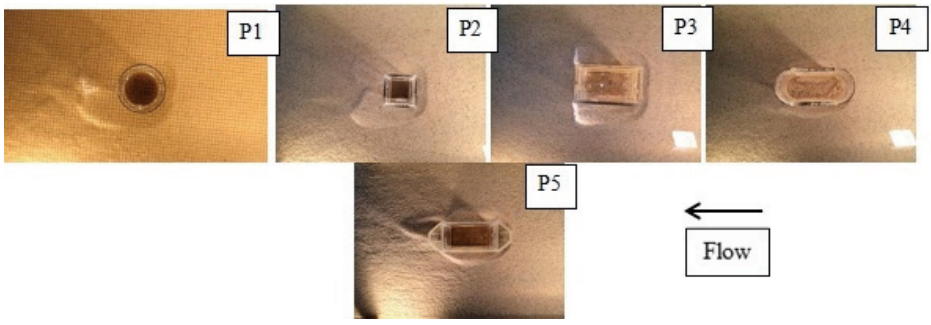

Figure 6 - Scour hole photographs at the end of the experiment P1 to P5 for Hid 1. [29]

It was also observed that maximum scour depths occurred at the upstream face of the rounded piers and at the upstream corners for angular piers. The maximum scour depth values at measurements points A, B and C are summarized in Table 4, for different hydrographs. In Table 4, d_{sA} (cm) denotes the maximum (equilibrium) scour depth at the upstream face of the pier, d_{sB} (cm) and d_{sC} (cm) are the maximum scour depths at the lateral and the downstream faces of the pier, respectively. The final surrounding bed configurations, determined at the end of each experiment, are presented in Fig. 7 to 11. The distances are in cm. The contour plots are generated by the measurements of the elevations using point gauge by Surfer program in order to indicate the scouring and deposition zones at the upstream and downstream regions of the pier. As stated in [5], [6] and [32], three scouring forms were observed around the piers. At the upstream of the piers (Point A) the frontal scour due to the horseshoe vortices was observed. At the lateral sides of the piers (Point B) the observed scouring was due to the flow separation and shear layers and the succeeding turbulent wakes induced the deformation of the bed at the downstream of the piers (Point C). The frontal scour was mostly developed in the cases of the square pier P2 and the rectangular pier P3, compared to the rounded piers such as the circular P1 and the rectangular with circular nose pier P4 and the rectangular with trapezoidal nose P5 piers. The equilibrium scour depth at lateral side (point B) was not significant for the r

ectangular with trapezoidal nose pier P5. The deposition was significant at point B for the circular pier P1 and the square pier P2.

Table 4 - Maximum scour/deposition depths measured at the end of hydrographs

Scour Depths (cm)		Hydrographs				
		Hid55-45 (HID 1)	Hid55-63 (HID 2)	Hid55-73 (HID 3)	Hid1010-63 (HID 4)	Hid2020-63 (HID 5)
P1	d_{sA}	3.8	6	6	6	6.5
	d_{sB}	3.4	5	4.5	3.6	5.5
	d_{sC}	0.8d	0.6d	0.5	0	1.7
P2	d_{sA}	4	6.5	7.5	6.5	7.5
	d_{sB}	2.9	4.5	7	6.5	7.5
	d_{sC}	0.8d	0.5	1.5	0.5	1.5
P3	d_{sA}	4.5	7.5	8.5	8	8
	d_{sB}	0.5	0.8	2	0	1.5
	d_{sC}	0.2d	1d	0.7d	1d	0.5d
P4	d_{sA}	4.2	4.4	6	4.4	5.5
	d_{sB}	0.5	0.6	1.5	0.4	2.5
	d_{sC}	0.1d	0.1d	0	0.1d	0.8d
P5	d_{sA}	2.2	4	5	4.5	5.5
	d_{sB}	0	0	0	0	1
	d_{sC}	1.3d	1.4d	1.6d	2.2d	1.2d

Note: “d” means deposition in d_{sC} point.

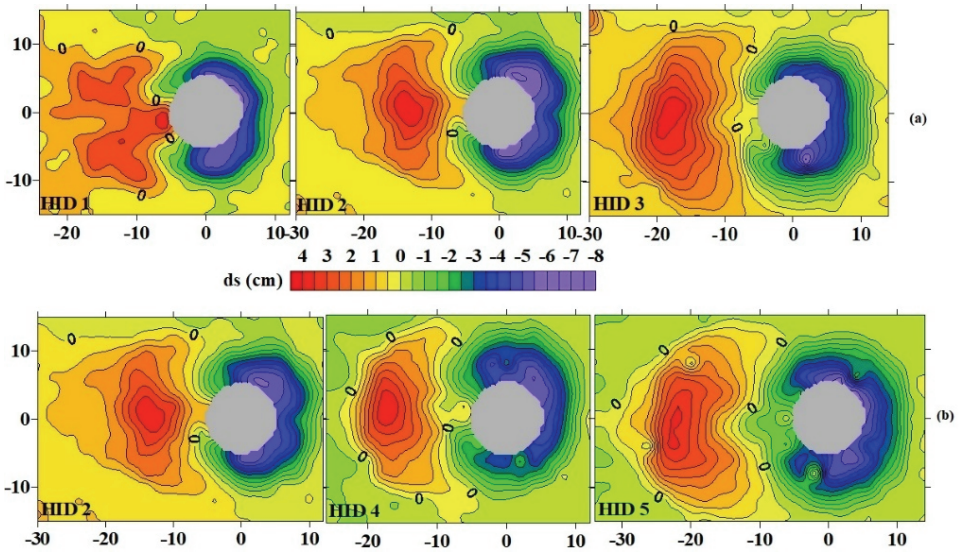

Figure 7 - Bed configurations in the case of the circular pier P1 for the hydrographs a) having the same duration and different flow rate peaks b) having the same flow rate and different durations.

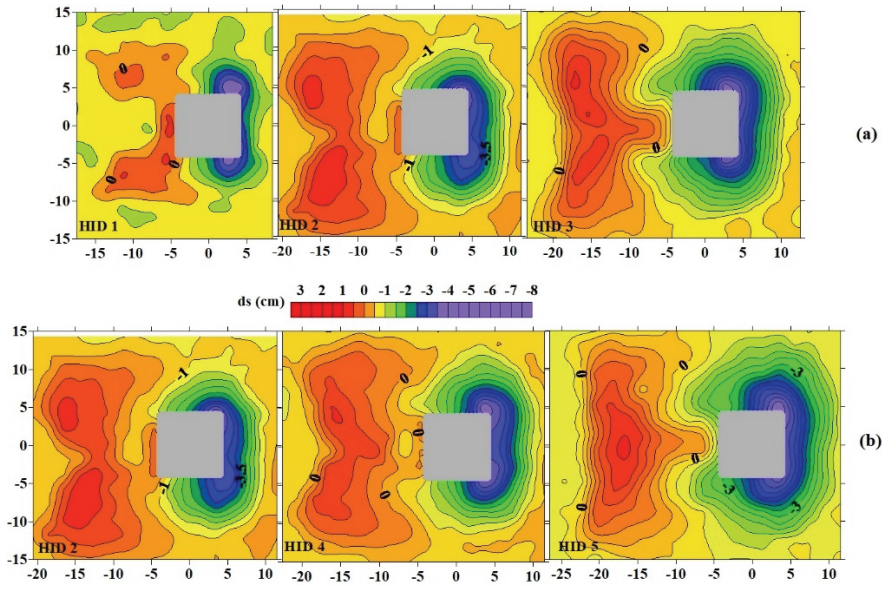

Figure 8 - Bed configurations in the case of the square pier P2 for the hydrographs a) having the same duration and different flow rate peaks b) having the same flow rate and different durations.

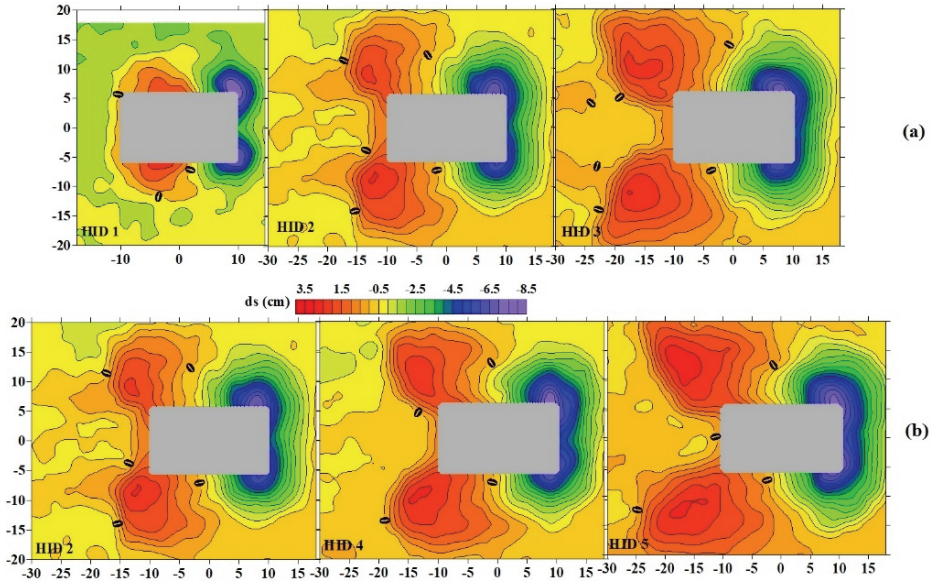

Figure 9 - Bed configurations in the case of the rectangular pier P3 for the hydrographs a) having the same duration and different flow rate peaks b) having the same flow rate and different durations.

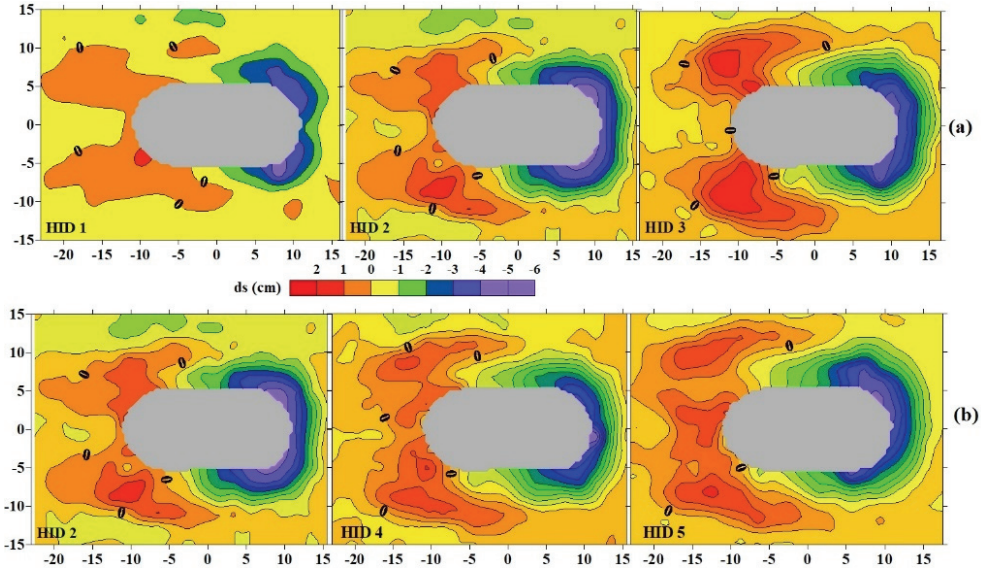

Figure 10 - Bed configurations in the case of the rectangular with the circular nose pier P4 for the hydrographs a) having the same duration and different flow rate peaks b) having the same flow rate and different durations.

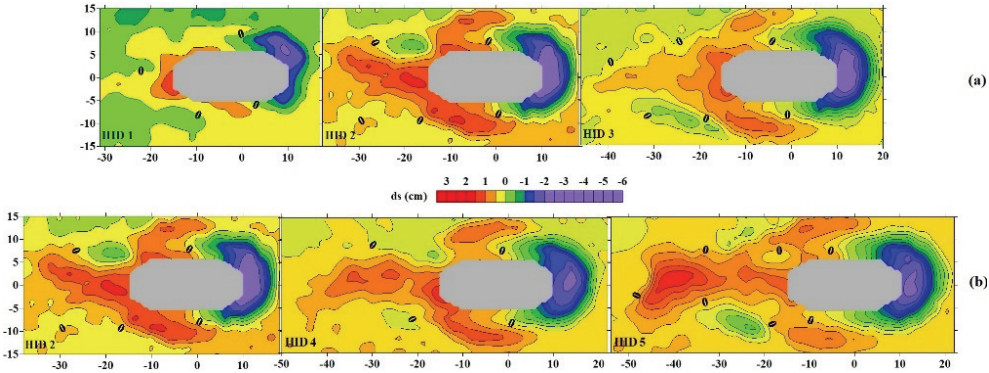

Figure 11 - Bed configurations in the case of the rectangular with the trapezoidal nose pier P5 for the hydrographs a) having the same duration and different flow rate peaks b) having the same flow rate and different durations.

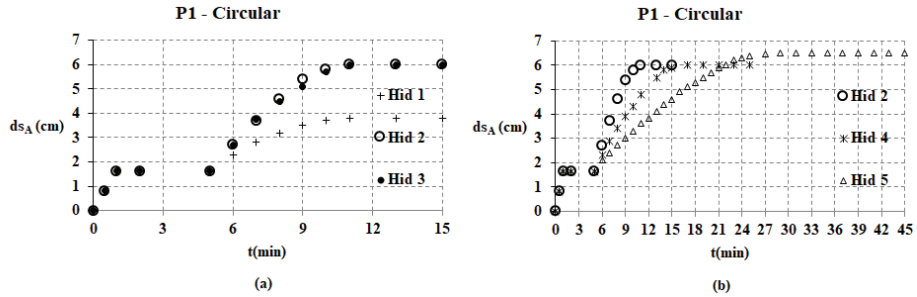

Figure 12 - Temporal variations of the scour depth at point A for the circular pier P1 for hydrographs a) with different peak flow rate b) with different duration

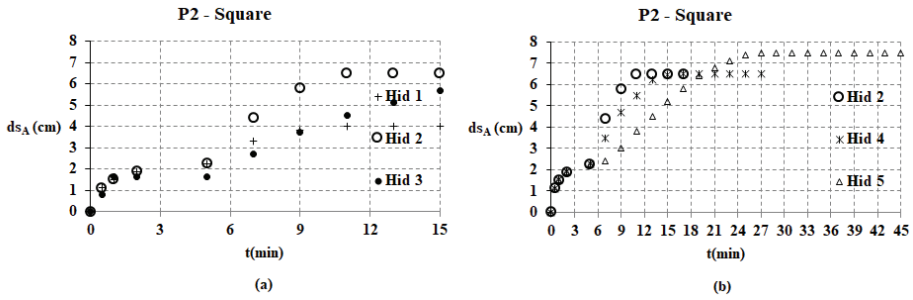

Figure 13 - Temporal variations of the scour depth at point A for the square pier P2 for hydrographs a) with different peak flow rate b) with different duration

The time dependent scour depths at point A for all experiments are given in Fig. 12 to Fig. 16. For each of the piers, the scour depth initially increased and reached a maximum at about peak flow rate. As expected, larger maximum scour depths were developed in the case of the piers P2 and P3, compared to the piers P1, P4 and P5. It was revealed that the peak flow rate values of the hydrographs effected the maximum scour depths much more than the durations of the hydrograph limbs.

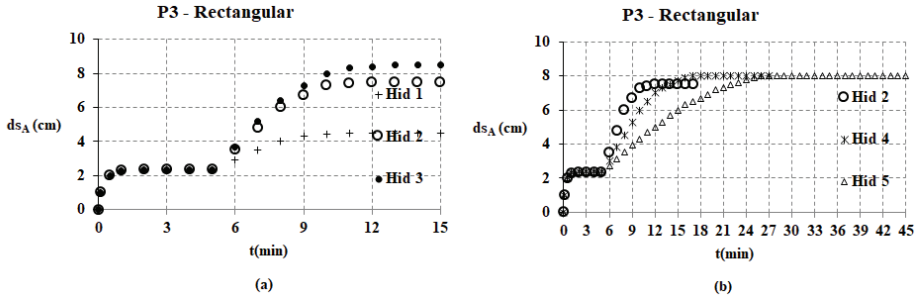

Figure 14 - Temporal variations of the scour depth at point A for the rectangular pier P3 for hydrographs a) with different peak flow rate b) with different duration

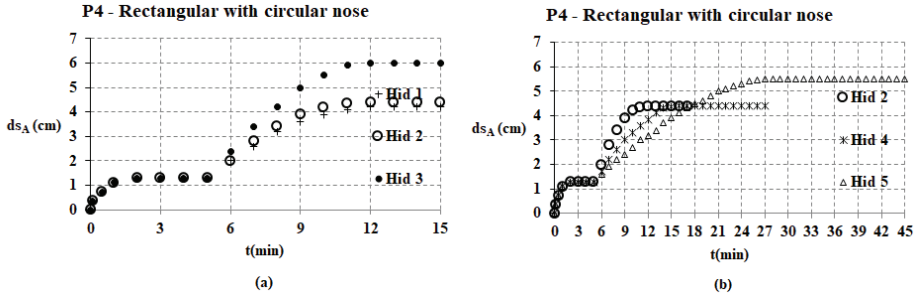

Figure 15 - Temporal variations of the scour depth at point A for circular nose pier P4 for hydrographs a) with different peak flow rate b) with different duration

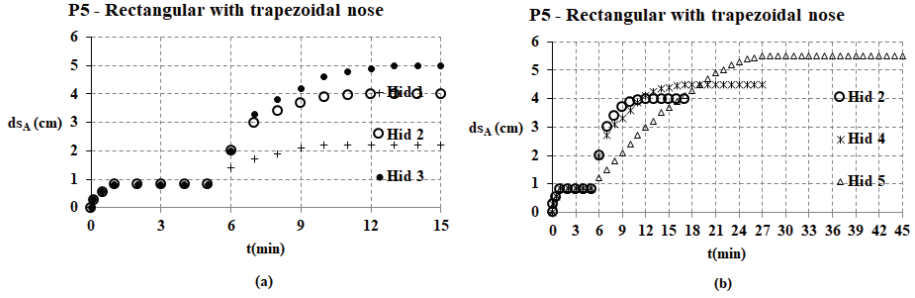

Figure 16 - Temporal variations of the scour depth at point A for the trapezoidal nose pier P5 for hydrographs a) with different peak flow rate b) with different duration

The fractional changes in the scour depth at point A with respect to the fractional changes in the peak flow rate were investigated by taking the smallest value (Q_p = 45 l/s) as reference value. The so obtained percentages are given in Table 5a.

For circular pier P1, when the flow rate was increased to 63 l/s (by 40%) and 73 l/s (by 62%), these increases caused the same change of 60% in the scour depth. In the case of square pier P2, when the flow rate was increased to 63 l/s and 73 l/s, these increases caused the changes of 62% and 88% in the scour depth, respectively. These changes were observed as 40% and 62% in the case of rectangular pier P3, 5% and 42% for rectangular pier with circular nose P4 and 82% and 130% for rectangular pier with triangular nose P5, respectively.

Table 5a - Fractional changes in the scour depth in terms of fractional changes in the flow rate

Pier type	**P1**		**P2**		**P3**		**P4**		**P5**	
ΔQ_p / Q_{pref} (%)	40	62	40	62	40	62	40	62	40	62
d_s / d_{so} (%)	60	60	62	88	67	88	5	42	82	130

The fractional changes in the scour depth at point A with respect to the fractional changes in the hydrograph rising limb duration were investigated by taking the smallest value (t_p = 5 min) as reference value. The so obtained percentages are given in Table 5b.

For circular pier P1, when the hydrograph rising limb duration was increased to 10 min (by 100%) and 15 min (by 200%), these increases caused 0% and 9% increase in the scour depth, respectively. In the case of square pier P2, when the hydrograph rising limb duration was increased to 10 min and 15 min, these increases caused 0% and 15% increase in the scour depth, respectively. These changes were observed as 8% and 8% in the case of rectangular pier P3, 0% and 25% for rectangular pier with circular nose P4, and 13% and 38% for rectangular pier with triangular nose P5, respectively.

Table 5b - Fractional changes in the scour depth in terms of fractional changes in the rising limb duration

Pier type	**P1**		**P2**		**P3**		**P4**		**P5**	
Δt / t_{ref} (%)	100	200	100	200	100	200	100	200	100	200
d_s / d_{so} (%)	0	9	0	15	8	8	0	25	13	38

The maximum scour depths were first observed at the lateral sides of the pier and then they migrated to the upstream of the pier. Higher flow velocities caused greater scour depths, as expected. For all the hydrographs, the maximum scour depth occurred after the peak flow rate was reached. [14], [12], [27] and [19] studied the temporal scour depth variations under unsteady flow conditions and showed that the recession period of hydrograph played a minor role in the scouring process. As seen in Table 5 and Fig. 12 to16 this fact was also observed

in our experiments. In Table 6, t_p and t_{se} denote times to reach the peak discharge and equilibrium scour depth, respectively.

Table 6 - Times to reach the peak discharge and equilibrium scour depth

Pier ID.	Hid55-45			Hid55-63			Hid55-73			Hid1010-63			Hid2020-63		
	tp	tse	%	tp	tse	%	tp	tse	%	tp	tse	%	tp	tse	%
P1	10	10.5	97	10	10.5	95	10	10.6	98	15	16	93	25	26.4	91
P2	10	10.5	95	10	10.6	98	10	10.6	99	15	16	98	25	26.5	98
P3	10	10.5	97	10	10.6	93	10	10.6	98	15	16.5	97	25	26.5	98
P4	10	10.5	98	10	10.5	98	10	10.5	99	15	16	98	25	26.4	98
P5	10	10.5	98	10	10.5	99	10	10.5	99	15	16	95	25	26.4	96

Note: % means percentage of the maximum scour depth at the peak time. t_p and t_{se} are in *minute*.

3.2. Comparison of the Measured Time Dependent Scour Depths ds(t) for Circular Pier P1 with the Equations Proposed by [27] and [33]

[27] and [33] proposed the empirical relations based on their experiments performed under unsteady flow conditions with triangular hydrographs. They used the reference length L_R that involves the pier width b (for circular piers b = D) and the approach flow depth h. The dimensionless time dependent scour depth $d_s(t)/L_R$ is expressed as:

$$\frac{d_s(t)}{L_R} = 0.068 K_s {\sigma_g}^{-0.5} {F_d}^{1.5} \log(T) \quad (3)$$

where $L_R = (hA)^{1/3}$, A= the cross sectional area of the pier, Ks = pier shape coefficient, σ_g = geometric standard deviation of particle size distribution, F_d = densimetric particle Froude number, $F_d = \frac{u}{\sqrt{g' D_{50}}}$, g'= reduced gravitational acceleration, $g' = \big((\rho_s - \rho)/\rho\big) g$ T is a dimensionless time parameter $T = \frac{t}{t_R}$, t and t_R being time and time scale with $t_R = \frac{\sigma_g^{\frac{1}{3}} \sqrt{g' D_{50}}}{L_R} t$. [33] developed the formula previously proposed by [27] and generalized temporal scour depth due to a single peaked flood wave. They combined [12] and [27] formula with Manning equation. [27] rewrote the formula as:

$$\frac{d_S(\gamma T_M)}{L_R} = 0.068 K_s {\sigma_g}^{-0.5} {F_d}^{1.5} \log(\gamma T_M) \quad (4)$$

where; the subscript *M* denotes the peak flow, $T_M = t/t_M$ is the normalized time and $\gamma = t_M/t_R$ such that $T = \gamma T_M$, with t_M = time to peak of the flood hydrograph. [33] used the following expression shown in Eq. 5.

$$Q_M = [T_M \, exp(1 - T_M)]^n \quad (5)$$

where n= the hydrograph shape parameter, n>1. In this study the shape factor was determined by using their procedure and the value of n was obtained as 5. The optimum computation step length ΔT_M value was taken as ΔT_M =0.01, as suggested. Fig. 17 represents the measured temporal scour depths and those calculated from [27] and [33] together with the band of ±25%. As seen from this figure, the experimental values were found not to be in agreement with those obtained from equation of [27]. The numerical results obtained from equation of [27] found to be underestimated in all cases. It was revealed that the compatibility between the values observed in the experiments and those obtained from [33] was better.

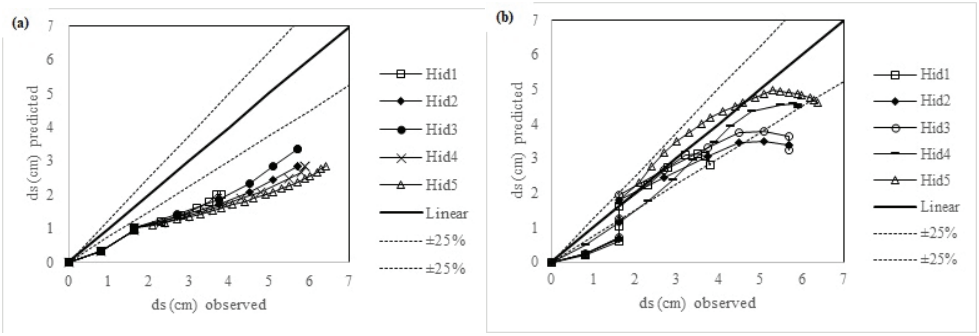

Figure 17 - Measured temporal variations of the scour depths and those calculated by using the equations proposed by a) [27] and b) [33]

3.3. Derivation of the Empirical Equation

The experimental findings were used to derive the empirical relations for the dimensionless scour depth ds (t) / L_R as proposed by [27] and [33] by performing nonlinear regression analysis. Depending upon the dimensionless parameters taken into consideration 3 different scenarios were studied (Table 7). The constant factor considered in the relations corresponds to the shape factor K_s which is assumed to be equal to 1 in the case of circular pier. The following scenarios are used considering the dimensionless variables indicated below:

Table 7 - Scenarios for nonlinear regression analysis

Scenario 1: $\frac{d_s(t)}{L_R} = f_1\left(F_d, I, \frac{h}{b}, \frac{b}{D_{50}}, T\right)$
Scenario 2: $\frac{d_s(t)}{L_R} = f_2\left(F_d, I, \frac{b}{D_{50}}, T\right)$
Scenario 3: $\frac{d_s(t)}{L_R} = f_3(F_d, I, T)$

The considered dimensionless parameters and so obtained empirical relations, together with the coefficients of determination are given in Tables 8 to 12. The largest coefficients of determination R^2 were obtained in the case of the Scenario 1.

Table 8 - Regression Equations for 3 different scenarios for P1

Scenarios	*Regression Equation*	R^2
f1	$\frac{d_s(t)}{L_R} = {F_d}^{2.256} I^{-2.226} \frac{h}{b}^{0.026} \frac{b}{D_{50}}^{-1.085} \log(T)$	*0.93*
f2	$\frac{d_s(t)}{L_R} = {F_d}^{2.410} I^{-2.382} \frac{b}{D_{50}}^{-1.130} \log(T)$	*0.91*
f3	$\frac{d_s(t)}{L_R} = {F_d}^{-0.968} I^{1.1914} \log(T)$	*0.76*

Table 9 - Regression Equations for 3 different scenarios for P2

Scenarios	*Regression Equation*	R^2
f1	$\frac{d_s(t)}{L_R} = 0.993 {F_d}^{2.256} I^{-2.226} \frac{h}{b}^{0.026} \frac{b}{D_{50}}^{-1.085} \log(T)$	*0.91*
f2	$\frac{d_s(t)}{L_R} = 0.993 {F_d}^{2.410} I^{-2.382} \frac{b}{D_{50}}^{-1.130} \log(T)$	*0.81*
f3	$\frac{d_s(t)}{L_R} = 0.890 {F_d}^{-0.968} I^{1.1914} \log(T)$	*0.48*

Table 10 - Regression Equations for 3 different scenarios for P3

Scenarios	*Regression Equation*	R^2
f1	$\frac{d_s(t)}{L_R} = 1.346 {F_d}^{2.256} I^{-2.226} \frac{h}{b}^{0.026} \frac{b}{D_{50}}^{-1.085} \log(T)$	*0.91*
f2	$\frac{d_s(t)}{L_R} = 1.352 {F_d}^{2.410} I^{-2.382} \frac{b}{D_{50}}^{-1.130} \log(T)$	*0.81*
f3	$\frac{d_s(t)}{L_R} = 0.808 {F_d}^{-0.968} I^{1.1914} \log(T)$	*0.51*

Table 11 - Regression Equations for 3 different scenarios for P4

Scenarios	*Regression Equation*	R^2
f1	$\frac{d_s(t)}{L_R} = 0.869 {F_d}^{2.256} I^{-2.226} \frac{h}{b}^{0.026} \frac{b}{D_{50}}^{-1.085} \log(T)$	*0.95*
f2	$\frac{d_s(t)}{L_R} = 0.873 {F_d}^{2.410} I^{-2.382} \frac{b}{D_{50}}^{-1.130} \log(T)$	*0.85*
f3	$\frac{d_s(t)}{L_R} = 0.491 {F_d}^{-0.968} I^{1.1914} \log(T)$	*0.58*

Table 12 - Regression Equations for 3 different scenarios for P5

Scenarios	***Regression Equation***	***R^2***
f1	$\frac{d_s(t)}{L_R} = 0.757{F_d}^{2.256} I^{-2.226} \frac{h}{b}^{0.026} \frac{b}{D_{50}}^{-1.085} \log(T)$	***0.94***
f2	$\frac{d_s(t)}{L_R} = 0.759{F_d}^{2.410} I^{-2.382} \frac{b}{D_{50}}^{-1.130} \log(T)$	***0.84***
f3	$\frac{d_s(t)}{L_R} = 0.465{F_d}^{-0.968} I^{1.1914} \log(T)$	***0.48***

Since experimental studies performed in unsteady flow conditions are relatively rare, our suggested relations were tested with limited data available in the literature. Experimental findings obtained by [27] and [34] were tested and obtained results are illustrated in Fig. 18a and 18b. An acceptable agreement was found in the case of scenario 1 for circular piers. The geometric and hydraulic parameters corresponding to these experiments are summarized in Table 13.

Table 13 - Geometric and Hydraulic Parameters of Previous Studies

Experiment No	D (cm)	hM (cm)	d50 (mm)	σg	FdM
OH_HYD 1	11	15	3.1	2.15	1.960
OH_HYD 2	11	17	3.1	2.15	2.260
OH_HYD 3	11	19	3.1	2.15	2.580
OH_HYD 4	11	17	3.1	2.15	2.280
Arkis - HYD 1	4	22.6	1.68	1.3	1.197
Arkis - HYD 1	8	22.6	1.68	1.3	1.197
Arkis - HYD 1	15	22.6	1.68	1.3	1.197
Arkis - HYD 1	20	22.6	1.68	1.3	1.197
Arkis - HYD 2	4	23.52	1.68	1.3	2.448
Arkis - HYD 2	8	23.52	1.68	1.3	2.448
Arkis - HYD 2	15	23.52	1.68	1.3	2.448
Arkis - HYD 2	20	23.52	1.68	1.3	2.448

In some of the existing studies, the experiments were carried out by using circular piers and the results were generalized for otherwise shaped piers by taking into consideration various shape factors. The shape factors suggested by different researchers including ([2]; [24]; [35];

[36]; [26]; [37]; [9]; [10]; [1]; [22]; [12]) are summarized in Table 14, together with those obtained from the experimental findings combined with the nonlinear regression analysis. The given coefficients concern the scenarios 1 and 2 which provided the highest coefficients of determination.

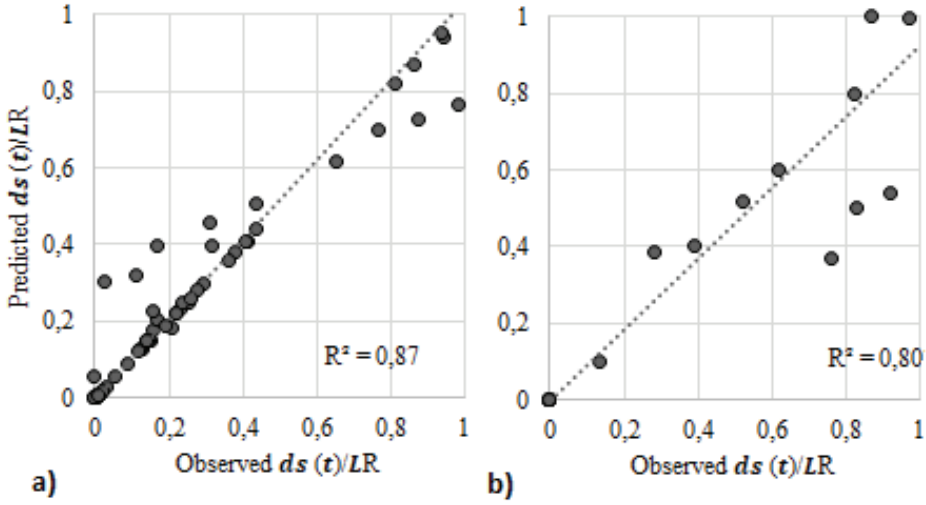

Figure 18 - Comparison of the dimensionless time dependent scour depth $d_s(t)/L_R$ computed from the suggested relation scenario 1 for P1 and those measured by a) [34] and b) [27]

Table 14 - Pier shape factor values Ks proposed by Researchers and those obtained in this study

Pier Type	Tison (1940)	Laursen and Toch (1956)	Chabert and Engeldinger (1956)	Dietz (1972)	Breusers et.al. (1977)	Mostafa (1994)	Melville (1997)	Hoffmans and Verheij (1997)	Richardson and Davis (2001)	Oliveto and Hager (2002)	Bennett (2002)	Ks(Calc.) (present study)	
												Sc 1	Sc 4
P1	1	0.9	1	1	1	1	1	1	1	1	1	1	1
P2	-	-	-	-	1.2	-	1.1	-	-	1.3	-	0.99	1.1
P3	1.4	1	1.1	1.1	1.3	1.3	1	1-1.2	1.1	1.2	1.1	1.35	1.34
P4	-	0.9	-	0.9	-	1.1	1	0.9	1	-	0.9	0.87	0.86
P5	-	-	-	-	-	-	-	-	-	-	-	0.76	0.76

3.4. Temporal Evolution of the Scour Holes Geometry

The scour hole measurements were performed both with data obtained from the camera and laser meter combined with Surfer software program and by using laser meter combined with AutoCAD drawings at the end of each experiment. Scour and deposition areas were drawn by means of the image processing technique by using the data of Video Camera 1 and then illustrated in AutoCAD. This process was performed for all piers and the results obtained for the circular pier are presented in Fig. 19, as an illustrative example.

The geometric characteristics of the scour holes around the piers are summarized in Table 15. The scour contours were found to be almost uniformly spaced. The shape of the scour hole around piers was approximately an inverted cone. For the pier placed along the channel axis, the scour contours were almost symmetrical with respect to the pier axis.

The surface area and volume of the scour hole around the bridge piers were computed using AutoCAD Civil 3D software based on the conic approximation method, by calculating the volume between two sectional areas. The two areas are being added along with the square root of their product and multiplied by a third of distance between the areas to determine the volume. Accordingly, in Fig. 20, the dimensionless surface area $A^* = \frac{A_{scour}}{A_{pier}}$ and dimensionless time $T = \frac{t}{t_R}$, were used. Variations of dimensionless area against dimensionless time are shown in Fig. 20 for each pier and for 5 different hydrographs. The scour hole evolution can be defined by means of a mathematical expression such as $A^* = aT^b$, a and b being coefficients [38]. In this study the same form of relation was investigated, and so obtained values are plotted as A^* versus T in Fig. 20. The so obtained coefficients a and b are given in Table 16.

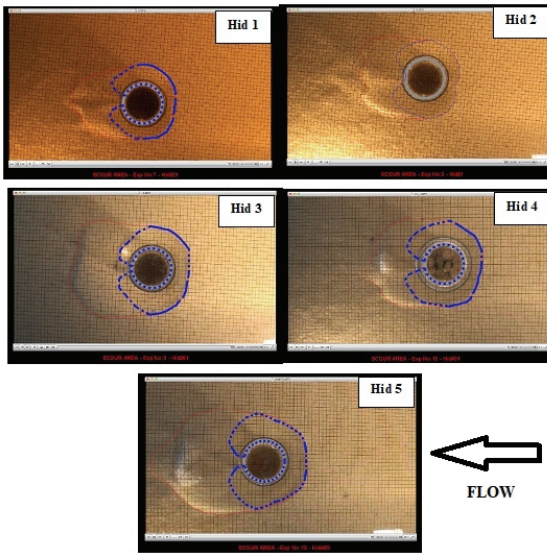

Figure 19 - Scour hole configuration for the circular pier after the image processing

Table 15 - Scour hole measurements for piers

Pier ID	Hyd. ID	b (cm)	d_{sA} (cm)	Area (cm^2)	Volume (cm^3)
	Hid 1	11	3.8	438	672
	Hid 2	11	5.8	472	977
P1	Hid 3	11	5.8	501	1219
	Hid 4	11	6.1	529	1028
	Hid 5	11	6.5	563	1443
	Hid 1	8.5	4.1	402	435
	Hid 2	8.5	6.6	420	785
P2	Hid 3	8.5	7.6	601	1255
	Hid 4	8.5	6.5	483	927
	Hid 5	8.5	7.7	716	1459
	Hid 1	11.5	4.5	283	442
	Hid 2	11.5	7.4	662	1447
P3	Hid 3	11.5	8.1	710	1819
	Hid 4	11.5	7.8	602	1460
	Hid 5	11.5	8	798	2006
	Hid 1	12	3.9	398	508
	Hid 2	12	4.2	490	770
P4	Hid 3	12	5.5	512	928
	Hid 4	12	4.4	537	942
	Hid 5	12	5.4	586	1078
	Hid 1	11	2	289	211
	Hid 2	11	3.7	420	595
P5	Hid 3	11	4.4	537	844
	Hid 4	11	4.2	446	644
	Hid 5	11	5.2	569	755

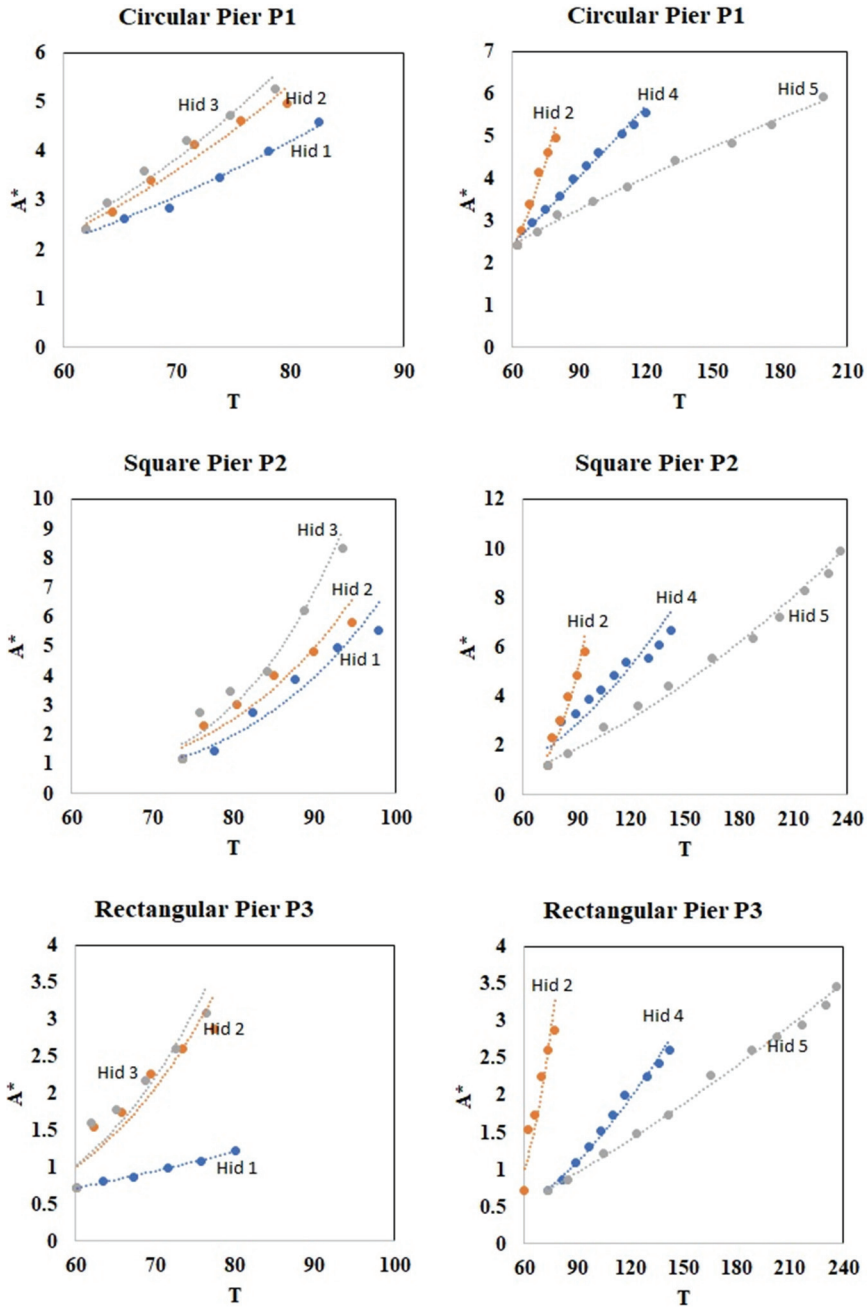

Figure 20 - Variation of A^* with respect to T

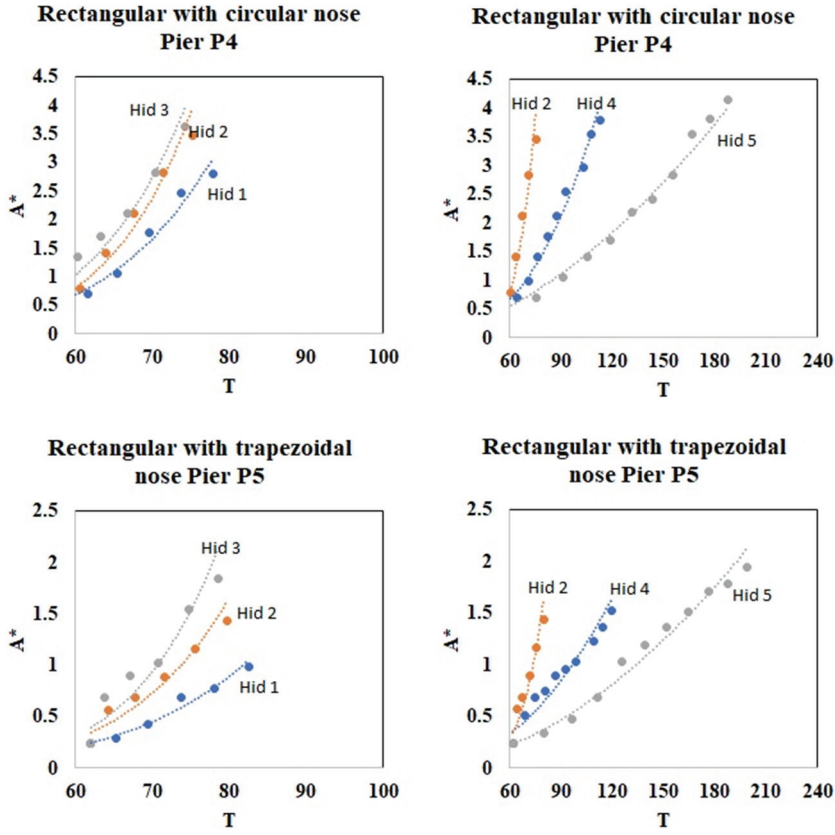

Figure 20 - Variation in A^* with respect to T (Continued)

Table 16 - Coefficients a and b of the mathematical expressions

		Hid55-45	**Hid55-63**	**Hid55-73**	**Hid1010-63**	**Hid2020-63**
P1	**a**	0.0002	$1x10^{-5}$	$6x10^{-6}$	0.017	0.12
	b	2.31	2.94	3.14	1.22	0.73
P2	**a**	$2x10^{-11}$	$4x10^{-11}$	$1x10^{-13}$	0.0003	0.0009
	b	5.83	5.7	7.02	2.07	1.7
P3	**a**	0.0004	$4x10^{-9}$	$1x10^{-9}$	0.0001	0.0026
	b	1.83	4.72	5	1.99	1.32
P4	**a**	$4x10^{-11}$	$3x10^{-13}$	$7x10^{-12}$	$5x10^{-6}$	0.0004
	b	5.77	7.02	6.23	2.89	1.74
P5	**a**	$2x10^{-10}$	$4x10^{-12}$	$7x10^{-14}$	$3x10^{-5}$	$9x10^{-5}$
	b	5.12	6.13	7.1	2.31	1.9

4. CONCLUSIONS

In this study, clear water scour experiments were performed for five different shapes of piers; circular, square, rectangular, rectangular with circular nose (lenticular) and rectangular with trapezoidal nose, for five triangular shaped hydrographs. It was revealed that there were substantial differences among the different scour holes related to the pier shapes and hydrograph characteristics.

- The peak flow rates were much more effective on the scour depths compared to the hydrograph durations. The scour depth evolutions were mainly influenced during the rising limb and the maximum scour depth occurred approximately at the peak flow rate, without significant change during the recession period of the hydrographs. It was observed from the experiments that about more than 90% of the maximum scour depth occurred initially for all pier shapes at about peak times of the experiments.
- From the inspection of Table 4, the maximum scour depth at measurement points A and B was found to be the smallest in the case of the pier P5. As shown in Table 4 the maximum scour depth at measurement point A was observed in the case of the pier P3.
- From the inspection of Table 5a, it was revealed that the pier P4 was affected least, while the pier P5 was influenced most. From the inspection of Table 5b, it was found that the pier P5 was influenced most from the fractional changes in the flow.
- There is a discrepancy between the measured dimensionless scour depths and those calculated from the relation suggested by [27]. The values calculated from this relation was found to be underestimated in all cases. The majority of the measured values and those calculated from the equation proposed by [33] were found to be in the interval of ± 25%.
- The derived empirical relations concerning the time dependent dimensionless scour depths were studied statistically. The so obtained determination coefficients revealed that the most effective parameters were $F_d, I, \frac{h}{b}, \frac{b}{D_{50}}$ and T.
- The regression analysis was performed to investigate the pier shape factor. As seen in Table 14 the average values are as follows: $K_s = 1.045$ for the pier P2, $K_s = 1.345$ for the pier P3 and $K_s = 0.865$ for the pier P4. These values are close to those existing in the literature.
- The pier shape factor in the case of the pier P5 (the rectangular shape with trapezoidal nose) was found to be equal to 0.760.
- From the inspection of the Fig. 20 it was revealed that the geometry of the pier shape effects the scour hole development directly. The larger value of the ratio of the scour area to the pier area for different shaped piers are found to be as follows: for pier P1 $A^* = 5$, for pier P2 $A^* = 8$, for pier P3 $A^* = 3.5$, for pier P4 $A^* = 4$ and for pier P5 $A^* = 2$.

- The empirical relation in the form $A^* = aT^b$ was found to be convenient to express the dimensionless scour hole surface area versus the dimensionless time.
- According to these results, the rectangle with trapezoidal nose shaped piers and the rectangle with circular nose shaped bridge piers were found to be more advantageous with respect to decrease in the magnitude of the scour depth.
- One can say that the volume of the scour hole depends on the cross section of the piers. Although the P4 (rectangular with circular nose) pier caused the largest scour depth, the scour hole with the smallest volume was observed for this pier.
- Similar investigations will be useful to exhibit the behavior of non-uniform sediment to reveal the influence of the sediment dimension and geometric standard deviation of particle size distribution. Various shaped hydrographs may also be generated in order to study the influence of the hydrograph shapes.

Symbols

A = Scour hole area (L^2)

b = pier width (L)

d_s = scour depth (L)

D_{50} = median grain size (L)

F_d = densimetric particle Froude number

F_r = Froude number

g = gravitational acceleration (LT^{-2})

g'= reduced gravitational acceleration $g' = \left((\rho_s - \rho)/\rho\right)g$

h = approach flow depth (L)

I = flow intensity ratio

K_s = pier shape factor

L_R = reference length

n = hydrograph shape parameter

Q = discharge (L^3/ T)

T = dimensionless time

t = time (T)

u = mean approach velocity (L/T)

u_c= mean approach critical velocity (L/T)

u_{*c} = critical shear velocity (L/T)

ρ = fluid density

ρ_s = sediment density

σ_g = geometric standard deviation of the particle size distribution

Subscripts

b = base flow

p = peak flow

M = peak flow (Hager and Unger (2010))

References

[1] Hoffmans. G.J.C.M., Verheij. H.J., Scour Manual, Rotterdam, Netherlands, 1997

[2] Chabert. J., Engeldinger. P., Etude des affouillements autour des piles de ponts (Study of scouring around bridge piers). Chatou, France: Laboratoire National d'Hydraulique, 1956.

[3] Laursen. E., M, An analysis of relief bridge scour. American Society of Civil Engineers, Journal of the Hydraulics Division, 89 (HY3), 93-118, 1963.

[4] Shen, H. W., Schneider, V. R., Karaki, S. S., Local scour around bridge piers. American Society of Civil Engineers, Journal of the Hydraulics Division, 95 (HY6), 1969.

[5] Melville, B.W., Local scour at bridge sites. University of Auckland, School of Engineering, 1975.

[6] Ettema, R., Kirkil, G., Muste, M., Similitude of Large-Scale Turbulence in Experiments on Local Scour at Cylinders. Journal of Hydraulic Engineering 132:33–40. doi: 10.1061/(ASCE)0733-9429(2006)132:1(33), 2006.

[7] Yanmaz, A.M., Altinbilek, H.D., Study of time-dependent local scour around bridge piers. J. of Hydraulic Eng., Vol. 117, No. 10, 1991.

[8] Kothyari, U.C., Raju, K.G.R., Garde, R.J., Live-bed scour around cylindrical bridge piers. Journal of Hydraulic Research 30:701–715. doi: 10.1080/00221689209498889,1992.

[9] Richardson, E. V., Davis, S.R., Evaluating scour at bridges - Third edition. Hydraulic Engineering Circular No. 18, Federal Highway Administration Publication No. FHWA HI 96-031, Washington, D.C., 1995.

[10] Melville, B.W., Raudkivi, A.J., Effects of Foundation Geometry on Bridge Pier Scour. Journal of Hydraulic Engineering 122:203–209. doi: 10.1061/(ASCE)0733-9429(1996)122:4(203), 1996.

[11] Melville, B.W., Chiew, Y.M., Time Scale for Local Scour at Bridge Piers. Journal of Hydraulic Engineering 125:59–65. doi: 10.1061/(ASCE)0733-9429(1999)125:1(59), 1999.

[12] Oliveto, G., Hager, W.H., Temporal Evolution of Clear-Water Pier and Abutment Scour. Journal of Hydraulic Engineering 128:811–820. doi: 10.1061/(ASCE)0733-9429(2002)128:9(811), 2002.

[13] Dey, S., Westrich, B., Hydraulics of Submerged Jet Subject to Change in Cohesive Bed Geometry. Journal of Hydraulic Engineering 129:44–53. doi: 10.1061/(ASCE)0733-9429(2003)129:1(44), 2003.

[14] Chang, W.Y., Lai, J.S., Yen, C.L., Evolution of Scour Depth at Circular Bridge Piers. Journal of Hydraulic Engineering 130:905–913. doi: 10.1061/(ASCE)0733-9429(2004)130:9(905), 2004.

[15] Köse, Ö., Experimental and analytical investigation of temporal variation of local scour at bridge abutments. Middle East Technical University, 2007.

[16] Diab, R., Experimental investigation on scouring around piers of different shape and alignement in gravel. Middle East Technical University, 2011.

[17] Guney, M.S., Bombar, G., Experimental Investigation of Time-Dependent Local Scour at Bridge Piers. In: River Corridor Restoration Conference. Switzerland, 2011.

[18] Mohammadpour, R., Ghani, A., Azamathulla, H.M., Prediction of equilibrium scour time around long abutments. Proceedings of the Institution of Civil Engineers - Water Management 166:394–401. doi: 10.1680/wama.11.00075, 2013.

[19] López, G., Teixeira, L., Ortega-Sánchez, M., Simarro, G., Estimating Final Scour Depth under Clear-Water Flood Waves. Journal of Hydraulic Engineering 140:328–332. doi: 10.1061/(ASCE)HY.1943-7900.0000804, 2014.

[20] Hamidifar, H.M., Nasrabadi, M.H.O., Using a bed sill as a scour countermeasure downstream of an apron. Ain Shams Engineering Journal, 2011.

[21] Vijayasree, B.A., Eldho, T.I., Mazumder, B.S., Ahmad, N., Influence of bridge pier shape on flow field and scour geometry. International Journal of River Basin Management 17:109–129. doi: 10.1080/15715124.2017.1394315, 2019.

[22] Bennetts, T.A., Local scour around bridge piers under steady and unsteady flow conditions. University of Hertfordshire, 2002.

[23] Das, S., Ghosh, R., Das, R., Mazumdar, A., Clear water scour geometry around circular piers. Ecol. Environ. Conserv. 20(2), 479–492., 2014.

[24] Tison, L.J., Local scour in rivers. Journal of Geophysical Research (1896-1977) 66:4227–4232. doi: 10.1029/JZ066i012p04227, 1961.

[25] Cunha, L.V., Time evaluation of local scour. In: IAHR (ed) International Association for Hydraulic Research, Eleventh International Congress. Sao Paulo, 1975.

[26] Breusers, H.N.C., Nicollet, G., Shen, H.W., Local Scour Around Cylindrical Piers. Journal of Hydraulic Research 15:211–252. doi: 10.1080/00221687709499645, 1977.

[27] Oliveto, G., Hager, W.H., Further Results to Time-Dependent Local Scour at Bridge Elements. Journal of Hydraulic Engineering 131:97–105. doi: 10.1061/(ASCE)0733-9429(2005)131:2(97), 2005.

[28] Dey, S., Fluvial Hydrodynamics.Springer, 2014.

[29] Bor, A.T., Experimental and Numerical Study of Local Scour Around Bridge Piers with Different Cross Sections Caused by Flood Hydrograph Succeeding Steady Flow. Dokuz Eylül University, 2015.

[30] Melville, B.W., Coleman, S.E., Bridge Scour. Water Resources Publications, Colorado,ABD, 2000.

[31] Lanca, R.M.M., Simarro, G., Fael, C.M.S., Cardoso, A.E., Effect of Viscosity on the Equilibrium Scour Depth at Single Cylindrical Piers. Journal of Hydraulic Engineering Vol.142 No:3 Pages: 06015022. doi: 10.1061/(ASCE)HY.1943-7900.0001102, 2016.

[32] Tsutsui, T., Fluid force acting on a cylindrical pier standing in a scour. In: Bluff Bodies Aerodynamics& Applications. Milano Italy, 2008.

[33] Hager, W.H., Unger, J., Bridge Pier Scour under Flood Waves. Journal of Hydraulic Engineering 136:842–847. doi: 10.1061/(ASCE)HY.1943-7900.0000281, 2010.

[34] Arkis, A., Köprü Uç Ve Orta Ayaklari Etrafindaki Yerel Oyulmalara Karşi Koruyucu Önlemlerin Araştirilmasi. Dokuz Eylül University, 2013.

[35] Laursen, E.M., Toch, A., Scour around bridge piers and abutments, Iowa Highways Research Board, Ames, IA., 1956.

[36] Dietz, J., Construction of long piers at oblique currents illustrated by the BAB-Main Bridge Eddersheim, and Systematic model tests on scour formation at piers. Mitteilungsblatt der Bundersanstalt fur Wasserbau, Karlsruhe, Germany 31:79–109, 1972.

[37] Mostafa, E.A., Scour around skewed bridge piers. Alexandria University, Alexandria, Egypt, 1994.

[38] Yanmaz, A.M., Kose, O., Surface Characteristics of Scouring at Bridge Elements. Turkish J Eng Env Sci 31:127–134, 2007.

TEKNİK DERGİ MANUSCRIPT DRAFTING RULES

1. The whole manuscript (text, charts, equations, drawings etc.) should be arranged in Word and submitted in ready to print format. The article should be typed on A4 (210 x 297 mm) size paper using 10 pt (main title 15 pt) Times New Roman font, single spacing. Margins should be 40 mm on the left and right sides and 52.5 mm at the top and bottom of the page.
2. Including drawings and tables, articles should not exceed 25 pages, technical notes 10 pages.
3. Your contributed manuscript must be sent over the DergiPark system. (http://dergipark.gov.tr/tekderg)
4. The text must be written in a clear and understandable language, conform to the grammar rules. Third singular person and passive tense must be used, and no inverted sentences should be contained.
5. Title must be short (10 words maximum) and clear, and reflect the content of the paper.
6. Sections should be arranged as: (i) abstract and keywords, (ii) title, abstract and keywords in the other language, (iii) main text, (iv) symbols, (v) acknowledgements (if required) and (vi) references.
7. Both abstracts should briefly describe the object, scope, method and conclusions of the work and should not exceed 100 words. If necessary, abstracts may be re-written without consulting the author. At least three keywords must be given. Titles, abstracts and keywords must be fitted in the first page leaving ten line space at the bottom of the first page and the main text must start in the second page.
8. Section and sub-section titles must be numbered complying with the standard TS1212.
9. Symbols must conform to the international rules; each symbol must be defined where it appears first, additionally, a list of symbols must be given in alphabetic order (first Latin, then Greek alphabets) at the end of the text (before References).
10. Equations must be numbered and these numbers must be shown in brackets at the end of the line.
11. Tables, drawings and photographs must be placed inside the text, each one should have a number and title and titles should be written above the tables and below the drawings and photographs.
12. Only SI units must be used in the manuscripts.
13. Quotes must be given in inverted commas and the source must be indicated with a reference number.
14. Acknowledgement must be short and mention the people/ institutions contributed or assisted the study.
15. References must be numbered (in brackets) in the text referring to the reference list arranged in the order of appearance in the text. References must include the following information:

    If the reference is an article: Author's surname, his/her initials, other authors, full title of the article, name of the journal, volume, issue, starting and ending pages, year of publication.

    Example : Naghdi, P. M., Kalnins, A., On Vibrations of Elastic Spherical Shells. J. Appl. Mech., 29, 65-72, 1962.

    If the reference is a book: Author's surname, his/her initials, other authors, title of the book, volume number, editor if available, place of publication, year of publication.

    Example : Kraus. H., Thin Elastic Shells, New York. Wiley, 1967.

    If the reference is a conference paper: Author's surname, his/her initials, other authors, title of the paper, title of the conference, location and year.

    If the source is a thesis: Author's surname, his/her initials, thesis title, level, university, year.

    If the source is a report: Author's surname, his/her initials, other authors, title of the report, type, number, institution it is submitted to, publication place, year.
16. Discussions to an article published in Teknik Dergi should not exceed two pages, must briefly express the addressed points, must criticize the content, not the author and must be written in a polite language. Authors' closing remarks must also follow the above rules.
17. A separate note should accompany the manuscript. The note should include, (i) authors' names, business and home addresses and phone numbers, (ii) brief resumes of the authors and (iii) a statement "I declare in honesty that this article is the product of a genuinely original study and that a similar version of the article has not been previously published anywhere else" signed by all authors.
18. Copyright has to be transferred to UCTEA Turkish Chamber of Civil Engineers. The standard copyright form signed by the authorised author should therefore be submitted together with the manuscript.

CONTENTS

ISSN: 1300-3453